A SEMI-CLASSICAL MODEL OF PROTON TUNNELLING IN HYDROGEN-BONDED COMPOUNDS

Michael Colin Lawrence

A thesis submitted to the
University of Cape Town
for the degree of
Doctor of Philosophy
August, 1980

ABSTRACT

Two back-to-back Morse potentials are used to model the protonic potential in a hydrogen bond. A mathematical method is developed to obtain semi-classical solutions for the eigenvalues and eigenfunctions of the potential. Particular care is taken over the form of approximation used in the vicinity of the barrier top. The double Morse potential is then used as the fundamental element in the analysis of the proton dynamics in a number of hydrogen-bonded species:

a) Chromous acid. A consistent, quantitative explanation is found for the $\nu_s(OH)/\nu_s(OD)$ bands in the mid-infrared spectra of CrOOH/CrOOD. The 226 cm^{-1} band in the far infrared and neutron scattering spectra of CrOOH is shown to be caused by the protonic tunnelling mode.

b) Carboxylic and Dicarboxylic acids. The 140 cm^{-1} protonic upper state splitting in dimeric formic acid proposed by Excoffon and Marechal (1972) is shown to be supported by the double Morse potential analysis. The analysis suggests however that the two hydrogen-bonded protons in $(HCOOH)_2$ tunnel independently. The anomalous $\nu_s(OH)/\nu_s(OD)$ intensity ratios observed in the infrared spectra of both adipic acid and dimeric formic acid could not be explained in terms of mechanical anharmonicity alone. The protonic tunnelling frequency in crystalline formic acid is shown to be about 23 cm^{-1}, which supports the order-disorder interpretation of the observed phase transition in this crystal.

c) Potassium Dihydrogen Phosphate (KDP). The crystallographic and infrared spectroscopic data for KDP and DKDP are

interpreted consistently using the double Morse potential. The bare single-particle tunnelling frequency Ω is estimated to be 320 ± 10 cm^{-1} and the overtone band at 4600 cm^{-1} in the infrared spectrum of KDP is shown to be a $|0\rangle \rightarrow |3\rangle$ single particle transition. The model is capable of predicting the temperature and pressure dependence of both the protonic tunnelling frequency and the protonic inter-site separation δ. The soft-mode Raman data of Peercy (1975) is re-analysed allowing for the temperature dependence of Ω. The analysis shows that i) the lattice polarization induced by the protonic tunnelling; ii) the modulation of the tunnelling frequency by non-polar optic phonons, and iii) the direct $B_{ij}S_i^xS_j^x$ protonic interactions are all essential factors in interpreting the soft-mode Raman response of KDP. The direct $J_{ij}S_i^zS_j^z$ protonic interaction is shown to increase in magnitude with increasing pressure and the relationship $J \propto \delta^2$ is criticised. The soft-mode damping is interpreted as arising from the modulation of the single-particle tunnelling frequency by the lattice modes.

ACKNOWLEDGEMENTS

Thanks and appreciation for the support and help given to me during the past three years as I worked on this thesis go to:

i) Dr. G.N. Robertson, for his enthusiastic supervision, ideas and encouragement;

ii) The Department of Physics at U.C.T., for its making available to me funds to attend the Fourth European Meeting on Ferroelectricity in Yugoslavia, and for their hospitality and friendliness;

iii) Dr. R.E. Nettleton, of the University of the Witwatersrand, for helpful discussions in October, 1979;

iv) African Explosives and Chemical Industries (Pty.) Ltd. (A.E.C.I.), for their generous financial support;

v) My wife, Lynne, as well as my parents, for their continual support and encouragement; and

vi) Penny Dobbie, for her careful and patient typing of the manuscript.

TABLE OF CONTENTS

CHAPTER ONE

INTRODUCTION

1.1 The Hydrogen Bond

In many molecular solids and liquids there is a tendency for a hydrogen atom which is covalently bonded to an electronegative atom such as O or N to form a second, weaker bond to another electronegative atom. This phenomenon is termed hydrogen bonding. A well-known example is ice, in which the association of the hydrogen atoms in one H_2O unit with the oxygen atoms in the neighbouring units causes an intricate polymeric structure to be built up. Other examples are the carboxylic acid molecules which form dimers in the vapour phase, held together by pairs of hydrogen bonds e.g. acetic acid:

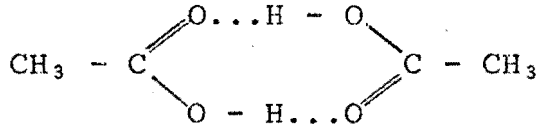

Hydrogen bonds are typically denoted either by A-H...B (as above) or more simply by AH...B, where A and B represent the heavier atoms at either end of the bond. The notation implies that the hydrogen atom H is more strongly bound to the A atom than it is to the B atom.

The most commonly used method of detecting the presence of hydrogen bonds in a given compound is by means of infrared (IR) spectroscopy and hence there is a considerable need to understand accurately the vibrational dynamics of the hydrogen bond.

Of the vibrational modes available to a hydrogen bond, by far the most important spectroscopically is the ν_s(AH)

stretching vibration $\vec{A}\overleftarrow{H}...\vec{B}$, as a strong downward shift occurs in the ν_s(AH) frequency as the hydrogen bond forms. The frequency of this vibration lies in the range 1000-3500 cm^{-1} (for bonds of the form OH...O), the lower end of the range being typically associated with relatively short hydrogen bonds (O...O distance 2.5Å) and the upper end of the range with longer bonds (O...O distance 2.8Å). See for example Novak (1974).

A rather poorly understood aspect of hydrogen bonding is that of proton tunnelling, the quantum mechanical "motion" of the proton from one site in the bond to the other, i.e. AH...A $\rightleftarrows$ A...HA. It is often difficult to detect this phenomenon crystallographically as the observed hydrogen probability distribution tends to be blurred out by the lattice motion leaving a broad, single-peaked distribution about the bond centre. This situation is easily misinterpreted to be a centralized hydrogen bond A-H-A. Spectroscopically, however, these two situations will give rise to very different vibrational bands. An example of this is chromous acid (CrOOH) in which tunnelling has only recently been crystallographically discerned (Nørlund Christensen, Hansen and Lehmann (1977), whereas earlier work suggested that the hydrogen atom was centrally situated (Hamilton and Ibers (1963)). Tunnelling is also of interest in some biological systems e.g. as a transport mechanism for protons through a biological membrane (Nagle and Morowitz (1978)).

This thesis is concerned with the development of a simple model which allows one to determine from spectroscopic and crystallographic data the extent of tunnelling in hydrogen-bonded species of the form AH...A and the way in which it is

affected by lattice vibrations, isotopic substitution, temperature changes and compression of the bond. It also allows one to make some estimate of the relative strengths of the various ν_s(AH) transitions and their bandshapes.

The remainder of this chapter discusses the theoretical background to the model and introduces the potential form to be used in the model. For a broader discussion of hydrogen-bonding, the reader is referred to one of the review works on the subject, e.g. that by Schuster, Zundel and Sandorfy (1975).

1.2 Theoretical Description of the ν_s(AH) vibrational mode

The system AH...A is usually treated by applying the Born-Oppenheimer approximation, which allows one to separate the electronic motion from that of the nuclei. Stationary states for the nuclear motion may then be determined from the Schrödinger equation

$$[T + V(\underset{\sim}{R})]\Psi(\underset{\sim}{R}) = \mathcal{E}\Psi(\underset{\sim}{R}) \qquad (1.1)$$

where T represents the kinetic energy operator for the nuclei, $\underset{\sim}{R}$ the coordinate describing the nuclear motion, $\mathcal{E}$ the energy eigenvalue associated with the nuclear motion and $V(\underset{\sim}{R})$ the average potential field generated by the electrons.

Olovsson and Jönsson (in Schuster *et al.* (1975)) have shown how for by far the majority of hydrogen bonds for which accurate crystallographic data are available, the bond angles lie in the range of 170-180°. Hence in the analysis of the ν_s(AH) vibration it is reasonable to consider the problem in one dimension only. Janoschek (also in Schuster *et al.*) shows how it is appropriate to use Jacobian coordinates to describe

the nuclear motion. In the case of potentials V which are symmetric about the centre of the bond (e.g. for bonds where appreciable tunnelling occurs in the low-lying states), these co-ordinates may be taken as the displacement q_1 of the proton from the centre of the bond and the relative displacement q_2 of the two A atoms from each other. The Schrödinger equation then becomes

$$\left[-\frac{\hbar^2}{2m_1}\frac{\partial^2}{\partial q_1^2} - \frac{\hbar^2}{2m_2}\frac{\partial^2}{\partial q_2^2} + V(q_1;q_2) + W(q_2)\right]\Psi(q_1,q_2) = \mathcal{E}\Psi(q_1,q_2) \quad (1.2)$$

where

$$m_1 = \frac{2m_A m_H}{2m_A + m_H} \quad \text{and} \quad m_2 = m_{A/2} \quad (1.3)$$

are the appropriate reduced masses and the potential $V(\underset{\sim}{R})$ has been separated for convenience into the sum of two terms: $V(q_1;q_2)$ representing the potential surface for the proton motion at given A...A distance q_2 and $W(q_2)$ the A...A repulsion.

As the proton is much lighter than either of the two atoms A, most authors adopt as an approximation q_2 = constant and $m_2 = \infty$. This is equivalent to introducing a second Born-Oppenheimer approximation which separates the proton motion from that of the heavier atoms, thus obtaining

$$\left[-\frac{\hbar^2}{2m_H}\frac{d^2}{dq_1^2} + V(q_1;q_2)\right]\Phi(q_1;q_2) = E(q_2)\Phi(q_1;q_2) \quad (1.4)$$

as the Schrödinger equation for the stationary states of the protonic motion alone, where $E(q_2) = \mathcal{E} - W(q_2)$.

This equation will be written more simply as

$$\left[-\frac{\hbar^2}{2m}\frac{d^2}{dx^2} + V(x)\right]\Phi(x) = E\Phi(x) \quad (1.5)$$

where $x = q_1$, $m = m_H$ and the dependence of E, V and Φ upon q_2 is left implicit. It is also convenient to introduce the variable R defined by $2R = q_2$.

Once a suitable form for the potential V has been determined, the energy level structure for the ν_s(AH) vibrations of a symmetric AH...A system can be obtained from equation (1.4). This should in some way correlate with the observed IR spectra.

1.3 Choosing a Potential V(x)

Qualitatively the potentials V(x) for AH...A bonds can be categorized as follows (Novak (1974)):

(i) Single minimum potentials. These occur in very short hydrogen bonds e.g. $KH(CH_2COO)_2$ ($2R=2.44\text{Å}$);

(ii) Asymmetric potentials. These occur in very long hydrogen bonds where the hydrogen atom remains associated with only one A atom e.g. ice ($2R=2.76\text{Å}$);

(iii) Symmetric double minimum potentials. The two minima represent the most likely places for the hydrogen atom to be situated in the bond. This category usually supports tunnelling e.g. chromous acid ($2R=2.49\text{Å}$).

Figure 1.1 illustrates these three categories. This thesis is concerned with potentials of the third type. It becomes appropriate then to consider only those vibrational states in the potential which have a definite parity and the IR-active transitions will then be those which occur between states of opposite parity. Figure 1.2 shows such a double minimum potential together with the first few low-lying states.

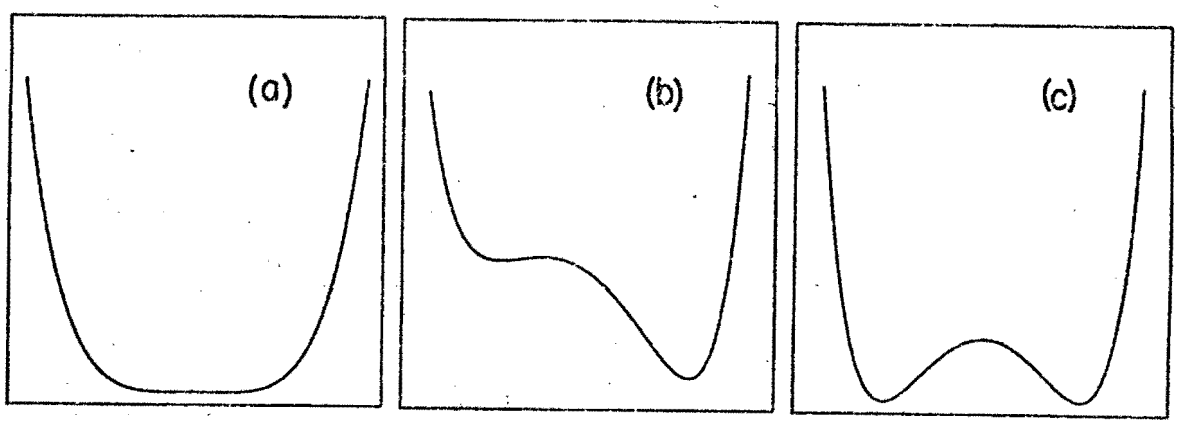

Figure 1.1. Hydrogen bond Potentials: (a) single minimum potential; (b) asymmetric potential; (c) symmetric double minimum potential.

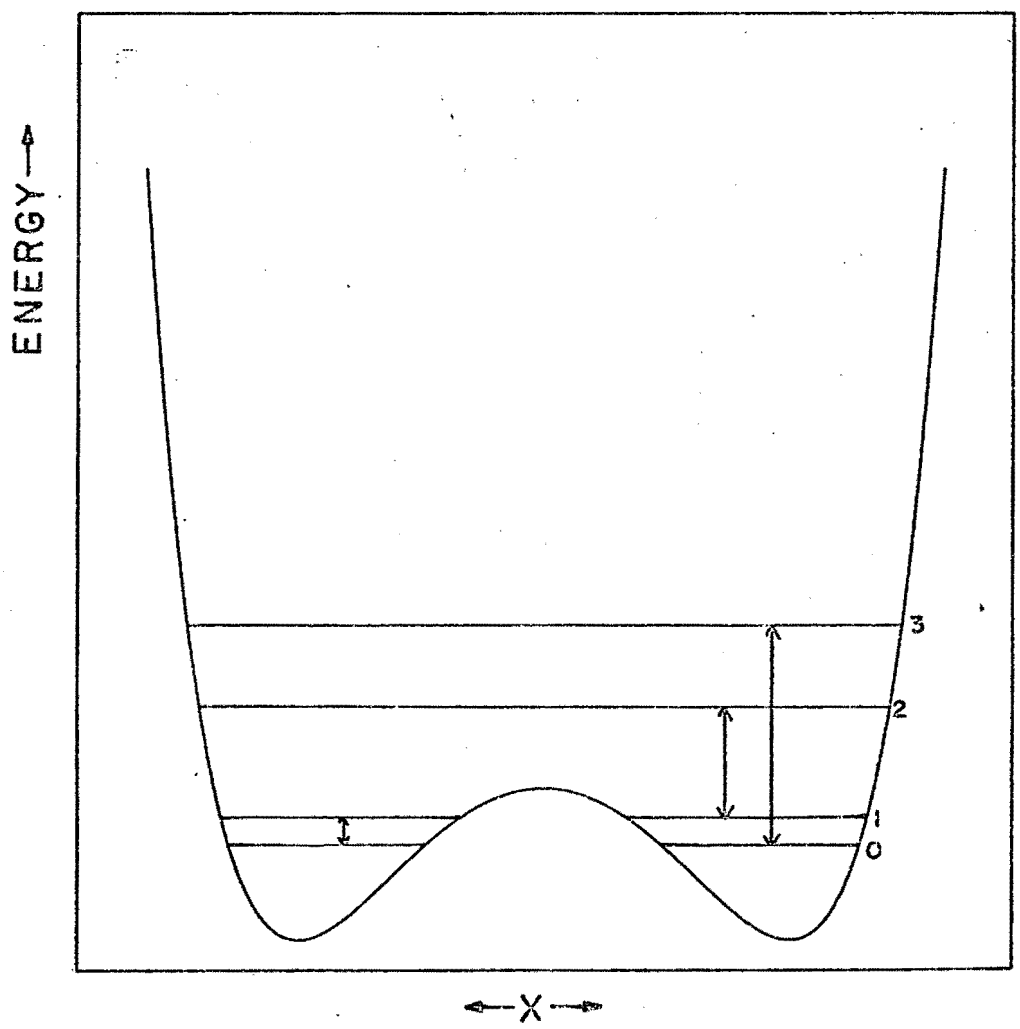

Figure 1.2. Infrared active transitions in a double minimum hydrogen bond potential.

It is very difficult to determine the potential V directly from the electronic motion and so it becomes imperative to choose some analytic form to characterize it, dependent upon a number of parameters. In choosing such a form, it is useful to take the following factors into account:

(i) The potential must in some sense be a physically reasonable representation of the actual potential involved, i.e. must have the characteristic double, or perhaps single minimum shape and must give a very small probability of locating the proton in the immediate vicinity of the A atoms at $x = \pm R$ respectively.

(ii) The parameters should ideally be determinable either directly or indirectly from available crystallographic and/or spectroscopic data.

(iii) The potential should be sufficiently simple mathematically so as to allow ready determination of the wavefunctions and energy eigenvalues from equation (1.5). Analytic solutions are usually far more useful than numerical solutions which can be gathered for only one species at a time.

1.4 Examples of Hydrogen Bond Potentials

Baker (1954) constructed a double minimum potential as the sum of two completely overlapping Morse potentials. From this the transition frequencies for an OH...O hydrogen bond were predicted as a function of the O...O distance. The Morse potential parameters used were simply those obtained spectroscopically for the single OH molecule. The energy levels were obtained by constructing the proton wavefunctions

as a linear combination of those for the single OH molecule. This method led to a systematic error of about 25% when compared with ν_s(OH) frequencies known at the time, and which could be attributed either to the approximations made in constructing the wavefunctions or to the failure of the potential used to approximate accurately the true potential.

Reid (1959) suggested using the sum of two Lippincott-Schroeder potentials to form the potential V and by incorporating an expression for W so modelled the entire potential surface for the nuclear motion. He also allowed for the minima being asymmetric, as would be the general case in hydrogen bonds. From this he was able to predict with some accuracy the values of R at which the well changes from a double to a single minimum shape. No detailed analysis of the wavefunctions involved was attempted.

Pshenichnov and Sokolov (1961) have constructed asymmetric wells out of three parabolic segments: one to form the potential barrier and two further pieces extending upwards from the minima on either side, leaving cusps at the bottom. The advantage of this method is that Schrödinger's equation can be solved exactly for parabolic barriers. The variation of the transition frequencies can be determined then for various A...B distances assuming certain values for the other well parameters.

Somorjai and Hornig (1962) constructed a double minimum asymmetric well by means of a fourth-degree polynomial and determined the corresponding wavefunctions as linear combinations of harmonic oscillator wavefunctions. No attempt was made to apply the method directly to any observed IR spectra.

Davis and Christoffersen (1973) have constructed the double minimum well out of two Morse potential segments (leaving a cusp at x = 0) and have applied it to the inversion of NH_3, ND_3 and NT_3 molecules. Although this problem is not the same as that of hydrogen bonding, it is worth mentioning as the wells involved are rather similar. The difficulty in using such a well to model hydrogen bonds would be that for low barriers the cusp becomes a nuisance (as it does in the case of NH_3).

1.5 The Double Morse Potential

Following Baker (1954) two Morse potentials superimpose to give

$$V(x) = U(R+x) + U(R-x) \qquad (1.6)$$

where $U(x) = D\{1 - \exp[\alpha(r_o-x)]\}^2$ is the usual form of a Morse potential characterized by the parameters D, α and r_o.

The advantages of this potential can be discussed in terms of the three points raised at the end of section 1.3:

(i) It is physically realistic. An AH ion (e.g. OH^-) is well-represented by a single Morse potential. It is plausible therefore that an AH...A or A...HA system is well represented by a pair of Morse potentials provided that the bonds remain asymmetric and the O...O distance remains relatively large.

When the bond length is relatively short or when the hydrogen atom is nearly central, such a construction cannot be expected to remain accurate if the parameters are taken to be those of the diatomic ion. However, if D, α and r_o are treated simply as parameters to be determined, this form becomes very

flexible. D then no longer represents the dissociation energy and the potential well is more readily characterized by quantities such as the barrier height, separation of the minima and curvature at the minima.

V(x) may be conveniently written as

$$V(x) = D\{2\exp[-2\alpha(R-r_o)]\cosh 2\alpha x - 4\exp[-\alpha(R-r_o)]\cosh\alpha x\} \quad (1.7)$$

with the additive constant 2D from (1.6) omitted.

From this form is can be simply shown that V(x) has a double minimum shape if and only if

$$\gamma \equiv \exp[\alpha(R-r_o)]/2 > 1 \quad (1.8)$$

in which case the central point is given by

$$V(0) = \frac{D}{2\gamma^2} - \frac{2D}{\gamma} . \quad (1.9)$$

The minima occur at $x = -x_m$ and $x = +x_m$ respectively where

$$\alpha x_m = \cosh^{-1}\gamma \quad (1.10)$$

and then

$$V(x_m) = -D - \frac{D}{2\gamma^2} .$$

Combining (1.9) and (1.11), the barrier height is seen to be

$$V(0) - V(x_m) = D\left(\frac{\gamma-1}{\gamma}\right)^2 \quad (1.11)$$

(ii) The bond length 2R is usually available from X-ray or neutron diffraction studies and so the free parameters left to characterize V are D, α and r_o. These must be determined from the remaining IR and crystallographic data.

(iii) As will be seen in the next chapter, this potential form yields itself very well to mathematical analysis

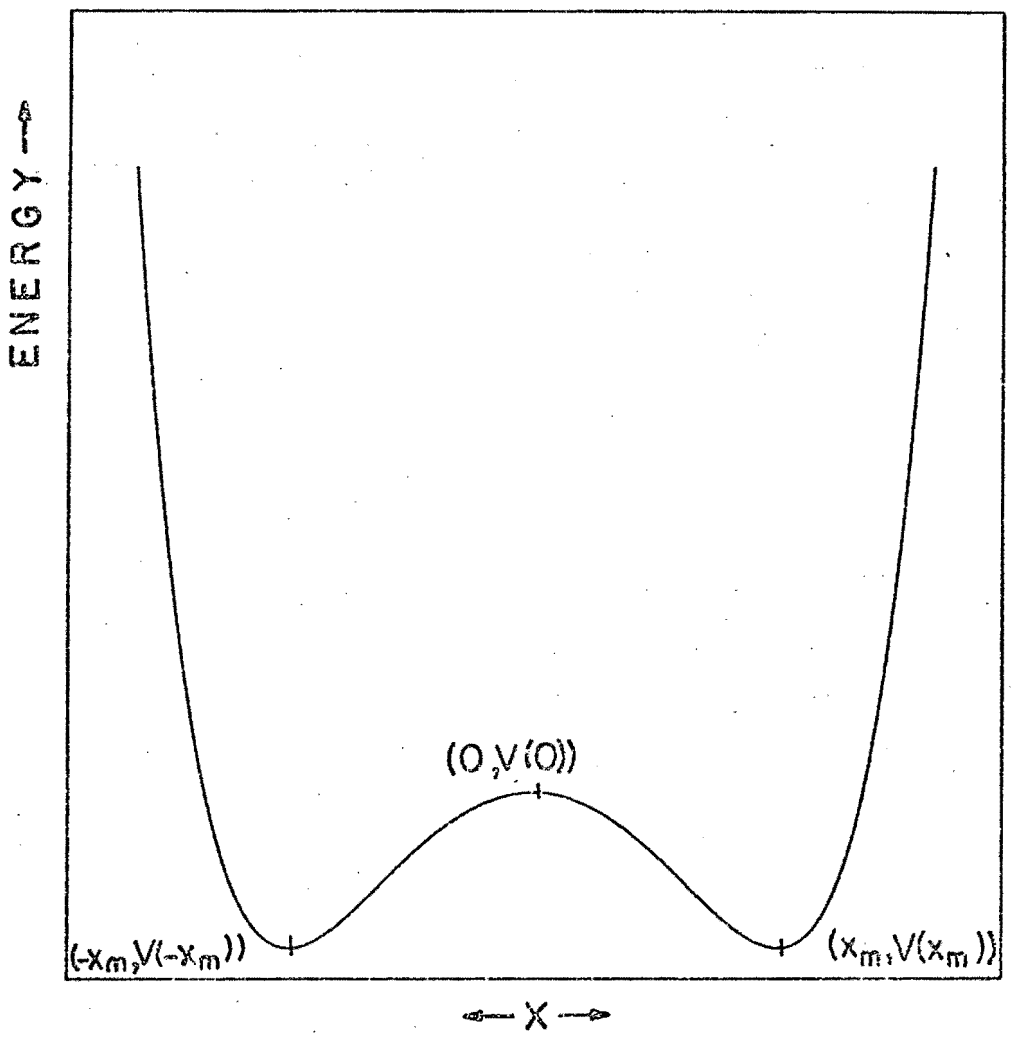

Figure 1.3. The double Morse potential. The co-ordinates of the barrier top and the two minima are (0,V(0)) and ($\pm x_m$,V($\pm x_m$)) respectively.

An asymptotic analysis technique will be developed to yield the wavefunctions.

An important advantage of this representation is that it suggests that the effects of a change in bond length, such as occurs on deuteration, cooling or the application of pressure, can be taken into account simply by varying R.

The double Morse potential is illustrated in Figure 1.3.

1.6 Outline of Remaining Chapters

Chapter 2 gives the details of the mathematical method used to obtain the energy eigenvalues and single particle wavefunctions associated with a particular double Morse potential. Chapter 3 applies the model to the OH...O bonds in crystalline chromous acid. This substance has particularly short hydrogen bonds ($2R = 2.49\text{Å}$) and should therefore provide a stringent test of the accuracy of the double Morse potential. Chapter 4 applies the model to certain carboxylic and dicarboxylic acids in both the crystalline and gaseous phases. These substances have relatively long hydrogen bonds and it is of particular interest to know the details of any proton tunnelling in their hydrogen bonds. Chapter 5 discusses in detail the proton dynamics in potassium dihydrogen phosphate (KDP), a well-known ferroelectric material. The double Morse potential is shown to be particularly suitable for determining pressure and thermal variations in the proton tunnelling frequency and to yield greater understanding of the proton-proton and proton-lattice interactions in KDP crystals. Chapter 6 concludes the thesis with a discussion of the overall success of the double Morse potential in characterizing protonic potentials in hydrogen bonds.

CHAPTER TWO

ASYMPTOTIC ANALYSIS OF THE DOUBLE MORSE POTENTIAL

The method developed in this chapter enables approximate wavefunctions and energy eigenvalues to be determined for the proton motion in the potential well described by equation (1.7). The method is based on a WKB-type analysis of the Schrödinger equation (1.5), but special care is taken to allow for the effects of the potential barrier, a well-known difficulty in normal WKB analysis (see for example Ford, Hill, Walkano and Wheeler (1959) or Miller (1968)). In Section 2.1 it will be shown how to select the most suitable asymptotic form of the wavefunctions to give approximate solutions to equation (1.5). Section 2.2 gives the transformations which must be applied to (1.5) to generate these asymptotic forms and section 2.3 then shows how these various forms can be connected together to give the total wavefunction. Section 2.4 discusses some of the computational problems that arise when determining the energy levels by this method and suggests how they can be overcome. Section 2.5 shows how the model can be used to calculate approximate bandshapes for the various ν_s(OH) transitions and section 2.6 discusses how estimates of the parameters R, D, α and r_o may be obtained in practice for a given species.

2.1 Choosing Asymptotic Forms

For each region of the potential V(x) the wavefunction Φ will be expanded in terms of an appropriate asymptotic series. To select the best such expansion, it is useful to know

approximately where in the potential well the energy levels lie.

Consider the equation

$$f(x;E) \equiv E-V(x) = 0. \tag{2.1}$$

For V(x) defined as above, f has four zeros (or turning points) at $x = \pm a, \pm b$ respectively and where a and b are given by

$$\alpha a = \cosh^{-1}[\gamma-(\gamma^2+\gamma^2 E/D+\tfrac{1}{2})^{\frac{1}{2}}]$$
$$\alpha b = \cosh^{-1}[\gamma+(\gamma^2+\gamma^2 E/D+\tfrac{1}{2})^{\frac{1}{2}}]. \tag{2.2}$$

Two cases can be distinguished:

Case I

If $V(x_m)<E<V(0)$ (i.e. the energy level lies below the barrier) then both a and b are real and $0<a<b$.

Case II

If $E>V(0)$ (i.e. the energy level lies above the barrier) then b is real and a is complex.

Figure 2.1 illustrates these two cases.

Interest is usually focussed on the first few low-lying levels. At least two of these states usually have energy eigenvalues E_n which are such as to place the respective energy levels $|n\rangle$ below the barrier.

The usual WKB approach to this type of problem (see for example ter Haar (1964) or Erdélyi (1956)) is to show that the wavefunctions can be asymptotically approximated by either "trigonometric" or "exponential" forms, i.e.

$$\Phi(x) \sim c_1 \ell^{\frac{1}{2}} \cos(\textstyle\int^x dx/\ell + c_2) \tag{2.3a}$$
$$\Phi(x) \sim \ell^{\frac{1}{2}}[c_3 \exp(\textstyle\int^x dx/\ell) + c_4 \exp(-\int^x dx/\ell)] \tag{2.3b}$$

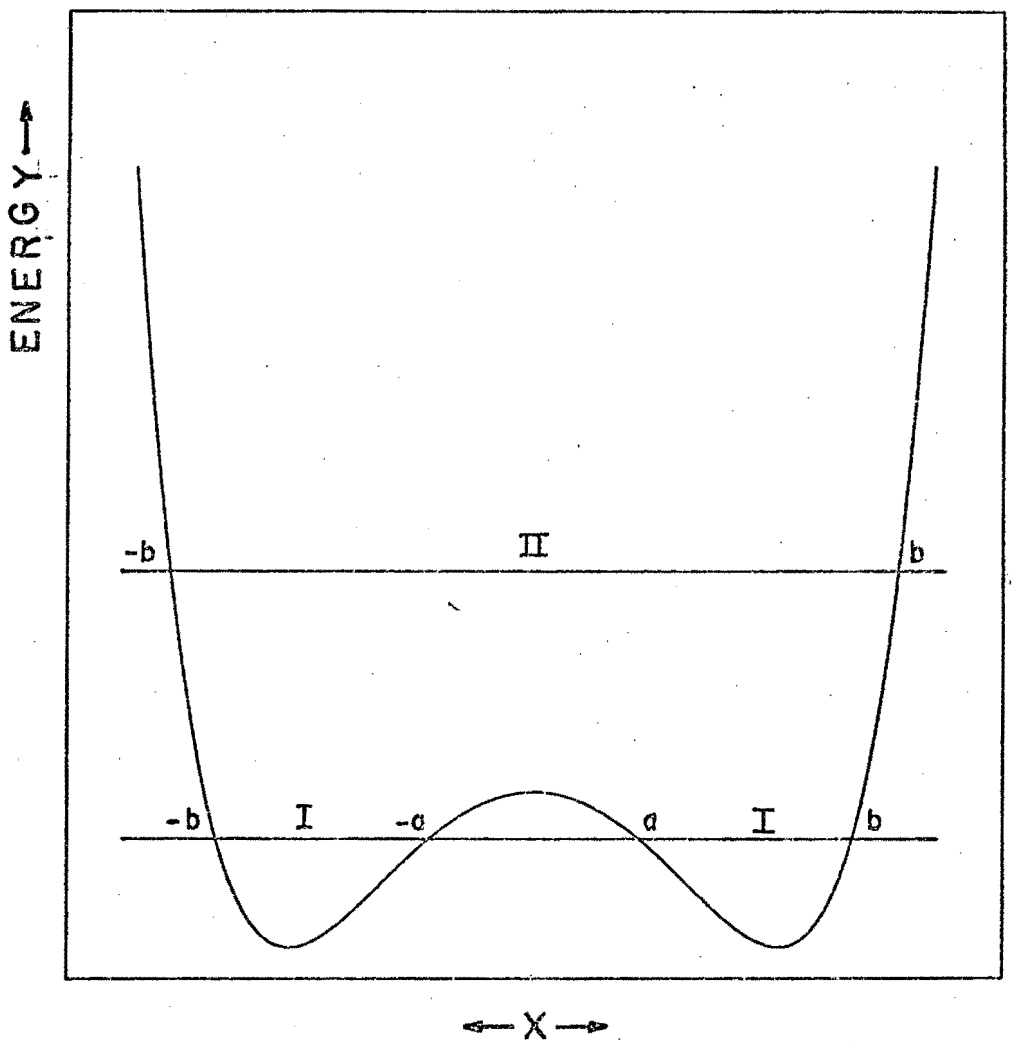

Figure 2.1. Semi-classical turning points in the double Morse potential. Case I: Energy level lying below the barrier top. Case II: Energy level lying above the barrier top.

respectively, where

$$\ell = (\hbar^2/2m)^{\frac{1}{2}}|V(x)-E|^{-\frac{1}{2}}. \qquad (2.3c)$$

As these forms are asymptotic in nature, they apply only when x is relatively "far" from the turning points. The first of these two forms applies to those regions where $E>V(x)$ and the second to those where $E<V(x)$, (so-called "classically allowed" and "classically forbidden" regions respectively). Notice that for a given turning point, the region immediately to one side of it will be classically allowed and immediately to the other side will be classically forbidden.

An approximate expression for the wavefunction in the immediate vicinity of a given turning point must still be found. A method must also be found to determine the coefficients c_1, c_2, c_3, c_4 above so that the expansions used both represent the same wavefunction.

The first step in the normal WKB analysis is the transformation of the Schrödinger equation to the Airy equation:

Define λ by $\lambda^2 = \frac{2m}{\hbar^2}$ and introduce the variables η and ξ by $\eta = \psi(x)\Phi$ and $\xi = \phi(x)$ (2.4)

where ψ and ϕ are functions of x yet to be defined.

Substitution into equation (1.5) yields

$$\frac{d^2\eta}{d\xi^2} + \frac{1}{\phi'}\left(\frac{\phi''}{\phi'} - \frac{2\psi'}{\psi}\right)\frac{d\eta}{d\xi} + \left[\frac{\lambda^2(E-V)}{\phi'^2} + \frac{\psi}{\phi'^2}\frac{d^2\psi^{-1}}{dx^2}\right]\eta = 0. \qquad (2.5)$$

Now put

$$\frac{\phi''}{\phi'} = \frac{2\psi'}{\psi} \quad (\text{i.e. } \psi = |\phi'|^{\frac{1}{2}}) \qquad (2.6)$$

to obtain

$$\frac{d^2\eta}{d\xi^2} + \lambda^2\left[\frac{E-V}{\phi'^2}\right]\eta = -\frac{\psi'}{\phi'^2}\frac{d^2\psi^{-1}}{dx^2}\eta$$

or

$$\frac{d^2\eta}{d\phi^2} + \lambda^2\left[\frac{E-V}{\phi'^2}\right]\eta = \rho(\phi)\eta \tag{2.7}$$

where

$$\rho(\phi) = \left[\frac{\phi'''}{2\phi'^3} - \frac{3\phi''^2}{4\phi'^4}\right]. \tag{2.8}$$

If the assumption

$$\frac{E-V}{\phi'^2} = \phi \tag{2.9}$$

is inserted into (2.7) then

$$\frac{d^2\eta}{d\phi^2} + \lambda^2\phi\eta = \rho(\phi)\eta. \tag{2.10}$$

Erdélyi shows that the first terms in an asymptotic expansion for Φ can then be obtained by solving the equation

$$\frac{d^2\eta}{d\phi^2} + \lambda^2\phi\eta = 0. \tag{2.11}$$

Putting $\phi = -\lambda^{2/3}\tau$ gives

$$\frac{d^2\eta}{d\tau^2} - \tau\eta = 0 \tag{2.12}$$

which is a standard form of the Airy equation, having two independent solutions $\eta = Ai(\tau)$ and $\eta = Bi(\tau)$. Ai and Bi are defined in Appendix A. Approximate wavefunctions are thus given by

$$\Phi(x) \approx Ai(\tau)/\psi(x) \text{ or } \Phi(x) \approx Bi(\tau)/\psi(x) \tag{2.13}$$

from (2.4).

It turns out that using the asymptotic forms for Ai and Bi (see Appendix A) in (2.13) on either side of the turning

point $\tau=0$ one obtains precisely expressions (2.3). This gives the relationship between the various c's as expressions (2.3) must approximate to the same Airy function in the vicinity of the turning point. This procedure can be easily extended to a series of turning points (see Erdélyi (1956), Jeffreys (1962), Jeffreys and Jeffreys (1956) or Heading (1962).)

However the standard WKB procedure cannot be applied directly to the problem at hand for three reasons (see Ford *et al.* (1959), Miller (1968)):

(i) the value of a may be too small to make the asymptotic expansions (2.3b) accurate in the region $|x|<a$;

(ii) also, if the energy level lies immediately above the top of the barrier, then the presence of the two complex turning points a of f close to the origin fails to make expansions of the form (2.3a) between the points $x = -b$ and $x = +b$ sufficiently accurate near $x = 0$;

(iii) below the barrier the turning points a and b for a given level may not be sufficiently far apart for the form (2.3a) to be at all accurate in the region $a<|x|<b$.

In order to overcome these difficulties, the following modifications must be introduced. Replace (2.9) by

$$\frac{E-V}{\phi'^2} = \phi^2 \pm A^2 \tag{2.14}$$

(using + sign above barrier, - sign below). Then

$$\frac{d^2\eta}{d\phi^2} + \lambda^2(\phi^2 \pm A^2)\eta = \rho(\phi)\eta. \tag{2.15}$$

Olver (1974) has shown that under suitable conditions $\rho(\phi)$, or more accurately $\rho(\phi;R)$, is a continuous function of

both ϕ and R and that the first terms of an asymptotic expansions for the wavefunctions Φ can then be obtained by considering solutions of

$$\frac{d^2\eta}{d\phi^2} + \lambda^2(\phi^2 \pm A^2)\eta = 0. \qquad (2.16)$$

Putting $\phi = \tau/(2\lambda)^{\frac{1}{2}}$ this becomes

$$\frac{d^2\eta}{d\tau^2} + (\tfrac{1}{4}\tau^2 \pm \frac{\lambda}{2}A^2)\eta = 0 \qquad (2.17)$$

which is a standard form of the parabolic cylinder equation (see Abramowitz and Stegun (1965)).

Two independent solutions

$$\eta = y_1(\tau;\mp A^2\lambda/2)$$

$$\text{and } \eta = y_2(\tau;\mp A^2\lambda/2) \qquad (2.18)$$

are chosen, where y_1 and y_2 are even and odd parabolic cylinder functions respectively. (Appendix A contains the definitions of these functions).

This transformation will thus overcome difficulties (i) and (ii) above for it can be used throughout the region $-b<-c<x<c<b$ where $0<c<b$.

To overcome difficulty (iii) the following procedure is adopted. Near to the points $x = \pm b$ the standard transformation mentioned above of the Schrödinger equation to the Airy equation will be retained but it will not be assumed that the wavefunctions so obtained can be replaced by expressions of the form (2.3b) anywhere in the region $|x|<b$. In fact, the precise Airy function asymptotic form (2.13) so obtained will be used throughout a region $c<|x|<\infty$, where $c \sim (a+b)/2$. For computational purposes c will be taken as equal x_m.

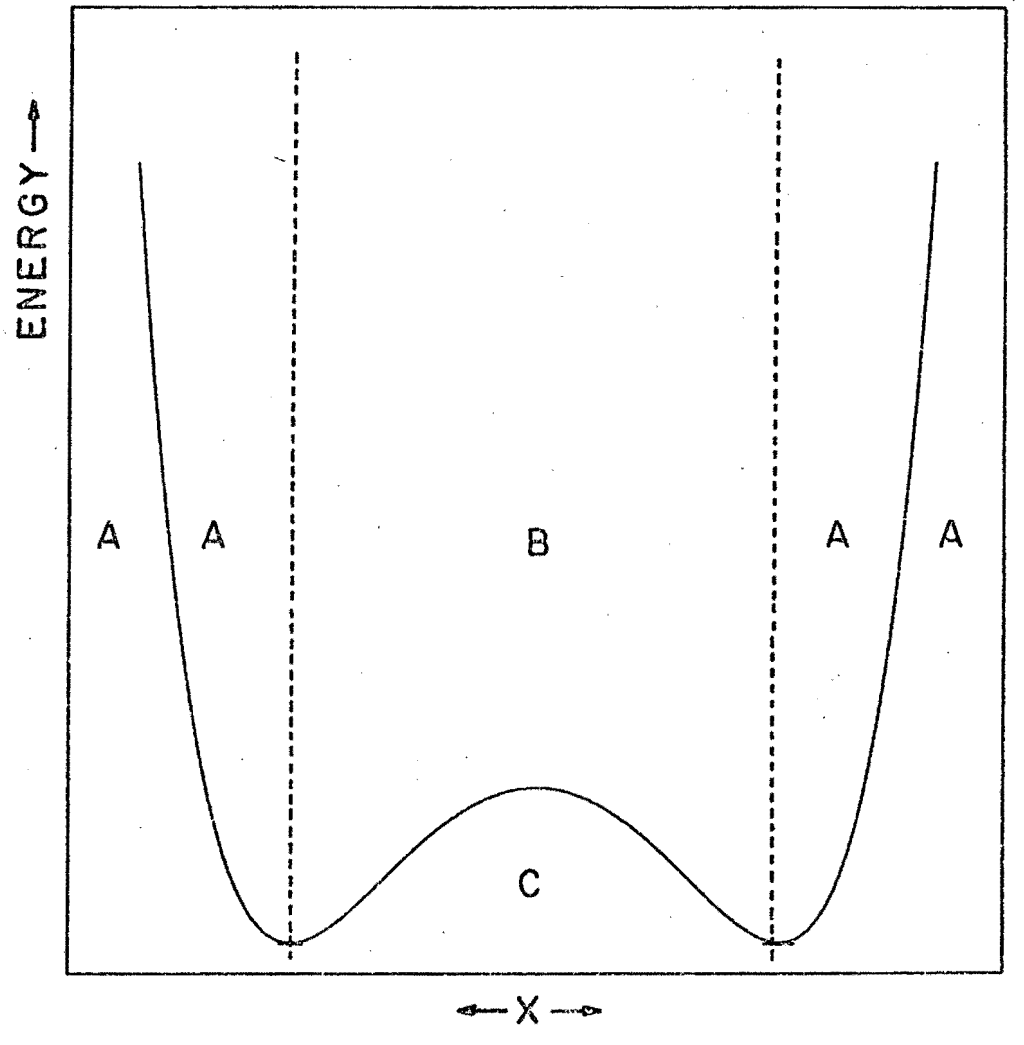

Figure 2.2. Transformations used in the semi-classical analysis of the double Morse potential.

A: Transform Schrödinger's equation to

$$\frac{d^2\eta}{d\tau^2} - \tau\eta = 0.$$

B: Transform Schrödinger's equation to

$$\frac{d^2\eta}{d\tau^2} + (\tfrac{1}{4}\tau^2 + \frac{\lambda}{2}A^2)\eta = 0.$$

C: Transform Schrödinger's equation to

$$\frac{d^2\eta}{d\tau^2} + (\tfrac{1}{4}\tau^2 - \frac{\lambda}{2}A^2)\eta = 0.$$

This method has the additional advantage of allowing a smooth transition in the form of approximation used when passing from levels immediately below the barrier to levels immediately above. Figure 2.2 summarizes the various transformations.

2.2 The Transformations

The transformations described above are termed "Liouville transformations". Before proceeding with the development of these transformations care must be taken to define accurately the nature of the turning points, the boundary conditions on Φ and the particular transformations for each region.

Consider the nature of the turning points a and b defined by (2.2). b is always real but a may assume values that are either real, conjugate imaginary or complex. It is essential to distinguish between the latter two cases for a.

It follows from the fact that $\cosh^{-1}(u) = i\cos^{-1}(u)$ that a will be pure imaginary if and only if

$$-1<\gamma-(\gamma^2+\gamma^2E/D+\tfrac{1}{2})^{\frac{1}{2}}<1. \qquad (2.19)$$

The right-hand inequality implies simply that the level E lies above the barrier top (otherwise a would be real) whereas the left-hand inequality becomes

$$(\gamma+1)^2>\gamma^2+\gamma^2E/D+\tfrac{1}{2}$$

$$\text{or } E<D(2/\gamma+1/2\gamma^2$$

$$\text{i.e. } E<V(0)+4D/\gamma \qquad (2.20)$$

Thus there exists a region immediately above the barrier where f has two real and two conjugate imaginary zeros. If the level E is any higher than the value $V(0)+4D/\gamma$, it turns out that the transformations outlined above are entirely unsuitable for treating the then complex values of a. (In all the examples which are later considered the levels of interest all lay well within the region

$$V(x_m)<E<V(0)+4D/\gamma \ ). \tag{2.21}$$

The asymptotic forms chosen must obey the same boundary conditions as the original wavefunction Φ. These boundary conditions are $\Phi(\pm\infty) = \Phi'(\pm\infty) = 0$.

Furthermore as the Hamiltonian in (1.5) commutes with the parity operator when V is defined by (1.7), attention can be restricted to solutions which have a definite parity i.e.

$$\text{either} \qquad \Phi(x) = \Phi(-x) \quad (\text{implying } \Phi'(0)=0)$$

$$\text{or} \qquad \Phi(x) = -\Phi(-x) \quad (\text{implying } \Phi(0)=0). \tag{2.22}$$

It is also necessary to define more carefully over what range of the independent variable x each asymptotic expansion is going to be valid. This will now be done using the insight of section 2.1.

Case I Below the Barrier

Region 1

$-x_m<x<x_m$: transform to parabolic cylinder equation.

Region 2

$|x|>x_m$: transform to Airy equation

and define the following subregions:

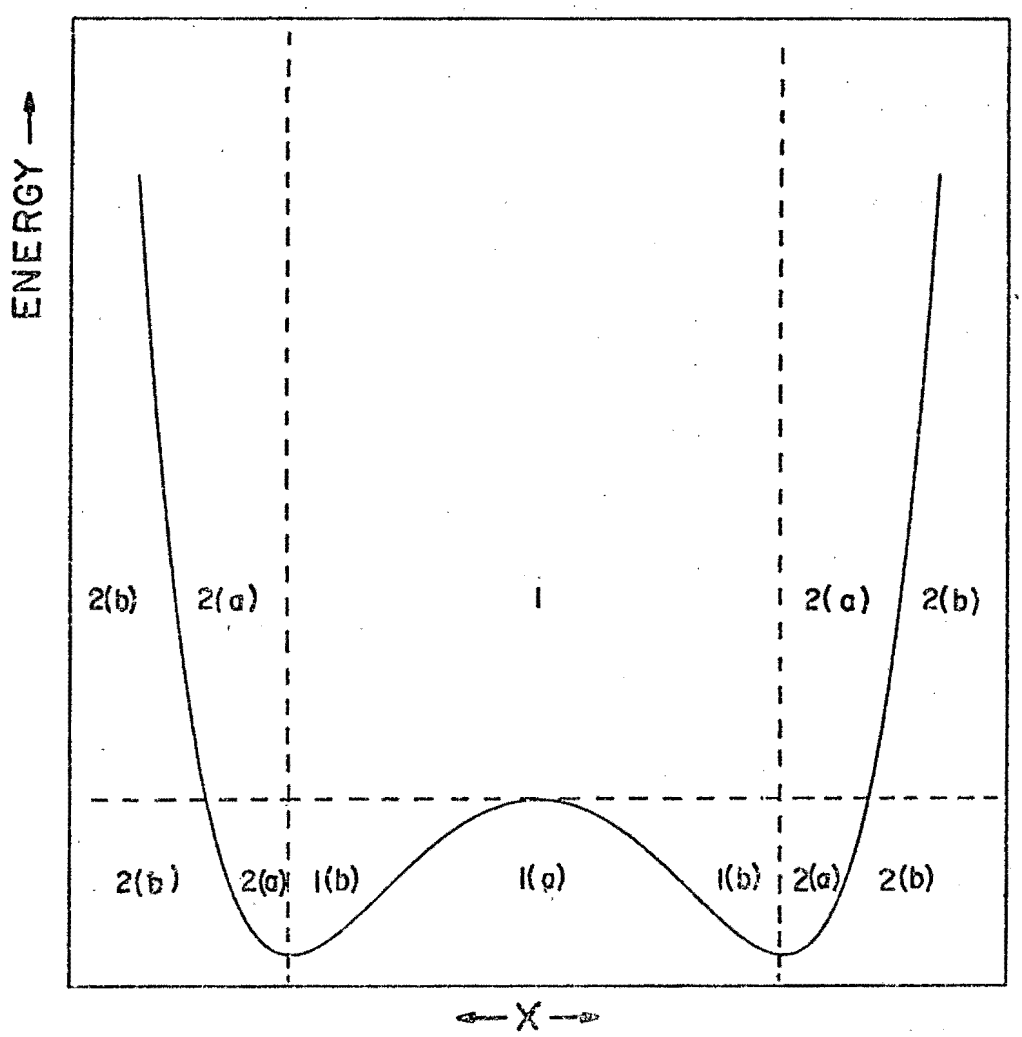

Figure 2.3. Definition of Regions 1 and 2 as used in the semi-classical analysis of the double Morse potential. Subregions 1(a), 2(a) and 2(b) are defined below the barrier; subregions 2(a) and 2(b) are defined below the barrier.

1(a) : $|x|<a$

1(b) : $a<x<x_m$, $-x_m<x<-a$

2(a) : $x_m \leqslant x<b$, $-b<x\leqslant -x_m$

2(b) : $|x|>b$.

Case II Above the Barrier

Region 1

$-x_m<x<x_m$: transform to parabolic cylinder equation.

Region 2

$|x|>x_m$: transform to Airy equation

and define subregions 2(a) and 2(b) as for Case I. (Region 1 need not be subdivided any further).

Figure 2.3 illustrates these regions.

The transformations can now be applied.

Case I Below the Barrier

Region 1

Put $$\frac{E-V}{\phi'^2} = \phi^2 - A^2, \qquad (2.23)$$

$V(\pm A) = E$ and define A by

$\phi(\pm a) = \pm A$.

Then from (2.4), (2.6) and (2.18),

$$\Phi = y_{1,2}(\tau; A^2\lambda/2)/|\phi'|^{\frac{1}{2}}, \quad \tau \equiv \phi(2\lambda)^{\frac{1}{2}}. \qquad (2.24)$$

It remains to determine ϕ from (2.23).

In region 1(a), (2.23) becomes

$\int_{\phi}^{A}(A^2-\phi^2)^{\frac{1}{2}}d\phi = \int_{x}^{a}(V-E)^{\frac{1}{2}}dx$ *

---

* In this integral and in some further integrals in this section the same symbol will be used for both the integration limit and the integration variable. Whereas this notation is not strictly correct, it makes the argument easier to follow at this stage than if a further symbol were introduced. No confusion can arise: the integration limit and the integration variable are always strictly distinct.

whence

$$\cos^{-1}w - w(1-w^2)^{\frac{1}{2}} = (2/A^2)\int_x^a (V-E)^{\frac{1}{2}}dx \qquad (2.25)$$

where

$$w = \phi/A.$$

In region 1(b), (2.23) becomes

$$\int_A^{\phi}(\phi^2-A^2)^{\frac{1}{2}}d\phi = \int_a^x (E-V)^{\frac{1}{2}}dx$$

whence

$$w(w^2-1)^{\frac{1}{2}} - \cosh^{-1}(w) = (2/A^2)\int_a^x (E-V)^{\frac{1}{2}}dx. \qquad (2.26)$$

Using $\phi(-a) = -A$, A is given from (2.25) as

$$A^2 = (2/\pi)\int_{-a}^{a}(V-E)^{\frac{1}{2}}dx \qquad (2.27)$$

Equations (2.25) and (2.26) determine ϕ implicitly as a function of x and (2.24-2.27) suffice in theory to yield an approximate wavefunction Φ in Region 1.

Region 2

Put $$\frac{E-V}{\phi'^2} = \phi \qquad (2.28)$$

with $V(b) = E$ and $\phi(b) = 0$.

The solution for Φ is then

$$\Phi = \mathrm{Ai}(\tau)/|\phi'|^{\frac{1}{2}}, \quad \tau \equiv -\phi\lambda^{-2/3}. \qquad (2.29)$$

from (2.4), (2.6) and (2.13).

It remains to determine ϕ from (2.28). Equation (2.28) may be written as

$$\phi' = -\left[\frac{E-V}{\phi}\right]^{\frac{1}{2}} \qquad (2.30)$$

as ϕ must be a decreasing function of x to give the correct behaviour in (2.29): $\mathrm{Ai}(\tau)$ must tend to zero as $x \to \infty$.

In region 2(a), $x_m < x < b$, and so (2.30) becomes

$$-\int_{\phi}^{0}\phi^{\frac{1}{2}}d\phi = \int_x^b (E-V)^{\frac{1}{2}}dx$$

or

$$\phi = \left[\frac{3}{2}\int_x^b (V-E)^{\frac{1}{2}}dx\right]^{2/3}. \qquad (2.31)$$

In region 2(b), $x>b$ and (2.30) becomes

$$-\int_o^{\phi}(-\phi)^{\frac{1}{2}}d\phi = \int_b^x (V-E)^{\frac{1}{2}}dx$$

or

$$\phi = -\left[\frac{3}{2}\int_b^x (V-E)^{\frac{1}{2}}dx\right]^{2/3} . \qquad (2.32)$$

Equations (2.31-2) determine ϕ as a function of x and together with (2.29) give an approximation for Φ in region 2.

Case II Above the Barrier

Region 1

Put $$\frac{E-V}{\phi'^2} = \phi^2 + A^2 \qquad (2.33)$$

with $V(\pm a) = E$ and define A by

$$\phi(\pm a) = \pm iA.$$

a is now taken to be pure imaginary, which will be the case if $E-V(>0)$ does not become too large.

From (2.4), (2.6) and (2.18)

$$\Phi = y_{1,2}(\tau;-A^2\lambda/2)/|\phi'|^{\frac{1}{2}}, \quad \tau \equiv \phi(2\lambda)^{\frac{1}{2}}. \qquad (2.34)$$

It remains to determine ϕ. From (2.33)

$$\int_o^{\phi}(\phi^2+A^2)^{\frac{1}{2}}d\phi = \int_o^x (E-V)^{\frac{1}{2}}dx$$

($\phi(0)=0$ as ϕ may be assumed to be odd in x from (2.33) and the condition $\phi(\pm a)=\pm iA$).

Hence

$$\sinh^{-1}w+w(1+w^2)^{\frac{1}{2}} = (2/A^2)\int_o^x (E-V)^{\frac{1}{2}}dx \qquad (2.35)$$

with $w = \phi/A$. This equation determines ϕ implicitly as a function of x. A may be obtained as follows. From (2.33)

$$\int_{-iA}^{iA}(\phi^2+A^2)^{\frac{1}{2}}d = \int_{-a}^{a}[E-V(z)]^{\frac{1}{2}}dz \qquad (2.36)$$

taking integrals along suitable paths in the complex plane.

The left-hand side of (2.36) reduces to $iA^2\pi/2$ and to treat the right-hand side consider an integration along the imaginary axis. The right-hand side becomes

$$\int_{-a}^{a} [E-V(z)]^{\frac{1}{2}}dz = -i\int_{-Im(a)}^{Im(a)}[E-V(iy)]^{\frac{1}{2}}dy$$

so

$$A^2 = -(2/\pi)\int_{-Im(a)}^{Im(a)} [E-V(iy)^{\frac{1}{2}}]dy. \qquad (2.37)$$

Note that

$$E-V(iy) = E-D\{2\ \exp[-2\alpha(R-r_o)]\cos 2\alpha y - 4\ \exp[-\alpha(R-r_o)]\cos\alpha y\}$$

which is real for real y.

Hence equations (2.34), (2.35) and (2.37) suffice in theory to yield approximate wavefunctions for Φ in region 1.

Region 2

Region 2 may be treated in exactly the same fashion as region 2 in Case I, yielding approximate wavefunctions of the form

$$\Phi = Ai(\tau)/|\phi'|^{\frac{1}{2}},\ \tau \equiv -\phi\lambda^{-2/3}.$$

The methods described above cannot be extended to the case where a is complex but, as already mentioned, this does not seriously hamper the applicability of the model.

2.3 Matching of Solutions

In order to obtain the complete wavefunctions out of the various segments already constructed, it is necessary to determine which asymptotic solution in Region 1 will match which asymptotic solution in Region 2, for both Cases. It will only be possible to achieve such a matching if the value of E corresponds to an eigenvalue E_n of the system. The

various segments will then all be approximations to the same Φ.

In the normal WKB methods, matching conditions are obtained by assuming that the Airy functions can be approximated by the first terms of their own asymptotic expansions (i.e. trigonometric or exponential forms) in regions far from the turning points. The matching conditions for a series of turning points are determined as follows.

Consider two turning points x_1 and x_2 and let $x_1<x_2$ with the region $x_1 < x < x_2$ classically allowed.

Let

$$\Phi(x) \sim c_1 \ell^{\frac{1}{2}} \cos\left(\int_{x_1}^{x} dx/\ell + c_2\right) \tag{2.38}$$

be the asymptotic form arising from considering an Airy function centred at $x = x_1$. Then the right-hand side of (2.38) can be written as

$$\cos\left(\int_{x_1}^{x} dx/\ell + c_2\right) = \cos\left(\int_{x_1}^{x_2} dx/\ell - \int_{x}^{x_2} dx/\ell + c_2\right)$$
$$= \cos\left(\int_{x}^{x_2} dx/\ell + c_2'\right)$$

where $c_2' = -c_2 - \int_{x_1}^{x_2} dx/\ell$.

Thus if

$$\Phi(x) \sim c_1 \ell^{\frac{1}{2}} \cos\left(\int_{x}^{x_2} dx/\ell + c_2'\right) \tag{2.39}$$

is the asymptotic approximation for Φ constructed in the classical region about the turning point $x = x_2$, the above expressions give the relationship between c_2 and c_2'. This is then the matching procedure.

However, as has already been pointed out in Section 2.1, the above form is not necessarily valid for this problem, as it depends upon exactly where the energy levels lie. Instead, an approximate matching will be made of the Airy functions of region 2 to the parabolic cylinder functions of

Region 1 at $x=x_m$ by demanding that they be equal in value and first derivative at this point.

The accuracy of this method is not readily determined analytically. A numerical estimate of the errors involved can be made by choosing points other than x_m for c and seeing what effect this has upon the energy level structure. (An analysis of this sort has been attempted in Appendix C).

The details of the method are as follows:

In region 1,

$$\Phi^{(1)}(x) = y_{1,2}[(2\lambda)^{\frac{1}{2}}\phi; \pm A^2\lambda/2]/|\phi'|^{\frac{1}{2}} \qquad (2.40)$$

from (2.24) and (2.34), where the + sign refers to levels below the barrier and the - sign to levels above. ϕ is chosen appropriately.

In region 2,

$$\Phi^{(2)}(x) = Ai(-\lambda^{2/3}\phi)/|\phi'|^{\frac{1}{2}} \qquad (2.41)$$

from (2.29) and ϕ is again chosen appropriately. Let the energy levels be labelled as E_o, E_1, E_2, ...etc. from the ground state upwards and let Φ_n be the corresponding wavefunctions. In order to obtain a matching of $\Phi^{(1)}$ to $\Phi^{(2)}$ in value at x_m, it is simply a matter of choosing the correct normalization factor C_n to apply to the wavefunction in one of the two regions.

Assume that

$$C_n\Phi_n^{(1)}(x_m) = \Phi_n^{(2)}(x_m). \qquad (2.42)$$

The matching condition thus becomes

$$C_n\Phi_n^{(1)'}(x_m) = \Phi_n^{(2)'}(x_m) \qquad (2.43)$$

or together with (2.42)

$$\Phi_n^{(1)'}(x_m)\Phi_n^{(2)}(x_m) - \Phi_n^{(1)}(x_m)\Phi_n^{(2)'}(x_m) = 0. \qquad (2.44)$$

In order to determine $\Phi^{(1)'}$ and $\Phi^{(2)'}$ it is necessary to treat the two energy level cases separately.

Case I Below the Barrier

Here

$$\Phi^{(1)} = \phi'^{-\frac{1}{2}} y_{1,2}\left[(2\lambda)^{\frac{1}{2}}\phi; A^2\lambda/2\right]$$

with

$$\phi' = \left(\frac{V-E}{A^2-\phi^2}\right)^{\frac{1}{2}}$$

so

$$\Phi^{(1)'} = -\tfrac{1}{2}\phi'^{-3/2}\phi'' y_{1,2}\left[(2\lambda)^{\frac{1}{2}}\phi; A^2\lambda/2\right] + \phi'^{\frac{1}{2}}(2\lambda)^{\frac{1}{2}} y'_{1,2}\left[(2\lambda)^{\frac{1}{2}}\phi; A^2\lambda/2\right] \qquad (2.45)$$

and

$$\phi'' = \tfrac{1}{2}\phi'^{-1}\left(\frac{V'+2\phi\phi'^3}{A^2-\phi^2}\right). \qquad (2.46)$$

Also

$$\Phi^{(2)} = \phi'^{-\frac{1}{2}} Ai(-\lambda^{2/3}\phi)$$

with

$$\phi' = -\left(\frac{E-V}{\phi}\right)^{\frac{1}{2}}$$

so

$$\Phi^{(2)'} = -\tfrac{1}{2}\phi'^{-3/2}\phi'' Ai(-\lambda^{2/3}\phi) - \lambda^{2/3}\phi'^{\frac{1}{2}} Ai'(-\lambda^{2/3}\phi) \qquad (2.47)$$

and

$$\phi'' = \tfrac{1}{2}\left(-\frac{V'}{\phi\phi'} - \frac{E-V}{\phi^2}\right). \qquad (2.48)$$

Substitution of (2.45) and (2.47) together with (2.46) and (2.48) into (2.44) gives the desired matching condition in this case.

Case II Above the Barrier

Here

$$\phi^{(1)} = \phi'^{-\frac{1}{2}} y_{1,2}\left[(2\lambda)^{\frac{1}{2}}\phi; -A^2\lambda/2\right]$$

with

$$\phi' = \left(\frac{E-V}{\phi^2+A^2}\right)^{\frac{1}{2}}$$

so

$$\Phi^{(1)'} = -\tfrac{1}{2}\phi'^{-3/2}\,\phi'' y_{1,2}\left[(2\lambda)^{\frac{1}{2}}\phi; -A^2\lambda/2\right] + \phi'^{\frac{1}{2}}(2\lambda)^{\frac{1}{2}} y'_{1,2}\left[(2\lambda)^{\frac{1}{2}}\phi; -A^2\lambda/2\right] \tag{2.49}$$

with

$$\phi'' = -\tfrac{1}{2}\phi'^{-1}\left(\frac{V'+2\phi\phi'^3}{\phi^2+A^2}\right). \tag{2.50}$$

$\Phi^{(2)'}$ is determined in the same way as outlined for Case I.

Substitution of (2.47-8) and (2.49-2.50) into (2.44) again yields the desired condition.

The wavefunctions thus obtained have therefore the following final form:

Even Parity Solutions (n even)

$$\Phi_n(x) = \begin{cases} \Phi_n^{(2)}(x) & x > x_m \\ C_n \Phi_n^{(1)}(x) & -x_m \leqslant x \leqslant x_m \\ \Phi_n^{(2)}(-x) & x < -x_m \end{cases} \quad \text{where } y_1 \text{ is chosen}$$

Odd Parity Solutions (n odd)

$$\Phi_n(x) = \begin{cases} \Phi_n^{(2)}(x) & x > x_m \\ C_n \Phi_n^{(1)}(x) & -x_m \leqslant x \leqslant x_m \\ -\Phi_n^{(2)}(-x) & x < -x_m \end{cases} \quad \text{where } y_2 \text{ is chosen}$$

and in both cases the wavefunctions Φ_n are continuous in their first derivatives at $x = \pm x_m$.

Notice that this method handles very neatly the troublesome barrier top. The same approximation form is used both above and below the barrier and all "quantum corrections" arising from the relative proximity of the points z=-a and z=a are taken into account by the use of the parabolic cylinder functions.

2.4 Computational Method

In the last section a method was derived enabling one to obtain approximate energy eigenvalues and the associated wavefunctions for the well described by equation (1.7), (given values for R, D, α, and r_o). However, a number of technical difficulties arise when this method is used for computational purposes:

i) The computation of the various phase integrals, generally of a form

$$\int_{z_1}^{z_2} |E-V(z)|^{\frac{1}{2}} dz.$$

ii) The difficulty in obtaining ϕ explicitly as a function of x from equations (2.25), (2.26) and (2.35).

iii) The computation of the Airy and parabolic cylinder functions and their respective derivatives as needed for the wavefunctions and the various matching conditions.

iv) The difficulty in determining the E_n so as to satisfy the matching condition (2.44).

As regards (i), the computation of the various phase integrals, Appendix B shows how all these integrals may be reduced to combinations of incomplete or complete elliptic integrals of the first, second or third kind. Standard

algorithms exist for evaluating these integrals and are referred to in the Appendix B. Similarly, numerical algorithms are also available for calculating the functions mentioned in (iii) and these are discussed in the Appendix A.

Regarding (ii) and (iv), it is seen that both these problems involve solving non-linear algebraic equations. Again, special algorithms exist for handling these tasks. In particular, in the programs developed the Harwell Subroutine Library* subroutine NBØ1A was used to solve these equations. This subroutine uses a bisection-interpolation technique and provided rapid solutions to both these equations. Care must be taken when computing energy eigenvalues with this technique to ensure that all the energy levels in a prescribed range are actually found. The method adopted was to search systematically for the first three even parity levels E_0, E_2 and E_4 and then to search between each consecutive pair of these even parity levels to detect the remaining levels E_1 and E_3. Levels with n>4 are not usually of interest.

2.5 Transition Intensities and Band Shapes

Once the wavefunctions Φ have been determined for a given potential well, rough estimates can be obtained of the transition intensities and of the band shapes. The probability of an electric dipole transition between the states $|m\rangle$ and $|n\rangle$ of the system is given by

$$P_{n\to m} \propto \left|\langle n|\underset{\sim}{\mu}.\underset{\sim}{E}|m\rangle\right|^2 \qquad (2.51)$$

where $|m\rangle$ and $|n\rangle$ are normalised state vectors,

$\underset{\sim}{\mu}$ is the electric dipole moment operator,

---

* See Appendix D.

$\underset{\sim}{E}$ is the perturbing electric field vector causing the transition

and ω_{nm} is the transition frequency $E_m - E_n$.

As a first approximation $\underset{\sim}{\mu}.\underset{\sim}{E}$ may be taken as proportional to the displacement x of the proton from the centre of the bond. (Janoschek, Weidemann, Pfeiffer and Zundel (1972) computed the dipole moment of the hydrogen bond in $H_5O_2^+$ using SCF-MO-LCGO calculations and their values show that although there is a considerable difference between the dipole moment of the proton in a hydrogen bond and the dipole moment of a bare proton, the dipole moment remains approximately proportional to the proton displacement x.) Thus

$$P_{n\to m} \propto \left| \langle \Phi_n(x) | x | \Phi_m(x) \rangle \right|^2 . \qquad (2.52)$$

Numerical integration can be used to normalize the wavefunctions obtained and then to calculate the matrix elements $\langle m|x|n\rangle$.

Allowance can also be made for stimulated emission from the upper state in (2.52) by means of a factor $[1-\exp(-\hbar\omega/kT)]$, if and when this becomes important.

The question of bandshapes is a far more difficult one and only the crudest computations can be made. One mechanism that will broaden the line at frequency ω_{nm} is the thermal motion of the oxygen atoms at either end of the bond. If one assumes that the proton states follow the oxygen-oxygen vibrations adiabatically then the change in frequency ω_{nm} with R can be readily determined from the model if the other parameters are assumed to remain constant. In this case the absorption intensity at frequency ω_{nm} due to the transition $|n\rangle$ to $|m\rangle$ is given by

$$I_{nm}(\omega) \propto \int_0^\infty P_{n\to m}(R)\,G(R)\,F(\omega-\omega_{nm}(R))\,\omega_{nm}(R)\,dR \qquad (2.53)$$

where G(R) represents the probability of the oxygen atoms being separated by a distance of 2R and F represents any other broadening mechanism that may occur.

In estimating G(R), the distribution function for the O...O distance, it is necessary to bear in mind that the oxygen vibrations are part of the lattice vibrations and hence the vibrations of neighbouring oxygen atoms are correlated.* Lawrence and Robertson (1979) have shown how the relative thermal vibration of two neighbouring oxygen atoms in an ice crystal can be as much as an order of magnitude smaller than the thermal amplitude of the individual oxygen atoms.

Other sources of broadening that may have to be considered in the formation of the function F include instrumental width (usually a relatively small effect), spontaneous decay of the excited state $|m\rangle$ (giving rise to an uncertainty in E_m) and coupling of the ν_s(OH) mode to the lattice modes.

2.6 Applying the Model to Specific Problems

Before the model can be applied to determining the energy level structure for the ν_s(OH) vibrations of a particular hydrogen bond, some estimates of the parameters R, D, α and r_o are needed.

As mentioned in Section 1.5, 2R is usually crystallographically available simply as the O...O distance, the bond being assumed linear. The OH distance is also sometimes available crystallographically, but is unfortunately not

---

* This applies, of course, only to hydrogen bonds in crystals.

directly related to the four parameters R, D, α and r_o. Instead it corresponds to the most probable proton position which is given approximately by the argument $x'=x'(R,D,\alpha,r_o,T)$ for which

$$\frac{\Phi_0^2(x)+\exp(-\hbar\omega_{01}/kT)\Phi_1^2(x)}{1+\exp(-\hbar\omega_{01}/kT)} \qquad (2.54)$$

is a maximum, where ω_{01} is the splitting of the ground state and T the temperature at which the OH distance was experimentally determined. (The higher levels are assumed to be negligibly populated).

The other source of information about the well is the infrared (IR) spectrum itself. If some attempt is made to determine which line or band in the spectrum corresponds to which IR-active transition in the well, this information can also help to fix D, α and r_o, for then

$$g_{nm}(D,\alpha,r_o,R)=\omega_{nm} \qquad (2.55)$$

where g_{nm} represents the transition frequency as calculated from the algorithms given in sections 2.1-2.4 and ω_{nm} represents the observed transition frequency. This, together with possibly an equation for the OH distance determined from (2.54), yields a system of linear equations which can then be solved numerically for D, α and r_o using a routine such as NSØlA in the Harwell Subroutine Library. However, it may be that, in the particular case considered, the number of equations of the above form that can be inferred from the experimental data is insufficient to determine all three parameters. It is then necessary to invoke some other estimate(s) for any undetermined parameter(s). r_o is usually fairly accurately known for the diatomic case and, unlike D and α (which determine more the well shape whereas r_o fixes

more the proton position in the diatomic case) does not vary very much between the diatomic and hydrogen-bonded cases. Thus r_o could be inserted directly into (2.55) or (1.7) leaving only D and α to be determined from the infrared data.

Another means of estimating D, α and r_o is to compare the data available for a particular hydrogen bond with that of its deuterated analogue. As pointed out in section 1.5 it seems reasonable to suppose that the wells involved in each case will have similar D, α and r_o values. Hence once the parameters have been estimated for one species the energy level structure of the other can readily be predicted simply by varying R. This method provides an additional check on the accuracy of the parameters used, and it will be tested extensively in the following chapters.

CHAPTER THREE

CHROMOUS AND COBALTIC ACID

3.1 The Chromous Acid Problem

Chromous acid (CrOOH) and deuterated chromous acid (CrOOD) are interesting hydrogen-bonded species from both crystallographic and spectroscopic points of view. In spite of a good deal of discussion in the literature, their peculiar mid-infrared spectra have defied adequate explanation. Similar problems arise in the interpretation of the spectra of cobaltic acid - a chromous acid isomorph. In this chapter the double Morse potential will be used in conjunction with the relevant crystallographic and spectroscopic data for these species to give quantitative, consistent and unified explanation of the spectral anomalies.

X-ray diffraction (Douglass (1957), Ibers, Holm and Adams (1961)) and neutron diffraction techniques (Hamilton and Ibers (1963), Nørlund Christensen, Hansen and Lehmann (1976,77)) have been used to determine the crystal structure of chromous acid. CrOOH crystallizes into either an α-form (space group $R\bar{3}m$) or a β-form (space group $P2_1nm$ or Pnnm).* CrOOD crystallizes into either an α-form (space group $R\bar{3}m$) or a β-form (space group $P2_1nm$ or Pnnm). In what follows the term 'chromous acid' will refer to the α-form. Similarly the notation 'CrOOH' and 'CrOOD' will also refer to the α-form. The β-form will not be considered any further as the spectroscopic work quoted has always been performed on crystals of the α-form.

---

* The neutron diffraction experiments failed to yield decisive results as to the space groups of the β-forms.

Qualitatively, the crystal can be described as having a layered structure with close-packed CrO_6 octahedra joined to each other by hydrogen bonds. Nørlund Christensen *et al.* have shown that in CrOOD the hydrogen bonds are non-centrosymmetric whereas in CrOOH the proton has equal probability of being located in either of two off-centre sites.

Table 3.1 summarizes the known crystallographic data for the OH...O and OD...O bonds in CrOOH and CrOOD respectively. Of particular interest is the large Ubbelohde effect: the O...O distance increase on deuteration has been determined by Hamilton and Ibers to be 0.06Å and by Nørlund Christensen *et al.* to be 0.10Å. This is one of the largest increases known.

In order to arrive at an explanation of the mid-infrared spectra it is necessary to piece together also the near-infrared, far-infrared and neutron inelastic scattering spectra for chromous acid. Tables 3.2 and 3.3 summarize the observed vibrational modes, based on the spectra of Temme and Waddington (1973), Rush and Ferraro (1966) and Snyder and Ibers (1962).

Figures 3.1 and 3.2 show the mid-infrared (IR) spectra for CrOOH and CrOOD respectively. The striking feature of the spectra is that CrOOH shows a broad single band (at about 1650 cm^{-1}) in the hydrogen bond stretching region whereas CrOOD shows a well-resolved doublet in the same region (peaks at 1613 cm^{-1} and 1923 cm^{-1} respectively at -196°C). It is also not obvious why the $\nu_s(OH)/\nu_s(OD)$ ratio is as low as 0.95 since this ratio is typically in the range 1.25 to 1.35 (see Novak (1974)).

Table 3-1

CrOOH/CrOOD hydrogen bond distances in angstroms

	CrOOH		CrOOD	
	(a)	(b)	(a)	(b)
O...O	2.49(2)	2.47(1)	2.55(2)	2.57(2)
O-H(D)	?	1.16(1)	0.96(4)	1.05(2)

(a) Hamilton and Ibers (1963)

(b) Nørlund Christensen *et al.* (1977)

Table 3-2

Infrared and neutron scattering bands for CrOOH (all frequencies in cm^{-1})

Neutron energy loss	Neutron energy gain	Infrared (24°C)	Infrared (-196°C)
		3400(w)	3400(w)
		∿1650(vs)	∿1650(vs)
1250(vs)		1202(s)	1229(s)
825(w)			
771(w)			
		620(w)	627(w)
541(w)			
477(w)	475	526(s)	518(s)
	226	224(m)	
	110		
	65		

Based on Temme and Waddington (1973), Rush and Ferraro (1966) and Snyder and Ibers (1962).

Table 3-3

Infrared and neutron scattering bands for CrOOD (all frequencies in cm^{-1})

Neutron energy gain	Infrared (24°C)	Infrared (-196°C)
	3400(w)	3400(w)
	1916(s)	1923(s)
	1671(w)	1663(m)
	1594(s)	1613(s)
836	836(s)	832(s)
	637(m)	648(s)
	556(s)	566(s)
	503(s)	508(s)
460	470(m)	475(m)
	431(w)	432(m)
180		
62		

Based on Temme and Waddington (1973), Rush and Ferraro (1966) and Snyder and Ibers (1962).

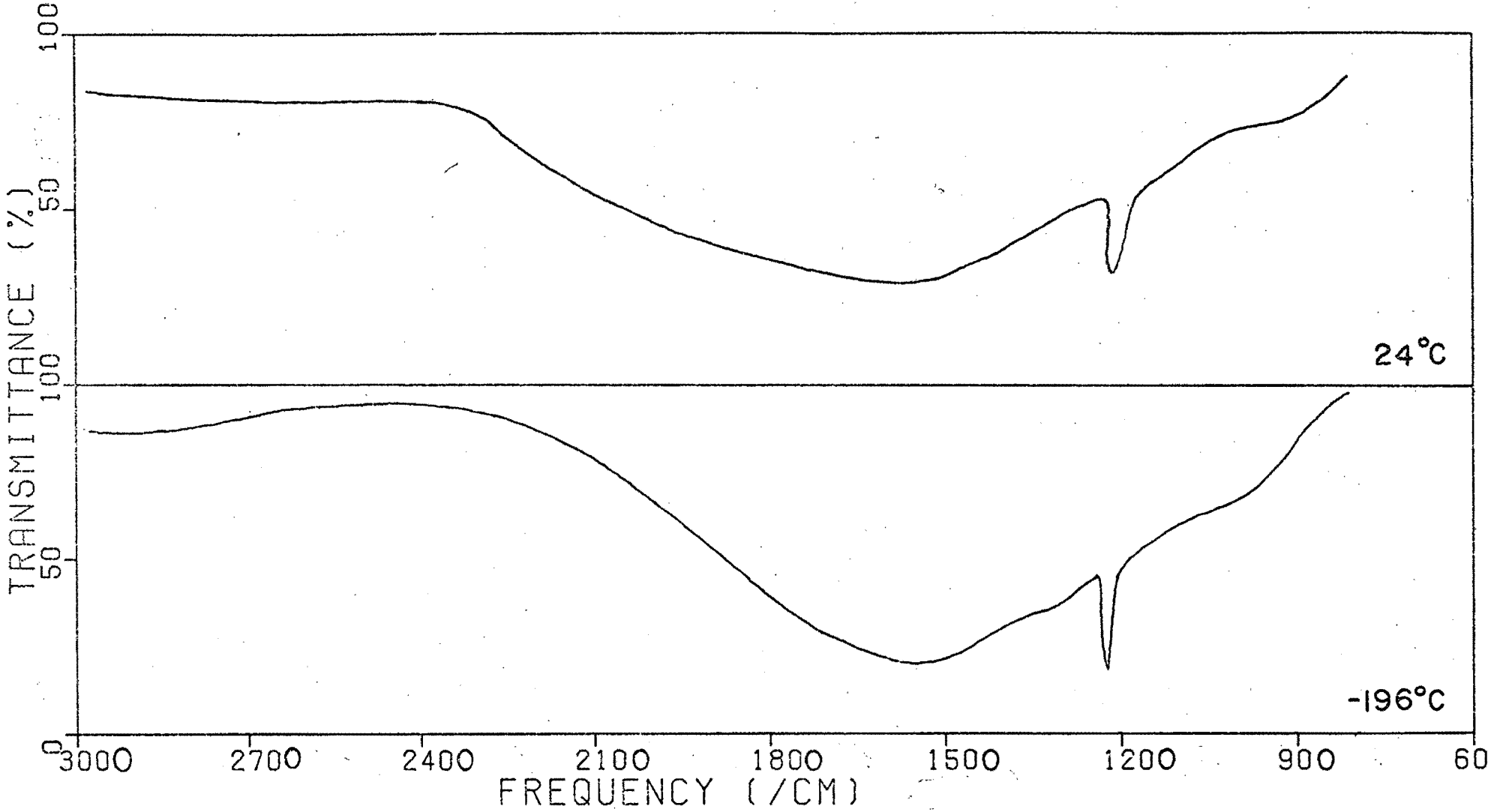

Figure 3.1. Infrared spectrum of CrOOH at 24°C and -196°C in the range 3000-700 cm^{-1}. Based on Snyder and Ibers (1962).

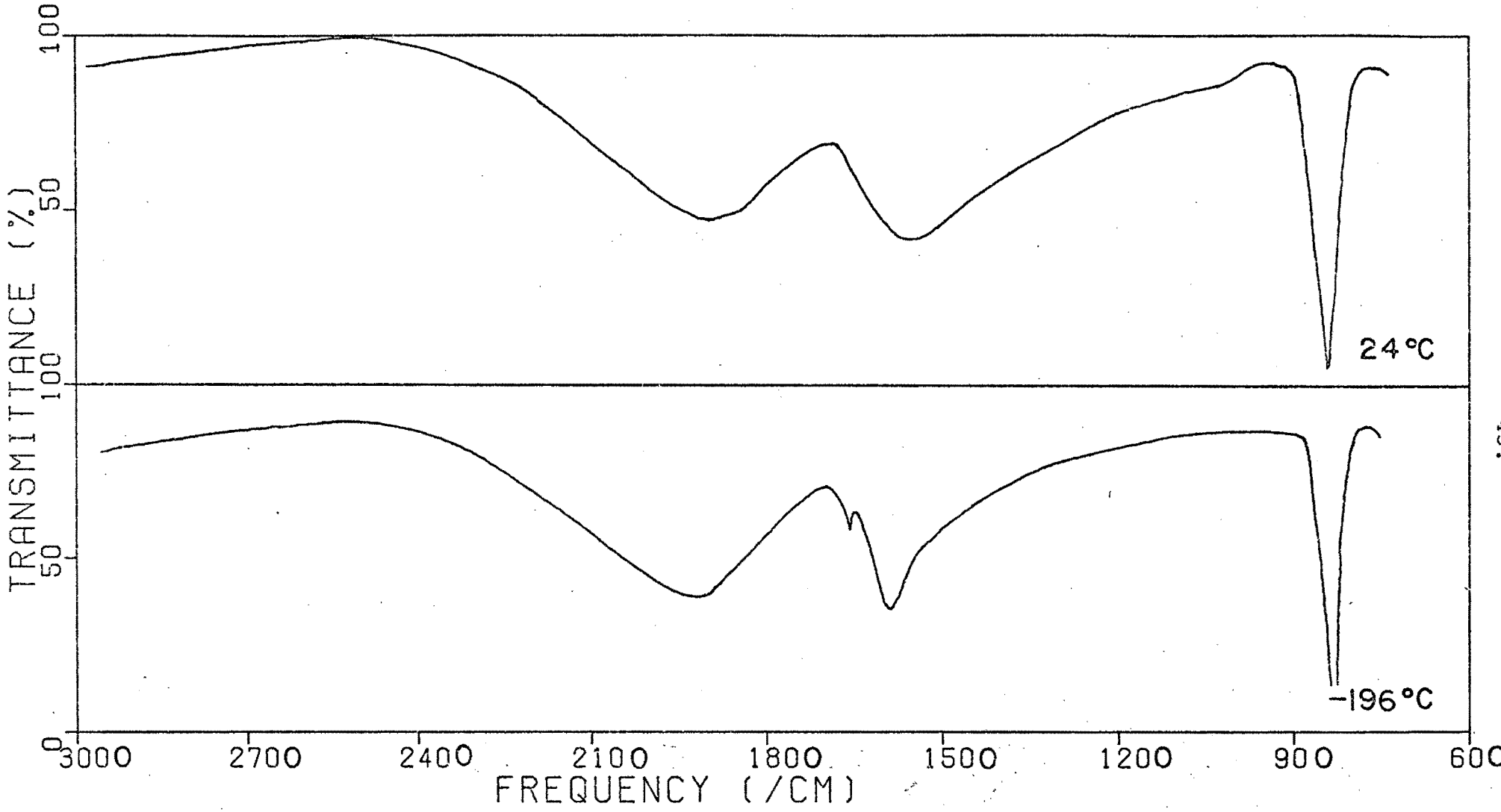

Figure 3.2. Infrared spectrum of CrOOD at 24°C and -196°C in the range 3000-700 cm^{-1}. Based on Snyder and Ibers (1962).

In the next section some of the current explanations of the chromous acid problem will be discussed, and thereafter the problem will be analysed using the double Morse potential model.

3.2 Interpretations of the Mid-Infrared Spectra

Snyder and Ibers (1962) suggested that the difference in the mid-IR spectra of CrOOH and CrOOD could be explained by using different potential energy curves for the OH...O and OD...O bonds respectively. In terms of their model the potential well for the OH...O bond in CrOOH is a double minimum potential with a very low potential barrier having all its energy levels situated above the barrier. The band observed at 1650 cm^{-1} resulted from the $|0\rangle \rightarrow |1\rangle$ IR-active transition. See Fig. 3.3. For CrOOD on the other hand the barrier would be much higher with the $|0\rangle$ and $|1\rangle$ energy levels situated close together near the bottom of the wells and with the $|2\rangle$ and $|3\rangle$ levels both lying near to each other at about the top of the barrier. The observed bands at 1923 cm^{-1} and 1613 cm^{-1} then resulted from the $|0\rangle \rightarrow |3\rangle$ and $|1\rangle \rightarrow |2\rangle$ IR-active transitions respectively. See Fig. 3.4. They were able to model the CrOOD potential well quite accurately in terms of a quartic potential function, obtaining the energy levels by an expansion of the wavefunctions in terms of an harmonic oscillator basis set.

Claydon, Sheppard, Stace and Upfield (1975) questioned this interpretation of the spectra saying that the potential energy curves used by Snyder and Ibers were too markedly different to be physically realistic. Instead they suggested that

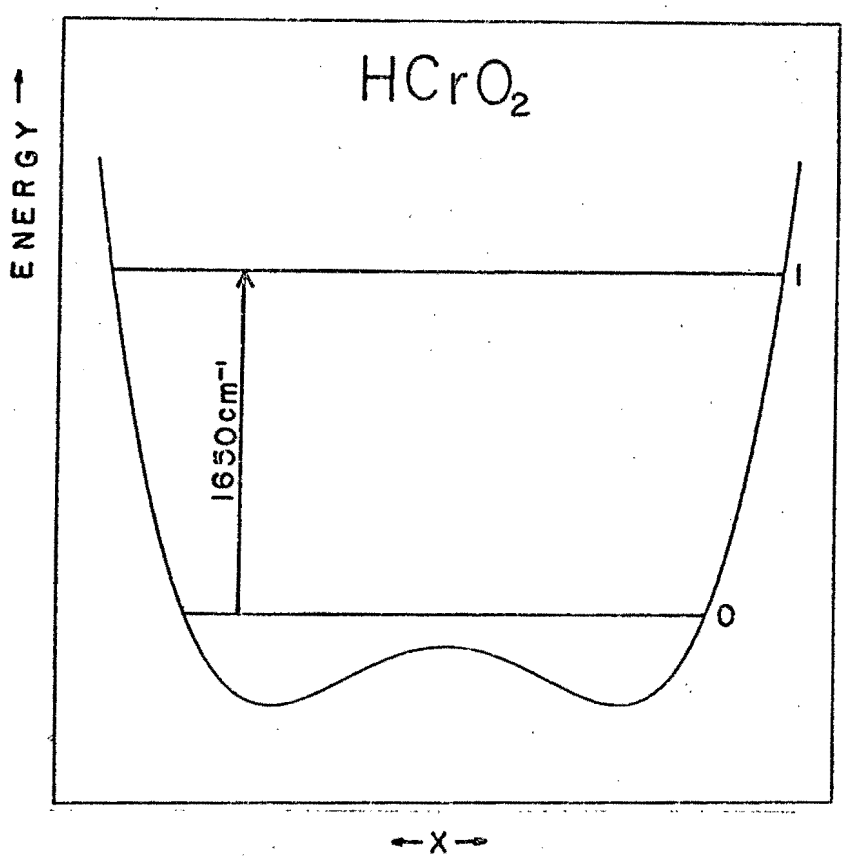

Figure 3.3. Energy level scheme for CrOOH as proposed by Snyder and Ibers (1962).

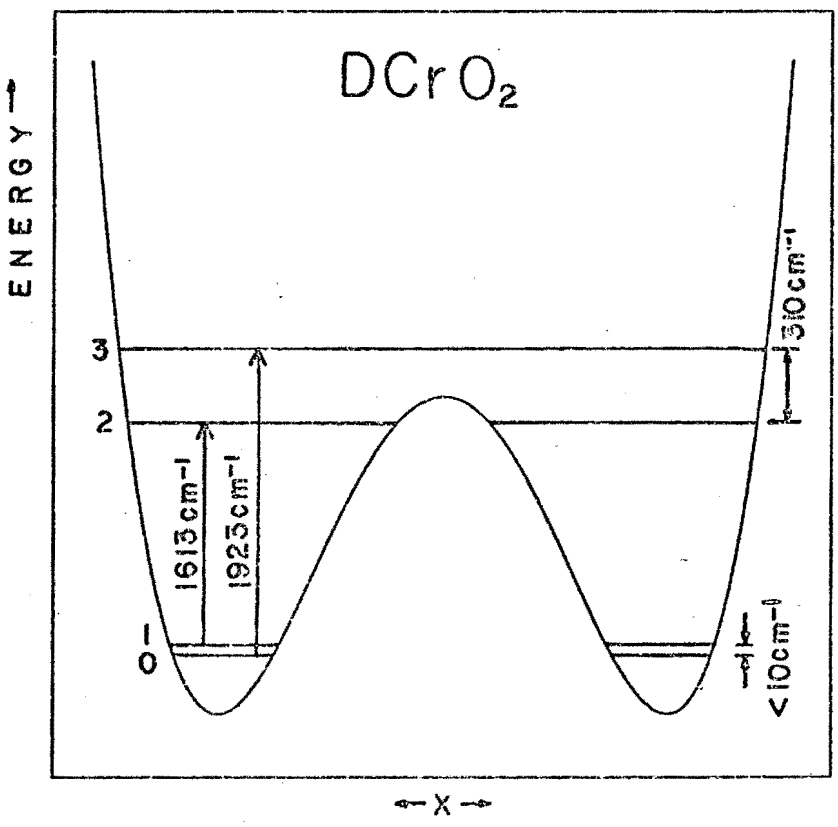

Figure 3.4. Energy level scheme for CrOOD as proposed by Snyder and Ibers (1962).

the doublet in the CrOOD spectrum resulted from an accidental Fermi resonance between the overtone of the δ(OD) bending frequency and the ν_s(OD) stretching vibration. The overtone frequency at 2δ(OD) lies very close to the centre of a broad singlet ν_s(OD) band, giving rise to the observed doublet. Such a resonance does not occur in CrOOH as the bending mode overtone 2δ(OH) lies at a much higher frequency than the ν_s(OH) band. They were however unable to explain the low $\nu_s(OH)/\nu_s(OD)$ ratio other than to point out that it must arise from the difference in the OH...O and OD...O potential curves.

Savel'ev and Sokolov (1975) have also questioned Snyder and Ibers' assumption of very different potential wells and concluded that a Fermi resonance explanation was the most convincing one. An analysis of an AH...B bond as a coupled oscillator then showed that the low $\nu_s(AH)/\nu_s(AD)$ ratios are indeed possible. However their analysis was too crude to yield accurate potential wells for the CrOOH/CrOOD system.

3.3 The Model applied to Chromous Acid

As an initial hypothesis we assume that the explanation of the CrOOD spectrum suggested by Snyder and Ibers is in fact the correct one. Then equation (2.55) becomes

$$g_{03}(D,\alpha,r_O,R) = 1923 \text{ cm}^{-1}$$
$$g_{12}(D,\alpha,r_O,R) = 1613 \text{ cm}^{-1} \qquad (3.1)$$

The analysis of these equations will be performed using the crystallographic data of Hamilton and Ibers and then again using that of Nørlund Christensen *et al.*, referred to hereafter as data sets I and II respectively. The important difference between the data sets is that the O...O distance

for CrOOH is 0.02Å shorter according to Nørlund Christensen than it is according to Hamilton and Ibers. Likewise the O...O distance for CrOOD is 0.02Å longer according to Nørlund Christensen than it is according to Hamilton and Ibers. (Hence the differences in the magnitudes of the Ubbelohde effect mentioned in Section 3.1).

3.3.1 Data Set I

According to Table 3.1, 2R=2.55Å for CrOOD. As the OD distance is poorly determined, equations (3.1) are solved simultaneously for D and α using various assumed values for r_O. If a solution is found for a given r_O, 2R is set to 2.49Å and, using the same D, α and r_O, a protonic energy level scheme is then computed for CrOOH. By comparing the resultant transition frequencies with the observed spectrum, it should be possible to select an r_O value which yields the most consistent interpretation of the CrOOH/CrOOD spectra.

Proceeding along these lines, solutions were found for D and α for all r_O values lying in the range 0.92(0.01) 0.97Å, using the Harwell Subroutine Library program NSØ1A. The results are given in Table 3.4, along with the barrier heights (B), minimum positions (x_m) and OD distances for the various wells. Exact convergence was not achieved when r_O was equal to the values 0.92, 0.96 and 0.97Å, but the results obtained from these values of r_O were accepted as being sufficiently accurate for the purpose at hand.

Table 3.5 gives the CrOOH predictions based on the parameters of Table 3.4. The $|0\rangle \rightarrow |1\rangle$ transition lies in the range 250-320 cm^{-1}, the $|1\rangle \rightarrow |2\rangle$ transition in the range 1500-1650 cm^{-1} and the $|0\rangle \rightarrow |3\rangle$ transition in the range 3250-3450 cm^{-1}.

Table 3-4

Data Set I

CrOOD potential well parameters: given r_o, $|0\rangle \rightarrow |3\rangle = 1923 cm^{-1}$, $|1\rangle \rightarrow |2\rangle = 1613 cm^{-1}$ and $2R = 2.55 Å$

r_o (Å)	D (eV)	α ($Å^{-1}$)	$R-r_o$ (Å)	x_m (Å)	OD (Å)	B (cm^{-1})	ω_{03} (cm^{-1})	ω_{12} (cm^{-1})	ω_{01} (cm^{-1})	$D\alpha^2$
.920	5.40	2.84	.355	.294	1.000	3177	1903	1607	8	43.5
.930	4.59	3.01	.345	.293	1.002	3173	1923	1613	10	41.7
.940	3.46	3.30	.335	.294	1.001	3180	1923	1613	9	37.7
.950	2.42	3.73	.325	.297	0.999	3180	1923	1613	8	33.6
.960	1.18	4.95	.315	.305	0.993	3190	1928	1609	8	28.9
.970	1.19	5.02	.305	.295	1.004	3100	1967	1583	10	30.1

Note: Convergence fails for r_o = 0.920, 0.960 and 0.970Å.

Table 3-5

Data Set I

CrOOH Potential well parameters and transition frequencies determined from CrOOD parameters. $2R = 2.49 Å$

r_o (Å)	$R-r_o$ (Å)	x_m (Å)	OH (Å)	B (cm^{-1})	ω_{03} (cm^{-1})	ω_{12} (cm^{-1})	ω_{01} (cm^{-1})
.920	.325	.248	1.052	1834	3341	1512	319
.930	.315	.248	1.051	1889	3378	1535	316
.940	.305	.253	1.043	2015	3343	1555	288
.950	.295	.259	1.034	2168	3308	1580	257
.960	.285	.272	1.018	2491	3269	1638	203
.970	.275	.261	1.032	2379	3448	1657	248

3.3.2 Data Set II

Here 2R=2.57Å for CrOOD. The OD distance is more accurately known in this data set and this suggests that the following set of equations

$$g_{03}(D,\alpha,r_O,R) = 1923 \text{ cm}^{-1}$$
$$g_{12}(D,\alpha,r_O,R) = 1613 \text{ cm}^{-1}$$
$$OD(D,\alpha,r_O,R) = 1.16\text{Å} \qquad (3.2)$$

be solved for D, α and r_O.

However, no solution could be found using the Harwell Subroutine NSØ1A. (See also the note on the re-parameterization of the potential well to speed convergence of the root-finding routine, Section 3.5). Hence it was decided to revert to using the same procedure as was applied to data set I, on the assumption that an inaccuracy in the OD distance in data set II was responsible for no solution being obtained. A little thought shows that the results for CrOOD given in Table 3.4 can be carried over to this case simply by increasing the r_O and OD values by 0.01Å to allow for the larger estimate of R, the other values in the table remaining the same. These results are now given as Table 3.6.

Table 3.7 shows the CrOOH transition frequencies and potential well details predicted in a similar fashion to those of data set I. The $|0\rangle \rightarrow |1\rangle$ transition lies in the range of 300-600 cm^{-1}, the $|1\rangle \rightarrow |2\rangle$ transition lies in the range 1500-1600 cm^{-1} and the $|0\rangle \rightarrow |3\rangle$ transition lies in the range 3600-3900 cm^{-1}.

3.3.3 The CrOOH Predictions and Proposed Interpretation

The problem is now to decide whether the observed

Table 3-6

Data Set II

CrOOD potential well parameters: given r_o, $|0\rangle \rightarrow |3\rangle = 1923 cm^{-1}$, $|1\rangle \rightarrow |2\rangle = 1613 cm^{-1}$ and $2R = 2.57 Å$

r_o (Å)	D (eV)	α ($Å^{-1}$)	$R-r_o$ (Å)	x_m (Å)	OD (Å)	B (cm^{-1})	ω_{03} (cm^{-1})	ω_{12} (cm^{-1})	ω_{01} (cm^{-1})	$D\alpha^3$
.930	5.40	2.84	.355	.294	1.010	3177	1903	1607	8	43.5
.940	4.59	3.01	.345	.293	1.012	3173	1923	1613	10	41.7
.950	3.46	3.30	.335	.294	1.011	3180	1923	1613	9	37.7
.960	2.42	3.73	.325	.297	1.009	3180	1923	1613	8	33.6
.970	1.18	4.95	.315	.305	1.003	3190	1928	1609	8	28.9
.980	1.19	5.02	.305	.295	1.014	3100	1967	1583	10	30.1

This table has been obtained from Table 3.4 by increasing r_o and OD by 0.01Å to allow for the larger R value in this data set.

Note: Convergence fails for r_o = 0.930, 0.970 and 0.980Å.

Table 3-7

Data Set II

CrOOH potential well parameters and transition frequencies determined from CrOOD parameters. $2R = 2.47 Å$

r_o (Å)	$R-r_o$ (Å)	x_m (Å)	OH (Å)	B (cm^{-1})	ω_{03} (cm^{-1})	ω_{12} (cm^{-1})	ω_{01} (cm^{-1})
.930	.305	.213	1.152	1098	3870	1519	571
.940	.295	.214	1.146	1171	3895	1540	560
.950	.285	.222	1.125	1336	3813	1543	507
.960	.275	.231	1.109	1549	3726	1549	445
.970	.265	.248	1.054	1611	3608	1611	333
.980	.255	.237	1.072	1899	3957	1653	398

CrOOH spectra can be interpreted in terms of either of the transition frequency schemes computed above, and, if so, whether the potential wells required are physically realistic.

If the predicted CrOOH transition frequencies of data set I are compared with the observed bands given in Table 3.2, the only possible *a priori* assignment is as follows:

$$\omega_{01} = 226 \text{ cm}^{-1}$$
$$\omega_{12} = 1650 \text{ cm}^{-1}$$
$$\omega_{03} = 3400 \text{ cm}^{-1}. \qquad (3.3)$$

On the other hand, a comparison of CrOOH frequencies of data set II with the observed frequencies suggests the following possible assignment:

$$\omega_{01} = 518 \text{ cm}^{-1}$$
$$\omega_{12} = 1650 \text{ cm}^{-1}$$
$$\omega_{03} = 3400 \text{ cm}^{-1}. \qquad (3.4)$$

Assignment (3.3) is judged more likely to be correct than assignment (3.4) for the following reasons:

i) The 518 cm^{-1} band in the CrOOH IR spectrum is probably associated with either the 566 cm^{-1} or 508 cm^{-1} band observed in the CrOOD IR spectrum, and is therefore unlikely to be a hydrogen vibration band. On the other hand, the 226 cm^{-1} band in the CrOOH neutron scattering spectrum does not appear to be associated with any such band in the CrOOD neutron scattering spectrum and is hence more likely to be the tunnelling mode.

ii) The 3400 cm^{-1} band coincides more closely with the $|0\rangle \rightarrow |3\rangle$ frequency predictions of data set I than with those of data set II.

iii) It also appears that the magnitude of the Ubbelohde effect (0.10Å) in data set II is exceptionally high. This seems unrealistic and is probably due to an error in the atom positions determined by Nørlund Christensen, as it is very difficult to determine accurately the proton position in a very short hydrogen bond.

iv) The values for the OD distance in Tables 3.4 and 3.6 accord more closely with Hamilton and Ibers' value of 0.96(4)Å than with Nørlund Christensen's value of 1.05(2)Å.

On these grounds assignment (3.4) can be rejected. It is now proposed that assignment (3.3) is the correct one, for the following reasons:

i) There appears to be no satisfactory explanation for the 226 cm^{-1} band other than to assign it to the tunnelling mode. Temme and Waddington assigned it to a Cr-O bending mode, but this does not explain the absence of the band in the CrOOD neutron scattering spectrum.*

ii) A further interpolation of Table 3.4 suggests that an r_o value of 0.958(5)Å gives the closest fit to (3.3). The results of this calculation appear in Table 3.8. This table shows that the potential wells for CrOOH and CrOOD are far more similar to each other than those used by Snyder and Ibers (the barrier heights are 2406 cm^{-1} and 3193 cm^{-1} respectively).

---

* It may possibly be the 180 cm^{-1} band in the CrOOD neutron spectrum, but then why is this band so much weaker here than in CrOOH?

Table 3-8

Refined potential well parameters for for CrOOH and CrOOD

	CrOOH	CrOOD
r_o(Å)	.958	.958
D(eV)	1.44	1.44
α (Å^{-1})	4.53	4.53
R-r_o (Å)	.287	.317
x_m(Å)	.269	.303
B (cm^{-1})	2406	3193
OH(D) (Å)	1.021	0.994
ω_{01} (cm^{-1})	214	7
ω_{03} (cm^{-1})	3264	1923
ω_{12} (cm^{-1})	1621	1613
Dα^2	29.7	29.7

The objections raised by Savel'ev *et al.* and Claydon *et al.* do then no longer apply.*

iii) As regards the frequency ratio $\nu_s(OH)/\nu_s(OD)$, it appears that to compute this ratio, one must consider the $\nu_s(OH)$ frequency as the average of $|0\rangle \rightarrow |3\rangle$ and $|1\rangle \rightarrow |2\rangle$ frequencies (and likewise for the $\nu_s(OD)$ frequency). If this is done, then $\nu_s(OH)/\nu_s(OD) = 1.4$, which is a more reasonable value.

iv) The protons in CrOOH are predicted to be disordered. This agrees with the neutron diffraction results of Nørlund Christensen *et al.* (Note: CrOOH hydrogen bonds are still *dynamically* symmetric because the rapid tunnelling causes a bimodal probability density function for the proton on the timescale of the neutron scattering experiment).

v) The predicted OH and OD distances (Table 3.8) are entirely reasonable.

vi) The transition probabilities, calculated by the method given in Section 2.4, are tabulated for $r_o = 0.958\text{Å}$ in Table 3.9. It is predicted that the $|1\rangle \rightarrow |2\rangle$ band is far stronger than both the $|0\rangle \rightarrow |1\rangle$ and $|0\rangle \rightarrow |3\rangle$ bands for CrOOH (provided that the Boltzmann factor is ignored - a point which will be discussed later).

---

* The possibility of a Fermi resonance is not necessarily excluded as such a resonance would merely enhance the already existing minimum in the $\nu_s(OD)$ doublet. It could also be that the Fermi resonance is responsible for the secondary minimum which appears in the doublet at $-196^{\circ}C$. See Figure 3.2.

Table 3-9

Relative transition probabilities for CrOOH and CrOOD

	Transition	Frequency (cm^{-1})	Relative dipole moment	Relative intensity
CrOOH	$\|0\rangle \rightarrow \|1\rangle$	214	77	41
	$\|0\rangle \rightarrow \|3\rangle$	3264	15	33
	$\|1\rangle \rightarrow \|2\rangle$	1621	44	100
CrOOD	$\|0\rangle \rightarrow \|1\rangle$	8	100	2
	$\|0\rangle \rightarrow \|3\rangle$	1923	21	27
	$\|1\rangle \rightarrow \|2\rangle$	1613	23	27

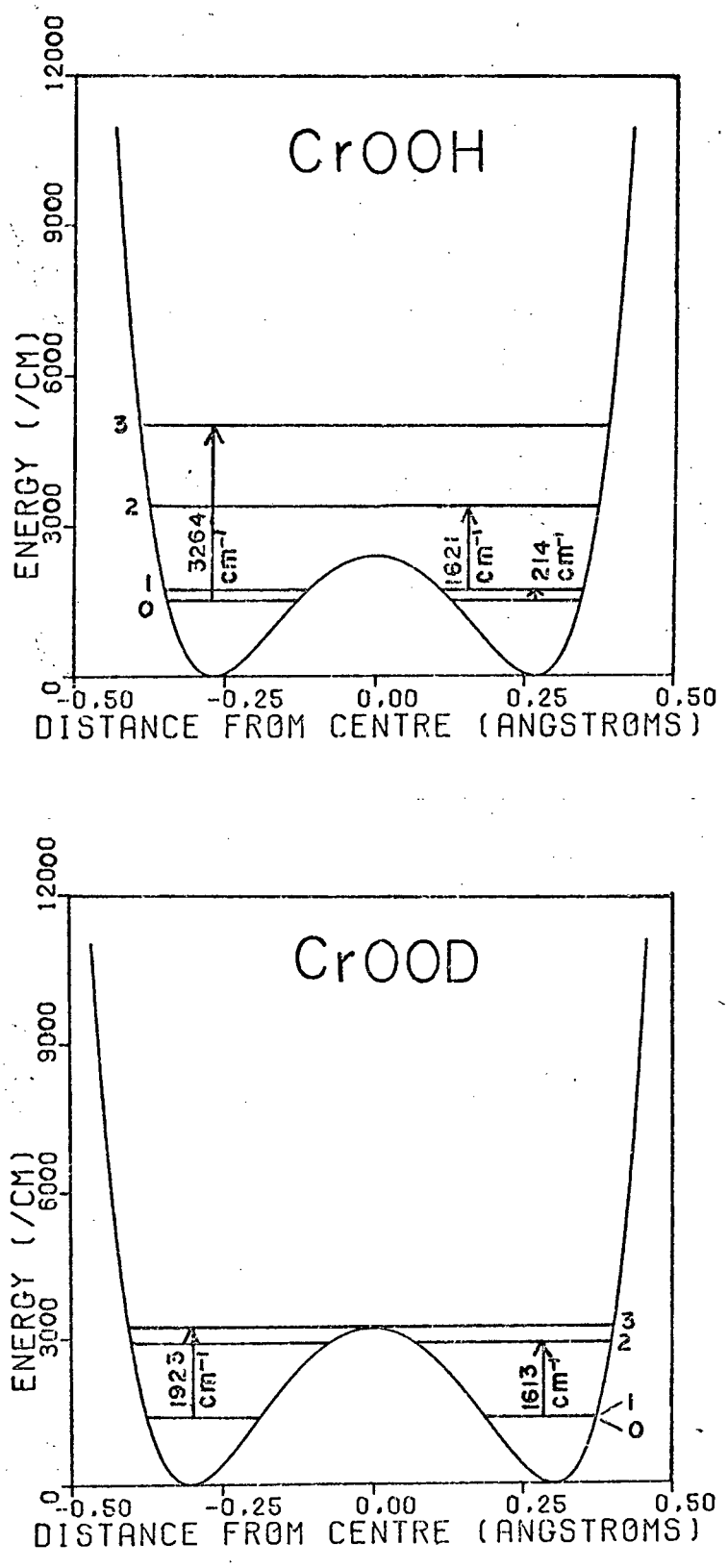

Figure 3.5. Double Morse Potentials for CrOOH and CrOOD. (The ground state splitting for CrOOD is about 7 cm^{-1}.)

This accords with the experimental strengths given in Tables 3.2 and 3.3.

Sheppard (1979) has subsequently favoured this interpretation of the spectra after a personal communication of these results to him.

The resulting energy level schemes are illustrated in Figure 3.5.

3.3.4 Questions Arising from the Assignments

i) Does the 226 cm^{-1} band appear in the far IR spectrum of CrOOD? As Temme and Waddington performed their far-IR work on CrOOH only and as Rush and Ferraro failed to locate this band in the spectrum of CrOOH, the latter authors' observation that there are no such bands in the far IR spectrum of CrOOD is inconclusive. Further experiments would be needed to resolve this point.

ii) Why is there no apparent temperature dependence of the 1650 cm^{-1} band (Figure 3.1)? Such a dependence should be easily observable upon cooling CrOOH from room to liquid nitrogen temperature, if the ground state splitting is really as much as 226 cm^{-1}. It is proposed that the CrOOH crystal should not be conceived of as consisting of independent double well oscillators but that it should rather be seen as supporting collective protonic modes which result in a ferrodistortive phase transition upon cooling. If such a transition occurred at a temperature just below room temperature, CrOOH would be an ordered

crystal at 77K. The proton is then "localized" in one or other of the potential minima and the true wavefunction consists of an approximately equal mixture of the symmetric ground state and antisymmetric first excited state. The single particle wavefunctions are no longer the eigenfunctions of the full crystal Hamiltonian. The population of the first excited state is maintained by the proton-proton interactions and would not be expected to vary much with temperature when the crystal is in the low temperature phase. (Proton-proton interactions in ferroelectric crystals will later be discussed extensively in Chapter 5). There seems to be no information in the literature regarding the ferroelectricity or otherwise of CrOOH (a recent monograph by Lines and Glass (1977) on ferroelectricity does not mention CrOOH). This lack of information could be due to the fact that large single crystals of chromous acid are very difficult to prepare.

iii) If the band at 3400 cm^{-1} is a hydrogen stretching mode for CrOOH then what is the explanation of the similar band in the CrOOD spectrum at 3400 cm^{-1}? This point is not clear. It is possible that both the observed bands are in fact overtones or combinations of stretching modes. The $|0\rangle \rightarrow |3\rangle$ transition is then overshadowed by the presence of this overtone band in the CrOOH spectrum. In the following section an analysis shows that such a $|0\rangle \rightarrow |3\rangle$ band is also likely to be very broad and so would not be readily

discerned in the observed spectrum. See also section 3.4 below on cobaltic acid for a discussion of the same point.

3.3.5 Band Shapes

The problem of predicting the band shapes for the various transitions is a difficult one. At best it is shown how the model can be used to predict fairly accurately in a qualitative sense the observed band shapes. The method used is that outlined in section 2.4

For CrOOD the integral (2.53) was computed for both the $|0\rangle \rightarrow |3\rangle$ and the $|1\rangle \rightarrow |2\rangle$ transitions and the results summed to obtain the intensity $I(\omega)$ at T = 295K:

Figure 3.6 shows the variation of the $|0\rangle \rightarrow |3\rangle$ transition frequencies and probabilities with respect to the O...O distance for CrOOD; D, α and r_o assumed to remain constant. Notice that the $|0\rangle \rightarrow |3\rangle$ transition frequency has a turning point at about R = 1.266Å. (This is an interesting phenomenon and will be discussed in greater detail at the end of this section.) As such a band head is not observed in the CrOOD spectrum other broadening mechanisms besides O...O modulation must be present.

The observed CrOOD bandshapes are fairly well reproduced in the following way:

i) The O...O distance 2R is assumed to follow a gaussian distribution with a standard deviation of σ = 0.02Å. (Lawrence and Robertson (1979) have pointed out that the fluctuation in the relative displacement of two neighbouring oxygen atoms in ice can be as much as an order of magnitude smaller than the r.m.s. displacements of the individual oxygen atoms. This is due to the high correlation between the individual motions as the oxygen atoms must be considered as part of the lattice. The r.m.s.

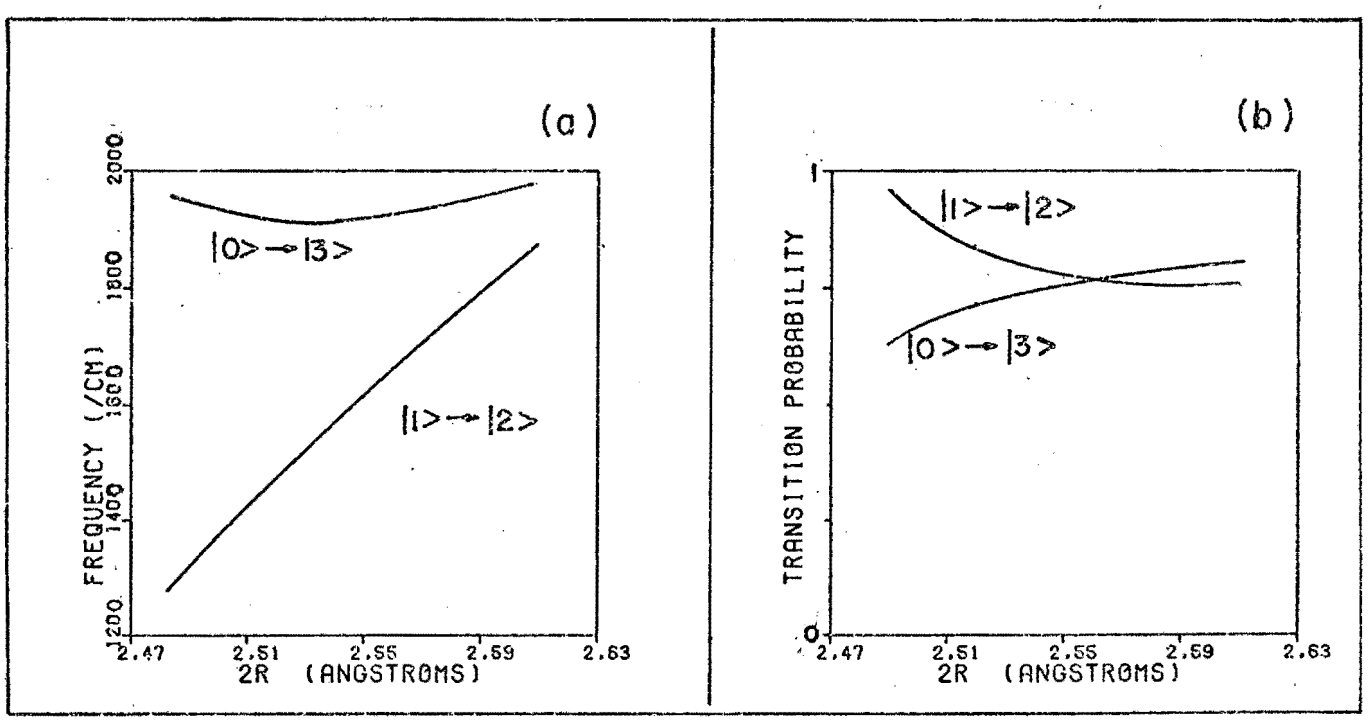

Figure 3.6. Variation in (a) predicted CrOOD transition frequencies and (b) predicted CrOOD transition probabilities with O...O distance.

thermal amplitude of the oxygen atoms in deuterated ice is known to be about 0.14Å (Peterson and Levy (1957)). Thus the above assumption is quite reasonable).

ii) Radiationless decay was introduced as a broadening mechanism for the $|0\rangle \rightarrow |3\rangle$ band, as its width calculated in terms of the above assumption alone was too narrow. The occurrence of such emission seems plausible as the energy difference between states $|3\rangle$ and $|2\rangle$ is quite small. $F(\omega - \omega_{nm}(R))$ in equation (2.53) thus describes a Lorentz profile:

$$\frac{1}{\pi} \frac{\Gamma_{03}/2}{[\omega - \omega_{nm}(R)]^2 + (\Gamma_{03}/2)^2}$$

where Γ_{03} is the decay width of the state. A mean life of 1.5×10^{-13}s (i.e. a width $\Gamma_{03} = 220\ cm^{-1}$) for state $|3\rangle$ was used to give the best qualitative agreement with the observed band shape.

iii) As the integral (2.53) had to be calculated numerically, a nominal instrumental width of 6 cm^{-1} was introduced to help smooth out the resultant $|1\rangle \rightarrow |2\rangle$ band shape.

Equation (2.53) thus becomes

$$I_{nm}(\omega) \propto \int_0^\infty P_{n\rightarrow m}(R)\, G(R) \frac{\Gamma_{nm}}{[\omega - \omega_{nm}(R)]^2 + (\Gamma_{nm}/2)^2}\, \omega_{nm}(R)\, dR$$

where G(R) represents the gaussian distribution mentioned above, $\Gamma_{03} = 220\ cm^{-1}$ and $\Gamma_{12} = 6\ cm^{-1}$.

For the $|0\rangle \rightarrow |3\rangle$ transition, the integration was performed numerically with the integration range restricted to $(R-\varepsilon, R+\varepsilon)$ where $\varepsilon = 0.03$Å. A total of 21 points were used for the integration. $I_{03}(\omega)$ was then computed at a

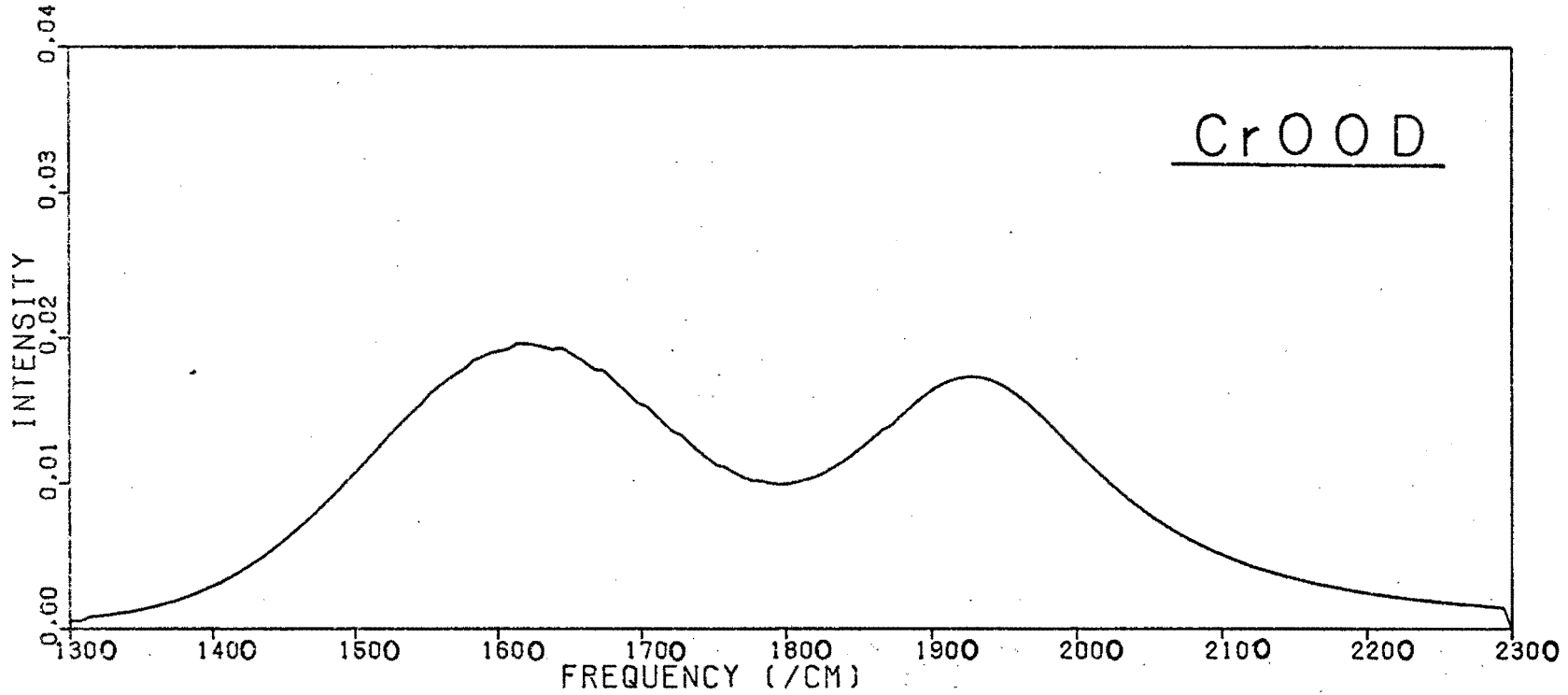

Figure 3.7. Predicted bandshapes for CrOOD infrared transitions. $\omega_{12} \sim 1613$ cm^{-1} and $\omega_{03} \sim 1923$ cm^{-1}.

total of 300 points in the range 1000-1800 cm^{-1}.

For the $|1> \rightarrow |2>$ transition, the integration range was restricted to the interval (R_1, R_2) where

$$\omega_{nm}(R_1) = \omega - 6 \text{ cm}^{-1}$$

$$\omega_{nm}(R_2) = \omega + 6 \text{ cm}^{-1}$$

A total of 41 points was used for the integration. $I_{12}(\omega)$ was then computed at the same 300 points as mentioned above.

The results are shown in Figure 3.7.

For CrOOH the situation is not so clear. Figure 3.8 shows the variation of the $|1> \rightarrow |2>$, $|0> \rightarrow |1>$ and $|0> \rightarrow |3>$ transition frequencies and probabilities with respect to the O...O distance. It appears that there is again a "band head" in the $|1> \rightarrow |2>$ transition at about $2R = 1.227\text{Å}$. This band is very narrow, quite contrary to the observed spectrum. No explanation can be advanced to explain the broadening of this band.

Assuming the same gaussian distribution for the O...O distance and introducing the same instrumental width 6 cm^{-1} for all of three transitions considered, the total intensity was calculated using equation (2.59) with T = 77K. In accordance with the point raised in section 3.3.4 regarding the possibility of co-operative protonic motion, the ground and first excited states were also assumed to be equally populated in this analysis. The results are shown in Figure 3.9.

Note about the "Band Heads": The predicted band heads are an artifact of the particular energy level scheme involved in the double Morse potential, as can be seen from the following argument. When R increases (D, α and r_o remaining constant) both the barrier height B and the minima

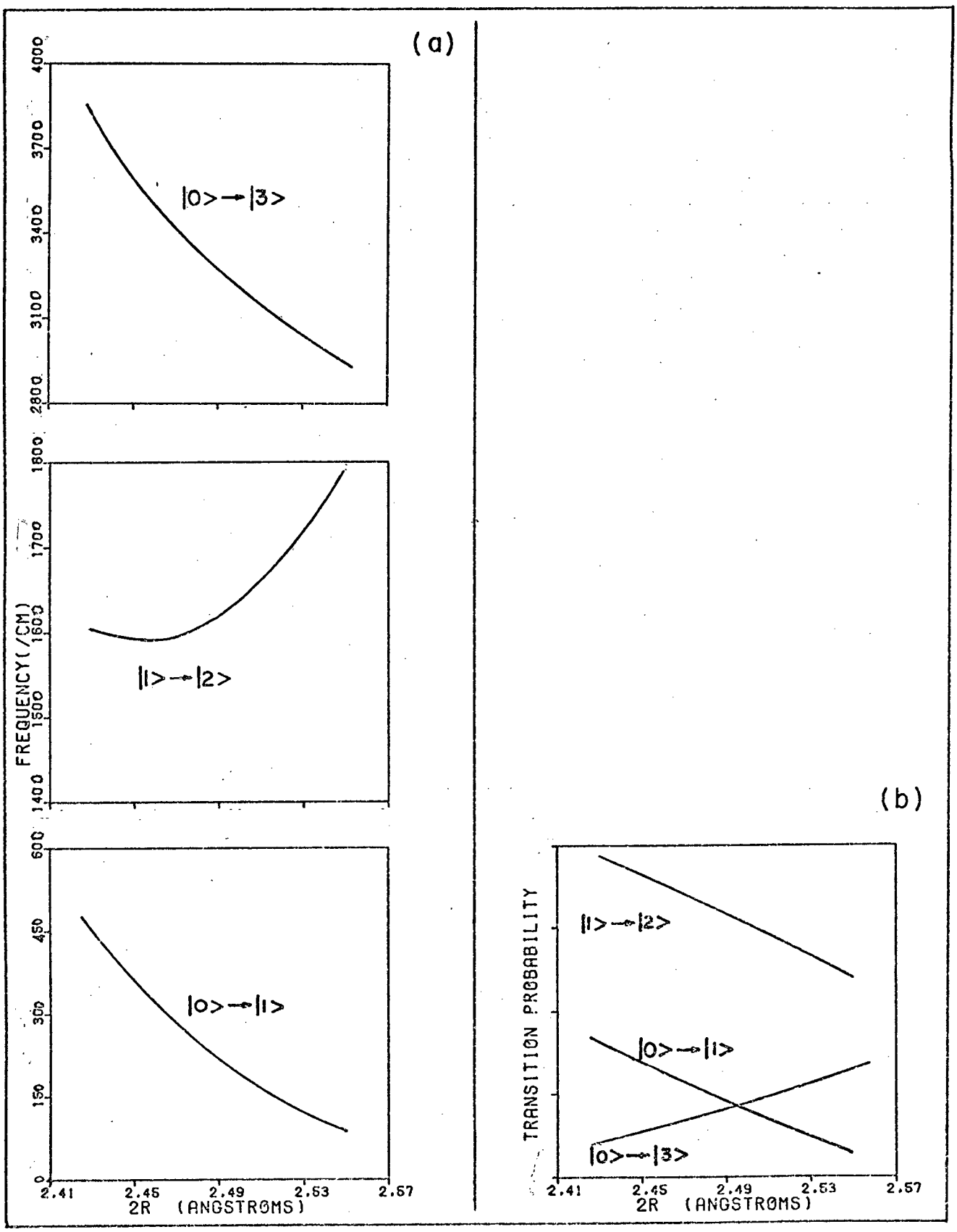

Figure 3.8. Variation in (a) predicted CrOOH transition frequencies and (b) predicted CrOOH transition probabilities with O...O distance.

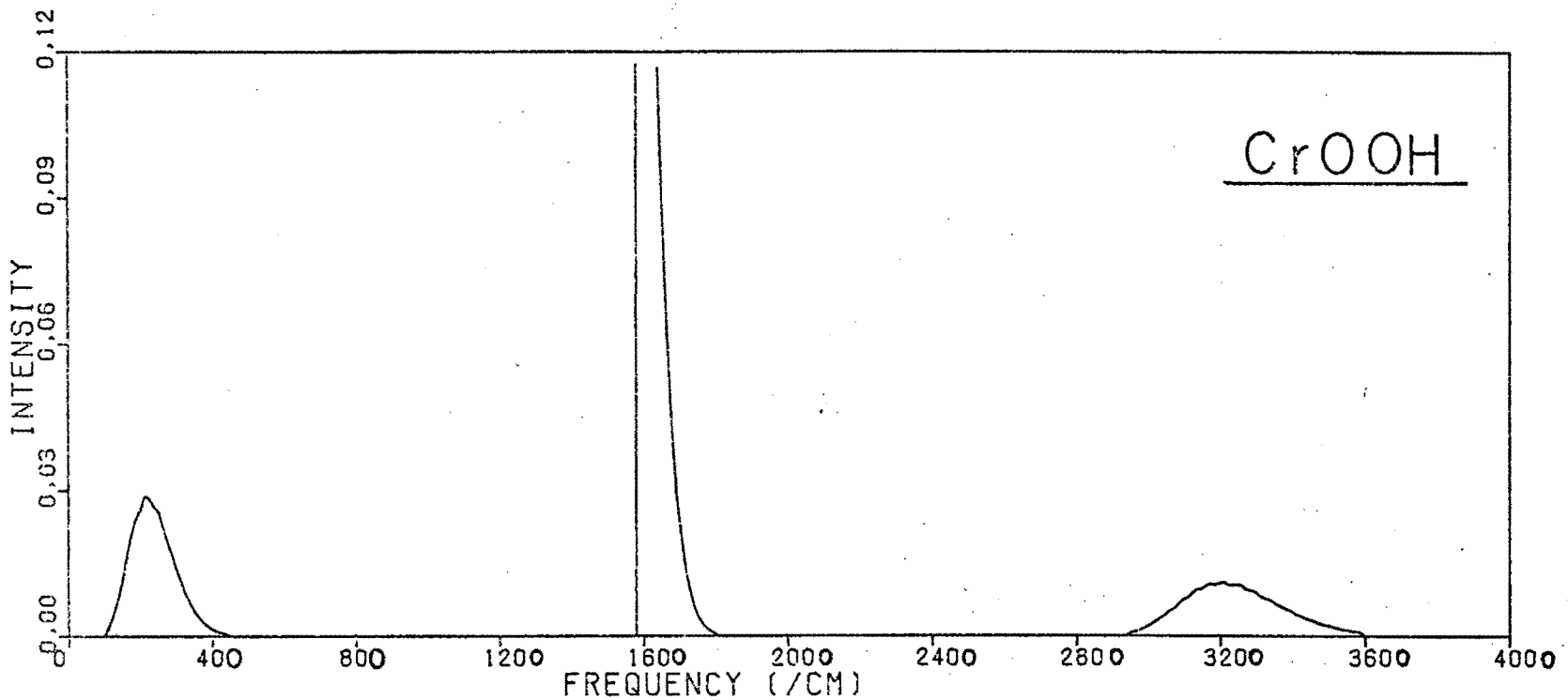

Figure 3.9. Predicted bandshapes for CrOOH infrared transitions. $\omega_{01} \sim 214$ cm^{-1}, $\omega_{12} \sim 1621$ cm^{-1} and $\omega_{03} \sim 3260$ cm^{-1}. Note the narrowness of the $|1\rangle \rightarrow |2\rangle$ transition band.

separation $2x_m$ increase. Consider a level E_n lying above the barrier. The standard semi-classical condition for determining the energy eigenvalue is

$$(n + \tfrac{1}{2})\pi = \int_{-\infty}^{\infty} \left|\frac{2m}{\hbar^2}[E - V(x)]\right|^{\frac{1}{2}} dx \qquad (3.5)$$

(see, for example, ter Haar (1964)). Equation (3.5) shows that the position of the given level E_n will depend in some sense upon the "area" enclosed in the potential well below the line $V(x) = E_n$ (neglecting any "quantum" effects caused by the proximity of imaginary turning points). The effect of the increase of R upon the level E_n will therefore be twofold:

i) It tends to lower the position of the level in the well as the outward motion of the outermost walls of the well introduce more "area" below the line $V(x) = E_n$. According to (3.5) this "area" must remain constant for given n and so the level moves down in position in the well to compensate.

ii) It tends to lift the position of the level in the well as the increase in the barrier height will reduce the "area" below the line $V(x) = E_n$. This "area" must again remain constant and so the level moves upward in position in the well to compensate.

These two effects compete with each other and thus a turning point can arise quite naturally in the transition frequencies if the position as R varies of the uppermost level in the transition is dominated first by the one effect and then by the other.

3.4 Cobaltic Acid

Cobaltic acid (CoOOH) has similar crystallographic and spectroscopic properties to chromous acid and the two compounds are often discussed together in the literature. A study of the IR spectra of cobaltic and deuterated cobaltic acid is therefore included for sake of completeness. The argument developed is similar to that of sections 3.1-3.3 and will not be repeated in detail.

Delaplane, Ibers, Ferraro and Rush (1969) have shown that the Ubbelohde effect upon deuteration of CoOOH is 0.07Å in magnitude with the hydrogen bond lengths being 2.50Å for CoOOH and 2.57Å for CoOOD (cf. Table 3.1). Tables 3.10 and 3.11 give the IR and neutron scattering frequencies observed for CoOOH and CoOOD by the same authors. The doublet frequencies for CoOOD are 1635 cm^{-1} and 1950 cm^{-1} respectively whereas the broad single band for CoOOH lies at about 1800 cm^{-1}. This last band appears considerably flatter than the corresponding band in the CrOOH spectrum. The neutron scattering spectrum for CoOOH shows a band at 264 cm^{-1} and Delaplane *et al.* were unable to arrive at a satisfactory explanation of its presence. Later Temme and Waddington (1973) observed a corresponding band at 221 cm^{-1} in the far IR for CoOOH and interpreted it as the Co-O bending mode, thus claiming to settle the difficulty.

As these data are qualitatively similar to the corresponding data for chromous acid, the same type of analysis can be performed. The CoOOD assignment is then

$$\omega_{12} = 1635 \text{ cm}^{-1}$$
$$\omega_{03} = 1950 \text{ cm}^{-1} \qquad (3.6)$$

(cf. (3.1)).

Table 3-10

Infrared and neutron scattering bands for CoOOH
(all frequencies in cm^{-1})

Neutron energy loss	Neutron energy gain	Infrared (24°C)	Infrared (-196°C)
		3400(m)	3450(m)
		∿1800(s)	∿1800(s)
1286(vs)	1300	1221(w)	1221(w)
755(w)	745		
570(vw)		578(s)	584(s)
468(sh)	530		475(w)
	264	221(m?)	
	150		
	65		

(Based on Delaplane, Ibers, Ferraro and Rush (1969) and Temme and Waddington (1973))

Table 3-11

Infrared spectral bands for CoOOD (frequencies in cm^{-1})

Infrared (24° C)	Infrared (-196°C)
3450(s)	3450(s)
1950(s)	1950(s,br)
1635(s)	1635(s)
858(s)	858(s)
832(sh)	832(sh)
655(w)?	655(w)
607(sh)	607(sh)
568(s)	572(s)
527(sh,w)	530(w)
510(sh,w)	510(w)
477(m)	480(s)

(Based on Delaplane, Ibers, Ferraro and Rush (1969) and Temme and Waddington (1973))

Table 3.12 shows the potential wells and transition frequencies predicted for CoOOD for various r_o values and Table 3.13 gives the corresponding CoOOH well parameters and transition frequencies. An r_o value of 0.959(5)Å was judged to give the best interpretation of the combined CoOOH/CoOOD spectra. Details of the predicted wells and transition frequencies are given in Table 3.14. The computed transition probabilities are given in Table 3.15.

The suggested CoOOH assignment is then

$$\omega_{01} = 221 \text{ cm}^{-1}$$

$$\omega_{12} = \sim 1800 \text{ cm}^{-1}$$

$$\omega_{03} = 3450 \text{ cm}^{-1} \qquad (3.7)$$

(cf. (3.4)).

The following points must also be noted:

i) Neutron inelastic scattering and IR spectra are not available for CoOOD. As in the CrOOH/CrOOD case, these spectra are of critical importance in assessing whether the 221 cm^{-1} band is caused by the tunnelling mode.

ii) A ferrodistortive phase transition is proposed for CoOOH at a temperature just below room temperature to account for Delaplane's observation that the 1800 cm^{-1} band shows no apparent temperature dependence. It is very difficult to obtain single crystals of cobaltic acid and it appears that no attempt has been made to detect such a transition. (cf. the corresponding discussion for CrOOH).

iii) The bands observed at 3450 cm^{-1} in the IR spectra of both CoOOH and CoOOD appear stronger than the

Table 3-12

CoOOD Potential well parameters: given r_o,

$|0\rangle \rightarrow |3\rangle = 1950 cm^{-1}$, $|1\rangle \rightarrow |2\rangle = 1635 cm^{-1}$ and $2R = 2.57\text{Å}$

r_o (Å)	D (eV)	α ($Å^{-1}$)	$R-r_o$ (Å)	x_m (Å)	OD (Å)	B (cm^{-1})	ω_{03} (cm^{-1})	ω_{12} (cm^{-1})	ω_{01} (cm^{-1})	$D\alpha^2$
.940	.518	8.90	.345	.349	0.971	3340	1950	1635	3	41.0
.950	.563	7.97	.335	.334	0.980	3370	1950	1635	4	35.8
.960	.657	6.94	.325	.323	0.989	3310	1950	1635	5	31.6
.970	1.406	4.63	.315	.302	1.005	3241	1949	1635	7	30.1

Table 3-13

CoOOH potential well parameters and transition frequencies determined from CoOOD parameters. $2R = 2.50\text{Å}$

r_o (Å)	$R-r_o$ (Å)	x_m (Å)	OH (Å)	B (cm^{-1})	ω_{03} (cm^{-1})	ω_{12} (cm^{-1})	ω_{01} (cm^{-1})
.940	.310	.310	0.990	3343	3166	1665	124
.950	.300	.299	0.999	3367	3227	1683	141
.960	.290	.287	1.010	2841	3281	1686	165
.970	.280	.262	1.036	2325	3382	1630	245

Table 3-14

Refined potential well parameters for CoOOH and CoOOD

	CoOOH	CoOOD
r_o (Å)	.969	.969
D(eV)	.913	.913
α (Å^{-1})	5.66	5.66
R-r_o (Å)	.281	.316
x_m (Å)	.311	.273
B(cm^{-1})	2583	3262
OH(D) (Å)	1.023	0.999
ω_{01} (cm^{-1})	202	7
ω_{03} (cm^{-1})	3338	1950
ω_{12} (cm^{-1})	1667	1635
$D\alpha^2$	29.3	29.3

Table 3-15

Relative transition probabilities for CoOOH and CoOOD

	Transition	Frequency (cm^{-})	Relative dipole moment	Relative intensity
CoOOH	$\|0\rangle \rightarrow \|1\rangle$	202	77	41
	$\|0\rangle \rightarrow \|3\rangle$	3338	15	25
	$\|1\rangle \rightarrow \|2\rangle$	1667	42	100
CoOOD	$\|0\rangle \rightarrow \|1\rangle$	7	100	2
	$\|0\rangle \rightarrow \|3\rangle$	1950	20	27
	$\|1\rangle \rightarrow \|2\rangle$	1635	22	27

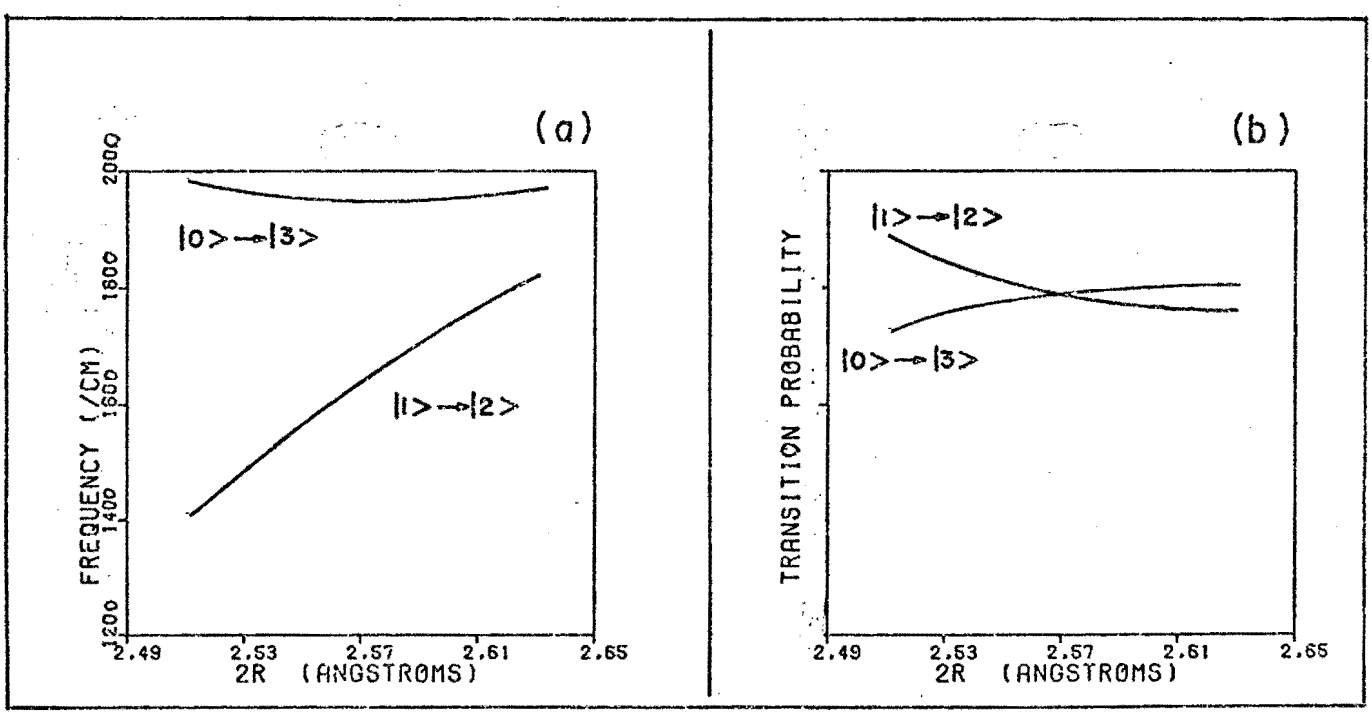

Figure 3.10. Variation in (a) predicted CoOOD transition frequencies and (b) predicted CoOOD transition probabilities with O...O distance.

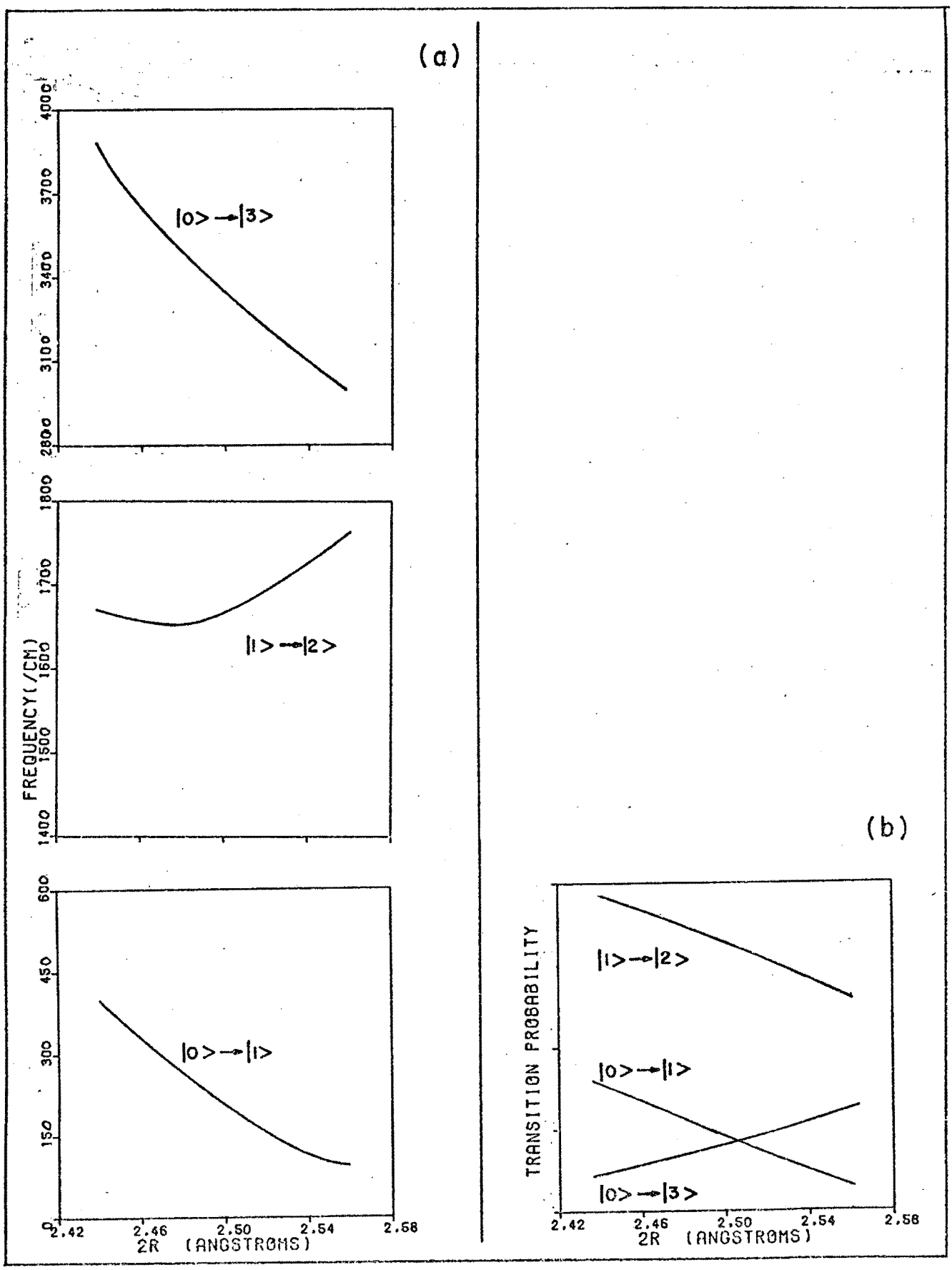

Figure 3.11. Variation in (a) predicted CoOOH transition frequencies and (b) predicted CoOOH transition probabilities with O...O distance.

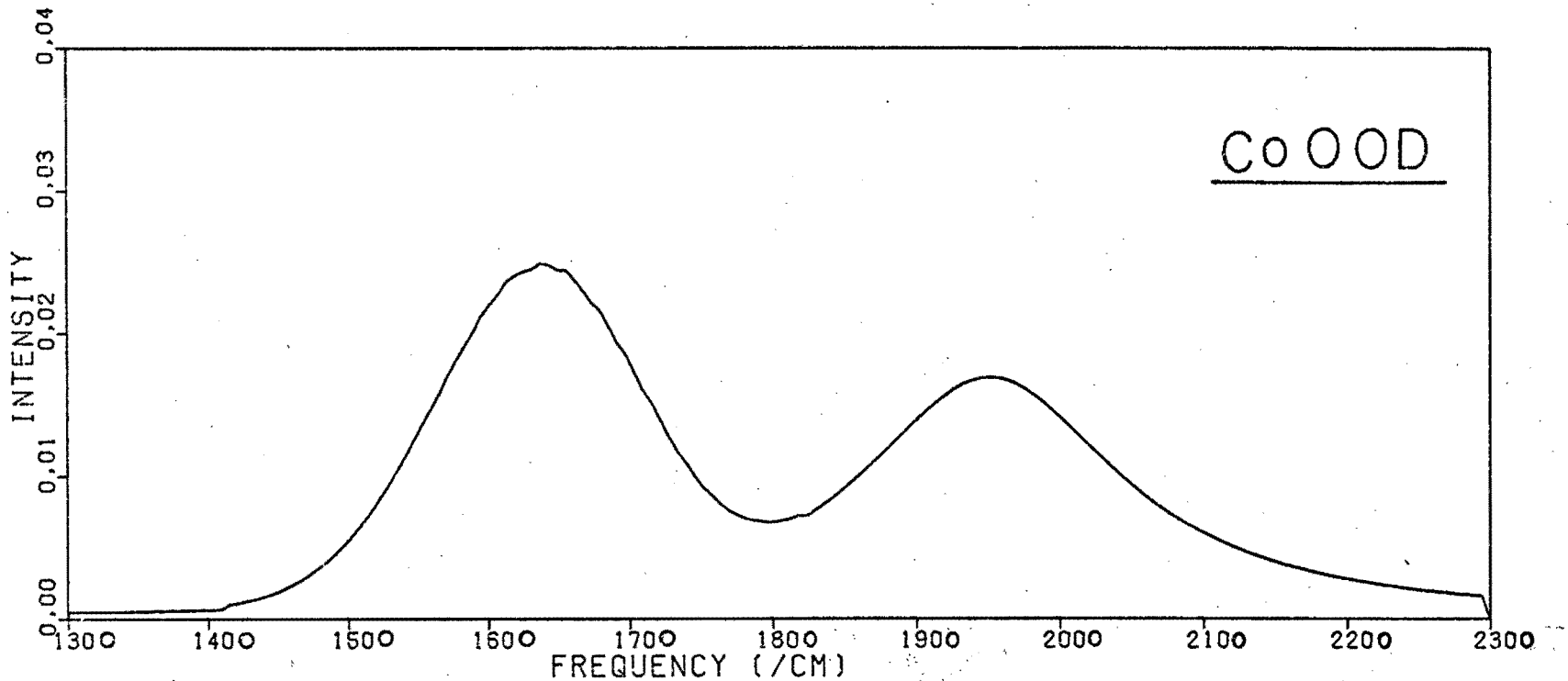

Figure 3.12. Predicted bandshapes for CoOOD infrared transitions. $\omega_{12} \sim 1635$ cm^{-1} and $\omega_{03} \sim 1950$ cm^{-1}.

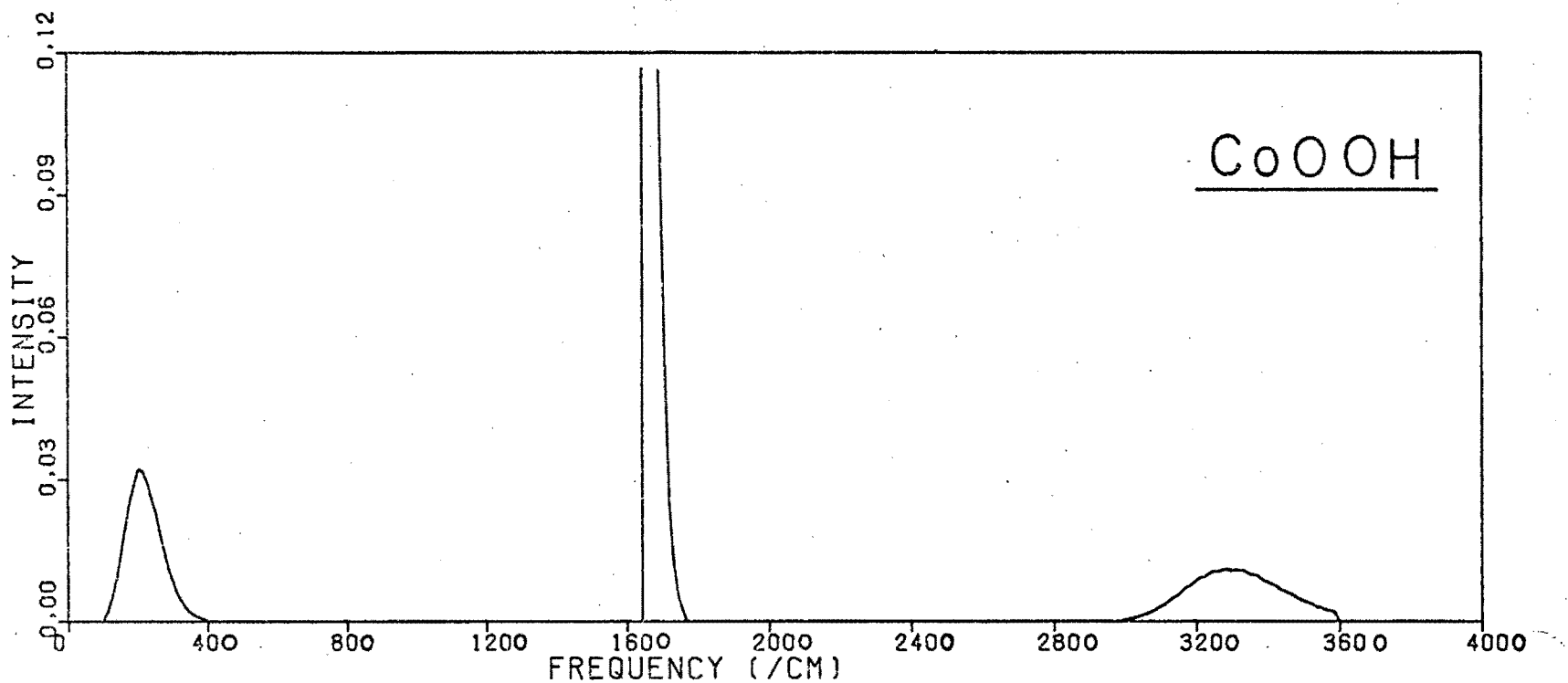

Figure 3.13. Predicted bandshapes for CoOOH infrared transitions. $\omega_{01} \sim 202$ cm^{-1} $\omega_{12} \sim 1670$ cm^{-1} $\omega_{03} \sim 3340$ cm^{-1}. Note the narrowness of the $|1\rangle \rightarrow |2\rangle$ transition band.

corresponding bands in the CrOOH/CrOOD spectra. This suggests that these bands may well be caused by overtones or combinations of stretching modes thus obscuring the $|0\rangle \rightarrow |3\rangle$ CoOOH transition, which is relatively weak.

An analysis of the band shapes of the transitions given in (3.5) and (3.7) was performed using the same O...O modulation and broadening mechanisms as were used in section 3.3.5. Figures 3.10 and 3.11 show the variation of the various transition frequencies and probabilities with respect to O...O distance and figures 3.12 and 3.13 show the predicted bandshapes. The narrowness of the $|1\rangle \rightarrow |2\rangle$ transition is again inexplicable for CoOOH.

3.5 Remarks on Computational Procedure

The wavefunctions for the protons and deuterons were computed at a total of 300 points and are displayed in figure 3.14 for CrOOH and CrOOD. As expected, the wavefunctions appear entirely smooth in their first derivative. These 300 points acted as the basis for a numerical integration to determine the normalization coefficients and the dipole matrix elements.

The convergence rate of the Harwell subroutine NSØ1A locating solutions for the systems (3.1), (3.2) and (3.6) was increased by re-parameterizing the well. $D\alpha^2$ was used instead of D as an unknown, and this gave faster convergence from a given starting approximation to the solution. For system (3.2) x_m also performed better as an unknown than r_o in the routine, even though this system proved later to be

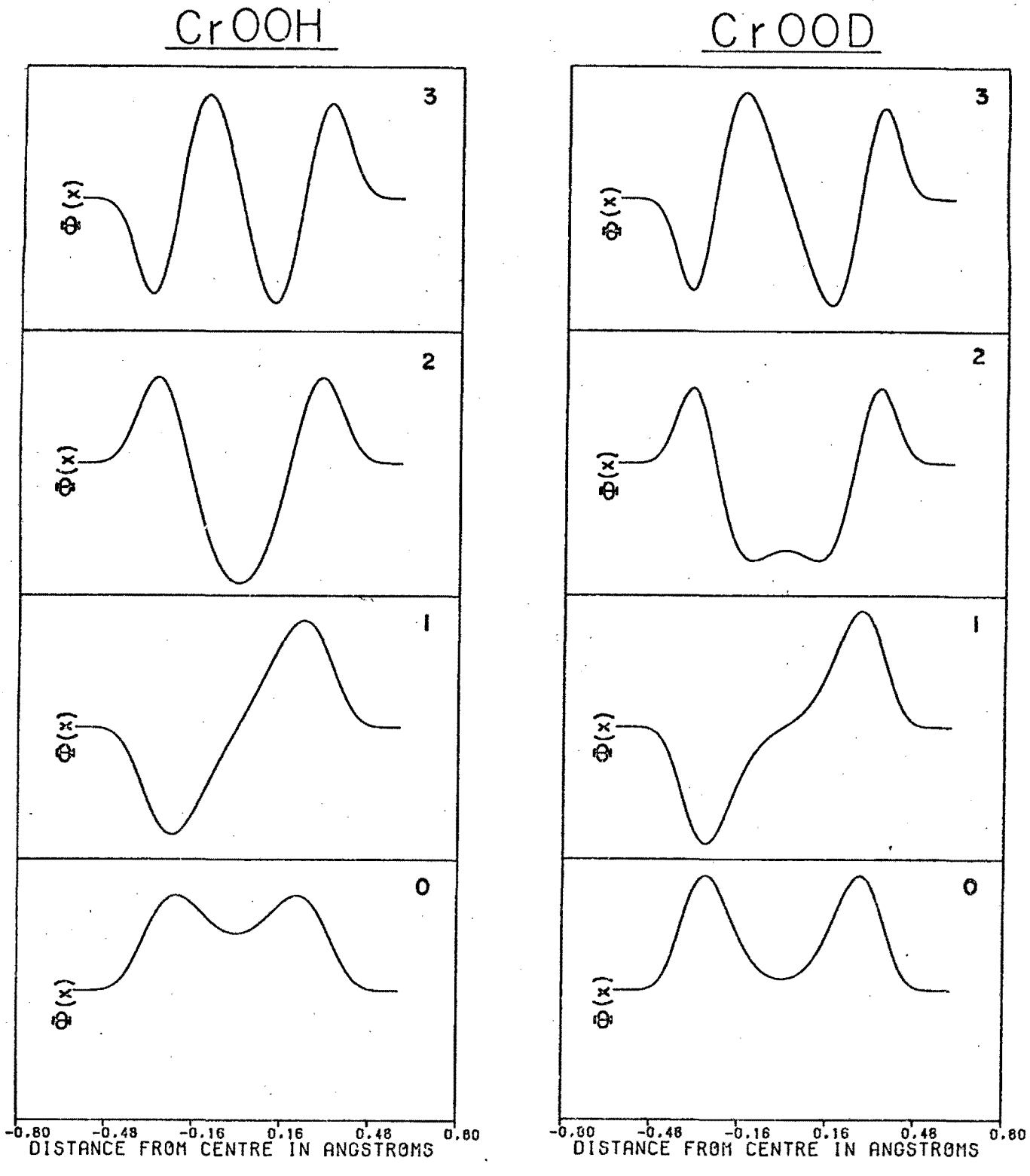

Figure 3.14. Double Morse Potential semi-classical wavefunctions for CrOOH and CrOOD. The numbers in the upper right hand corner refer to the eigenstates.

Table 3-16

Approximate UNIVAC 1100/81 Computer running times

Task	Time
Evaluate energy level scheme (first four levels)	7 secs
Evaluate energy level scheme and wavefunctions (first four levels)	20 secs
Solve for D and α, given R, r_o and two transition frequencies	2→5 mins
Compute band profiles	2.5 mins

mathematically inconsistent. This is borne out by an inspection of Tables 3.4 and 3.12 where it is seen that for a relatively small change in r_o, D and α change quite considerably. On the other hand $D\alpha^2$ and x_m appear to vary far more slowly with r_o.

All in all, no major computational difficulties arose and the computer (UNIVAC 1100/81) used performed the calculations quite rapidly. Table 3.16 gives some approximate computing times for the various types of calculations performed.

3.6 Conclusions

The model has given a remarkably consistent and quantitative explanation of the chromous acid IR spectral frequencies. The best assignment of the ν_s(OH) and ν_s(OD) bands is as follows:

$$\begin{aligned} \text{CrOOH} &: \omega_{01} = 221 \text{ cm}^{-1} \\ &\quad \omega_{12} = 1650 \text{ cm}^{-1} \\ &\quad \omega_{03} = 3400 \text{ cm}^{-1} \\ \text{CrOOD} &: \omega_{12} = 1613 \text{ cm}^{-1} \\ &\quad \omega_{03} = 1923 \text{ cm}^{-1} \end{aligned} \qquad (3.8)$$

The barrier heights for CrOOH and CrOOD are found to be 2406 cm^{-1} and 3193 cm^{-1} respectively with the OH and OD distances being 1.021Å and 0.994Å respectively.

This interpretation agrees with Snyder and Ibers regarding the ν_s(OD) band being composed of a $|0\rangle \rightarrow |3\rangle$ and a $|1\rangle \rightarrow |2\rangle$ transition. The presence of a Fermi resonance in the centre of the ν_s(OD) band (as proposed by Claydon *et al.* and Savel'ev and Sokolov) is not however denied,

but the prime cause of the doublet is put down to the separation of the $|2\rangle$ and $|3\rangle$ levels in the CrOOD energy level spectrum. This interpretation also gives an entirely new explanation of the ν_s(OH) spectrum. The 226 cm^{-1} band observed by Temme and Waddington is assigned to the $|0\rangle \rightarrow |1\rangle$ protonic transition and the 3400 cm^{-1} band observed by Rush and Ferraro is now assigned as the $|0\rangle \rightarrow |3\rangle$ transition, although the band may consist largely of overtone modes and combinations of stretching modes.

The crystallographic data of Hamilton and Ibers gave more consistent results in the analysis than those of Nørlund Christensen, Hansen and Lehmann. The latter data seemed to suggest that the $|0\rangle \rightarrow |1\rangle$ transition for CrOOH lay in the 500 cm^{-1} region, a result which could not be reconciled with the effect of deuteration on the IR spectra. The OD distances given by Nørlund Christensen *et al.* also seemed to be too high whereas that of Hamilton and Ibers appeared to be closer to the true distance.

An attempt was made to predict the bandshapes for the ν_s(OH) and ν_s(OD) transitions. Whereas good predictions are obtained for the ν_s(OD) transitions, the predicted bandwidth of the $|1\rangle \rightarrow |2\rangle$ transition in CrOOH is too narrow. This result needs closer examination.

The analysis was also performed on cobaltic acid and deuterated cobaltic acid (chromous acid isomorphs) and the results are qualitatively very similar to those for chromous acid.

The double Morse potential function gave a good account of the barrier changes when the O...O distance was varied by 0.06Å on deuteration. As this is a particularly

large Ubbelohde effect, the model should be equally successful in this regard for other species, where the Ubbelohde effect is usually smaller. This suggests that it should also be useful for analysing KDP-type ferroelectrics where the O...O distance is known to change with not only isotopic substitution but also with temperature and pressure. Tunnelling is known to occur in KDP and the model should provide a means of calculating the temperature and pressure variation of the tunnelling integrals. The proton dynamics of KDP will be examined in detail in Chapter 5.

CHAPTER FOUR

TUNNELLING IN CARBOXYLIC AND DICARBOXYLIC ACIDS

The carboxylic and dicarboxylic acids contain in some phases $(COOH)_2$ hydrogen-bonded cycles:

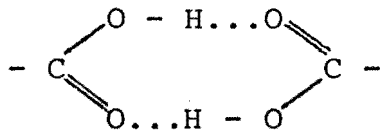

e.g. gaseous formic acid and crystalline adipic acid. This particularly simple structure lends itself well to the study of hydrogen bond properties. Another carboxylic acid structure that is of particular interest is that of crystalline formic acid, the molecules of which are joined together by single hydrogen bonds to form long chains.

Considerable effort has been made over the past few years to explain the IR spectra of many of these systems, but no complete theory exists at present. One of the open questions is whether proton tunnelling takes place on a sufficiently short time-scale to influence the spectra. In section 4.1 some of experimental results for these systems will be discussed and in the subsequent sections the question of tunnelling will be investigated using the double Morse potential model to represent the hydrogen bond dynamics.

4.1 Experimental Results

4.1.1 Dimeric and Crystalline Formic Acid

Excoffon and Marechal (1972) have carefully measured the IR spectra of various carboxylic acid dimers and their deuterated analogues. A species of particular interest is

formic acid HCOOH, which is dimeric in the vapour phase.

The IR spectrum of dimeric formic acid $(HCOOH)_2$ is reproduced in figure 4.1. It shows a complex structure in the 2400-3400 cm^{-1} $\nu_s(OH)$ stretching region with two intense absorptions at about 2967 cm^{-1} and 3207 cm^{-1} respectively and a number of weaker absorptions in the 2400-2900 cm^{-1} region.

The IR spectrum of the deuterated formic acid dimer $(HCOOD)_2$, reproduced in figure 4.2, is simpler with two strong absorptions at 2068 cm^{-1} and 2299 cm^{-1} respectively.

Excoffon and Marechal show how these spectra can be understood in terms of transitions between vibrational states of the system. These states are considered to arise from coupled $\nu_s(OH)$ and $\nu_\sigma(O...O)$ modes. Two low frequency ν_σ (O...O) modes exist in the dimer: the Q^+ mode which is symmetric with respect to rotation about the two-fold axis of symmetry of the dimer and the Q^- mode which is antisymmetric with respect to this axis of symmetry. The eigenvalue spectrum of these modes will vary according to the degree of excitation of the $\nu_s(OH)$ modes: Excoffon and Marechal consider a completely symmetric vibration of the two protons and the two modes Q^+ and Q^-, described by a Hamiltonian H^+, and a completely antisymmetric excited vibration of the same system, described by a Hamiltonian H^-. These two vibrations are inseparable when a single proton is excited. In the initial development of the theory proton tunnelling is ignored. The IR transitions then arise in the form $|u',v';0\rangle \rightarrow |u,v;1^+\rangle$ or $|u';v';0\rangle \rightarrow |u,v;1^-\rangle$ where u' and v' are the quantum numbers describing the Q^+ and Q^- modes respectively, with the $\nu_s(OH)$ modes in their ground state 0, and u and v are the quantum

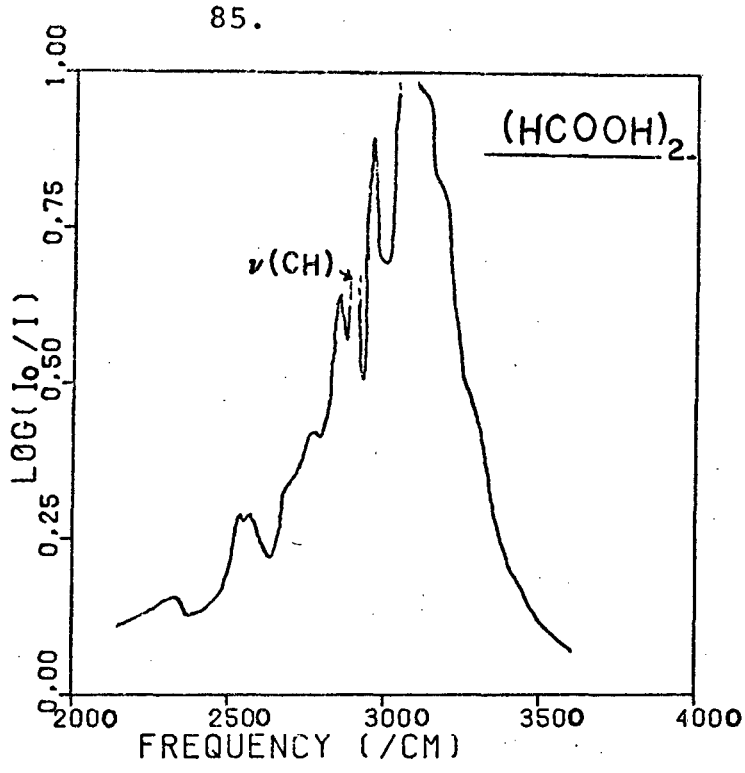

Figure 4.1. Mid-infrared spectrum of dimeric formic acid. Based on Excoffon and Marechal (1972).

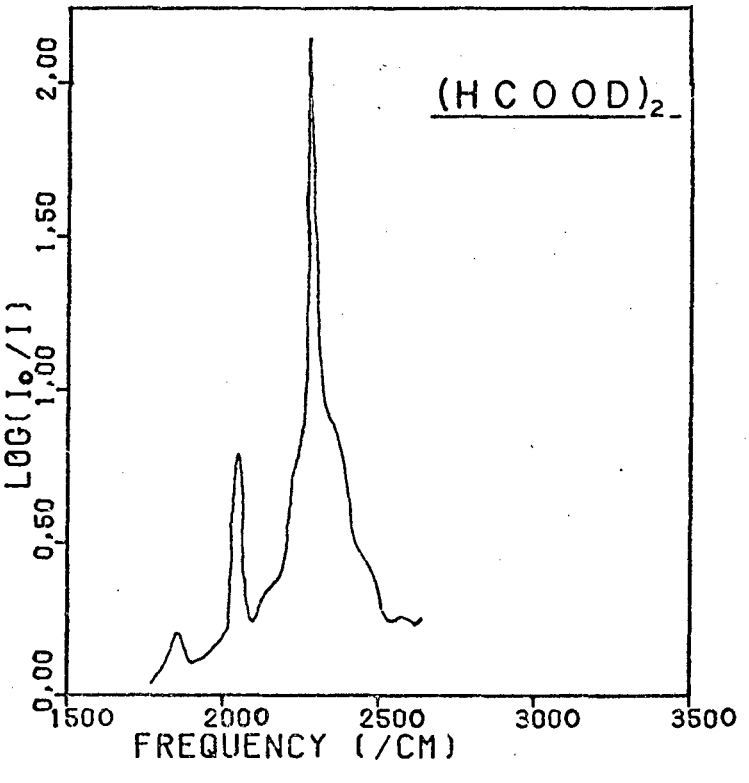

Figure 4.2. Mid-infrared spectrum of deuterated dimeric formic acid. Based on Excoffon and Marechal (1972).

numbers describing the Q^+ and Q^- modes when the ν_s(OH) modes are in either of the two excited states 1^+ and 1^- (depending on the resultant symmetry). These transitions will be subject to selection rules as described in the original paper.

Thus far the protons have been considered as localized within their respective wells on opposite sides of the molecules. However Excoffon and Marechal found that the IR spectrum of $(HCOOH)_2$ could only be understood in terms of this model if the upper vibrational state of each of the protons was split by 140 cm^{-1} due to tunnelling. This effectively doubles the number of predicted bands. They assume further that the protons tunnel in concert when they are both excited:

(i.e. the dipolar interaction between the hydrogen bonds is sufficiently strong to prevent both protons becoming localized on the same side of the molecule.)

For $(HCOOD)_2$ on the other hand, Excoffon and Marechal were able to explain the spectrum in terms of their model without having to invoke tunnelling. This is as would be expected: any splitting due to deuteron tunnelling would be very much smaller than that due to proton tunnelling since the tunnelling frequency is an exponentially decreasing function of the particle mass for a given barrier height. Furthermore, the height of the potential barrier is probably greater due to the increased O...O distance on deuteration (cf. chromous acid).

Bournay and Marechal (1975) measured the integrated intensities of various bands in the IR spectra of the formic

acid $(HCOOH)_2$, $(DCOOH)_2$, $(HCOOD)_2$ and $(DCOOD)_2$ gas phase dimers. They found that the ratios $P_{OH...O}/P_{OD...O}$ (CH group) and $P_{OH...O}/P_{OD...O}$ (CD group) were 1.99 and 2.06 respectively, where P denotes the respective transition probability for the $\nu_s(OH)$ or $\nu_s(OD)$ mode. Both of these ratios are considerably larger than $\sqrt{2}$, the value that would be expected if the vibrations were harmonic. A similar anomalous intensity ratio was detected in the IR spectra of crystalline formic acid by Zelsmann and Marechal (1974, 1977a). They found that the ratios $P_{OH...O}/P_{OD...O}$ (CH group) and $P_{OH...O}/P_{OD...O}$ (CD group) were 1.50 and 1.94 respectively for these crystals. As formic acid crystals do not contain the $(COOH)_2$ cycles, this seemed to indicate that the anomalous intensity ratio was an intrinsic property of the hydrogen bonds themselves, rather than of the cyclic arrangement of the two bonds. They attempted to explain the phenomenon in terms of an electrical and mechanical anharmonicity in the $\nu_s(OH)$ vibration (Zelsmann and Marechal (1977b)). It was shown that if the $\nu_s(OH)$ mode was strongly coupled to the $\nu_\sigma(O...O)$ mode, with the dipole moment operator depending on the O...O distance 2R as well as on the displacement x of the proton from its equilibrium position:

$$\mu(x;R) = \mu_o + \mu_1 x[1 + \varepsilon(R - R_o)]$$

(electrical anharmonicity), then the effect could be explained. μ_o, μ_1 and ε are constants and R_o is the equilibrium value of R.(ε=0 corresponds to the absence of electrical anharmonicity.)

The appearance of the $\nu_s(OH)$ spectral bands of crystalline formic acid are very different from those of the gas phase dimer and are far more difficult to reconstruct. The complication is due to the O...O vibrations now being part

of the whole system of lattice modes and no longer simply localized internal vibrations. In formic acid the crystal consists of long chains of HCOOH molecules linked together by single hydrogen bonds (see section 4.1.3) and the O...O vibrations clearly cannot be treated as being localized. Lawrence and Robertson (1979) have shown that the mean amplitude of the O...O vibrations in a hydrogen-bonded crystal can be as much as an order of magnitude smaller than the mean amplitude of vibration in the gas phase. This results in the band shape being considerably different in the crystalline and gaseous phases.

The difference in the spectra may also be caused in part by the fact that the O...O distance in the formic acid crystal is 0.12Å shorter than it is in the gas phase dimer. Proton tunnelling is thus far more likely to be important in the crystal than it is in the dimer. This will be discussed in detail in section 4.2 and 4.4.

4.1.2 Adipic Acid Crystals

Adipic acid crystallises so as to contain $(COOH)_2$ cycles:

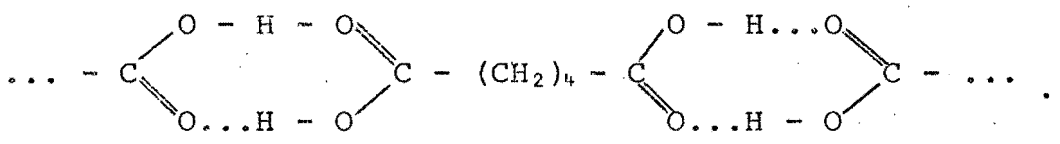

Auvert and Marechal (1979a,b,c) recently studied the IR spectra of adipic and deuterated adipic acid crystals. These spectra are reproduced in figures 4.3 and 4.4 respectively.

The following observations were made:

i) The ν_s(OH) band, spread over the range 2500 - 3200 cm^{-1}, is strongly polarized. Furthermore, the angle

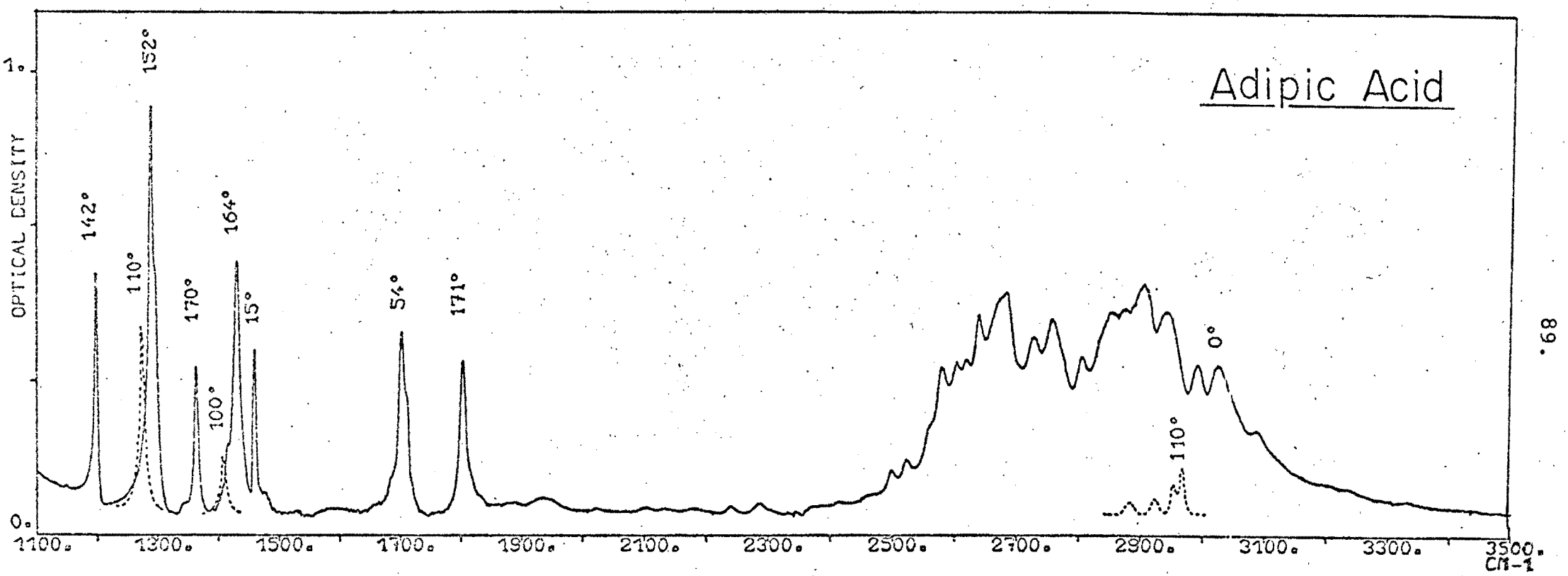

Figure 4.3. Infrared spectrum of crystalline adipic acid. From Auvert and Marechal (1979a). The spectrum is polarized in the a,c plane and θ represents the angle of polarization of the electric field in this plane. The solid line corresponds to $\theta = 0^{o}$, the angle which gives maximum ν_s intensity. The dotted lines correspond to $\theta = 90^{o}$, which gives minimum ν_s intensity. The values of θ which give maximum intensity for the remaining bands are also indicated. T = 10K.

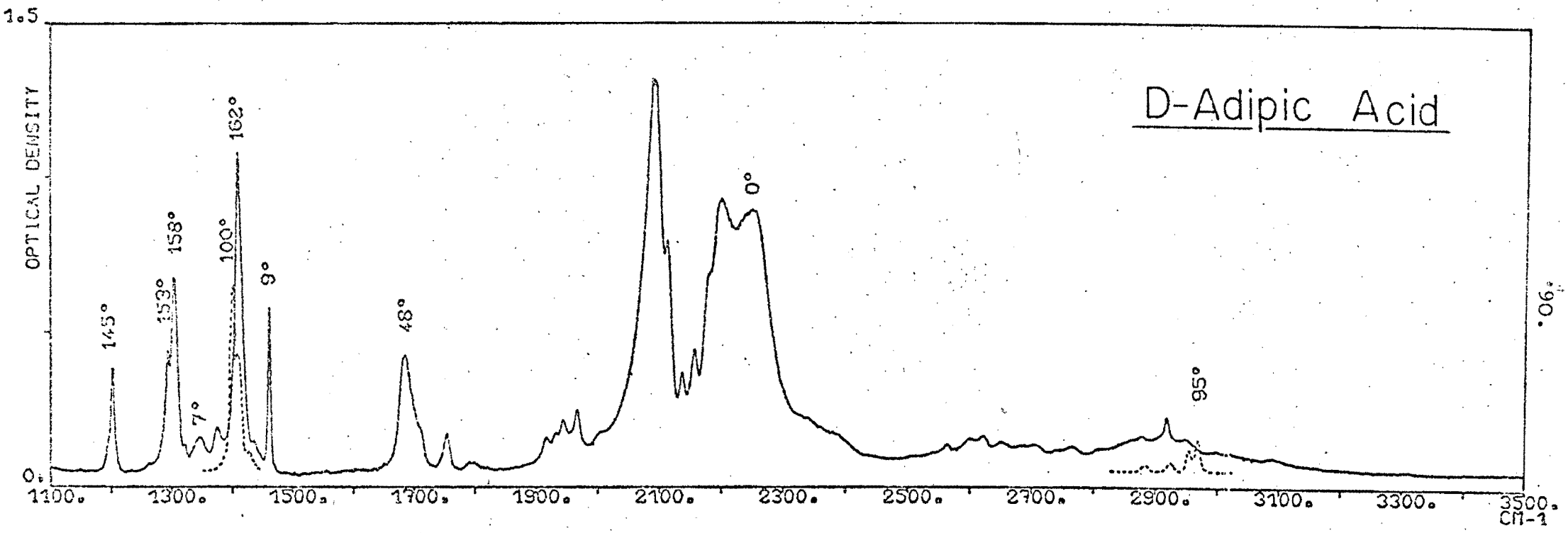

Figure 4.4. Infrared spectrum of crystalline deuterated adipic acid. From Auvert and Marechal (1979a). The spectrum is polarized in the $\vec{a},\vec{c}$ plane and θ represents the angle of polarization of the electric field in this plane. The solid line corresponds to $\theta = 0^{\circ}$, the angle which gives maximum ν_s intensity. The dotted lines correspond to $\theta = 90^{\circ}$, which gives minimum ν_s intensity. The values of θ which give maximum intensity for the remaining bands are also indicated. T = 10K.

of polarization varied across the band by about 9^{o} at room temperature. It also appeared that the band might consist of a low frequency part with one polarization and a high frequency part with a different polarization. However, the presence of such a discontinuity in the polarization of the band could not be firmly established. A similar result was found for the deuterated adipic acid ν_s(OD) band, where the polarization angle changed by about 8^{o} across the band.

ii) The $P_{OH...O}/P_{OD...O}$ ratio was also found to be of the order of 2.0 for this system. Whereas this ratio remained relatively constant when the temperature was varied from 10K to 300K, the values of both $P_{OH...O}$ and $P_{OD...O}$ dropped by about 20% as the temperature increased across this range. This result was surprising as a previous analysis of the same phenomenon in acetic acid dimers (Bournay and Marechal (1974)) predicted that both $P_{OH...O}$ and $P_{OD...O}$ should increase with temperature.

iii) The $\nu_{C=O}$ band appeared strongly polarized in both adipic and deuterated adipic acid crystals. At 10K the band was completely extinguished at a direction of 90^{o} to that of maximum absorption. However, when the temperature was raised to 300K, the extinction was no longer complete and the minimum intensity was now of the order of 10% of the maximum intensity.

A number of explanations were put forward to explain these observations and in order are:

i) The ν_s(OH) frequency is known empirically to depend on the O...O distance in the hydrogen bond (Novak (1974)). Auvert and Marechal suggested that the varying polarization of the ν_s(OH) band could therefore be best explained by considering a coupling of the δ(OH...O) bending mode with the ν_σ(O...O) mode. If the equilibrium position of the bending mode depended on the O...O distance it would mean that the polarization direction of the ν_s(OH) band would depend on its frequency via the dependence of both on the O...O distance.

It was also suggested that tunnelling in the upper state of the proton from one site in the hydrogen bond to the other could result in different ν_s(OH) polarizations for the two configurations if the bonds were non-linear. This is illusrated in figure 4.5. A neutron diffraction study (Auvert and Marechal (1979a)) failed to detect conclusively the presence of both these forms in the crystals.

ii) In order to explain quantitatively the 20% decrease in $P_{OH...O}$ and $P_{OD...O}$ as the temperature increased from 10K to 300K, it was necessary to postulate that the O...O distance in the dimer was 0.03Å longer at 300K than at 30K - which appears to be quite reasonable in comparison with known OH...O thermal expansions (cf. potassium dihydrogen phosphate crystals, discussed in the next chapter). As the dipole moment operator depends on the O...O distance when electrical anharmonicity is present, the decrease in transition probability with increasing temperature might then follow

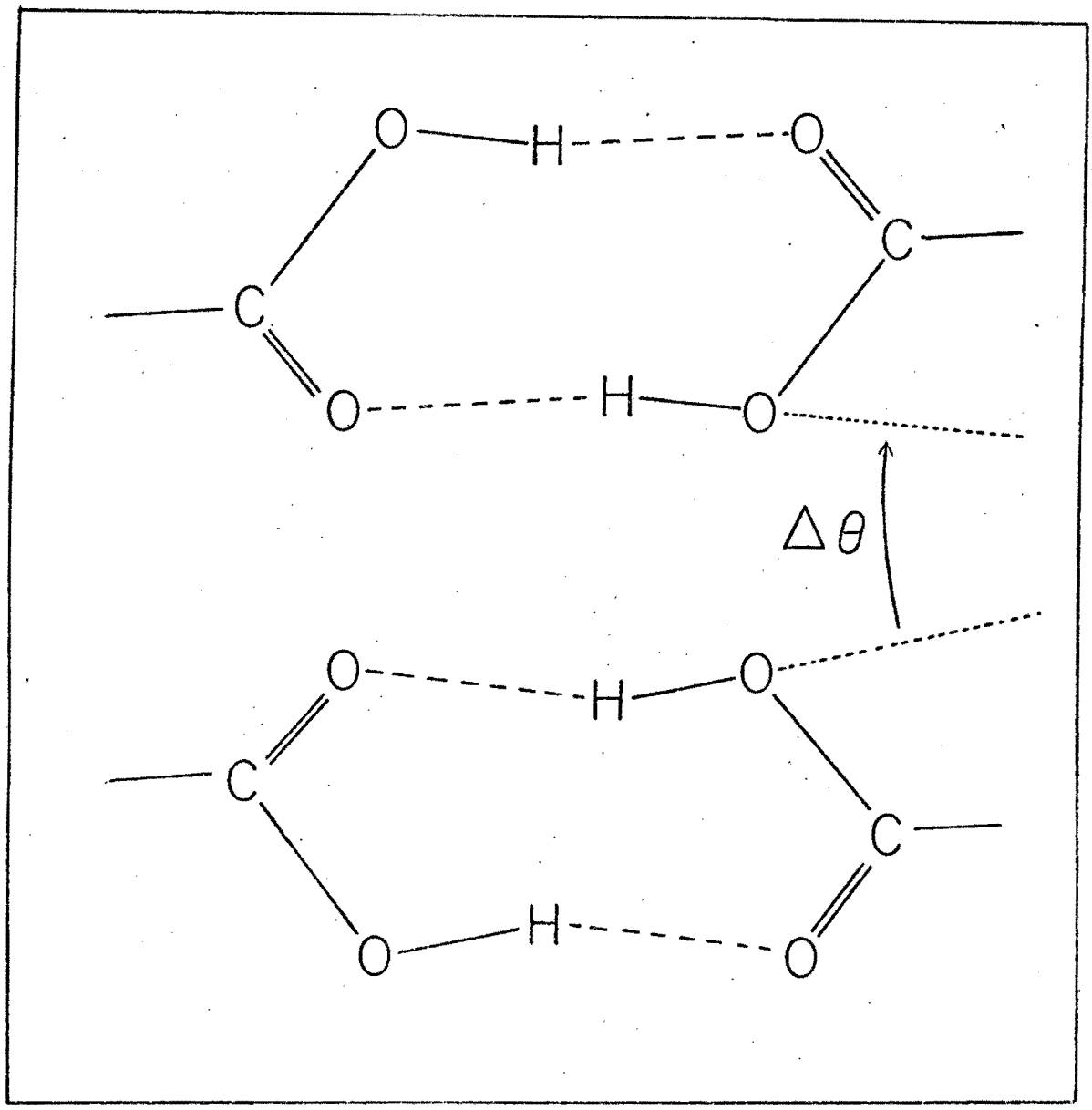

Figure 4.5. Postulated non-linearity of hydrogen bonds in crystalline adipic acid. Protonic tunnelling results in varying polarization of ν_s(CH) band.

quite naturally.

iii) Auvert and Marechal proposed that if both the configurations mentioned in (i) above were present in the crystal, then one configuration would have an energy that was 700K (490 cm^{-1}) higher than that of the other, relative to the lattice. (This energy estimate is based on the fact that from observation (iii) above, the configuration populations are in the ratio 1 to 10.) This higher energy configuration is a defect in the otherwise ordered crystal, the ordering being maintained by interactions between the protons in neighbouring cycles. At low temperatures only the first configuration would exist whereas at higher temperatures the concentration of the higher energy configuration would increase. The C=O bonds lie in different directions in the two configurations and hence the absorption in the high temperature case cannot be extinguished. However as noted in (i) above, the existence of these two possible configurations in a given crystal could not be firmly established.

4.1.3 Polymorphism in Formic Acid Crystals

Zelsmann, Bellon, Marechal and Bullemer (1970) discovered a first-order structural phase transition in crystalline formic acid. The ν_s(OH) and $\nu_{C=O}$ bands both showed marked changes in shape with temperature. When the crystal was heated, the changes occurred at 218±1K and when it was cooled the changes occurred at 207±5K. Differential thermal analysis showed that the transition was first order. The

transition was described as an order-disorder one: below the transition temperature all the (hydrogen-bonded) protons in a given molecular chain are localized either "left" or "right" (see figure 4.6a), whereas above the transition temperature both configurations can occur within a given chain (figure 4.6b). This interpretation is further supported by structural experiments, the results of which are summarized in table 4.1. As can be seen from the table, the microwave experiments, which were performed on the gaseous formic acid monomer (Lerner, Dailey and Friend (1957) and Kwei and Curl (1960)), and the electron diffraction experiments, performed on either the gaseous monomer or the gaseous dimer (Schomaker and O'Gorman (1947), Karle and Karle (1954) and Almenningen, Bastiansen and Motzfeldt (1970)), suggest that the C-O bond length is significantly longer than that of the C=O bond. On the other hand, X-ray crystallography (Holtzberg, Post and Fankuchen (1953)) suggests that the C-O and C=O bonds are of comparable length. Some explanation must be found for this discrepancy. In the monomeric form the C-O and C=O bonds must clearly be distinct. In the gas phase dimer however, simultaneous tunnelling of both protons involved in the hydrogen-bonding may occur, in which case the C-O and C=O bonds would interchange as the protons tunnelled in concert. But if the tunnelling takes places on a time-scale that is much longer than the rotational period of the dimer then the C-O and C=O bonds will still be distinguishable in the analysis of the electron diffraction experiment. On the other hand, X-ray crystallography determines the atom positions averaged over a period of minutes or hours and so proton tunnelling, which may occur many times during the sampling

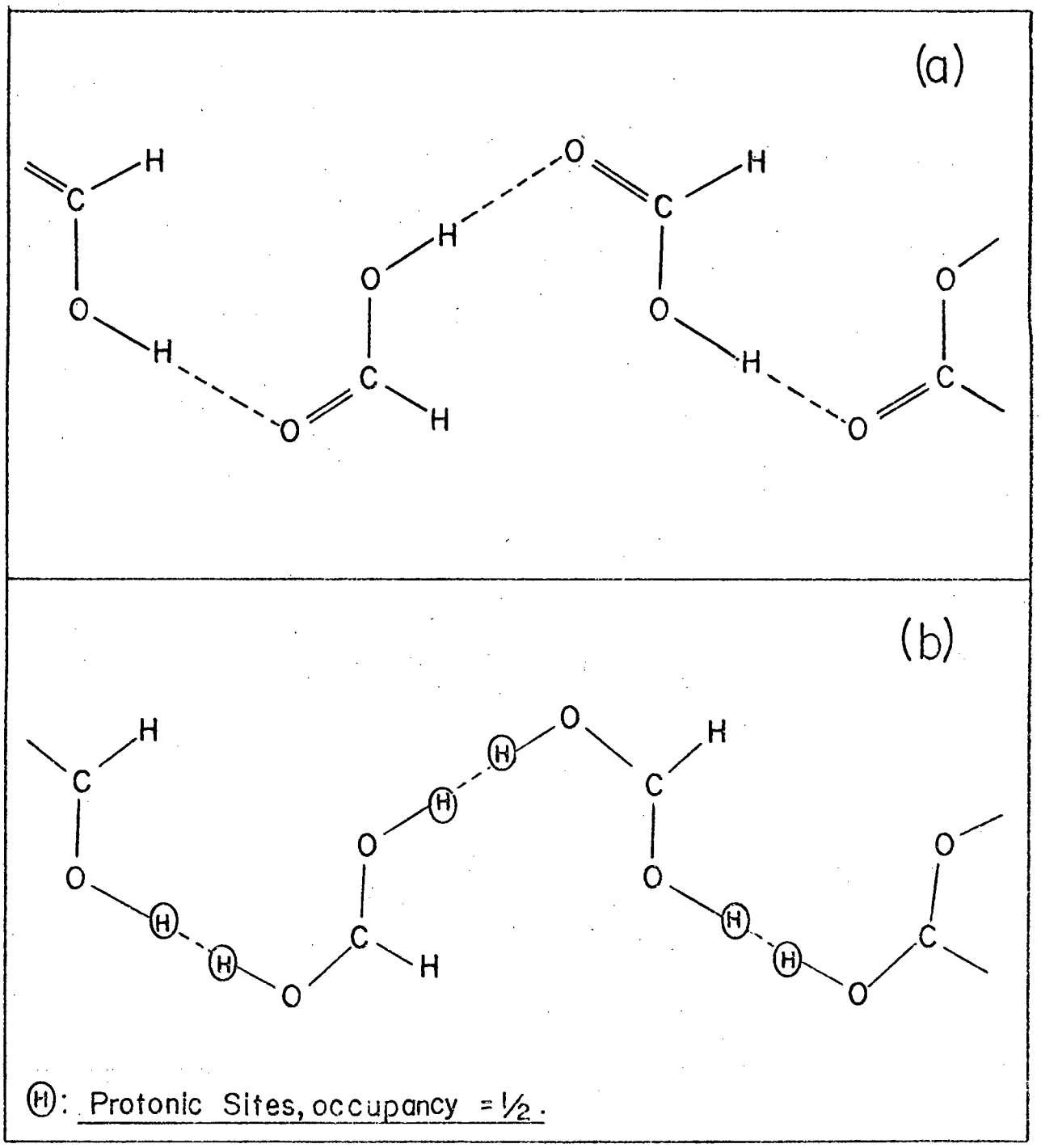

Figure 4.6. Polymorphism in formic acid crystals.
a) Low temperature phase: protons ordered on "left" site.
b) High temperature phase: protonic tunnelling results in symmetrical protonic distributions. The C-O and C=O bands are indistinguishable.

Table 4-1

Formic acid C-O and C=O bond lengths in the monomeric, dimeric and crystalline phases

Phase	Experimental technique	C=O (Å)	C-O (Å)	Reference
monomer	electron diffraction	1.213(26)	1.368(34)	(a)
monomer	electron diffraction	1.23(1)	1.36(1)	(b)
monomer	microwave spectroscopy	1.245(2)	1.312(2)	(c)
monomer	microwave spectroscopy	1.202(10)	1.343(10)	(d)
dimer	electron diffraction	1.220(3)	1.323(3)	(e)
crystal	X-ray diffraction	1.23(3)	1.26(3)	(f)

(a) Schomaker and O'Gorman (1947)
(b) Karle and Karle (1954)
(c) Lerner, Dailey and Friend (1957)
(d) Kwei and Curl (1960)
(e) Almenningen, Bastiansen and Motzfeldt (1970)
(f) Holtzberg, Post and Fankuchen (1953)

period, will make it impossible to distinguish between the C-O and C=O bonds within a given molecule.

The question thus arises as to whether proton tunnelling does actually occur in formic acid; and if so, whether the tunnelling time scale is of the right order of magnitude to confirm the above interpretation.

In the next section it will be shown how the double Morse potential model can be used to offer interpretations of the ν_s(OH) IR bands of formic and adipic acids as well as to indicate to what extent the anomalous intensity ratios are a consequence of proton tunnelling in these species.

4.2 Analysis of IR Spectra of Dimeric Formic Acid

One difficulty that arises with Excoffon and Marechal's treatment of the vibrational modes of the $(HCOOH)_2$ dimer is that they assume that joint tunnelling of the two protons can occur when one proton is in its excited state. But whereas one proton might readily tunnel in its excited state, the other proton, being in the ground state, will experience a far greater barrier to tunnelling. Thus if the protons are indeed coupled as Excoffon and Marechal suggest, then the joint tunnelling frequency is probably quite small (considerably less than 140 cm^{-1}).

In the treatment below we will choose rather to neglect the proton-proton interactions in the first excited state and consider the protons as independent. Haurie and Novak (1966) have pointed out that the infrared spectra of isotopically mixed CH_3COOH-CH_3COOD dimers appear to be the superposition of the isotopically pure dimeric spectra. In mixed

dimers the excitation of the ν_s(OH) mode could not be transferred to the ν_s(OD) mode. This suggests therefore that the coupling between the protons may indeed be small. When *both* the protons are in their ground states, the dipolar interaction is however sufficiently strong to keep the protons localized on opposite sites in the two bonds. This seems plausible as the splitting of the ground state for a single proton is likely to be very small. However, when one proton is excited we will assume that it is free to tunnel between opposite sites in the bond due to the splitting of the upper state. The other proton will remain localised in its respective site in the other bond. The tunnelling frequency of the excited (de-localized) proton is assumed to be 140 cm^{-1}. The IR active transitions thus arise in the form $|0\rangle \rightarrow |3\rangle$ and $|1\rangle \rightarrow |2\rangle$ where the 0 and 1 are quantum numbers describing the symmetric and antisymmetric states which mix to give the localized protonic ground state, and the 2 and 3 are quantum numbers describing the two levels which comprise the split upper single protonic state. These two transitions, taken together with changes in the quantum numbers of the Q^+ and Q^- modes, are thus responsible for the observed ν_s(OH) band.

In the previous chapter the double Morse potential model gave good results for the relatively short hydrogen bonds in chromous acid. Almenningen, Bastiansen and Motzfeldt (1970) have performed electron diffraction experiments on formic $(HCOOH)_2$ and deuterated formic $(HCOOD)_2$ acid dimers and their observed hydrogen bond lengths are given in table 4.2. As can be seen, the Ubbelohde effect is relatively small: $\Delta(O...O) = 0.019\text{Å}$, and the hydrogen bonds are relatively long ($\sim 2.70\text{Å}$). The double Morse potential model may

Table 4-2

Hydrogen bond lengths for $(HCOOH)_2$ and $(HCOOD)_2$

	$(HCOOH)_2$	$(HCOOD)_2$
O...O	2.703(7)Å	2.722(7)Å
O-H(D)	1.036(17)Å	1.058(17)Å

Based on Almenningen, Bastiansen and Motzfeldt (1970).

thus be expected to give at least as good a representation for the protonic potential for formic acid dimers, as these hydrogen bonds are longer and the potential is even closer to being two entirely separated Morse potentials (see section 1.5).

Does this model give intensity ratios which are in any way compatible with those observed by Excoffon and Marechal? To answer this, it is necessary to postulate an assignment for the various ν_s(OH) bands. We assume that the two strongest bands at 3107 cm^{-1} and 2967 cm^{-1} are the $|0\rangle \rightarrow |3\rangle$ and $|1\rangle \rightarrow |2\rangle$ transitions respectively. This retains Excoffon and Marechal's 140 cm^{-1} splitting of the upper state.

2R is set equal to 2.703Å (table 4.2) and the system

$$\begin{aligned} g_{03}(D,\alpha,r_o,R) &= 3107\ cm^{-1} \\ g_{12}(D,\alpha,r_o,R) &= 2967\ cm^{-1} \end{aligned} \qquad (4.1)$$

is then solved for various values of r_o.* The results are given in table 4.3. Similar numerical techniques to those outlined for chromous acid were used and solutions were obtained for all r_o values in the range 0.90(0.01)0.95Å.

2R is then set equal to 2.722Å and, keeping the other parameters constant, an energy level structure is predicted for $(HCOOD)_2$. The results are given in table 4.4. In order to select the best r_o value, the transition frequencies for

---

* The OH and OD distances given by Alemenningen *et al.* suggest that the D-D site-site separation is actually shorter than the H-H site-site separation. This is contrary to what would be expected considering the longer bond-length in $(HCOOD)_2$ and the heavier mass of the deuteron. It was therefore decided that these OH and OD distances could not be relied upon and were thus not used for estimating well parameters.

Table 4-3

$(HCOOH)_2$ Potential well parameters given r_o, $\omega_{03} = 3107\ cm^{-1}$, $\omega_{12} = 2967\ cm^{-1}$ and $2R = 2.703\text{Å}$

r_o (Å)	D (eV)	α ($Å^{-1}$)	$R-r_o$ (Å)	x_m (Å)	OH (Å)	B (cm^{-1})	ω_{03} (cm^{-1})	ω_{12} (cm^{-1})	ω_{01} (cm^{-1})	$D\alpha^2$
0.920	1.04	6.31	0.432	0.431	0.950	6316	3107	2967	1	41.3
0.930	1.15	5.81	0.422	0.421	0.959	6322	3107	2967	1	38.6
0.940	1.33	5.23	0.412	0.409	0.969	6339	3107	2967	1	36.4
0.950	1.80	4.42	0.402	0.395	0.981	6377	3107	2968	1	35.3
0.960	2.37	3.90	0.392	0.379	0.996	6117	3075	2890	2	36.0
0.980	2.15	4.20	0.372	0.360	1.015	5862	3146	2854	5	38.0

Note: Convergence fails for $r_o = 0.960\text{Å}$ and $r_o = 0.980\text{Å}$

Table 4-4

$(HCOOD)_2$ Potential well parameters and ν_s(OD) transition frequencies determined from $(HCOOH)_2$ parameters. $2R = 2.722\text{Å}$

r_o (Å)	$R-r_o$ (Å)	x_m (Å)	OD (Å)	B (cm^{-1})	ω_{03} (cm^{-1})	ω_{12} (cm^{-1})	ω_{01} (cm^{-1})
0.920	0.442	0.441	0.940	6433	2469	2470	0
0.930	0.432	0.431	0.949	6471	2439	2438	0
0.940	0.422	0.420	0.960	6536	2411	2409	0
0.950	0.412	0.406	0.972	6662	2380	2382	0
0.960	0.402	0.390	0.987	6481	2343	2340	0
0.980	0.382	0.372	1.005	6215	2389	2382	0

$(HCOOD)_2$ are compared with the observed spectrum. When r_o = 0.95Å the predicted $(HCOOD)_2$ transition frequencies are as follows: $|1\rangle\rightarrow|2\rangle$ = 2380 cm^{-1} and $|0\rangle\rightarrow|3\rangle$ = 2382 cm^{-1} with negligible ground state splitting ($\sim 7 \times 10^{-3}$ cm^{-1}) and virtually no upper state splitting. Comparing this result with the experimental $(HCOOD)_2$ spectrum (figure 4.2) it appears that this very close doublet may be the band at 2299 cm^{-1}, experimentally unresolved. (Interestingly enough the analogous bands in the IR spectrum of the deuterated acetic acid dimer shows a slight doublet structure. See Excoffon and Marechal (1972).) This r_o value is the one which yields predicted transition frequencies as close as possible to the 2299 cm^{-1} band.

The details of double Morse potential wells for this value of r_o are summarized in table 4.5. From this table we note that the ground state splitting for $(HCOOH)_2$ is very small (1.4 cm^{-1}), while the upper state is split by 140 cm^{-1} (as desired) and that the barrier height is considerably higher than in the chromous acid case. This is as expected considering the relatively long hydrogen bond lengths in the formic acid dimers. The positions of the energy levels in the potential well are shown for $(HCOOH)_2$ in figure 4.7a and for $(HCOOD)_2$ in figure 4.7b.

The transition probabilities were computed using (2.52) and are given in table 4.6. The two bands in the $(HCOOD)_2$ doublet are predicted to have equal transition probability while the $|0\rangle\rightarrow|3\rangle$ transition has a slightly higher probability than the $|1\rangle\rightarrow|2\rangle$ transition in $(HCOOH)_2$. This accords with the qualitative appearance of the observed spectra.

Table 4-5

Best potential well parameters for $(HCOOH)_2$ and $(HCOOD)_2$

	$(HCOOH)_2$	$(HCOOD)_2$
r_o (Å)	0.950	0.950
D(eV)	1.81	1.81
α ($Å^{-1}$)	4.42	4.42
$R-r_o$(Å)	0.402	0.412
x_m (Å)	0.395	0.406
B (cm^{-1})	6377	6662
OH(D) (Å)	0.981	0.972
ω_{01} (cm^{-1})	1.4	0
ω_{03} (cm^{-1})	3107	2382
ω_{12} (cm^{-1})	2967	2380
$D\alpha^2$	35.3	35.3

Table 4-6

Relative ν_s(OH) transition probabilities for $(HCOOH)_2$ and $(HCOOD)_2$

	Transition	Frequency (cm^{-1})	Relative transition probability	Relative intensity
$(HCOOH)_2$	$\|0\rangle \rightarrow \|3\rangle$	3107	100	100
	$\|1\rangle \rightarrow \|2\rangle$	2967	99	94
$(HCOOD)_2$	$\|0\rangle \rightarrow \|3\rangle$	2382	68	52
	$\|1\rangle \rightarrow \|2\rangle$	2380	68	52

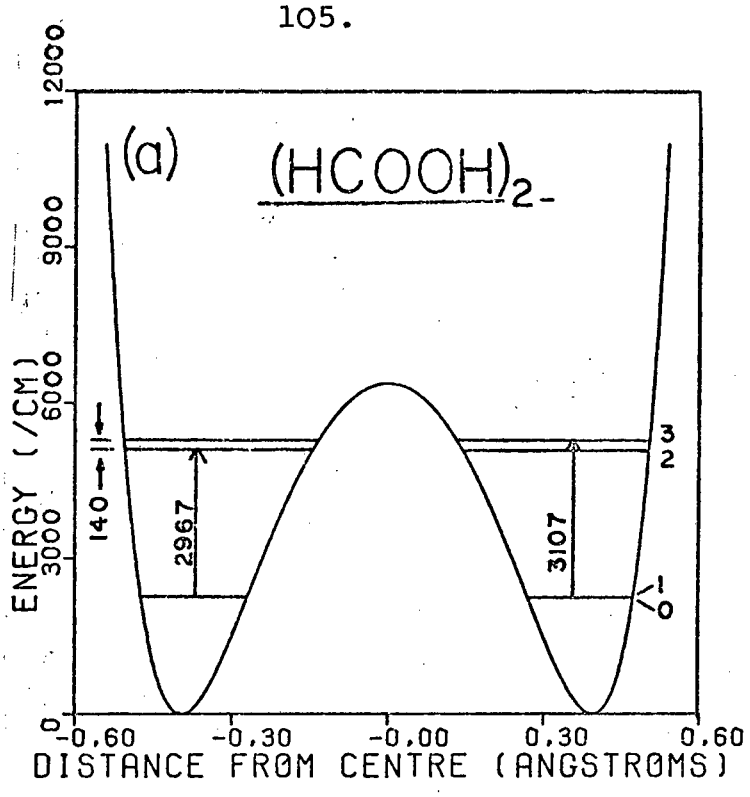

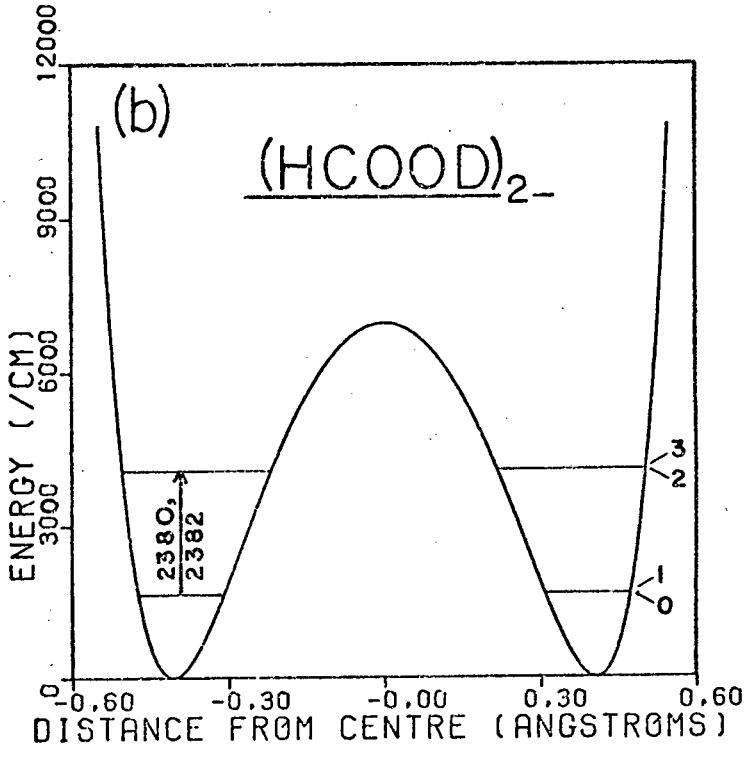

Figure 4.7. Double Morse potentials for
a) $(HCOOH)_2$
b) $(HCOOD)_2$

An approximate integrated intensity ratio may then be calculated:

$$\frac{P_{OH\ldots O}}{P_{OD\ldots O}} \approx \frac{P^{(H)}_{1\to 2} + P^{(H)}_{0\to 3}}{P^{(D)}_{1\to 2} + P^{(D)}_{0\to 3}} = 1.48.$$

This is close to the harmonic oscillator value of $\sqrt{2}$. It is therefore concluded that proton tunnelling cannot by itself explain the anomalous intensity ratio.

Of course, any conclusions drawn from the calculations are critically dependent on the assignment of the transitions in (4.1) being correct. Although (4.1) seems an obvious first choice (and the simplest possibility), other assignments are possible in view of the unknown contribution of sum and difference bands involving changes in the quantum numbers of the Q^+ and Q^- modes.

Indeed, Excoffon and Marechal proposed a different assignment, viz.

$$\omega_{12} = 2688\ \text{cm}^{-1}$$

$$\omega_{03} = (2688 + 140)\ \text{cm}^{-1} = 2828\ \text{cm}^{-1}. \qquad (4.2)$$

However, no parameters could be found for the double Morse potential model which would yield this assignment.

The only other assignment which is substantially different from either of the above is one of the form

$$\omega_{12} \approx 2550\ \text{cm}^{-1}$$

$$\omega_{03} \approx 3000\ \text{cm}^{-1} \qquad (4.3)$$

which attempts to identify the two main features of the spectrum with the $|1\rangle\to|2\rangle$ and $|0\rangle\to|3\rangle$ transitions respectively. It was possible to obtain double Morse potential parameters which yielded this assignment and at the same time predicted that the 2299 cm^{-1} band was a $(|1\rangle\to|2\rangle) - (|0\rangle\to|3\rangle)$ doublet

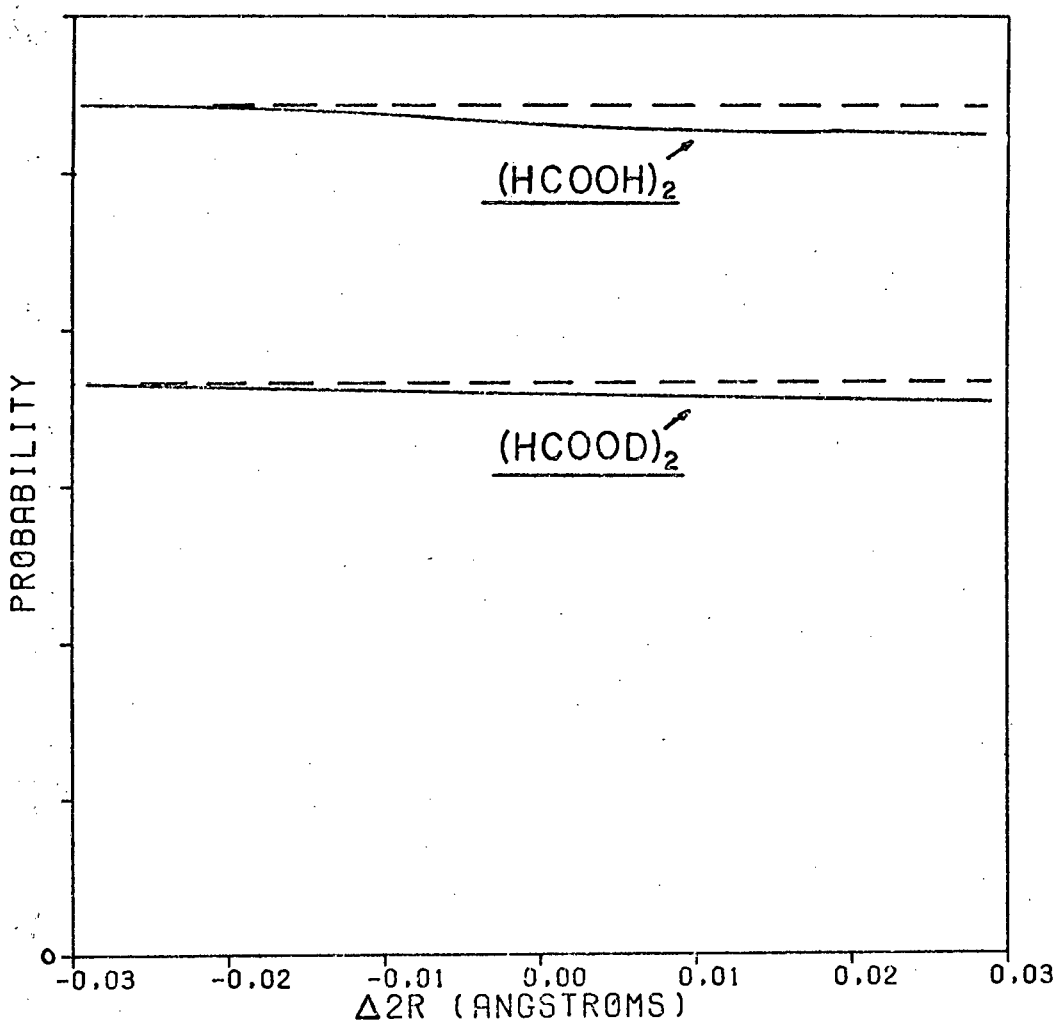

Figure 4.8. Transition Probability ratios for $(HCOOH)_2$ and $(HCOOD)_2$, as functions of O...O distance.

to 300K), whereas the above analysis yields only a 2.5% decrease in $P_{OH...O}$ and a 1.7% decrease in $P_{OD...O}$ for the same increase in 2R. So while this effect is in the right direction, it is unlikely that the decrease in $P_{OH...O}$ and $P_{OD...O}$ can be explained entirely in terms of the change in the well shape with temperature. This provides indirect support for Auvert and Marechal's suggestion that electrical anharmonicity is responsible for the decrease in $P_{OH...O}$ and $P_{OD...O}$ with temperature.

Finally an attempt was made to predict the bandshapes for formic acid and deuterated formic acid dimers, using the assignment (4.1) and proceeding by a method similar to that used for the chromous acid bandshapes. Without adding any other broadening mechanisms beside O...O thermal variations of r.m.s. amplitude of 0.01Å and an instrumental width of 6 cm^{-1}, it was found that the qualitative features of the bandshapes could be reproduced. i.e. the narrow single band centred at about 2300 cm^{-1} for $(HCOOD)_2$, the broad band stretching from about 2600 cm^{-1} to 2900 cm^{-1} for the $|1>\rightarrow|2>$ $(HCOOH)_2$ transition and the strong narrow band at about 3000 cm^{-1} for the $|0>\rightarrow|3>$ $(HCOOH)_2$ transition. These predicted profiles are reproduced in figures 4.9 and 4.10.

Of course this represents only a very crude calculation of the envelope of the underlying vibrational transitions, which involve changes in the quantum numbers of both the ν_s(OH) and ν_σ(O...O) modes. These were calculated in considerable detail by Excoffon and Marechal, but without including protonic tunnelling directly into the Hamiltonian of the system.

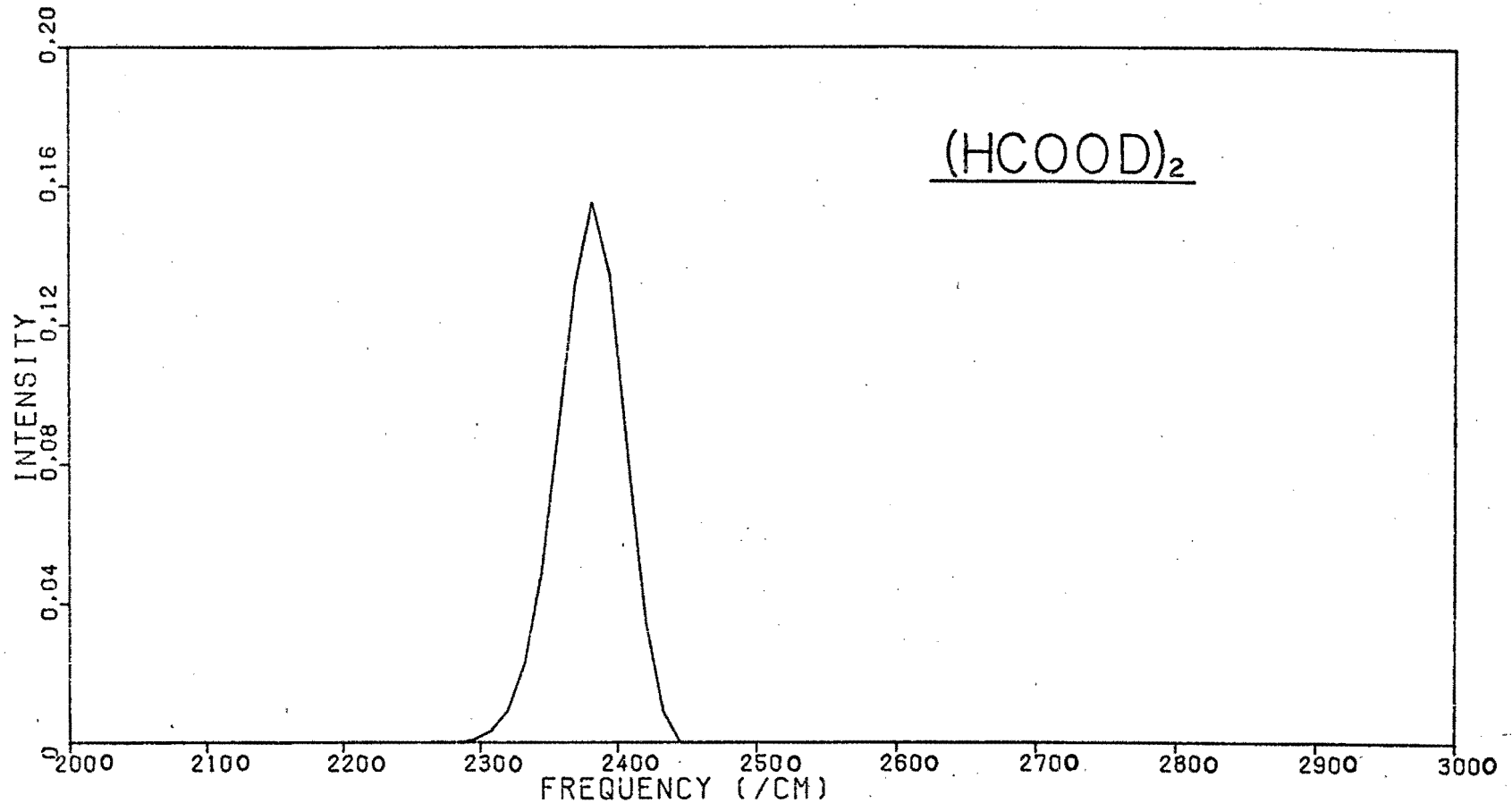

Figure 4.9. Predicted $(HCOOD)_2$ infrared band profile. The major peak is an unresolved doublet. cf. Figure 4.2.

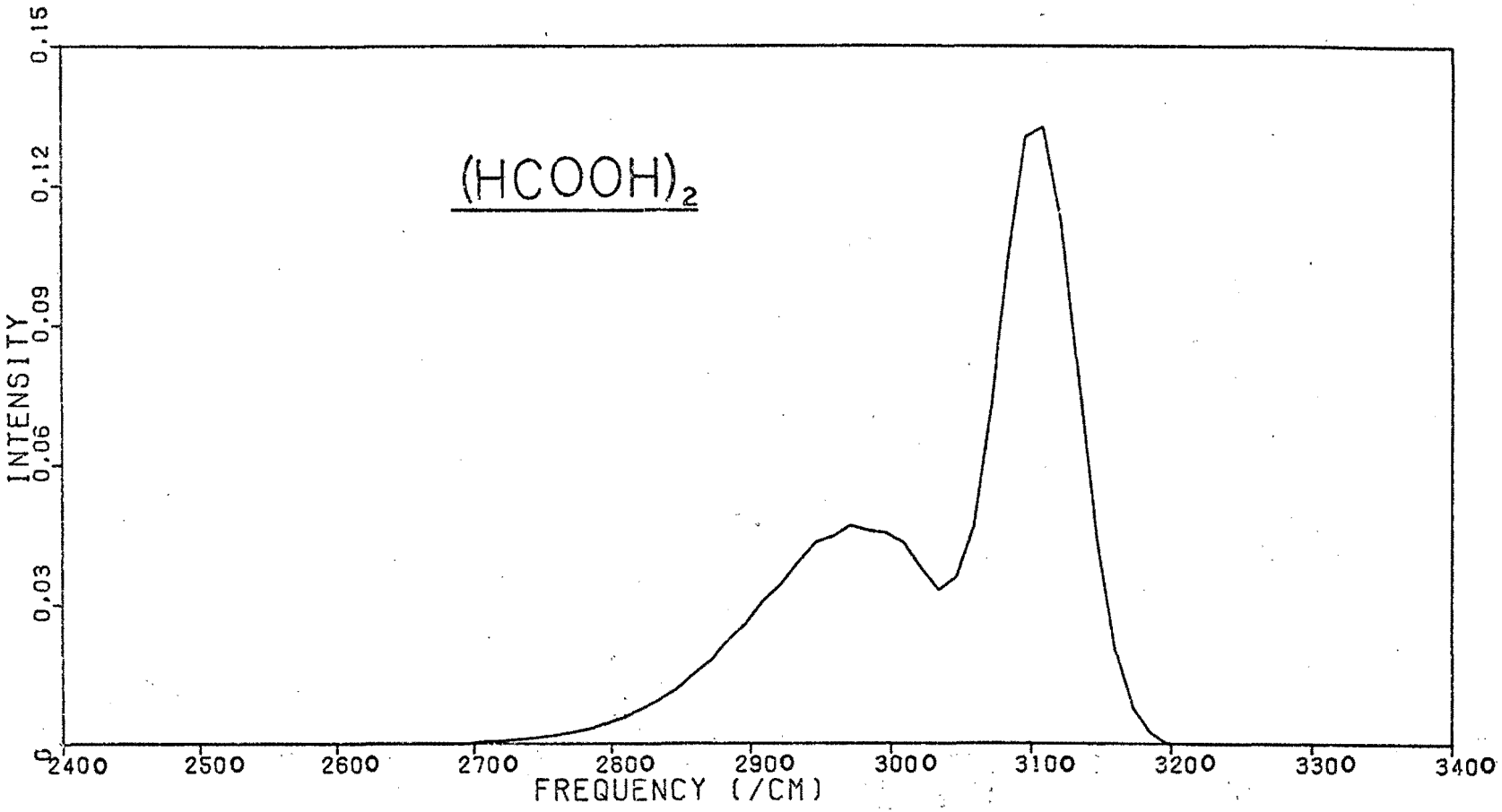

Figure 4.10. Predicted $(HCOOH)_2$ infrared band profile. cf. Figure 4.1.

4.3 Adipic Acid IR Spectra

The above analysis of the spectra of formic acid dimers cannot be repeated in as much detail for adipic acid crystals because

i) there appear to be no crystallographic data available at present for deuterated adipic acid and

ii) the IR spectrum of the ν_s(OH) vibrations in the crystal is even more difficult to interpret, and no detailed assignment of the underlying transitions has been published.

Instead, a simple and rather crude method will be used to estimate the adipic acid protonic potential wells directly from the formic acid results.

According to Housty and Hospital (1965) the O...O distance in adipic acid crystals is 2.64Å, i.e. 0.06Å shorter than the O...O bond length in the gas phase formic acid dimer. However, as both these substances contain similar $(COOH)_2$ cycles, it seems reasonable to assume that the protonic potential well in the adipic acid cycle can be modelled in terms of the double Morse potential by using the same parameters D, α and r_o (but not, of course, R) as were obtained for the formic acid cycles. Thus putting $2R = 2.64$Å to correspond to the above mentioned O...O distance and using the D, α and r_o given in table 4.5 for formic acid, the adipic acid transition frequencies were predicted to be

$$\omega_{03} = 3034 \text{ cm}^{-1}$$

$$\omega_{12} = 2679 \text{ cm}^{-1}.$$

If this is compared with the experimental spectrum, figure 4.3, it appears to be reasonable as the ν_s(OH) observed band

stretches from 2500 cm^{-1} to 3200 cm^{-1} and appears to be divided into two main sub-bands, with similar intensities. The ground state splitting is calculated to be about 6.2 cm^{-1}.

To predict the transition frequencies for deuterated adipic acid by this method, it will be necessary to assume some value for the O...O distance. This was taken to be 2.66Å on the assumption that the magnitude of the Ubbelohde effect is the same for adipic and formic acids. The computed transition frequencies are then

$$\omega_{03} = 2300 \text{ cm}^{-1}$$
$$\omega_{12} = 2290 \text{ cm}^{-1}. \qquad (4.5)$$

This again appears to be reasonable if one assumes that this predicted band corresponds to the observed one at about 2250 cm^{-1} and that the observed band is an unresolved doublet. The details of these double Morse potentials used for adipic and deuterated adipic acid are given in table 4.7.

The transition probabilities were calculated for adipic acid using the above parameters and equation (2.51). Table 4.8 summarizes the resulting transition probabilities. The ratio $P_{OH...O}/P_{OD...O}$ was found to be 1.51, again closer to the harmonic oscillator result of $\sqrt{2}$ than to the observed value of about 2. The variation of $P_{OH...O}$ and $P_{OD...O}$ with R were calculated and, assuming that both the OH...O and OD...O distances decreased by 0.03Å on cooling from room temperature to 30K, the temperature variation of these quantities determined. The variation was again estimated to be about 2%, far less than the 20% variation observed by Auvert and Marechal. As in the case of formic acid (see above) one is led to conclude that

Table 4-7

Estimated potential well parameters for Adipic and deuterated Adipic Acid

	Adipic acid	Deuterated adipic acid
r_o (Å)	0.950	0.950
D (eV)	1.81	1.81
α ($Å^{-1}$)	4.42	4.42
$R-r_o$ (Å)	0.37	0.37
x_m (Å)	0.36	0.37
B (cm^{-1})	5420	5730
OH(D) (Å)	0.985	0.975
ω_{01} (cm^{-1})	6.2	0.1
ω_{03} (cm^{-1})	3034	2297
ω_{12} (cm^{-1})	2679	2285
$D\alpha^2$	35.3	35.3

Table 4-8

Relative ν_s(OH) transition probabilities for Adipic and deuterated Adipic acid crystals

	Transition	Frequency (cm^{-1})	Relative transition probability	Relative intensity
Adipic acid	|0>→|3>	3034	92	100
	|1>→|2>	2679	100	96
D-adipic acid	|0>→|3>	2297	64	53
	|1>→|2>	2285	64	53

i) the anomalous intensity ratio cannot be explained in terms of the oscillator well shape alone and

ii) although the model predicts both $P_{OH...O}$ and $P_{OD...O}$ to decrease with increasing temperature, the observed effect is far more pronounced than that calculated.

Both these considerations tend to support Auvert and Marechal's hypothesis regarding the importance of electrical anharmonicity.

Regarding the structure of the ν_s(OH) band, it appears that it is indeed composed of two bands, with maxima given approximately by (4.4), which may well have somewhat different polarizations considering that the bond is bent. The upper state splitting is estimated to be 355 cm^{-1} (511K). This therefore supports Auvert and Marechal's interpretation of the varying ν_s(OH) polarization given in section 4.1.2.

4.4 Polymorphism, Proton Tunnelling and Crystal Defects

An approximate protonic energy level scheme for crystalline formic acid can be computed in a way similar to that which was used for crystalline adipic acid in the previous section. The values of D, α and r_o obtained for the dimer (table 4.5) are retained and 2R is set equal to the crystalline O...O distance of 2.58Å (Holtzberg *et al.* (1953)) and the energy eigenvalues are then computed. This leads to the following transition frequencies:

ω_{01} = 23 cm^{-1}

ω_{12} = 2323 cm^{-1}

ω_{03} = 3023 cm^{-1}

The frequencies ω_{12} and ω_{03} are in good qualitative agreement with the observed ν_s(OH) band for the crystal - see Zelsmann and Marechal (1974).

The $|0\rangle \rightarrow |1\rangle$ transition frequency of 23 cm^{-1} (6.9 x 10^{11} s^{-1}) implies that in the absence of strong interactions between neighbouring protons (see below) the protons will tunnel rapidly from one site to the other and any X-ray diffraction experiment will "see" the averaged proton motion and also the C=O and C-O bond lengths as averaged out. In such a case it is not appropriate to speak of the proton as being localized in one or other of the potential minima, but it is rather more accurate to refer to the proton as being in either the symmetric ground state or the antisymmetric first excited state (represented by wavefunctions similar to those in figure 3.14). The tunnelling frequency of dimeric formic acid has been calculated to be about 1.4 cm^{-1} (4.2 x 10^{10} s^{-1}) in section 4.2 above which is certainly slow enough for gas phase electron diffraction experiments to "see" the proton as localized in one or other of the potential minima and thus also to distinguish between the C=O and C-O bond lengths. The above evidence confirms the order-disorder interpretation of the phase transition in crystalline formic acid given by Zelsmann *et al.* (see section 4.1.4 above).

Below the transition temperature the interactions between neighbouring protons are strong enough to cause a collective ordering of the protons in the crystal. X-ray diffraction experiments performed below the transition temperature should therefore see the C=O and C-O bonds as distinct. (Such experiments would provide a useful test of

this interpretation of the phase transition).

The dynamics of the protons in a chain of formic acid molecules in the crystal can be treated as a first approximation in terms of the transverse Ising model. As a very crude approximation consider the protons to be independent oscillators in a double minimum potential and occupying either of the two lowest-lying (symmetric and antisymmetric) states. This type of approximation has yielded good results for the KDP (potassium dihydrogen phosphate) system where there are four protons per unit cell. (See chapter 5.) The Hamiltonian of the system may be written as

$$H = -\Omega\Sigma_i S_i^x - \tfrac{1}{2}\Sigma_{i,j} J_{ij} S_i^z S_i^z$$

where S_i^x and s_i^z are pseudospin operators (defined in chapter 5), Ω is the single particle tunnelling frequency and J_{ij} is the interaction between the ith and jth proton. A random phase approximation treatment of this Hamiltonian shows that the system exhibits an order-disorder transition at a temperature T_c given implicitly by

$$J = 2\Omega \tanh(\Omega/2kT_c)$$

where $J = \Sigma_i J_{ij}$ is the interaction of a single proton with the remaining hydrogen-bonded protons in the chain.

If $\Omega = 23$ cm^{-1} and $T_c = 207$K for crystalline formic acid, then $J = 576$ cm^{-1}. (This is of the same order of magnitude as the values obtained for KDP.) Should a single proton be displaced from its position in an otherwise ordered crystal of formic acid, then this value also represents the energy associated with the defect.

4.5 Conclusion

In the above analysis it has been shown how the IR spectrum of certain carboxylic acids can be interpreted using the double Morse potential model. For formic acid cyclic dimers an argument has been presented which suggests that each proton tunnels independently of the other when it is in its excited state. The ground state splitting is however not large enough to permit any tunnelling of the protons when they are both in their ground states. The dipolar interaction also then keeps the protons localized on opposite sides of the molecule, i.e. one "left" and one "right". For formic acid dimers, the ν_s(OH) band was shown to be comprised of two bands, one at 2967 cm^{-1} and the other at 3107 cm^{-1}, corresponding to the $|1\rangle\rightarrow|2\rangle$ and the $|0\rangle\rightarrow|3\rangle$ transitions respectively. The ν_s(OD) band at 2299 cm^{-1} for deuterated formic acid dimer was predicted to be a doublet consisting of both the $|1\rangle\rightarrow|2\rangle$ and the $|0\rangle\rightarrow|3\rangle$ transitions. These assignments are slightly different from those of Excoffon and Marechal, but the 140 cm^{-1} upper state splitting suggested by these authors is confirmed.

For adipic acid crystals, approximate calculations showed that the ν_s(OH) band was actually composed of two separate bands, one at 3034 cm^{-1} and the other at 2679 cm^{-1}, which correspond to the $|1\rangle\rightarrow|2\rangle$ and the $|0\rangle\rightarrow|3\rangle$ transitions respectively. The ν_s(OD) band for deuterated adipic acid crystals was predicted to be a doublet consisting of both the $|1\rangle\rightarrow|2\rangle$ and the $|0\rangle\rightarrow|3\rangle$ transitions. This agrees with the suggestion of Auvert and Marechal that, on the basis of polarization measurements, the ν_s(OH) band does consist of

two separate bands. It also agrees with their postulate that tunnelling in the upper state is possible and that this may lead to the non-extinguishability of the C=O band at high temperatures.

Regarding the anomalous intensity ratios, it was found that although the model (which neglected electrical anharmonicity) predicted that $P_{OH...O}/P_{OD...O}$ was greater than $\sqrt{2}$ for both these substances, the difference was nowhere near as great as that observed. This forces one to conclude that the effect cannot be interpreted in terms of the well shape or its change on deuteration alone and that electrical anharmonicity should be taken into account. However, in the case of short hydrogen bonds, cf. chromous acid, a probability ratio of about 2 can arise quite naturally from the shape of the potential function and from the presence of a relatively large Ubbelohde effect. This can be seen qualitatively as follows. The transition probability (given by (2.52)) depends on the dipole transition matrix element of the proton between the two states involved. Figure 4.11 illustrates the potential wells for CrOOH and CrOOD, together with the energy levels and wavefunctions for the $|1\rangle$ and $|2\rangle$ single particle states. The barrier height for the CrOOD potential is higher than that for CrOOH and the n=1 and n=2 energy levels are situated lower down in the CrOOD wells than they are in the CrOOH wells. This results in the outermost peaks of the CrOOD wavefunctions being considerably narrower than those of the CrOOH wavefunctions. The dipole matrix elements $\langle 1|x|2\rangle$ will thus be considerably larger for CrOOH than for CrOOD, as borne out by Table 3.9.

CrOOH

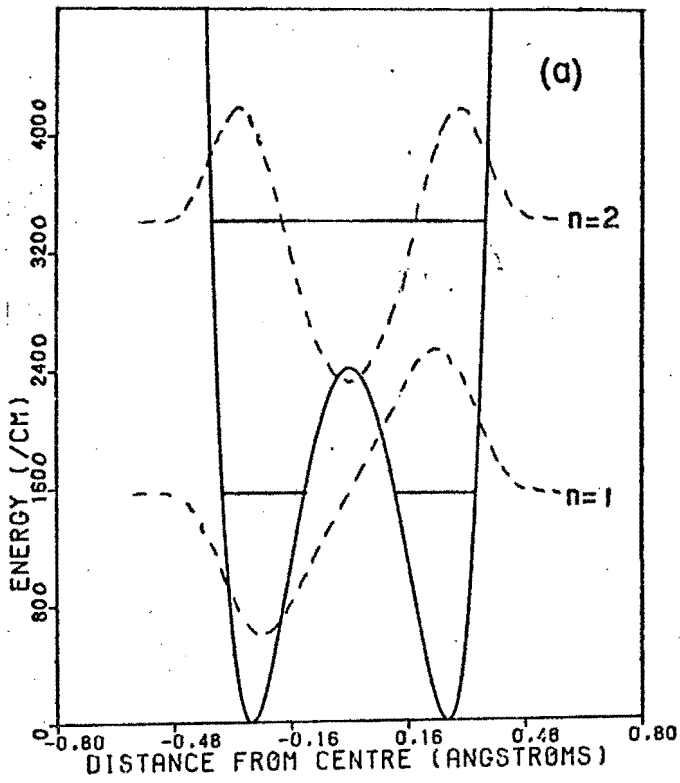

CrOOD

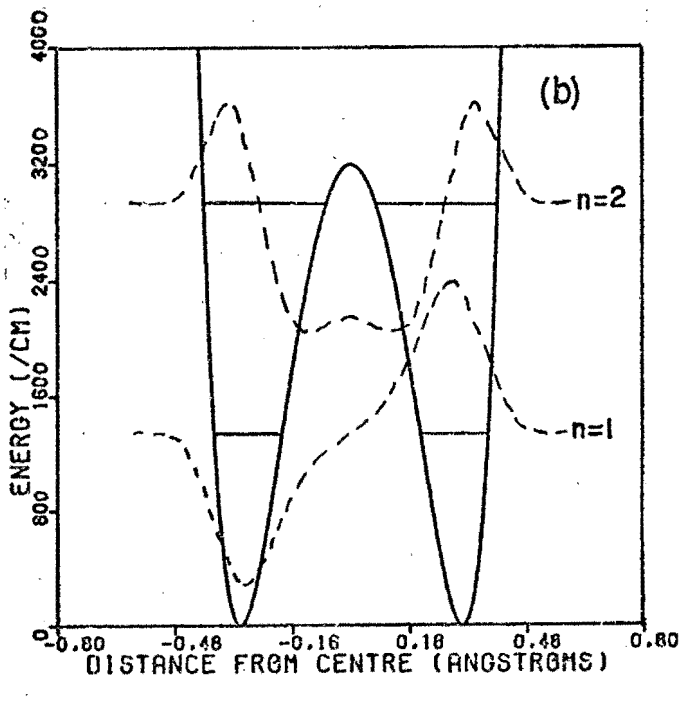

Figure 4.11. Overlap of CrOOH and CrOOD wavefunctions. Note that the peaks in the CrOOD wavefunctions are considerably narrower than the corresponding peaks for CrOOH. The amplitudes however remain comparable.

$P_{OH...O}$ and $P_{OD...O}$ are also predicted from the model to increase as 2R decreases, but again this amount is insufficient to account for the observed effect. Electrical anharmonicity must be taken into account. If tunnelling is indeed significant, as the above calculations have suggested, then Excoffon and Marechal's theory of the coupling between the ν_s(OH) and ν_σ(O...O) modes in the hydrogen-bonded cyclic dimers needs revision. Instead of treating the ν_s(OH) motion as an harmonic oscillator, it should be treated as a particle moving in a double minimum potential. The wavefunctions so obtained should be used to define the effective potentials for the ν_σ(O...O) modes in different states of ν_s(OH) excitation. Clearly such calculations would be very difficult. No attempt has been made in this chapter to study the coupling, which is responsible for the band broadening and structure.

It is also important to take into account the extent to which in the crystalline state the O...O vibrations can be treated as localized modes. Complete localization has been assumed by Zelsmann and Marechal in their treatment of formic acid and by Auvert and Marechal in their treatment of adipic acid. Whereas this might be a reasonable assumption in the case of the latter crystals, it is more difficult to justify in the case of formic acid crystals. Our own treatment of attempting to estimate the bandshapes in terms of the mean square displacement of the O...O distances is very crude and cannot replace a full dynamical treatment of the system.

The phase transition in crystalline formic acid has been discussed. The magnitude of the proton tunnelling frequency has been shown to be of the right order of magnitude to support the order-disorder interpretation of the phase transition. Similarities have been pointed out between this system and the ferroelectric KDP. It would be of interest to develop a theory of the phase transition in crystalline formic acid using the ideas contained in the KDP theory.

CHAPTER FIVE

TUNNELLING IN KDP-TYPE FERROELECTRICS

5.1 Introduction

The phenomenon of ferroelectricity may be described as the onset of spontaneous polarization in a crystal when it is cooled below a specific temperature. This spontaneous polarization must also be reversible or at least re-orientable under the influence of an external stress or electric field in order for the crystal to be termed "ferroelectric".

One class of ferroelectrics that is particularly interesting from the lattice-dynamical point of view is the KDP-type of ferroelectric, KDP standing for potassium dihydrogen phosphate (KH_2PO_4), which is the prototype of the class. Other members of the class include RbH_2PO_4, CsH_2PO_4, KH_2AsO_4 RbH_2AsO_4 and CsH_2AsO_4 and the deuterated forms of all the preceding compounds. KDP was first discovered to be ferroelectric in 1935 and has since then been the subject of intensive theoretical and experimental research, especially during the last 20 years.

The ferroelectric phase transition in KDP can be briefly described as follows. In the tetragonal high-temperature phase (space group $I\bar{4}2d$) the crystal structure has four $K\text{-}PO_4$ groups per unit cell, with hydrogen bonds in the x-y plane joining neighbouring PO_4 tetrahedra. See Figure 5.1. When the temperature of the crystal is below the transition (or Curie) temperature of 123K, the protons are displaced away from the centre of the hydrogen bonds in an ordered fashion in the crystal, two protons being associated with each PO_4 tetrahedron. The protonic ordering is accompanied

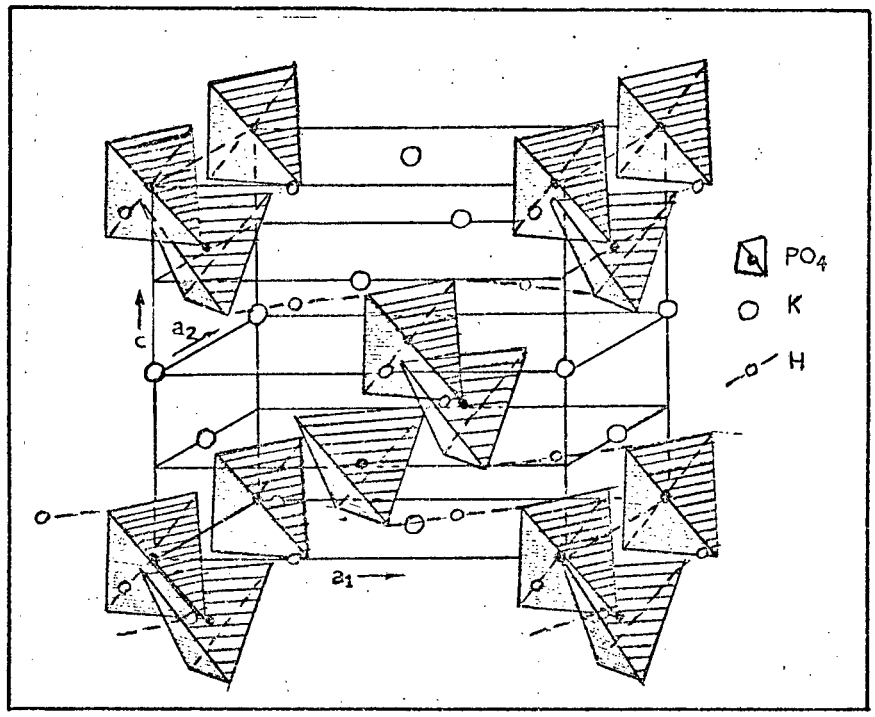

Figure 5.1. Structure of KH_2PO_4. From Slater (1941)

by a distortion of the $K-PO_4$ sub-lattice which results in a spontaneous polarization along the c-axis, at approximately 90° to the plane of the hydrogen bonds, cf. Bacon and Pease (1953, 1955) and Frazer and Pepinsky (1955). The application of an external electric field is then capable of causing each proton to change position in its bond to a symmetrically displaced site on the opposite side of the centre, cf. Bacon and Pease (1955). This describes the low-temperature or 'ferroelectric' phase of the crystal and is characterized by the space group Fdd2. Above the Curie temperature, each proton has an elongated probability distribution about the centre of the bond and it has not yet been possible to distinguish crystallographically whether

i) The protons are making large-amplitude anharmonic vibrations about the centre of the bond, or

ii) The protons are randomly distributed between the two off-centre sites mentioned above or

iii) Proton tunnelling within each bond is causing the two off-centre sites each to have an occupancy of half a proton, cf. Bacon and Pease (1955).

This describes the 'paraelectric' phase of the crystal and is characterized by the space group $I\bar{4}2d$.

Two fundamental components of the dynamics of the phase transition in KDP are

i) The collective protonic ordering mechanism and

ii) The coupling between the protonic system and the lattice modes of the remainder of the crystal.

Neither the protonic ordering or the heavy atom displacements have alone been able to explain the dynamics of the phase

transition. Although a large number of models have been developed, they tend either to be too simple to account for all the observed phenomena, or to involve so many undetermined parameters as to be incapable of verification.

A major difficulty, as has been seen from the discussion of the crystal structure, is that little is known about the form of the potential in which the proton moves. The main advance made in this thesis is that a much more precise protonic potential is used than in any previous work. This enables one to take into account both the temperature and pressure dependence of the proton tunnelling frequency. Hitherto the temperature dependence has always been neglected. The temperature and pressure dependence will be determined entirely from the existing crystallographic and infrared spectroscopic data using the ideas originally put forward by Lawrence and Robertson (1980). Having available a theoretical estimate of the temperature and pressure dependence of the proton tunnelling frequency allows us to re-analyse the temperature and pressure dependence of the existing soft-mode Raman scattering data, and to achieve a synthesis of the neutron diffraction, Raman and infrared spectroscopy data. Some aspects of the existing controversy regarding the nature of the proton-proton interactions will also be resolved.

Section 5.2 presents a brief resumé of the development of KDP theories and Section 5.3 some of the relevant experimental data. No attempt has been made at completeness, but sufficient background is presented to cover the subsequent analyses. (For a more complete discussion of the KDP problem, the reader is referred to the reviews by Blinc and Žekš (1974) and

Lines and Glass (1977)). Section 5.4 shows how estimates of the tunnelling frequencies of KDP and DKDP can be obtained from the available infrared spectra. Section 5.5 discusses the renormalization of the single-particle tunnelling frequency that is necessary when considering the interactions of the protonic system with the remainder of the lattice. Section 5.6 re-analyses existing Raman soft-mode data and Section 5.7 shows how estimates of the temperature and pressure variation of the proton-proton interaction J may be obtained from this re-analysis. Section 5.8 examines the problem of the soft-mode damping in the light of the preceding sections. Section 5.9 summarizes the chapter and suggests further development.

5.2 Microscopic Models of the Phase Transition

Initial attempts at explaining the phase transition mechanism in KDP concentrated only on the thermodynamics of the phase transition and made no attempt to explain the underlying microscopic dynamics. This review nevertheless starts with a description of the early models as they form the basis of recent, more refined models.

5.2.1 Static Descriptions

Slater (1941) was the first to suggest that protonic ordering was responsible for the ferroelectric phase transition in KDP. In terms of his model, the only possible ordered configurations that can arise for the protons about any given PO_4 tetrahedron in the ferroelectric phase are those which associate two protons with each given tetrahedron. (All other configurations are considered to be high-energy

configurations and are neglected.) Six possible two-proton (low-energy) configurations exist and are of two types, illustrated in Figure 5.2:

i) Those that place the two protons at vertices that lie in the same x-y plane about the tetrahedron, and

ii) Those that place the two protons at vertices of the tetrahedron that lie in different x-y planes.

The former configurations are taken to have energy 0 and the latter configurations then have a slightly higher energy ε. Only the former configurations give rise to a dipole moment along the c-axis. A thermodynamic analysis of this system then showed that it did indeed exhibit the required order-disorder phase transition at a non-zero transition temperature. Neutron diffraction results (Bacon and Pease (1955)) later confirmed the existence of this protonic ordering in the ferroelectric phase. However, the theory predicts a first-order phase transition, whereas the observed transition is near second-order.

Takagi (1948) showed that the second-order nature of the phase transition could be explained by also taking into account configurations having one proton or three protons associated with a given PO_4 tetrahedron. These configurations have a higher energy w, where $w>\varepsilon>0$. However, neither model can explain why the Curie temperature changes on deuteration from 123K to 229K. Isotopic substitution probably does not in itself appreciably change the Slater energies and hence the phase transition temperature would be expected on grounds of the Slater-Takagi model to be little changed on deuteration. This suggested that the role of the protons in the

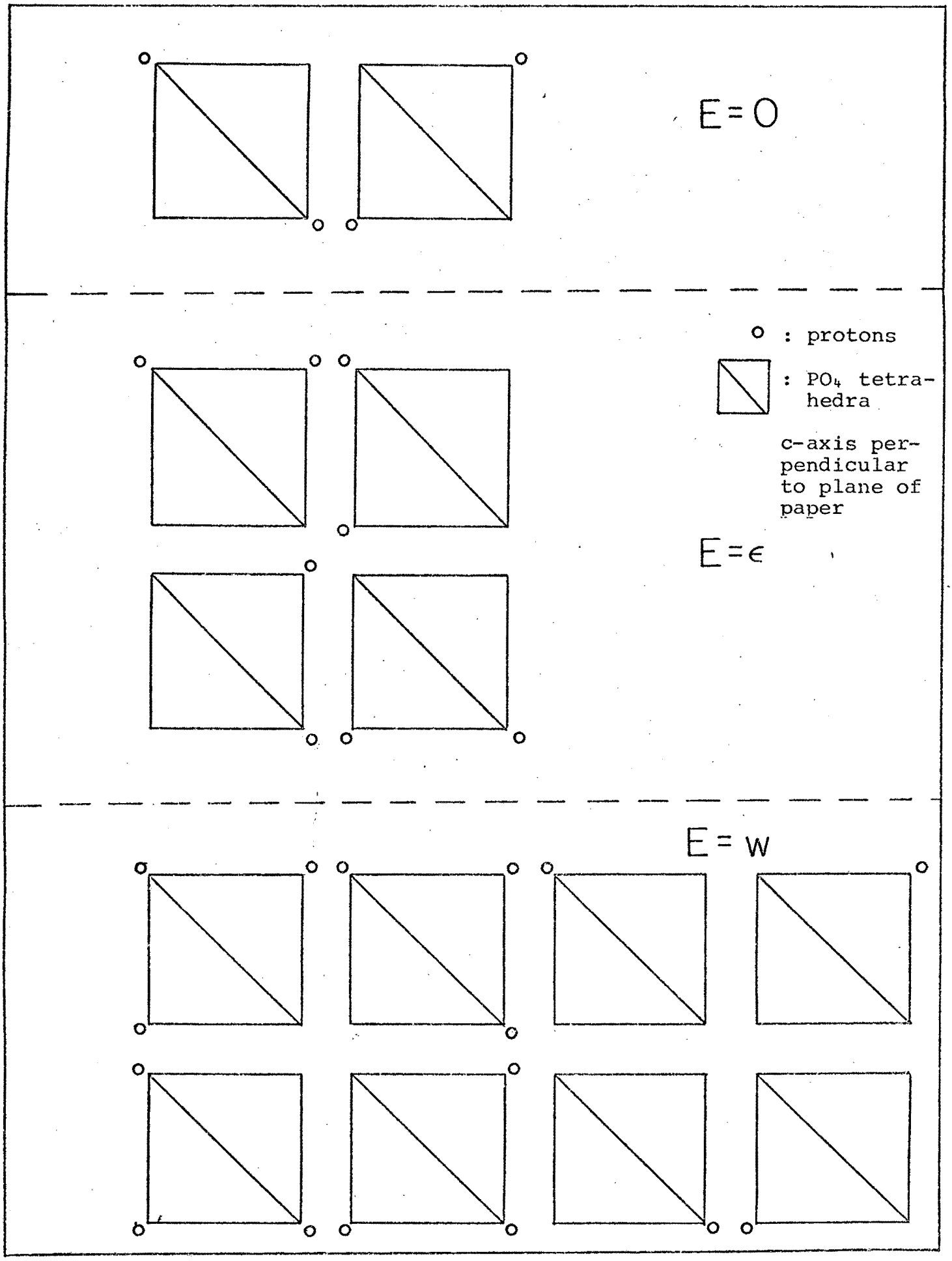

Figure 5.2. Slate-Takagi protonic configurations. The six two-proton configurations with energies E=0 or E=ε are those considered by Slater. Takagi includes eight further one- or three-proton configurations with energy E=w>>ε.

phase transition was by no means yet fully understood. X-ray diffraction (Frazer and Pepinsky (1953)) and neutron diffraction experiments (Bacon and Pease (1953)) were also later to establish that the bulk of the spontaneous polarization was in fact due not to the ordering of the protons but rather to the simultaneous displacement of the heavy atoms themselves along the c-axis.

Blinc (1960) invoked proton tunnelling in the hydrogen bonds to account for the observed change in Curie temperature on deuteration. As protons tunnel more freely than deuterons in a given double minimum potential and as any tunnelling motion would tend to oppose the onset of order with diminishing temperature, this would account for the relatively lower Curie temperature in KDP when compared with DKDP. The crucial drawback of this theory is that it neglects the heavy ion motion and hence cannot explain why the crystal becomes polarized along the c-axis. Furthermore, it is not clear that tunnelling is necessary if the Slater parameters change on deuteration.

Silsbee, Uehling and Schmidt (1964) examined an extended Slater-Takagi model of Senko (1961) which took into account both long and short-range protonic interactions, but neglected proton tunnelling. They applied this to the shape of the spontaneous polarization curve for DKDP and showed it could be well predicted but that the transition entropy was overestimated. It also appeared that the isotope effect on the Curie temperature can to some extent be reproduced if the Slater energy ε for different particles in the hydrogen bond is assumed to vary as the square of the off-centre

distance of the particle. (It is important to note at this stage that this assumption was made only in the context of deuteration. As will be seen in Section 5.7, later authors followed this uncritically, assuming that it gave an indication of how the Slater parameters changed on lattice compression. We will show that this is fallacious.)

Blinc and Svetina (1966a,b) performed a cluster analysis of the protonic system in KDP, assuming that the protons are rigidly coupled to the lattice through dipolar interactions. Both long- and short-range proton-proton interactions were taken into account: the short-range interactions being those between protons about a given PO_4 group and the long-range interaction being that between a given proton and the remaining protons in the lattice not belonging to the same PO_4 group. Proton tunnelling was included, as well as the polarizing effect of the proton tunnelling motion on the lattice, as originally put forward by Blinc and Ribarič (see Section 5.5). Blinc and Svetina assume, following Silsbee, Uehling and Schmidt, that the Slater energies vary as the square of the off-centre displacement of the particle (proton or deuteron) on deuteration. The model was developed in the zero-order (molecular field) approximation as well as in the two-particle cluster approximation (which takes into account some of the short-range interactions) and the four-particle cluster approximation (which takes into account all the short-range interactions). Blinc and Svetina predicted, using the latter approximation, that the phase transition in KDP could be of either first or second order, depending on the values of the parameters involved. Realistic transition

entropies were also obtained. A major difficulty with the Blinc-Svetina theory is that the rigid coupling of the proton system to the lattice is unphysical.

Blinc and Žekš (1968) extended the Blinc-Svetina static four-particle cluster model to analyse the experimental results of Umebayashi, Frazer, Shirane and Daniels (1967) and Samara (1967) concerning the effects of hydrostatic pressure on the Curie temperature and Curie constant for KDP and DKDP. The model used a double harmonic oscillator model (described in Section 5.3 below) to estimate the change in the tunnelling frequency on compression. They assumed, as a first approximation, that the sole effect of compression is to change the separation δ between the two off-centre protonic sites in the hydrogen bonds. If this is true, then the Slater parameter ε as well as the long-range interaction parameter γ vary in proportion to δ^2 on compression. The model was then capable of adequately explaining the variation of the Curie temperature and Curie constant with pressure. It was also shown that it was only by retaining proton tunnelling in the Blinc-Svetina model that the change in $\partial T_c/\partial P$ with isotopic subsitution could be explained.

Vaks and Zinenko (1973) examined the Blinc-Svetina model and showed that by making expansions in terms of small parameters, explicit expressions could be obtained for the free energy of the system. Blinc and Svetina only managed to obtain the free energy numerically and thus the Vaks-Zinenko results are of more ready application to other KDP-type ferroelectrics. Following Vaks and Larkin (1965), Vaks and Zinenko also showed explicitly how the direct proton-proton interaction depends on the lattice dimensions as well as on the

proton-proton separation. More will be said about this later.

Torstveit (1979) developed the Blinc-Svetina four-particle cluster model to allow in a consistent fashion for the pressure and deuteration dependence of the various parameters. Torstveit assumed with Blinc and Žekš (1968) that the parameters ε and w and the long-range interaction parameter γ are all proportional to the square of the off-centre distance of the proton or deuteron on compression of the lattice. The pressure dependence of the protonic tunnelling frequency was also estimated from the double harmonic oscillator potential and allowance was made for a possible pressure-dependence of the Blinc-Ribaric polarization factor (mentioned above). The four-particle cluster model yielded sets of ε_D, w_D and γ_D values from a fit to the spontaneous polarization curve at atmospheric pressure. It was then shown how, by assuming appropriate values for the ratio δ_H^2/δ_D^2, (which then yields ε_H, w_H and γ_H), values consistent with experiment could be obtained for the various Landau coefficients in the expression for the free energy. The pressure dependence of the various microscopic parameters then depends on the pressure dependence of δ. It was shown how, by assuming appropriate values for Ω_H and $\partial\Omega_H/\partial P$, good agreement can be obtained with the observed pressure dependence of the Landau coefficients.

5.2.2 Dynamic Descriptions

Cochran (1960) made an important advance in the general theory of ferroelectrics by showing that ferroelectric phase transitions can arise as a 'soft-mode' transition, i.e.

a heavy-atom lattice mode instability that results in a zero-frequency vibration at a certain temperature. Cochran (1961) suggested that there is in KDP a heavy-ion soft mode which results in the spontaneous polarization along the c-axis in the ferroelectric phase. The protons are then coupled to this mode and as the temperature approaches the Curie point, the protons order in such a fashion so as to enhance the local polarization set up by the soft mode.

Tokunaga and Matsubara (1966) developed a microscopic model of the protonic system in terms of the pseudospin formalism proposed earlier by de Gennes (1963). The Hamiltonian of the protonic system may be written as

$$H_p = \sum_i H_1(i) + \sum_{i>j} H_2(ij) \qquad (5.1)$$

where $H_1(i)$ denotes the single-particle part of the Hamiltonian for the ith proton and $H_2(ij)$ denotes the two-body part of the Hamiltonian for the interaction between the ith and the jth proton. Higher order interactions are neglected. Each proton is assumed to be localized in either the 'left' or 'right' hand site of its hydrogen bond.

It must be mentioned at this stage that complete localization only occurs in the limit of the splitting (due to tunnelling) of the ground state being small. If the ground state splitting is not small then the protonic wavefunctions are not completely localized.

The wavefunction of the protonic system may then be written as

$$\Psi(\underset{\sim}{r}) = \sum_i \{a_L^i \phi_L^i(\underset{\sim}{r}) + a_R^i \phi_R^i(\underset{\sim}{r})\} \qquad (5.2)$$

where the subscript L and R denote the two above-mentioned sites respectively. The coefficients a_L^i and a_R^i are considered to be Fermi operators obeying the usual commutator relationships

$$[a_L^{i\dagger}, a_L^j]_+ = [a_R^{i\dagger}, a_R^j]_+ = \delta_{ij}$$

(all mixed commutators being zero) together with the condition

$$a_L^{i\dagger} a_L^i + a_R^{i\dagger} a_R^i = 1$$

which permits only one proton to occupy any given bond. Pseudospin operators S_i^x, S_i^y and S_i^z are then defined by

$$S_i^x = \tfrac{1}{2}(a_L^{i\dagger} a_R^i + a_R^{i\dagger} a_L^i)$$

$$S_i^y = \tfrac{1}{2}(a_L^{i\dagger} a_R^i - a_R^{i\dagger} a_L^i)$$

$$S_i^z = \tfrac{1}{2}(a_L^{i\dagger} a_L^i - a_R^{i\dagger} a_R^i). \qquad (5.3)$$

The Hamiltonian then becomes

$$H_p = -\Omega \Sigma_i S_i^x - \tfrac{1}{2} \Sigma_{ij} [J_{ij} S_i^z S_j^z + K_{ij} S_i^x S_j^x + L_{ij}(S_i^x S_j^z + S_j^x S_i^z)]$$

where

$$\Omega = -2h_{LR} - \tfrac{1}{2}\Sigma_j [v_{ij}(LR,LL) + v_{ji}(LR,LL) + v_{ij}(LR,RR) + v_{ji}(LR,RR)]$$

$$J_{ij} = 2v_{ij}(LL,RR) - v_{ij}(LL,LL) - v_{ij}(RR,RR)$$

$$L_{ij} = 2v_{ij}(LR,RR) - 2v_{ij}(LR,LL)$$

$$K_{ij} = -4v_{ij}(LR,LR)$$

with

$$h_{LR} = \int \phi_L^{i*}(\underset{\sim}{r}) H_1(i) \; \phi_R^{i}(\underset{\sim}{r}) dV$$

$$v_{ij}(\mu\nu,\gamma\delta) = \int \phi_\mu^{i*}(\underset{\sim}{r}) \phi_\nu^{j*}(\underset{\sim}{r}') H_2(ij) \phi_\gamma^{j}(\underset{\sim}{r}) \phi_\delta^{i}(\underset{\sim}{r}') dV dV';$$

$$\mu,\nu,\gamma,\delta = L,R .$$

Tokunaga and Matsubara then write this as

$$H_p = -\Omega \Sigma S_i^x - \tfrac{1}{2} \Sigma_{ij} J_{ij} S_i^z S_j^z \qquad (5.4)$$

where

$$\Omega = -2h_{LR}$$

$$J_{ij} = 2v_{ij}(LL,RR) - v_{ij}(LL,LL) - v_{ij}(RR,RR)$$

as they assume that the protons are localized on different sites and hence that the integrals involving products of wavefunctions at different sites can be neglected. (This is not necessarily true if tunnelling is appreciable in the ground state.) An analysis of this Hamiltonian using the molecular field approximation showed that the system exhibited a phase transition at a temperature T_o given by

$$\frac{2\Omega}{J} = \tanh\left(\frac{\Omega}{2kT_o}\right) \qquad (5.5)$$

where

$$J = \Sigma_j J_{ij}.$$

(The notation used above is the same as that used in the review of Blinc and Žekš (1972), although the argument presented above is essentially that of Tokunaga and Matsubara. In particular Blinc and Žekš use the symbol Ω whereas Tokunaga and Matsubara replace this by the symbol 2Ω. Throughout the remainder of this thesis we will retain the convention of Blinc and Žekš.)

It is appropriate at this stage to introduce an alternative derivation of the Hamiltonian (5.4), given by Blinc and Žekš (1972, 1974). They consider each proton as occupying either the ground symmetric state of the double minimum potential well of the hydrogen bond (the + state, having energy E_0) or the 1st excited antisymmetric state (the - state, having energy E_1). This is a more general derivation as it does not pre-suppose localization of the protons. In the limit of negligible ground state splitting $E_1 - E_0$, the symmetric and antisymmetric states are related by a linear transformation to the left-right representation. However, if the splitting is appreciable, then the same linear transformations do not fully localize the protons and the resultant wavefunctions do not represent true eigenstates of the Hamiltonian. Thus the discussion in terms of symmetric/antisymmetric states is more accurate. The operators associated with these states are related in the limit of small ground state splitting to those given by Tokunaga and Matsubara by

$$a_+^i = \frac{1}{\sqrt{2}}(a_L^i + a_R^i), \quad a_+^{i\dagger} = \frac{1}{\sqrt{2}}(a_L^{i\dagger} + a_R^{i\dagger})$$

$$a_-^i = \frac{1}{\sqrt{2}}(a_L^i - a_R^i), \quad a_-^{i\dagger} = \frac{1}{\sqrt{2}}(a_L^{i\dagger} - a_R^{i\dagger})$$

and the pseudospin operators become

$$S_i^x = \tfrac{1}{2}(a_+^{i\dagger}a_+^i - a_-^{i\dagger}a_-^i)$$

$$S_i^y = \tfrac{1}{2}(a_+^{i\dagger}a_-^i - a_-^{i\dagger}a_-^i)$$

$$S_i^z = \tfrac{1}{2}(a_+^{i\dagger}a_-^i + a_-^{i\dagger}a_+^i). \qquad (5.6)$$

The Hamiltonian is then

$$H_p = -\Omega\Sigma_i S_i^x - \tfrac{1}{2}\Sigma_{ij} J_{ij} S_i^z S_j^z - \tfrac{1}{2}\Sigma_{ij} B_{ij} S_i^x S_j^x \qquad (5.7)$$

where

$$\Omega \approx E_1 - E_0 \quad \text{(the ground state splitting)}$$

$$J_{ij} = -4v^{ij}_{+-+-}$$

$$B_{ij} = 2v^{ij}_{++--} - v^{ij}_{++++} - v^{ij}_{----}$$

and

$$v^{ij}_{\mu\nu\delta\gamma} = \int \phi^{i*}_{\mu}(\underset{\sim}{r})\phi^{j*}_{\nu}(\underset{\sim}{r}')H_2(ij)\phi^{j}_{\gamma}(\underset{\sim}{r})\phi_{\delta}(\underset{\sim}{r}')\,dv\,dv';$$

$$\mu,\nu,\gamma,\delta = +,- \ .$$

If the term B_{ij} is neglected, then the Hamiltonian (5.7) is essentially the same as (5.4).

From (5.3) and (5.6) the pseudospin operator S^x_i is seen to be the tunnelling operator, which transfers protons in the L state to the R state and vice versa, S^y_i is seen to be the local current operator and S^z_i the co-ordinate dipole moment operator, giving the difference in occupation between the 'left' and 'right' hand sites.

Tokunaga and Matsubara showed that the above model is formally related to the Slater-Takagi model if the tunnelling term is neglected and only the nearest neighbour proton-proton interactions are taken into account. They also showed that by using a cluster approximation analysis of the Hamiltonian (5.4) the isotope effect on the Curie temperature could be explained. However, a difficulty encountered by the theory was that it predicted a substantial change on deuteration in the magnitude of the maximum spontaneous polarization, whereas none was observed.* This could only

---

* Samara (1973) has since shown that the apparent lack of isotopic effects on the Curie constant and the magnitude of the spontaneous polarization concluded by previous authors is erroneous and that both these quantities increase significantly on deuteration.

be overcome by modifying the model to include heavy-ion displacements as the source of the spontaneous polarization rather than it being caused through the protonic ordering itself.

Tokunaga (1966) discussed the dynamics of the Hamiltonian (5.4) and showed that the frequency of the protonic mode is given by

$$\Omega_0^2 = \Omega^2\left(1 - \frac{J}{\Omega} <S^x>\right) \qquad (5.8)$$

where $<S^x>$ is the expectation value of S_i^x in the molecular field approximation, given by

$$<S^x> = \tfrac{1}{2} \tanh(\Omega/2kT) . \qquad (5.9)$$

At the protonic ordering temperature T_o, $\Omega_0 = 0$ from (5.5), (5.8) and (5.9). This analysis was thus able to show how the onset of order in the protonic system did actually arise from the softening of a protonic mode, viz. $\Omega_0(T) \rightarrow 0$. Tokunaga pointed out that it is essential to include the heavy-ion displacements in order to understand the phase transition. However it could not be firmly established at that stage whether or not it was essential to include the protonic tunnelling. Structural changes on deuteration might well change the Slater parameters to a sufficient extent to account for the observed isotopic effects.

Kobayashi (1968) extended the model of Tokunaga and Matsubara so as to include explicitly the dynamics of the heavy-ion lattice. The heavy-ion motion was assumed to be coupled to the tunnelling motion of the protons and this coupling then entered into the Hamiltonian (5.4) via further terms in S_i^z. The system was then analysed in the random

phase approximation (RPA) and shown to exhibit a soft mode whose frequency in the paraelectric phase was given by

$$\omega_-^2 = \tfrac{1}{2}(\omega_j^2 + \Omega_0^2) - \{[\tfrac{1}{2}(\omega_j^2 - \omega_0^2)^2 + 4\langle S^x\rangle\Omega|G_i|^2\}^{\frac{1}{2}} \quad (5.10)$$

where Ω_0 is the proton ordering frequency, ω_j is the frequency of the optic phonon mode with which the protonic system interacts and G_i is the proton-lattice interaction.

This system undergoes a phase transition when $\omega_- = 0$ i.e. when $T = T_-$ given by

$$\frac{2\Omega}{\tilde{J}} = \tanh\left(\frac{\Omega}{2kT_-}\right) \quad (5.11)$$

with

$$\tilde{J} \equiv J + 4|G_i|^2/\omega_j \equiv J + 4G^*. \quad (5.12)$$

This transition temperature was estimated to be about 10K higher than the protonic ordering temperature T_o and thus illustrated the importance of the proton-lattice S^z coupling.

Cochran (1969) revised his earlier ideas concerning the heavy-ion soft mode in KDP (see above) and agreed with Kobayashi that it is the protonic collective mode, coupled to the lattice mode, that has the soft mode character. However, he pointed out that the direct proton-proton interactions are alone insufficient to cause the onset of the phase transition: it is rather the lattice-mediated protonic interactions that are responsible for the onset of the transition. The hypothetical protonic ordering temperature was estimated to be close to zero.

Godzik and Blumen (1974) considered a model similar to that of Kobayashi in construction, but assumed that the proton lattice coupling gives rise to S^x terms as well

as S^z terms in the Hamiltonian. A coupling of this nature was suggested by the fact that there are stretching displacements of the oxygen atoms in the x-y plane upon cooling through T_c. An analysis of this model using infinite order perturbation theory suggested that both the tunnelling frequency Ω and the proton-proton interactions J are reduced by the presence of the proton-lattice interaction. The formal results are very complicated and it is difficult to estimate the parameters involved from experiment. However it was shown that if reasonable values were assumed for the parameters involved then the isotope effect on the Curie temperature could to some extent be explained.

One of the most recent models of KDP is that of Havlin and Sompolinsky (1979) who attempted to analyse the dynamics of the KDP system by employing a cluster expansion for the interactions of the protons in the four hydrogen bonds about a given PO_4 group and a molecular field term for the proton lattice interactions. Their dynamical cluster model reduces in the static limit to the ordinary cluster model of Blinc and Svetina. As a cluster model it treats the short-range proton-interactions more accurately than the conventional single pseudospin per unit cell transverse Ising model. In particular the behaviour of the soft mode in the vicinity of the transition point agreed more closely with its observed behaviour. Whereas the RPA analyses of Kobayashi had predicted that $\omega_-^2 \propto (T - T_c)/T$ in the temperature region above the Curie point, this model gave $\omega_-^2 \propto (T - T_c)$ which is in far better agreement with the experimental data.

Blinc, Žekš, Sampaio, Pires and Sa Barreto (1979) have re-examined the model of Tokunaga and Matsubara (1966) and its extension by Kobayashi (1968) and have investigated the effect on the system of the inclusion of various other terms in the Hamiltonian. These additional terms include

i) A $B_{ij}S_i^xS_j^x$ term describing the effect of the tunnelling of one proton on that of another,

ii) An S^x coupling to the non-polar optical phonons,

iii) An S^x coupling with polar optical phonons, and

iv) A strong S^x coupling with the lattice, the lattice then being described by a pseudospin formalism.

The random phase approximation was used to evaluate the effect of these various terms. One of the most important results of this analysis was that inclusion of terms of the form (i) and (ii) could lead to an increase in the effective tunnelling frequency, suggesting that these effects should also be taken into account when analysing the coupled mode responses (cf. the reduction in Ω due to polarization suggested by Blinc and Ribarič (1963), referred to above). However, as will be seen later, the linear coupling which Blinc *et al.* assume between the protons and the non-polar optic phonons is inappropriate. Thus the conclusions of this paper are open to criticism in this regard.

5.3 Experimental Results

5.3.1 Infrared Spectra

Blinc and Hadži (1958) analysed the IR spectra of a number of KDP-type ferroelectrics and endeavoured to assign the ν_s(OH) bands to transitions in a double minimum potential

for these systems. For KDP the ν_s(OH) band was taken to be the doublet at 2400 cm^{-1} and 2750 cm^{-1}, these two frequencies corresponding to the $|1\rangle \rightarrow |2\rangle$ and $|0\rangle \rightarrow |3\rangle$ IR-active transitions respectively. For DKDP the ν_s(OD) band was taken to be the doublet at 1770 cm^{-1} and 2050 cm^{-1}, these frequencies also corresponding to the $|1\rangle \rightarrow |2\rangle$ and $|0\rangle \rightarrow |3\rangle$ transitions respectively. The band occurring at 1580 cm^{-1} in KDP (1200 cm^{-1} in DKDP) was assigned as a δ(OH) bending mode for KDP (δ(OD) bending mode for DKDP). The ν_s(OH) and ν_s(OD) transition frequencies were then used to determine the parameters defining a protonic potential well consisting of two overlapping harmonic oscillators:

$$V(x) = \begin{cases} \frac{1}{2}k(x + \ell)^2, & -\infty < x < B/2k\ell \\ \frac{1}{2}k(x - \ell)^2 + B, & B/2k\ell < x < \infty \end{cases} \qquad (5.13)$$

2ℓ being the distance between the potential minima, k the force constant and B an asymmetry term. A perturbation-theory analysis was used to determine the energy eigenvalues. The calculations suggested that the protonic ground state splitting was about 50 cm^{-1} and the protonic first excited state splitting was about 400 cm^{-1}. However, as will be shown later, this potential well proves to be too crude for use in any detailed study of the tunnelling.

Imry, Pelah and Wiener (1965) studied the IR absorption spectra of KDP and DKDP powder in KBr pellets at a number of temperatures both above and below the Curie temperature. Their IR spectra for KDP and DKDP are reproduced in figure 5.3. An examination of the low frequency spectrum of KDP in its paraelectric phase shows the existence of a broad band in the region 250-450 cm^{-1} and a sharp band at 530 cm^{-1}.

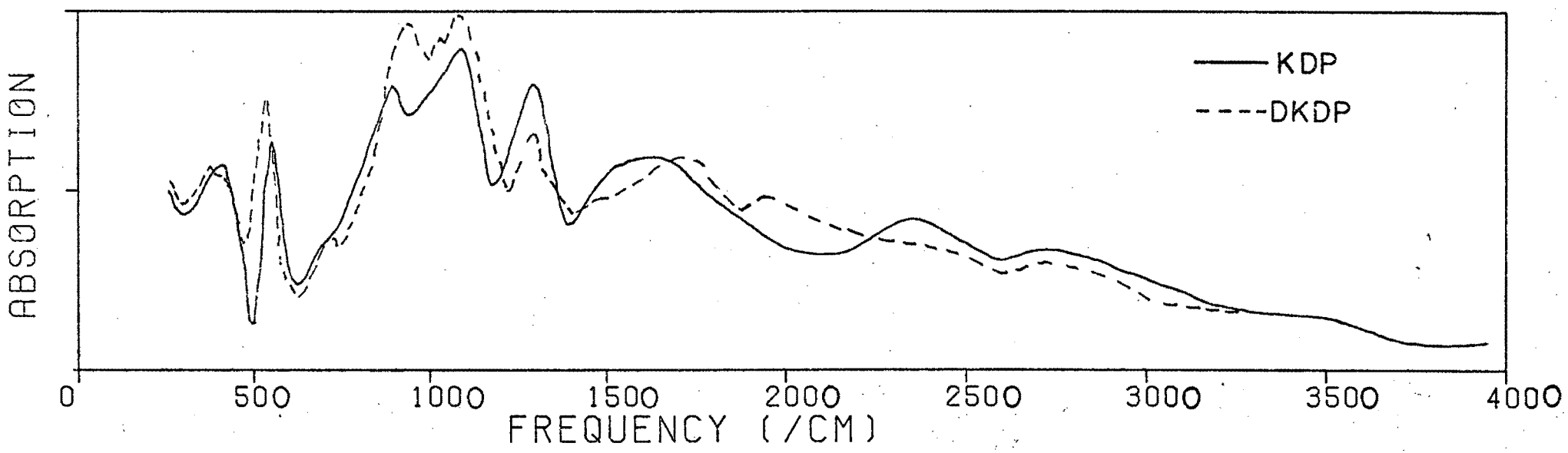

Figure 5.3. Infrared spectra of KDP and DKDP (∿90%D) at room temperature. Based on Imry, Pelah and Wiener (1965).

However, neutron inelastic scattering spectra obtained by the same authors showed only a single broad band in this region. Systematic study of the IR and the neutron inelastic scattering spectra of related compounds then led to the conclusion that the two peaks seen in the infrared were PO_4 vibrations whereas the broad band seen in the neutron inelastic scattering spectrum consisted of these two PO_4 modes superimposed on a low frequency protonic tunnelling mode at about 400 cm^{-1}. Imry, Pelah and Wiener argued that this latter mode was not seen in the IR spectra as asymmetries in the two potential minima reduced the probability of transition between the two levels of the split ground state. Further verification of this assignment came from the observation that below the Curie temperature the low frequency PO_4 absorptions became sharper, for if the PO_4 modes were broadened by coupling to a protonic tunnelling mode above the Curie temperature, then the disappearance of this mode below the Curie temperature would lead to the narrowing of these bands.

The asymmetric double harmonic oscillator model of Blinc and Hadži described above was then used in trial calculations and it was found that a ground state splitting of 400-500 cm^{-1} was consistent with the slightly asymmetric double minimum potential. The predicted $\nu_s(OH)$ assignments of Imry *et al.* (although not explicitly given) are then different from those of Blinc and Hadži, as the latter assignment gave an upper state splitting of 400 cm^{-1} and a ground state splitting of only 50 cm^{-1}.

Hill and Ichiki (1968) studied the polarized IR spectra of KDP and DKDP single crystals at various temperatures.

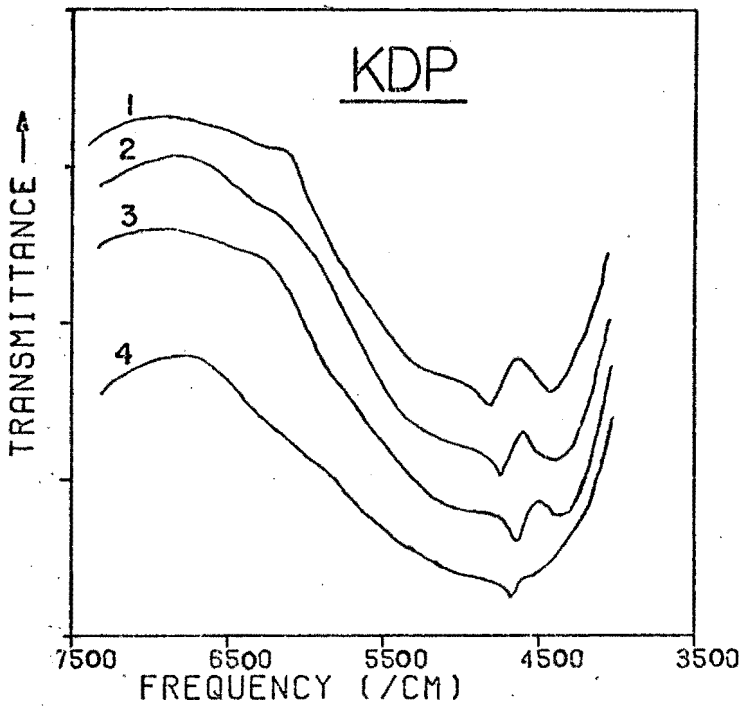

Figure 5.4. Infrared overtone spectra of KDP, polarization X(Z).
(1) T = -196°C
(2) T = 25°C
(3) T = 140°C
(4) T = 175°C

The change in the band shape with temperature is unexplained. Based on Viswanath and Miller (1979).

They concluded that for KDP the two bands at 2400 cm^{-1} and 2600 cm^{-1} were of the same polarization (viz. polarized perpendicular to the z-axis) whereas the band at 1720 cm^{-1} appeared as polarized parallel to the z-axis. This latter band was shifted to 1850 cm^{-1} in the low temperature phase but remained polarized parallel to the z-axis. They thus associated this band with a hydrogen bond vibration along the z-axis and suggested that the change in frequency on cooling was due to the onset of order below T_c. The bands at about 2400 cm^{-1} and 2800 cm^{-1} showed little variation with temperature (a result already commented upon by Imry *et al.* (1965)) and on this basis Hill and Ichiki concluded that there could be very little ground state splitting, so that if the well did have a double minimum shape it would have to have a relatively high potential barrier.

Viswanath and Miller (1979) examined the spectrum of KDP in the region of 4000-7200 cm^{-1} and detected a broad band centred at about 4600 cm^{-1} (figure 5.4). This band showed some marked changes with temperature and by comparison with similar bands in the IR spectra of other KDP-type ferroelectrics, they concluded that this band must also be associated with ν_s(OH) vibrational modes and was probably an overtone vibration of one of fundamental ν_s(OH) modes.

5.3.2 Raman Scattering

Kaminow and Damen (1968) performed Raman scattering experiments on KDP at various temperatures. The Raman spectrum exhibited a single overdamped mode centred at $\omega = 0$ which they then analysed in terms of a simple damped harmonic

oscillator model. The analysis showed that the spectrum consisted of a single low frequency mode, the frequency of which became zero at the Curie temperature. This mode could then be interpreted to be either the collective protonic tunnelling mode described by Tokunaga and Matsubara or the soft mode described by Cochran. The mode had a frequency of 99 cm^{-1} at high temperatures and in terms of the tunnelling model this would correspond to the single particle tunnelling frequency Ω. No explanation was put forward as to the cause of the damping, which appeared to be temperature independent.

She, Broberg, Wall and Edwards (1972) studied the Raman spectrum of KDP over a larger frequency range than had Kaminow and Damen, and showed that the overdamped mode observed by Kaminow and Damen is strongly coupled to another mode of the same symmetry and that this coupling must be taken into account when analysing the Raman spectrum. A coupled mode analysis was performed assuming a real coupling between the modes and the temperature dependence of the soft mode frequency determined. It was found that the transition temperature of the uncoupled soft mode was 30K whereas the transition temperature of the coupled mode was 116K. They concluded that the protonic ordering temperature is thus much lower than the Curie temperature, illustrating the importance of taking into account the mode coupling. The system could be interpreted in terms of the Kobayashi model and is formally equivalent to it in the limit of small damping, the two modes being the protonic collective mode and the polar optic phonon vibration respectively. However, one

disturbing result was that the square of the uncoupled soft mode frequency had a linear dependence on temperature, whereas the collective protonic mode RPA models predicted a $(T - T_c)/T$ temperature dependence.

Lagakos and Cummins (1974) using high resolution Brillouin scattering showed that there was yet a third mode, which was an x-y transverse acoustic mode, that could be resolved from the light scattering spectrum and this mode also had to be taken into account when analysing the spectrum. A coupled three-mode analysis was performed and it was shown how this accounted for the discrepancy between the Curie temperature of 123K and the coupled two-mode "clamped" Curie temperature of 116K determined by She *et al.* and mentioned above.

5.3.3 Pressure Effects

Samara (1971) investigated the effect of hydrostatic pressure on the ferroelectric phase transition in KDP and showed that the Curie temperature decreased with increasing pressure and finally reduced to OK at 17 kbar (see figure 5.5). The ferroelectric phase is thus suppressed below 17 kbar. He explained this phenomenon as being the consequence of the O...O distance, and hence also the H-H site-site separation δ, becoming shorter with increasing pressure. In terms of the Kobayashi model it was seen that the most important parameters of the theory viz. Ω, J and G all depend strongly upon δ and hence this result might follow naturally from the Kobayashi model. In fact at high pressure δ should tend to zero as the double minimum potential degenerates

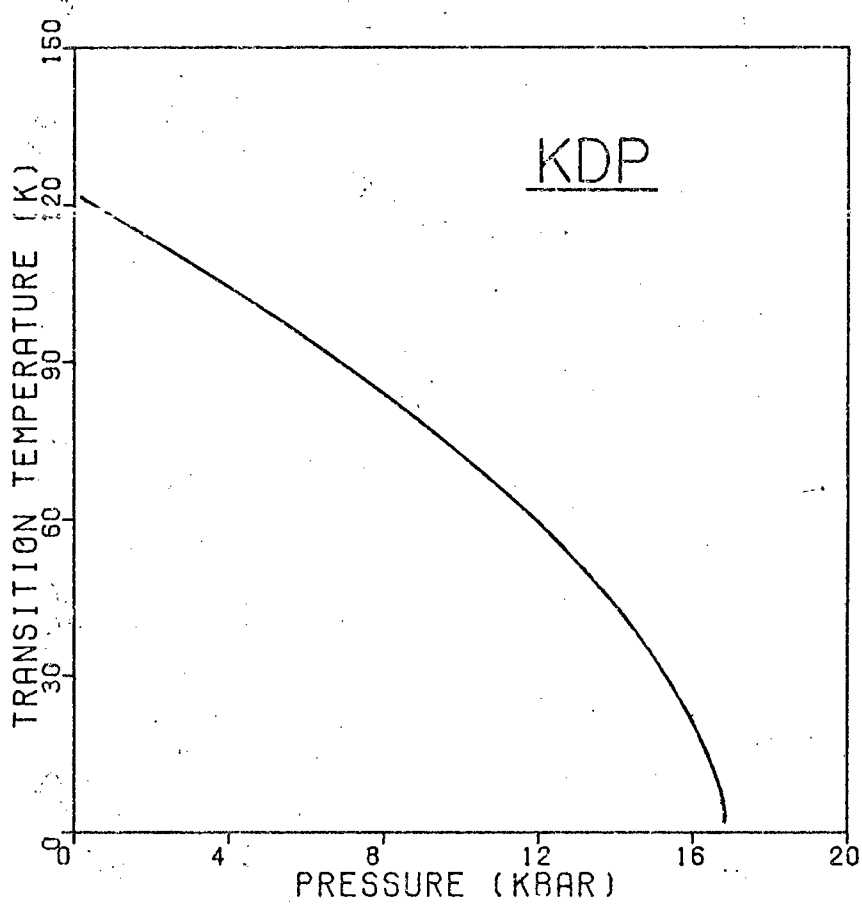

Figure 5.5. Pressure dependence of the Curie temperature for KDP. Based on Samara (1971).

into a single minimum well, in which case the phase transition will clearly be suppressed.

Peercy (1973) discovered that the overdamped Raman active mode observed by Kaminow and Damen became underdamped when a pressure of greater that 6 kbar was applied. This showed that the protonic mode is propagating rather than dissipative and that it has a pressure-dependent damping. If the damping is due to the collective mode being well-defined only over a short correlation length, then an increase in pressure, by shortening the proton-proton separation, will affect the proton-proton interaction in such a way as to increase the correlation length and so reduce the damping.

Peercy (1975) examined the pressure and temperature dependence of the soft mode Raman spectra of KDP and obtained

(i) The temperature dependence of the Raman spectra at 6.54 kbar (a pressure at which the soft mode is underdamped),

(ii) The pressure dependence of the Raman spectra at room temperature and

(iii) The pressure dependence of the Raman spectra at 140K.

The analysis was first conducted using a coupled mode model with an imaginary coupling constant and then conducted again using a coupled mode model with a real coupling constant. The former method is equivalent to interpreting the system in terms of a pure tunnelling model such as that of de Gennes (no proton-lattice coupling) and the latter method is shown to be equivalent, in the limit of small damping, to the coupled proton-optic mode model of Kobayashi. The first method led to the conclusion that the tunnelling model without phonon coupling could not describe the temperature

dependence of the Raman response. Attention was then concentrated on the second method. In the case of small damping Γ and real coupling Δ between the modes, the measured Raman response frequencies ω_- and ω_+ of the system are related to the uncoupled mode frequencies ω_a and ω_b by the relationship

$$\omega_{\pm} = \tfrac{1}{2}(\omega_b^2 + \omega_a^2) \pm \{[\tfrac{1}{2}(\omega_b^2 - \omega_a^2)]^2 + \Delta^4\}^{\frac{1}{2}}. \qquad (5.14)$$

This is formally the same as the expression for the coupled mode response frequencies given by equation (5.10) for the Kobayashi model; viz.

$$\omega_{\pm}^2 = \tfrac{1}{2}(\omega_j^2 + \Omega_0^2) \pm \{[\tfrac{1}{2}(\omega_j^2 - \Omega_0^2)^2 + 4\langle S^x\rangle\Omega|G_i|^2\}^{\frac{1}{2}} \qquad (5.10)$$

(where (G_i) is the proton lattice interaction, ω_j is the optic mode frequency and Ω_0 the protonic collective frequency) if the identification $\omega_b \leftrightarrow \omega_j$, $\omega_a \leftrightarrow \Omega_0$, $\Delta^4 \leftrightarrow 4\Omega\langle S^x\rangle|G_i|^2$ is made.

An analysis of the Raman response then yields the microscopic parameters of the Kobayashi model. The resulting temperature dependence of ω_a and ω_b at 6.54 kbar is displayed in figure 5.6 and the pressure dependence of ω_a and ω_b at room temperature is displayed in figure 5.7. Peercy concluded further that the coupling term Δ showed little temperature dependence at 6.54 kbar, whereas the damping Γ_a of the ω_a mode decreased with pressure (as expected). The proton collective mode with frequency Ω_0 determined by the above method directly from ω_a, can now be analysed within the tunnelling model of de Gennes. In terms of this model

$$\Omega_0^2 = \Omega^2\left[1 - \frac{J}{2\Omega}\tanh(\Omega/2kT)\right]$$

$$= \Omega^2\left[1 - \frac{\tanh(\Omega/2kT)}{\tanh(\Omega/2kT_c)}\right] \qquad (5.15)$$

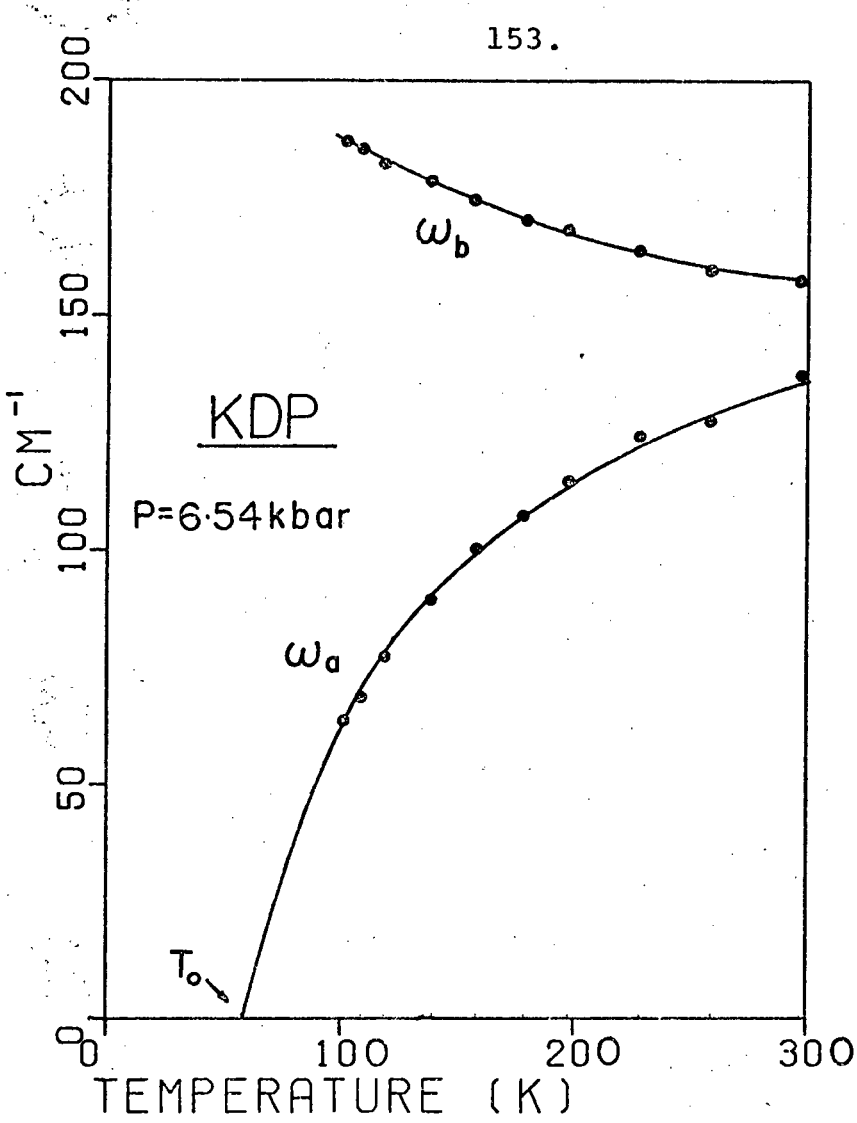

Figure 5.6. Temperature dependence of ω_a and ω_b at P = 6.54 kbar for KDP. The solid curve for ω_a is based on the model $\omega_a^2 = \Omega^2[1-\tanh(\Omega/2kT)/\tanh(\Omega/2kT_o)]$ with Ω = 178 cm^{-1} and T_o = 58K. From Peercy (1975).

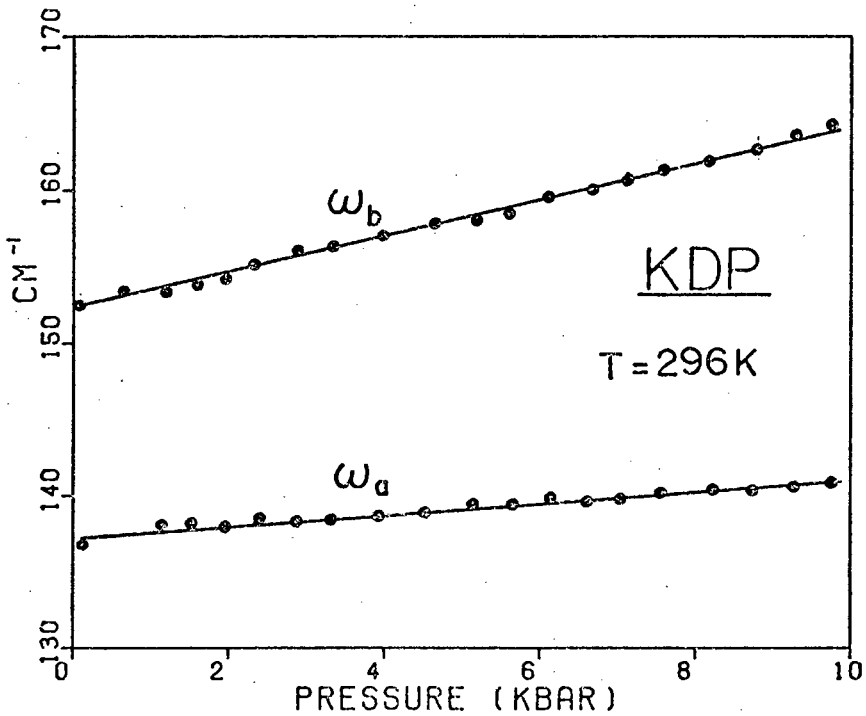

Figure 5.7. Pressure dependence of ω_a and ω_b at room temperature for KDP. From Peercy (1975).

provided that the proton-proton interaction J and the tunnelling frequency Ω are assumed to be temperature independent. This equation was fitted to the ω_a vs. T points in figure 5.6. and Ω and T_o were determined to be 178 cm^{-1} and 58K respectively. The value of T_o is rather poorly determined as $\tanh(\Omega/2kT_o) \approx 1$.

In terms of the Kobayashi model the transition temperature T_- (i.e. the "clamped" Curie temperature) is given by

$$\frac{2\Omega}{\tilde{J}} = \tanh\left(\frac{\Omega}{2kT_-}\right) \qquad (5.11)$$

where J is the renormalized proton-proton interaction defined by

$$\tilde{J} \equiv J + 4|G_i|^2/\omega_j \equiv J + 4G^*. \qquad (5.12)$$

As T_- = 86K (the temperature at which ω_- vanishes at 6.54 kbar), $\tilde{J}$ can be determined. The pressure dependence of ω_a is used to evaluate the pressure dependence and atmospheric pressure value of Ω. This together with the atmospheric pressure value of T_- yield the atmospheric pressure value of $\tilde{J}$, T_o being assumed pressure independent as Ω is relatively insensitive to T_o). Thus the pressure variations of J and Ω can be calculated. These results are given in table 5.1. By assuming (since $\tanh(\Omega/2kT_o) \approx 1$) that $J \approx 2\Omega$, the pressure dependence of J and G* can be determined. Peercy's conclusion was that the pressure dependence of J arises predominantly from the pressure dependence of G*, which seems most unlikely. Another difficulty is that Δ is found experimentally to be nearly temperature independent. If Peercy's identification of ω_a and ω_b with the two frequencies of the Kobayashi model is correct,

Table 5-1

Kobayashi Model Parameters and their Pressure Derivatives (Peercy (1975))

	$\Omega/2$ (cm^{-1})	$\tilde{J}$ (cm^{-1})	T_- (K)	T_0 (K)	J (cm^{-1})	G^* (cm^{-1})
x	86.2[1]	440[1]	117.8[1]	58[2]	345.1[1]	24[3]
$\partial \ell nx/\partial P$ (% kbar)	0.5	-1.5	-4.0		0.5	-8.7

(1) Value at atmospheric pressure

(2) Value at 6.54 kbar

(3) Value at atmospheric pressure and room temperature

one would expect Δ to vary with temperature as $\Delta^4 = 2|G_i|^2 \tanh(\Omega/2kT)$. This implies that G_i is temperature dependent, which seems unlikely.

5.3.4 Neutron Diffraction

A number of recently-performed neutron diffraction experiments on KDP-type ferroelectrics have been reviewed by Nelmes (1980). Table 5.2 (based on a similar table given by Nelmes) summarizes the relevant crystallographic results. Nelmes pointed out that:

i) δ is very much larger in RbDP than in KDP, yet their O...O distances are very much the same and their Curie temperatures differ by no more than 20%. The change in δ between these species is as large as that which is believed to account for the suppression of the ferroelectric transition (i.e. $T_c \to 0K$) at high pressure (see section 5.3.3 above). Hence it seems that the transition temperature is not strongly dependent on δ alone.

ii) There is a considerable change in both O...O distance and δ as KDP is cooled to a temperature just above T_c. In fact the changes are similar to those that accompany the application of 6 kbar pressure and at this pressure the soft mode becomes underdamped. This suggests that either these temperature dependences should be taken into account in the theory or that, as concluded in (i) above, the change in δ does not significantly alter the dynamics of the soft mode.

iii) The orientation θ of the tetrahedra has a different response to pressure than it has to temperature and

Table 5-2

Temperature and Pressure Dependence of Structural Parameters for RbDP, KDP and DKDP (Nelmes (1980))

Substance:	RbDP	RbDP	KDP	KDP	KDP	DKDP	DKDP
Pressure:	1 bar	1 bar	1 bar	1 bar	14 kbar	1 bar	1 bar
Temp. (K):	295	T_c+5	295	T_c+5	295	363	T_c+5
a(Å)	7.607(1)	7.586(3)	7.4521(4)	7.426(1)	7.34(1)	7.479(1)	7.459(1)
T_c(K)	146	146	123	123	46	222	222
δ (Å)	0.420(14)	0.387(9)	0.367(2)	0.341(1)		0.451(2)	0.449(1)
O...O(Å)	2.498(2)	2.486(4)	2.4949(5)	2.4831(5)	2.473(5)*	2.527(1)	2.523(1)
θ°	58.81(2)	59.08(5)	60.89(1)	60.99(1)	61.69(9)	61.35(3)	61.57(2)

* Corrected value: based on reduced data set (Meyer *et al.* (1980))

hence the change in T_c with pressure might well be linked to the change in θ rather than to the change in δ.

Now according to the Kobayashi model, the transition temperature is dependent on both the tunnelling frequency and the proton-proton interaction J. The only model that attempts to calculate Ω microscopically is the double harmonic oscillator model of Blinc and Hadži (1958): in terms of this model $\Omega \propto \delta\exp(-a\delta^2)$ where a is a constant. Furthermore, J has been assumed proportional to δ^2 on hydrostatic compression of the crystal: see Blinc and Žekš (1968), Blinc and Žekš (1974) and Mačkowiak, Stankowski, Žekš and Blinc (1979). (This assumption will be discussed in detail in section 5.7). Nelmes therefore concluded that there were fundamental discrepancies between the existing neutron diffraction data and the current theories of KDP. In particular, it seems inconsistent to regard Ω as temperature independent - which has been done in all models to date.

Meyer, Nelmes and Vettier (1980) performed a high pressure (c.a. 14 kbar) neutron diffraction study on KDP with the aim of determining the H-H site-site separation δ as accurately as possible. Unfortunately the geometry of the pressure cell in the apparatus greatly restricted the number of reflections that were accessible and thus the accuracy of the work was necessarily limited. δ is also difficult to determine as one is trying to represent a rather flat-topped protonic distribution about the centre of the bond observed experimentally by two overlapping gaussians. Furthermore, the centres of the gaussian distributions do not necessarily

correspond to the actual proton sites, because of the anharmonicity of the potential well. However, their results seemed to indicate that a large amount of the lattice compression is taken up by the rotation of the tetrahedra, with the O...O distance being reduced by merely 1/3 of the amount that would be expected if there were no rotation of the PO_4 tetrahedra. They concluded that the balance of the crystallographic evidence favours a variation of δ given by $\Delta(O...O) < \Delta\delta < 2\Delta(O...O)$ on application of 14 kbar pressure. The possibility of $\Delta\delta$ being greater than $2\Delta(O...O)$ was rejected. This was shown to be equivalent to rejecting the assumption made by Blinc and Žekš (1968) that the tetrahedra do not rotate on the application of pressure. (Assuming that the tetrahedra do not rotate on compression implies that $\Delta\delta = \frac{1}{2}\Delta a$ and Meyer *et al.* show that $\frac{1}{2}\Delta a$ is significantly greater than $2\Delta(O...O)$.)

5.4 Interpretation of the IR Spectra

5.4.1 Difficulties in the Previous Analyses

As mentioned in section 5.3.1 above the quantitative analyses of both Blinc and Hadži (1958) and Imry *et al.* (1965) of the IR spectrum of KDP have been based on a double harmonic oscillator description of the protonic potential. Whereas this model can be expected to yield a reasonable first approximation to the protonic energy level scheme, it has a number of drawbacks for more exact calculations, viz.

i) The potential well rises equally steeply on either side of the potential minimum, whereas even for an isolated OH bond, the side of the potential furthest

from the heavy atom is known to rise more gently than the side nearest to the heavy atom. In an OH...O bond this difference is likely to be even more marked (cf. Vaks and Zinenko (1973)).

ii) The barrier shape is also unrealistic in that it has a cusp at its highest point. This prevents the positions of energy levels lying near to the top of the barrier from being accurately determined.

iii) In the applications by both Blinc and Hadži (1958) and Imry *et al.* (1965) the hydrogen positions are taken to coincide with the potential minima. As has been pointed out by Vaks and Zinenko (1973), this is only an approximation as the true hydrogen positions are likely to be appreciably closer to the centre of the bond due to the asymmetry of the potential well.

iv) Furthermore the mean position of the hydrogen atoms in the disordered phase might well change with temperature even in a static well as the position of the probability maxima of the ground and first excited state do not necessarily correspond with each other. No such effect is taken into account by this model when assigning the hydrogen positions.

One must conclude that the double harmonic oscillator potential cannot really be expected to yield accurate results when it is used to calculate sensitive quantities such as the pressure variation of the tunnelling frequency. (Nevertheless the model has been used in this way by Blinc and Žekš (1968), Blinc and Žekš (1974), Mačkowiak, Stankowski, Žekš and Blinc (1979) and Torstveit (1979).)

In the following section the double Morse potential will be used to re-analyse the IR spectrum of KDP. This potential is clearly more realistic than the double harmonic oscillator one and its use overcomes all the drawbacks mentioned above.

5.4.2 Application of the Double Morse Potential

Methods similar to those used in chapters 3 and 4 will now be employed to analyse the IR spectra of KDP and DKDP.

Four parameters are required to characterize the double Morse potential viz. R,D,α and r_o. For KDP 2R will be taken as equal to 2.4945Å and δ as equal to 0.367Å (Table 5.2) at 295K and atmospheric pressure.

δ is calculated from the double Morse potential (see chapter 2 section 6) as the distance between the peaks in the proton probability distribution function, allowing for the fact that the protons occupy both of the two lowest-lying levels.

The IR spectra of KDP and DKDP are fairly complicated and a number of qualitatively different assignments are possible for the ν_s(OH) bands. These will now be systematically investigated.

Assignment 1. (Based on Blinc and Hadži (1958)). We assume that ω_{03} = 2750 cm^{-1} and ω_{12} = 2400 cm^{-1} and attempt to solve the coupled equations

$$g_{03}(D,\alpha,r_o,R) = 2750 \text{ cm}^{-1}$$

$$g_{12}(D,\alpha,r_o,R) = 2400 \text{ cm}^{-1}$$

$$\delta(D,\alpha,r_o,R) = 0.367\text{Å}$$

$$2R = 2.4945\text{Å}$$

for R,D,α and r_o using the Harwell subroutine NSØ1A (cf. chapter 2 section 6).

Result: No solution to the coupled equations could be found: the smallest sum of squared residuals was four orders of magnitude greater than the convergence criterion. This assignment was therefore rejected. (Blinc and Hadzi's assignment has been previously criticised by Imry *et al.* - see section 5.3.1 - on the grounds that the ground state splitting required is probably too low.)

Assignment 2. Same as Assignment 1, but assumes that ω_{12} = 1800 cm^{-1} instead of 2400 cm^{-1} (ignoring for the moment the results of Hill and Ichiki (1968) which militate strongly against such an assignment).

Result: Again NSØ1A generated physically meaningless parameters and the assignment was therefore rejected.

Assignment 3. This assignment retains the $|0\rangle \rightarrow |3\rangle$ transition at 2700 cm^{-1} but, instead of attempting to assign the $|1\rangle \rightarrow |2\rangle$ transition, tries various values for ω_{01}. Thus solutions are sought for the following system:

$$g_{03}(D,\alpha,r_o,R) = 2700 \text{ cm}^{-1}$$

$$g_{01}(D,\alpha,r_o,R) = 100,\ 250,\ 500 \text{ cm}^{-1}$$

$$\delta(D,\alpha,r_o,R) = 0.367\text{Å}$$

$$2R = 2.4945\text{Å}$$

Result: NSØlA generates physically meaningless parameters and the residual sum of squares remains high. The assignment is therefore rejected. It is clear at this stage that the band at 2700 cm^{-1} cannot be a $|0\rangle \rightarrow |3\rangle$ transition.

Assignment 4. Same as Assignment 3, but the 2700 cm^{-1} band is now assigned as a $|1\rangle \rightarrow |2\rangle$ transition.

Result: No solution is obtained but the residual sum of squares is three orders of magnitude lower than that achieved by Assignments 1, 2 and 3 and only one order of magnitude larger than the convergence criterion. This suggests that the assignment is at least plausible. The $|0\rangle \rightarrow |3\rangle$ transition was predicted to lie approximately in the 4000-5000 cm^{-1} region.

Assignment 5. This assignment is based on the results of Assignment 4. Assume that $\omega_{03} = 4600\ cm^{-1}$, i.e. identifying the band observed by Viswanath and Miller with a $|0\rangle \rightarrow |3\rangle$ transition. Various values are now tried for ω_{01} as in Assignments 3 and 4.

Result: "Exact" convergence (i.e. to within the convergence criterion) was not obtained but further attempts were made using other values for ω_{01}. "Exact" convergence was finally obtained when ω_{01} was confined to the range 315-370 cm^{-1}.

Assignment 5 is thus the only possible assignment which allows the available infrared, overtone and crystallographic data to be reconciled in terms of the double Morse potential model. However, a number of questions about this assignment still arise:

i) Does the above assignment predict realistic values for the $|1\rangle \rightarrow |2\rangle$ transition frequency?

ii) If D,α and r_o remain constant on deuteration (an assumption that seemed to be satisfactory during the calculations of the preceding two chapters) and if 2R is set equal to its DKDP value, are the predicted transition frequencies and is the predicted site-site separation for DKDP compatible with experiment?

iii) Are the experimental temperature and pressure variations of the proton intersite separation, as determined by Nelmes, reproduced by the double Morse potential model? (To a first approximation D,α and r_o can be assumed to remain unchanged on thermal contraction and hydrostatic compression. δ would thus vary with R and could be predicted directly from the double Morse potential.)

iv) Can the value of ω_{01} be more closely refined?

These questions will now be looked at in turn. The calculations of D,α and r_o were performed for Assignment 5 with ω_{01} set equal to 315, 320, 330, 340, 350, 360 and 370 cm^{-1} in turn. Each resulting set of parameters was then used to perform the various calculations suggested by questions (i)-(iii) above. The results are presented in table 5.3. An inspection of this table shows the following:

i) If the predicted $|1\rangle \rightarrow |2\rangle$ transition frequency for KDP is compared with the observed band it appears that whereas the predicted transition frequencies lie in the range 2050-2300 cm^{-1}, the observed spectrum exhibits a broad feature stretching from 2200-2800 cm^{-1}, divided into two bands by an absorption minimum at 2600 cm^{-1}. However, the minimum at 2600 cm^{-1} can be explained in terms of a Fermi resonance

Table 5-3

Predicted double Morse potential parameters for KDP and DKDP

(given δ = 0.367Å, ω_{03} = 4600 cm^{-1}, and 2R = 2.4945Å for KDP; 2R = 2.527Å for DKDP; and an assumed ω_{01} value for KDP.)

KDP				KDP				DKDP				
ω_{01} (cm^{-1})	D (eV)	α (Å^{-1})	r_o (Å)	R-r_o (Å)	B (cm^{-1})	ω_{12} (cm^{-1})	ω_{03} (cm^{-1})	R-r_o (Å)	B (cm^{-1})	ω_{01} (cm^{-1})	ω_{12} (cm^{-1})	ω_{03} (cm^{-1})
315	4.44	4.10	0.9895	0.2587	3312	2290	4600	0.2740	4356	16	2235	2742
320	2.94	4.68	0.9998	0.2475	3259	2263	4601	0.2637	4114	19	2131	2700
330	1.63	5.75	1.0090	0.2383	3180	2214	4601	0.2545	3790	25	1979	2640
340	1.09	6.76	1.0113	0.2360	3119	2167	4600	0.2522	3577	29	1867	2595
350	.824	7.74	1.015	0.2368	3071	2121	4599	0.2530	3421	33	1773	2558
360	.669	8.72	1.0083	0.2390	3042	2078	4600	0.2552	3314	36	1695	2528
370	.590	9.52	1.0061	0.2412	3034	2046	4605	0.2574	3257	38	1641	2510

at this frequency of the ν_s(OH) vibration with an overtone of the observed mode at 1300 cm^{-1} (probably a δ(OH) bending vibration). Similar resonances have already been mentioned in the analysis of the infrared spectrum of chromous acid in chapter 3. Thus if the observed band is considered to be a single $|1\rangle \rightarrow |2\rangle$ band overlaid with a Fermi resonance at 2600 cm^{-1}, then there is reasonable agreement between the predicted and observed values for ω_{12}, provided that ω_{01} is closer in value to the lower end of the frequency range used.

ii) For DKDP it is seen that the predicted ground state splitting is about 15-40 cm^{-1}. This confirms that the tunnelling frequency in DKDP is very much smaller than that in KDP. The predicted $|1\rangle \rightarrow |2\rangle$ transition frequency lies in the range 1650-2250 cm^{-1}, depending on the precise parametrization of the potential well, and this is to be compared with an observed band centred at 1750 cm^{-1}. The predicted $|0\rangle \rightarrow |3\rangle$ transition frequency lies in the range 2500-2750 cm^{-1} and it seems plausible that this corresponds to the weak band observed in the same region (see figure 5.3). An absorption minimum again occurs at 2600 cm^{-1} and is probably again due to a Fermi resonance, considering the band observed at 1300 cm^{-1} - although in this case the origin of this latter band is not clear. Of the various values suggested for ω_{01} in table 5.3, ω_{01} = 350 cm^{-1} probably agrees best with the above assignment.

Table 5-4

Predicted site-site separations for KDP and DKDP for selected values of ω_{01}

KDP ω_{01} (cm^{-1})	KDP δ(295K) (Å)	KDP δ(128K) (Å)	KDP δ(14 kbar) (Å)	DKDP δ(363K) (Å)	DKDP δ(228K) (Å)
315	0.367	0.334	0.313	0.451	0.445
320	0.367	0.337	0.319	0.448	0.443
330	0.367	0.340	0.326	0.446	0.441
340	0.367	0.342	0.330	0.448	0.442
350	0.367	0.344	0.333	0.449	0.444
360	0.367	0.345	0.335	0.451	0.447
370	0.367	0.345	0.336	0.453	0.449
Exptl. (Table 5.2)	0.367(2)	0.341(1)	0.358(9)*	0.451(2)	0.449(1)

* Meyer *et al.* (1980)

iii) If the computed values of δ_H(T=128K), δ_D(T=363K) and δ_D(T=228K), given in table 5.4, are compared with those given by Nelmes in table 5.2 (and recorded again in table 5.4) there is agreement for KDP at about 340 cm^{-1} and for DKDP at about 360 cm^{-1}. In order to calculate δ at 14 kbar pressure it must be noted that the crystallographic determinations at 14 kbar were based upon a smaller set of crystallographic reflections than were used at atmospheric pressure due to the obstructing presence of the high pressure cell (Meyer *et al.* (1980)). If the smaller set of reflections is also used for the analysis at atmospheric pressure, the results can be compared with those obtained using the full data set at atmospheric pressure and so some estimate of the systematic error involved obtained. The O...O distance is thus seen to be 0.021Å shorter at 14 kbar than at atmospheric pressure (both measurements based on the restricted data sets). This value of 0.021Å will be subtracted from the O...O distance at atmospheric pressure as determined from the full set of reflections so as to obtain a (hopefully) better estimate of the O...O distance at 14 kbar (as indicated in table 5.2). Using this revised estimate of 2R at 14 kbar, δ_H(14 kbar) is then calculated for the various ω_{01}. An inspection of the various values for δ_H(14 kbar) shows that they are all somewhat lower than that given by Meyer *et al.*, but are all consistent with the conclusion of that paper, viz. that the balance of evidence favours a change in δ with the range Δ(O...O) < $\Delta\delta$ < 2Δ(O...O) on application

of 14 kbar pressure.

iv) If the remarks (i)-(iii) immediately above are all taken into account the best value for ω_{01} is probably in the range 320 $\pm$ 10 cm^{-1}.*

Assignment 5 above thus appears to be compatible with both crystallographic and infrared data, yielding a value of about 320 $\pm$ 10 cm^{-1} for the single particle tunnelling frequency. In the following sections of this chapter this estimate of Ω will be used to analyse the Raman data discussed in sections 5.3.3 and 5.3.4 above. A method will also be developed whereby the double Morse potential determined for Ω = 320 cm^{-1} above can be used to estimate the variation of Ω and δ with temperature and pressure.

5.5 Renormalization of the Tunnelling Frequency

This section explains why it is necessary to renormalize the single-particle tunnelling frequency when analysing the Raman spectra in terms of the coupled mode models. A good deal of confusion has arisen in the literature as authors have not always indicated whether the tunnelling frequency they are discussing is the static single-particle one or a renormalized version.

In the analysis of the Raman response by Peercy (1975) (section 5.3.4 above) the single-particle tunnelling frequency was determined to be 172 cm^{-1} at atmospheric pressure. Now in terms of the work of Blinc and Ribarič (1963) the tunnelling frequency determined by an analysis such as Peercy's is lower in value by a factor A than the static single-particle tunnelling frequency determined from an infrared study. This renormalization is necessary since the proton, being charged,

---

* The higher ω_{01} values predict an unrealistic value for ω_{12} for KDP.

polarizes the lattice as it moves so that there is a strong coupling between it and the lattice modes. This does not greatly affect the frequencies of the $|0\rangle \rightarrow |3\rangle$ and $|1\rangle \rightarrow |2\rangle$ infrared transitions as they occur on a shorter timescale than the lattice vibrations and the potential well may then be treated as essentially static. However when interpreting Raman soft-mode spectra, the timescale of the observed lattice vibrations is comparable with that of the single-particle tunnelling motion and hence these electrostatic interactions must be included. Peercy's value of 172 cm^{-1} for the tunnelling frequency is therefore less by a factor A than its hypothetical value in absence of lattice polarization. Equation (5.15) should thus become

$$\Omega_0^2 = (A\Omega)^2\left[1 - \frac{J}{A\Omega}\langle S^x\rangle\right] \qquad (5.16)$$

and (5.9) should become

$$\langle S^x\rangle = \tfrac{1}{2}\tanh(A\Omega/2kT) \qquad (5.17)$$

where Ω now represents the static single-particle tunnelling frequency and $A\Omega$ = 172 cm^{-1}.

Some estimates of the renormalization factor A will now be mentioned.

If the estimate of 400 cm^{-1} for the tunnelling frequency obtained by Imry *et al.* (section 5.3.1 above) is correct then Peercy's data yields $A \approx 172\ cm^{-1}/400\ cm^{-1} = 0.4$. Blinc and Žekš (1968) estimated Ω to be about 430 cm^{-1} on the basis of double harmonic oscillator calculations and by comparing this value with estimates of the (renormalized) tunnelling frequency obtained from static dielectric measurements obtained a value for A of about 0.6. Torstveit (1979)

used the same estimate for Ω as Blinc and Žekš above and concluded that A = 0.3, having estimated a renormalized Ω of about 140 cm^{-1} from a four-particle cluster model treatment of the static dielectric properties. He also attempted to take into account possible pressure dependences of A, but concluded that any such pressure dependence could probably be disregarded.

These calculations of A are rather crude but it would be very difficult to do much better due to the complicated dependence of A upon the details of the dynamics of the proton lattice interaction. However the effect is clearly important and must be taken into account when attempting to correlate infrared and Raman estimates of the tunnelling exquency.

Blinc, Žekš, Sampaio, Pires and Sa Barreto (1979) (see section 5.2 above) have shown how it may be necessary to add additional terms to the Hamiltonian of the Kobayashi model so as to take into account further proton-proton and proton-lattice couplings. These all have the effect of further renormalizing the single-particle tunnelling frequency in order to obtain its effective value in the model. At this stage the extent to which the inclusion of these terms alters the effective single-particle tunnelling frequency is uncertain, but in the re-analysis of the Raman data of Peercy (1975) that is to follow some of these terms will indeed be seen to be important.

5.6 Re-analysis of the Soft-Mode Raman Spectrum

5.6.1 Determination of $\Omega(T,P)$

The above discussion of the experimental data for KDP has revealed the need for a careful study of the effect of temperature on the tunnelling frequency. Nelmes (1980) (see table 5.2) has pointed out that the decrease in O...O distance for KDP on cooling from room temperature to just above T_c is comparable with that which occurs on application of 6 kbar hydrostatic pressure. As this degree of pressure has a significant effect on the dynamics of the phase transition, the change in O...O distance on cooling cannot be neglected. Peercy's analysis of the temperature dependence of the collective mode frequency ω_- on the other hand treats Ω as constant and the success of the analysis suggests that Ω depends little, if at all, on temperature.

The double Morse potential model gives a simple method of estimating both the pressure and temperature dependence of Ω. If the O...O distance for KDP is assumed to vary linearly with both temperature and pressure over the range of Nelmes's experiments and if the OH...O bonds are assumed (as an approximation) to be always linear, then the data of table 5.2 leads to the following expression for 2R:

$$2R = 2.4945\text{Å} + c_1(T - 295) - c_2P$$

where $c_1 = 6.826 \times 10^{-5}$ Å/K

and $c_2 = 1.5 \times 10^{-3}$ Å/kbar.* (5.18)

---

* The "corrected" O...O distance at 14 kbar has been used to determine the pressure coefficient in this equation. See section 5.4.2 for a discussion of this point.

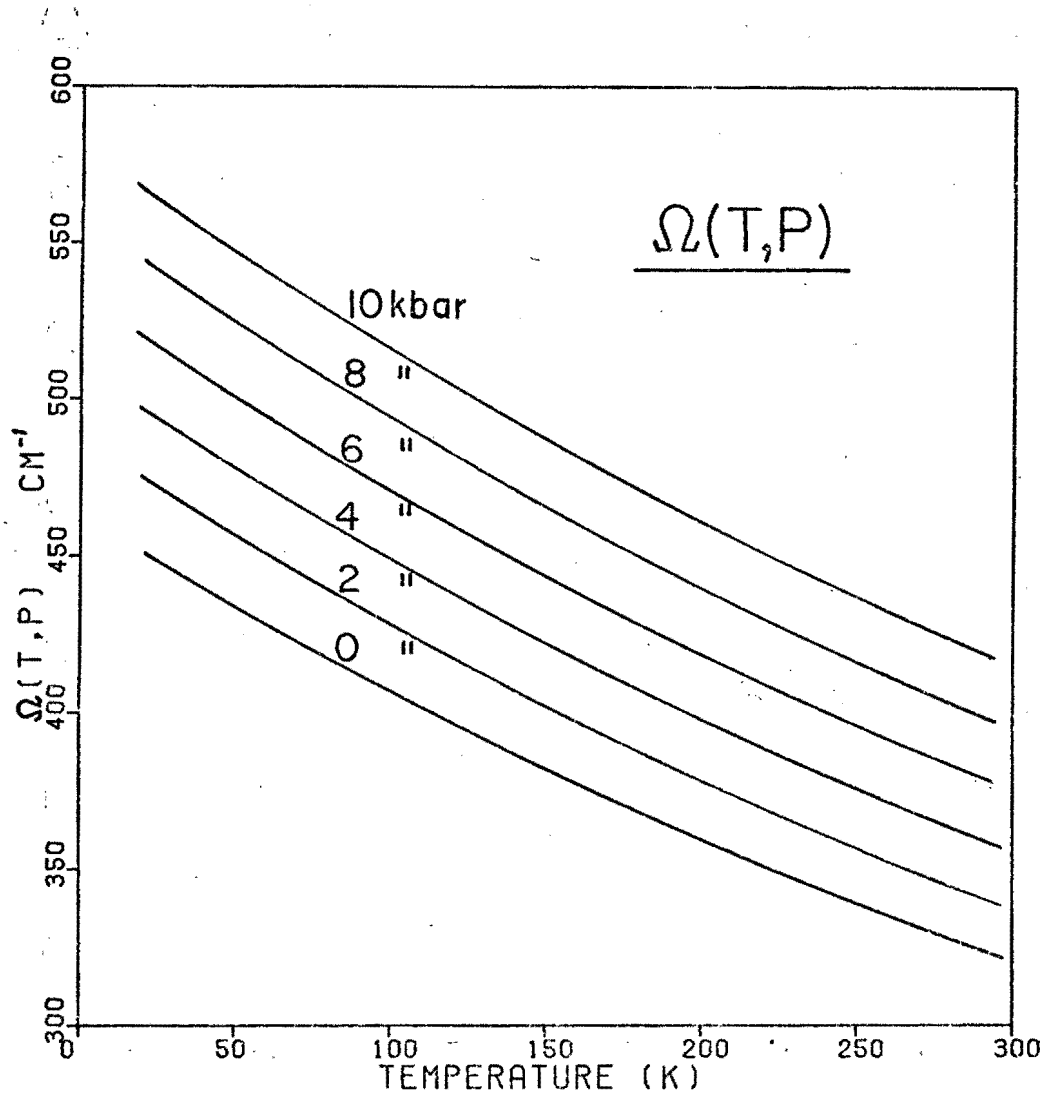

Figure 5.8. Predicted Temperature and Pressure dependence of the "bare" protonic tunnelling frequency Ω, assuming that Ω(295K, 1bar) = 320 cm^{-1}.

If D,α and r_o are assumed to remain constant on the application of pressure and/or on cooling, then these parameters together with R given by equation (5.18) suffice to yield Ω at any given temperature and pressure. (D,α and r_o have already been determined from the infrared data in section 5.5). The only justification for this assumption is that in the chromous acid problem (chapter 3) the way in which the potential changed on deuteration, with the O...O distance increasing by 0.06Å, could be well represented by assuming that only 2R changed, D,α and r_o remaining constant.

Ω(T,P) has been calculated by this method for various values of T and P on the assumption that Ω(295K,1 bar) = 320 cm^{-1}, the value estimated in section 5.4. The results are displayed in figure 5.8. It is important to note that the temperature variation of Ω is comparable with its pressure variation over the range of temperature and pressure accessible to experiment.

5.6.2 Models for ω_a^2

Peercy's model for the collective protonic mode frequency (equation 5.16) can be written as

$$\omega_a^2(T,P) = A\Omega(T,P)[A\Omega(T,P) - J(T,P)\langle S^x\rangle] \qquad (5.19)$$

where

$$\langle S^x\rangle = \tfrac{1}{2}\tanh[A\Omega(T,P)/2kT] \qquad (5.20)$$

including explicitly the temperature and pressure dependence of ω_a, J and Ω. The proton ordering temperature $T_o(P)$ at pressure P is then given implicitly by

$$\frac{A\Omega(T_o,P)}{J(T_o,P)} = \tfrac{1}{2}\tanh[A\Omega(T_o,P)/2kT_o] \equiv \langle S^x \rangle_0 \quad . \qquad (5.21)$$

An attempt will now be made to use this basic model to determine A, J(T,P) and $T_o(P)$ directly from the Raman soft-mode response. Four different variations of (5.19) will be made in an attempt to understand the Raman spectra. The initial assumption is that Peercy's analysis of the Raman response in terms of two coupled damped harmonic modes and his identification of the frequencies of these modes with those of the Kobayashi model is essentially correct. However each variation will use an expression for the temperature dependence of the protonic collective mode frequency that is fundamentally different from that used by Peercy. Each model will be fitted in a regression analysis to Peercy's original data points for ω_a vs. T at 6.54 kbar. The regression analyses all include a temperature and pressure dependent Ω, determined by the above method. Seven regressions will be performed with each model using the seven values for Ω(295K, 1 bar) ($=\omega_{01}$) given in table 5.3.

Model A

We assume that at a given pressure the ratio J(T,P)/Ω(T,P) is temperature independent. This is less stringent than requiring both J and Ω to be individually temperature independent as has been done in all previous attempts to analyse the soft-mode Raman response.

Then equation (5.19) may be written as

$$\omega_a^2(T,P) = [A\Omega(T,P)]^2\left[1 - \frac{J(T,P)}{A\Omega(T,P)} \langle S^x \rangle\right]$$

$$= [A\Omega(T,P)]^2[1 - \langle S^x \rangle / \langle S^x \rangle_0] \,. \qquad (5.22)$$

A and $\langle S^x \rangle_0$ are then determined by fitting equation (5.22) to the nine data points for ω_a vs. T presented in figure 5.6.* The regression was performed using the Harwell Subroutine Library program VBØ1A with regression parameters $p_1 = A$ and $p_2 = 2\langle S^x \rangle_0$ for various assumed values of Ω(295K, 1 bar).

The results, together with estimates of the standard deviations of the regression parameters, are presented in table 5.5. For comparison purposes the results of Peercy's regression of equation (5.22) on the nine data points given in figure 5.6 are also included in the table. The statistic s^2 = (sum of squared residuals)/(no. of degrees of freedom) provides a useful means of comparing the goodness of fit of the various models. The values of s^2 show that the fit of equation (5.22) to the data is considerably worse than that of Peercy's model. This seems strange as model A, by including a temperature-dependent Ω, is a refinement of Peercy's original model. Hence *either* Peercy's good fit is coincidental (possibly the results of cancelling errors) and model A has to be refined further in order to obtain the same accuracy of fit, *or* Peercy's model is adequate and the method of calculating the temperature dependence of Ω in model A is suspect.

---

* The point at T = 259K, ω_a = 127 cm^{-1} consistently gave exceptionally high residuals and was therefore ignored in the regression.

Table 5-5

Model A: Results of regression analysis

$p_1 = A$ and $p_2 = 2\langle S^x \rangle_0$

Ω(295K, 1 bar) cm^{-1}	p_1	p_2	$\sigma(p_1)$	$\sigma(p_2)$	s^2 $(cm^{-1})^2$
315	0.434	0.985	0.013	0.007	18.7
320	0.440	0.983	0.011	0.007	15.1
330	0.445	0.982	0.010	0.006	11.0
340	0.445	0.980	0.009	0.005	8.6
350	0.442	0.980	0.008	0.005	7.0
360	0.437	0.979	0.007	0.005	5.3
370	0.430	0.978	0.007	0.005	5.3
Peercy (1975) ($p_1 = \Omega(cm^{-1})$)	178	0.974	1	0.002	0.56

In view of the good results obtained with the double Morse potential in analysing the crystallographic and infrared data in section 5.4 and the existing difficulties in the theory, the second alternative seems unlikely. Serious attention will now be directed to the first.

Model B

A further refinement of model A is the inclusion of the coupling terms suggested by Blinc *et al.* (1979), mentioned in section 5.5.

The direct $B_{ij}S_i^xS_j^x$ proton-proton interaction is usually neglected in the RPA treatment of the proton dynamics as the coefficient B_{ij} depends on the square of the overlap integral of the "localized left" and "localized right" protonic wavefunctions (see Blinc and Žekš (1972)). If the ground state splitting is very small then the left-right overlap integral is effectively zero and the shape of the proton probability distribution function is essentially the same in the ground (symmetric) and first excited (antisymmetric) state. (Note: "first excited state" refers here to the upper level of the split ground state.) However, as has been noted in section 5.4.1, the probability maxima for the ground state are displaced away from those of the first excited state by nearly 0.02Å since the potential wells are skew, having different curvature on either side of the local minima. Thus the direct $B_{ij}S_i^xS_j^x$ coupling term may be of more importance than is suggested by the rather unrealistic double harmonic oscillator model of Blinc which neglects the skewness of the wells entirely.

Blinc treats the coupling of the protonic tunnelling with the non-polar optic phonons in a linear approximation:

$$\Omega(Q) = \Omega(0) + \left(\frac{\partial\Omega}{\partial Q}\right)_0 Q \qquad (5.23)$$

where Q is a co-ordinate describing the O...O displacement from its equilibrium length. Blinc shows that this leads to an indirect $B_{ij}S_i^xS_j^x$ coupling term in the RPA analysis of the resulting Hamiltonian. In terms of their investigation $\Omega(T,P)$ in equation (5.19) is replaced by $\Omega + B\langle S^x\rangle$ where B represents the joint effect of the direct $S_i^xS_j^x$ coupling between protons and indirect $S_i^xS_j^x$ coupling which results from the coupling of the pseudospins with non-polar optic phonons.

Equations (5.19) and (5.20) then become

$$\omega_a^2(T,P) = [A\Omega(T,P) + B\langle S^x\rangle][A\Omega(T,P) - (J(T,P) - B)\langle S^x\rangle] \qquad (5.24)$$

with

$$\langle S^x\rangle = \tfrac{1}{2}\tanh\left[\frac{A\Omega(T,P) + B\langle S^x\rangle}{2kT}\right]. \qquad (5.25)$$

If the ratio $[J(T,P) - B]/\Omega(T,P)$ is assumed temperature independent (in analogy with the assumption made in model A), equation (5.24) becomes

$$\omega_a^2(T,P) = [A\Omega(T,P) + B\langle S^x\rangle]A\Omega(T,P)\left[1 - \frac{J(T,P)-B}{A\Omega(T,P)}\langle S^x\rangle\right]$$

$$= [A\Omega(T,P) + B\langle S^x\rangle]A\Omega(T,P)[1 - \langle S^x\rangle/\langle S^x\rangle_0] \qquad (5.26)$$

where $\langle S^x\rangle_0$ is now determined from (5.25) with $T = T_o$.

Equation (5.26) was used as a regression on the nine data points for ω_a vs. T at 6.54 kbar with regression parameters $p_1 = A$, $p_2 = 2\langle S^x\rangle_0$ and $p_3 = B$. The regression was

Table 5-6

Model B: Results of regression analysis

$p_1 = A$, $p_2 = 2\langle S^X \rangle_0$ and $p_3 = B$

Ω(295K, 1 bar) cm^{-1}	p_1	p_2	p_3 cm^{-1}	$\sigma(p_1)$	$\sigma(p_2)$	$\sigma(p_3)$ cm^{-1}	s^2 $(cm^{-1})^2$
315	0.770	0.600	1135	0.022	0.007	76	0.31
320	0.732	0.634	952	0.019	0.003	64	0.32
330	0.687	0.676	754	0.018	0.003	53	0.34
340	0.653	0.704	642	0.017	0.004	49	0.38
350	0.626	0.726	567	0.016	0.004	47	0.41
360	0.602	0.742	515	0.016	0.004	46	0.45
370	0.583	0.752	480	0.016	0.004	46	0.48

performed using the Madison Academic Computing Centre (MACC) nonlinear regression package NREG*- a routine which gives greater control over the analysis than does the Harwell routine VBØ1A. One difficulty in performing the regression is that equation (5.26) has to be solved explicitly for $\langle S^x \rangle$ - this was achieved by means of the Harwell subroutine NBØ1A (cf. section 2.4).

The results are summarized in table 5.6. Although the values of s^2 are obtained are all lower than the value of s^2 obtained from Peercy's model, the large negative values for B are disconcerting. B consists of the sum of two terms: one due to the proton-optic phonon coupling (which, according to Blinc's analysis can only increase the effective tunnelling frequency) and a second due to direct $B_{ij}S_i^xS_j^x$ coupling. This latter term must therefore be large and negative. If the values of B are compared with the values of J given in table 5.1, the direct $B_{ij}S_i^xS_j^x$ coupling is seen to be as important as the direct $J_{ij}S_i^zS_j^z$ coupling. This seems most unlikely. Thus although the inclusion of $S_i^xS_j^x$ couplings in the Hamiltonian leads to a somewhat better fit to the Raman response, the model cannot be accepted as the parameter values required are physically unrealistic.

Model C

Blinc's argument for the addition of an "indirect" $S_i^xS_j^x$ coupling term in the Hamiltonian treats the proton-photon coupling in a linear approximation. However, this is by no means accurate, for even if a double harmonic oscillator potential is assumed Ω has an exponential rather than a linear

* See Appendix D

dependence on the O...O displacement (cf. Blinc and Hadzi (1958)).

It would be very difficult to include such a highly non-linear coupling in the Kobayashi model. Instead a model will be developed which takes this exponential dependence into account in another way.

Figure 5.9 shows the typical variation of Ω with R computed from the double Morse potential model, with $\Omega(295K, 1\ bar) = 320\ cm^{-1}$. Over a small R range equation (5.23) is more accurately written as

$$\Omega(Q) = \Omega(0)\exp(-bQ) \qquad (5.27)$$

where $\Omega(0)$ represents the value of Ω when the O...O distance is at its equilibrium value. This expression must then be used to replace the constant Ω in the Hamiltonian (5.7).

Now if Q is considered to be an internal co-ordinate defining a local harmonic mode then

$$\begin{aligned} \langle\Omega(Q)\rangle &= \langle\Omega(0)\exp(-bQ)\rangle \\ &= \Omega(0)\langle\exp(-bQ)\rangle \\ &= \Omega(0)\exp(-b\langle Q\rangle_c + \tfrac{1}{2}b^2\langle Q^2\rangle_c) \\ &= \Omega(0)\exp(\tfrac{1}{2}b^2\langle Q^2\rangle) \end{aligned} \qquad (5.28)$$

where the subscript c denotes a cumulant average (Kubo (1962a)) and we have used the fact that for $n > 3$, $\langle Q^n\rangle_c = 0$ as Q obeys a gaussian distribution law. This result holds even when the O...O motion is considered as part of the whole system of lattice modes, provided that it is justifiable to treat the heavy-atom dynamics in the harmonic approximation. This can

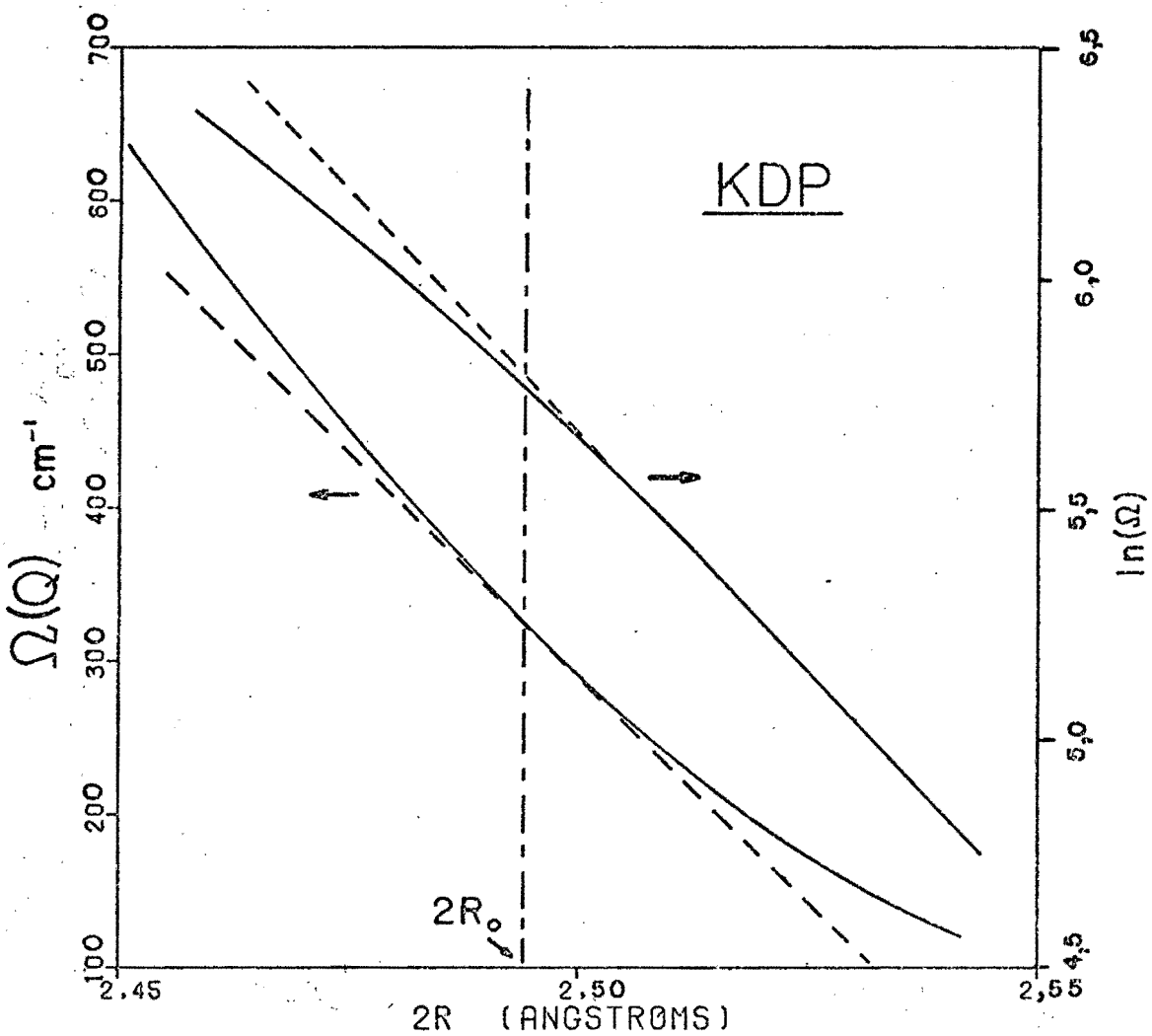

Figure 5.9. Predicted dependence of the "bare" protonic tunnelling frequency on O...O distance. Ω(295k, 1bar) = 320 cm^{-1}, $2R_o$ = 2.4945 Å (cf. table 5.2) and Q = 2R - $2R_o$.

be seen as follows. The internal co-ordinate Q can be obtained from the set of lattice normal co-ordinates by a linear transformation. If the amplitudes of the normal co-ordinates are regarded as independent gaussian random variables, the internal co-ordinate Q must itself be a gaussian random variable. Hence equation (5.28) still holds.

Maradudin, Ipatova, Montroll and Weiss (1971) show that if the lattice modes are taken into account then the expectation value $\langle Q^2 \rangle$ is given by

$$\langle Q^2 \rangle = \frac{\hbar}{NM} \sum_{j=1}^{3r} \sum_{\underset{\sim}{k}} [\omega_j(\underset{\sim}{k})]^{-1} f(\underset{\sim}{k},j) \coth\left[\frac{\hbar\omega_j(\underset{\sim}{k})}{2kT}\right](1 - \cos(\underset{\sim}{k}.2\underset{\sim}{R})) \tag{5.29}$$

where N is the number of atoms in the crystal, M is the mass of the oxygen atom, r is the number of atoms per unit cell, $w_j(\underset{\sim}{k})$ are the eigenfrequencies of the dynamical matric corresponding to the wavevector $\underset{\sim}{k}$ and $f(\underset{\sim}{k},j)$ is a further factor depending on the eigenvalues of the dynamical matrix (cf. equation 7.3.8 in the above reference). If the system is treated in the classical limit $\hbar\omega_j(\underset{\sim}{k}) >> kT$ then

$$\langle Q^2 \rangle \approx \frac{\hbar}{NM} \sum_{j=1}^{3r} \sum_{\underset{\sim}{k}^2} [\omega_j(\underset{\sim}{k})]^{-1} f(\underset{\sim}{k},j) \frac{2kT}{\hbar\omega_j(\underset{\sim}{k})}(1 - \cos(\underset{\sim}{k}.2\underset{\sim}{R})) \tag{5.30}$$

and hence $\langle Q^2 \rangle \propto T$. For simplicity, we shall assume that the classical limiting approximation can be justified in the high temperature paraelectric phase.

Now equation (5.30) is equivalent to that which would be obtained if Q described a single classical localised harmonic mode i.e. $\langle Q^2 \rangle = kT/(m\omega^2)$, Thus combining this with equation (5.28), $\langle \Omega(Q) \rangle = \langle \Omega(T,P) \rangle$ may be written as

$$\langle\Omega(T,P)\rangle = \Omega_0(T,P)\exp(cT) \qquad (5.31)$$

where $c = \frac{1}{2}b^2k/(m\omega^2)$ and $\Omega_0(T,P) = \Omega(Q=0)$ provided that

i) T is sufficiently high so as to make the classical approximation (5.30) valid and

ii) m and ω^2 are not necessarily identified respectively with a reduced O...O mass or an internal local mode frequency.

Equation (5.19) now becomes

$$\omega_a^2(T,P) = A\Omega_0(T,P)\exp(cT)[A\Omega_0(T,P)\exp(cT) - J(T,P)\langle S^x\rangle] \qquad (5.32)$$

or

$$w_a^2(T,P) = [A\Omega_0(T,P)\exp(cT)]^2\left[1 - \frac{J(T,P)}{A\Omega_0(T,P)\exp(cT)}\langle S^x\rangle\right]$$

$$= [A\Omega_0(T,P)\exp(cT)]^2[1 - \langle S^x\rangle/\langle S^x\rangle_0] \qquad (5.33)$$

where

$$\langle S^x\rangle = \tfrac{1}{2}\tanh\left[\frac{A\Omega_0(T,P)\exp(cT)}{2kT}\right] \qquad (5.34)$$

if $J(T,P)/[\Omega_0(T,P)\exp(cT)]$ is assumed temperature independent.

A non-linear regression of equation (5.33) on the nine data points of figure 5.6 was performed, using the MACC package with regression parameters $p_1 = A$, $p_2 = 2\langle S^x\rangle_0$ and $p_3 = c$. The results are summarized in table 5.7. The goodness of fit obtained, as measured by s^2, is comparable with that achieved by Peercy's analysis.

The question arises as to whether the values for parameter p_3 are realistic. Exp (cT) evaluated at T = 295K for Ω(295K, 1 bar) = 320 cm^{-1} equals 1.45, using the value for c given in table 5.7. Alternatively, b can be estimated from the curve in figure 5.9: at P = 1 bar and T = 295K b is

Table 5-7

Model C: Results of regression analysis

$p_1 = A$, $p_2 = 2\langle S^X \rangle_0$ and $p_3 = c$

Ω(295K, 1 bar) cm^{-1}	p_1	p_2	p_3 10^{-3} K	$\sigma(p_1)$	$\sigma(p_2)$	$\sigma(p_3)$ 10^{-3} K	s^2 $(cm^{-1})^2$
315	0.311	0.9728	1.41	0.006	0.0015	0.08	0.45
320	0.326	0.9728	1.26	0.007	0.0016	0.08	0.47
330	0.346	0.9729	1.07	0.007	0.0016	0.08	0.48
340	0.357	0.9730	0.94	0.007	0.0017	0.08	0.48
350	0.362	0.9730	0.85	0.007	0.0017	0.08	0.48
360	0.363	0.9730	0.77	0.007	0.0016	0.08	0.48
370	0.362	0.9730	0.73	0.007	0.0017	0.08	0.50

approximately equal to 12Å^{-1}. $\langle Q^2 \rangle$ can be estimated as follows from a plot of the variation of the $|0\rangle \rightarrow |3\rangle$ IR-active transition frequency with O...O distance. Assume that the modulation of ν_s(OH) frequency by the O...O vibrations is responsible for the width of the band at 4600 cm^{-1} and that a quasi-static "slow-modulation" limit is appropriate (Kubo (1962b)), then the half-width of this band can be used to predict directly from the plot the mean square deviation of the O...O distance due to thermal vibration (cf. Lawrence and Robertson (1979)). $\langle Q^2 \rangle$ is estimated by this method to be about $(0.07\text{Å})^2$. Hence $\exp(\frac{1}{2}b^2\langle Q^2 \rangle) = 1.42$. This value for $\exp(cT)$, which was estimated entirely from the infrared results, is thus comparable with the value estimated from the Raman response. Although the above bandwidth estimate is rather crude, the agreement between the two independent estimates of $\exp(\frac{1}{2}b^2\langle Q^2 \rangle)$, $(= \exp(cT))$, is very good and the values for p_3 can therefore be regarded as realistic.

Model D

Even though model C takes into account the effect of the non-linearity of the coupling between the pseudospin system and the non-polar optic phonons, it can be refined further to include the direct $B_{ij}S_i^xS_j^x$ proton-proton coupling, as was done in model B. The combined result is then

$$\omega_a^2(T,P) = [A\Omega_0(T,P)\exp(cT) + B\langle S^x \rangle][A\Omega_0(T,P)\exp(cT) - (J(T,P) - B)\langle S^x \rangle] \quad (5.35)$$

where

$$\langle S^x \rangle = \tfrac{1}{2}\tanh\left[\frac{A\Omega_0(T,P)\exp(cT) + B\langle S^x \rangle}{2kT}\right] \quad (5.36)$$

and B now represents only the direct $S_i^x S_j^x$ coupling arising from the difference between the form of the proton probability distribution functions in the ground and first excited states.

If the ratio $[J(T,P) - B]/[\Omega(T,P)\exp(cT)]$ is assumed temperature independent (in analogy with previous assumptions), equation (5.36) becomes

$$\omega_a^2(T,P) = [A\Omega_0(T,P)\exp(cT) + B\langle S^x\rangle]A\Omega_0(T,P)\exp(cT)$$
$$[1 - \langle S^x\rangle/\langle S^x\rangle_0] \quad (5.37)$$

where $\langle S^x\rangle_0$ is now determined from (5.36) with $T = T_o$. A regression of equation (5.37) on the nine data points in figure 5.6 was performed using the MACC package and regression parameters $p_1 = A$, $p_2 = 2\langle S^x\rangle$, $p_3 = B$ and $p_4 = c$. The Harwell routine NBØ1A was again used to determine $\langle S^x\rangle$ explicitly from (5.36).

The results are summarised in table 5.8. The values of s^2 are the lowest achieved thus far. The only difficulty is that the $\langle S^x\rangle_0$ values are slightly greater than 0.5, which from equation (5.36) is not permissible. However the discrepancy is not so great as to cause concern. It simply means that T_o cannot be determined accurately and is probably close to OK. This seems to agree with the interpretation of the phase transition that has been proposed by Cochran (1969), namely that the (hypothetical) ordering temperature of the bare protonic collective mode is not the principal factor which determines the Curie temperature but that it is the coupling of the protonic mode to the heavy-atom vibrations which is important. The other parameters appear to be entirely reasonable. A is similar to the values previously mentioned

Table 5-8

Model D: Results of regression analysis

$p_1 = A$, $p_2 = 2\langle S^X \rangle_0$, $p_3 = B$ and $p_4 = c$

Ω(295K, 1 bar) cm^{-1}	p_1	p_2	p_3 cm^{-1}	p_4 10^{-3} K	$\sigma(p_1)$	$\sigma(p_2)$	$\sigma(p_3)$ cm^{-1}	$\sigma(p_4)$ 10^{-3} K	s^2 $(cm^{-1})^2$
315	0.297	1.020	92	1.37	0.006	0.011	26	0.08	0.28
320	0.312	1.020	92	1.23	0.066	0.012	26	0.08	0.27
330	0.331	1.021	94	1.03	0.006	0.011	25	0.08	0.27
340	0.341	1.021	95	0.90	0.007	0.011	25	0.09	0.28
350	0.345	1.021	96	0.80	0.007	0.011	25	0.09	0.27
360	0.347	1.021	96	0.73	0.007	0.011	25	0.09	0.27
370	0.346	1.021	96	0.68	0.007	0.011	25	0.09	0.27

in section 5.5, B is now considerably less than the $S_i^x S_j^x$ coupling coefficient J (cf. table 5.1) and the values for c are similar to those obtained in model C.

A room temperature estimate of $\tilde{\Omega} \equiv A\Omega_0 \exp(cT) + B\langle S^x \rangle$ can then be obtained from table 5.8, assuming $\Omega_0 = 320\ cm^{-1}$ and obtaining $\langle S^x \rangle$ from a solution to equation (5.36). This gives $\tilde{\Omega} = 143\ cm^{-1} + B\langle S^x \rangle = 143\ cm^{-1} + 17\ cm^{-1} = 160\ cm^{-1}$.

No detailed statistical analysis can be performed for any of these models owing to a lack of information about the errors in the published ω_a vs. T data. The standard deviations σ given in tables 5.5-5.8 for the various parameters were determined by the MACC package using a linearized model about the optimal point in parameter space. In model D, B is poorly determined and an inspection of the partial correlation coefficients computed by the subroutine showed that B is highly correlated with $\langle S^x \rangle_0$. The other variables all appeared to be well determined and to be little correlated.

More data points in the region T > 300K (together with all the error bars) would be needed to establish conclucively that model D gives the best fit of all the models to the Raman data. If this is true then the other models should give progressively worse fits as the temperature range is extended.

Finally it must be noted that the fit achieved with model D is very good indeed: the root mean square residual is about 0.4 cm^{-1}, which is probably less than the expected error in the data points. This implies that the assumption that was made in the development of the model, viz. that $[J(T,P) - B]/[\Omega_0(T,P)\exp(cT)]$ is temperature independent, is

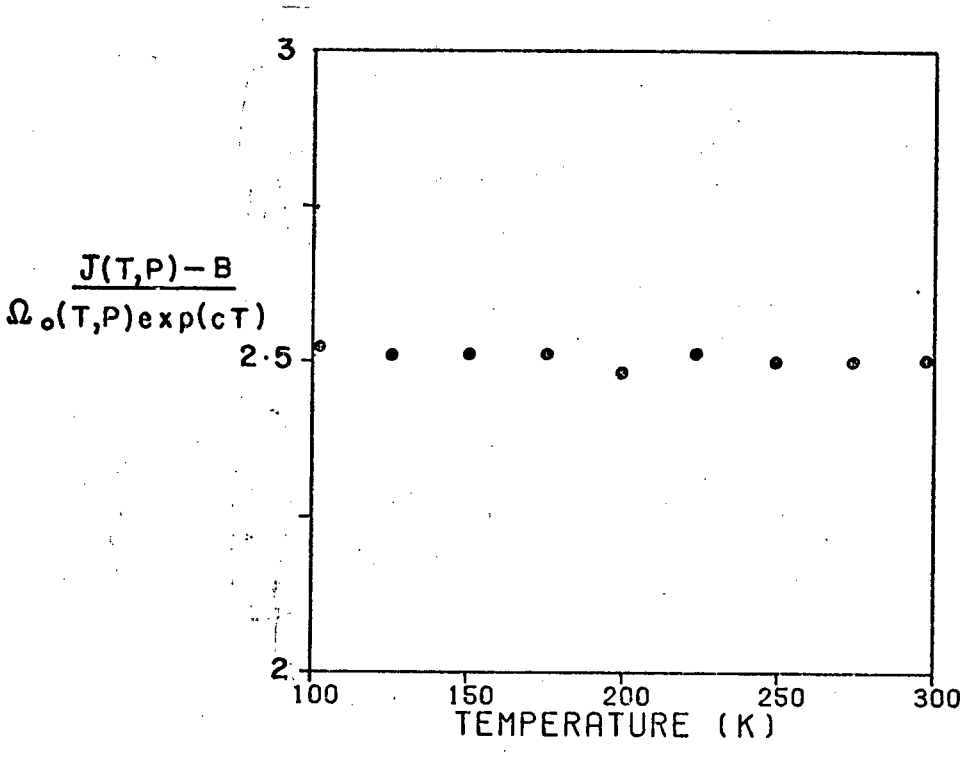

Figure 5.10. Predicted temperature dependence of the quantity $[J(T,P) - B]/[\Omega_o(T,P)\exp(cT)]$. This quantity shows no systematic variation with temperature, which supports the hypothesis that it is temperature independent. P = 6.45 kbar.

supported by the data. This quantity is plotted as a function of temperature in figure 5.10: it is evident that any systematic temperature variation is small.

5.6.3 Discussion

The above analysis has shown that

i) The Blinc-Ribarič polarization factor A,

ii) The direct $B_{ij}S_i^xS_j^x$ coupling between the pseudospins,

iii) The dynamic modulation of the tunnelling frequency by the lattice modes, and

iv) The temperature dependence of the tunnelling frequency due to lattice thermal expansion

are all essential factors in understanding the temperature dependence of the collective mode frequency.

Furthermore the analysis permits a far clearer understanding of the existing Raman and crystallographic data:

Firstly, the results of attempting to fit model B to the Raman response show that assuming a linear dependence of Ω on the O...O distance in the coupled mode model fails to explain the temperature dependence of the protonic collective mode frequency. Model C on the other hand shows that the temperature dependence of the collective mode frequency can be adequately explained by including explicitly the exponential dependence of Ω on the O...O distance and treating the O...O thermal motion as a stochastic process.

Secondly, the results of model C explain why Peercy's original model gave a good fit to the ω_a vs. T data even with a temperature-independent Ω. The temperature dependence of Ω is the result of two combined effects: i) the thermal

contraction of the O...O bond on cooling and ii) the modulation of the tunnelling frequency by the thermal fluctuations of the lattice. The first effect increases Ω exponentially with decreasing temperature whereas the second effect decreases $\langle\Omega\rangle$ exponentially with decreasing temperature. The two exponential rates are approximately the same (but of opposite sign) and hence Ω remains approximately temperature independent.

Thirdly it resolves the difficulty pointed out by Nelmes regarding the change in O...O distance on cooling. This variation in O...O distance must be taken into account but so must the modulation of the tunnelling frequency by the lattice vibrations. The resultant effect on the single particle tunnelling frequency is not nearly as great as might be anticipated from the thermal contraction alone. The application of pressure, on the other hand, affects only the O...O distance and not the magnitude of the O...O fluctuations. Thus the application of pressure has a much greater effect on the effective single-particle tunnelling frequency than does the thermal contraction of the O...O bond.

Fourthly, it explains why there are so many different estimates of Ω in the literature. The estimate obtained for Ω will depend on the experimental method and upon which particular interactions have been taken into account in the theory. The above analysis distinguishes between the following:

i) The bare (static) single-particle tunnelling frequency Ω, such as would be detected in the ν_s(OH) infrared spectra. The double Morse potential analysis of the infrared and crystallographic data in section 5.4 has

estimated Ω to be 320 $\pm$ 10 cm^{-1} at room temperature and atmospheric pressure.

ii) $A\Omega$, the static renormalized single-particle tunnelling frequency, renormalized by the factor A to allow for proton self-trapping caused by lattice polarization (Blinc and Ribarič (1963)). A has been estimated from the soft-mode Raman data to be 0.31 (cf. table 5.8) and thus $A\Omega$ is about 99 cm^{-1} at room temperature and atmospheric pressure.

iii) $A\Omega_0 \exp(\frac{1}{2}b^2\langle Q^2\rangle)$, which is an effective single-particle tunnelling frequency corrected for self-trapping and lattice modulation. This is approximately temperature independent and is estimated from the analysis of soft-mode Raman data to be about 143 cm^{-1} at room temperature and atmospheric pressure.

iv) $A\Omega_0 \exp(\frac{1}{2}b^2\langle Q^2\rangle) + B\langle S^x\rangle$, which also contains a correction for the effect of skewness of the single-particle potential on the proton-proton interactions. This leads to further terms proportional to $\langle S^x\rangle$ in the mean field approximation to the transverse Ising model Hamiltonian and thus to a correction in the tunnelling frequency. The magnitude of this correction is estimated to be about 17 cm^{-1} at room temperature and atmospheric pressure and thus the effective tunnelling frequency is about 160 cm^{-1}.

The above analysis stresses the importance of being able to take into account accurately the temperature and pressure dependence of the single-particle tunnelling frequency.

5.7 Determination of the Proton-Proton Interaction J

The coefficient $J = \sum_j J_{ij}$ describes the interaction between a given proton and its neighbours in the lattice. De Gennes (1963), who first introduced the pseudospin formalism in the context of KDP, pointed out that J comprises both long-range (dipolar) terms and short-range lattice-mediated terms, together with further components arising from the coupling of the protons to the lattice modes. In the literature (see references below) J has often been assumed to be described by the relationship $J \propto \delta^2$ where δ is the protonic inter-site separation. This is indeed the case if J is an exclusively dipolar interaction. For then J is proportional to the product of the dipole moments of adjacent OH...O bonds and as each dipole moment is itself proportional to the off-centre distance of the proton in the bond, J is proportional to δ^2. This would lead to $J_H/J_D = \delta_H^2/\delta_D^2$ on deuteration, assuming that the predominant change in the lattice structure on deuteration is that in the site-site separation of the hydrogen-bonded particle.

A similar result for J on deuteration can be derived quantum-mechanically without making explicit assumptions about dipole interactions. Vaks and Larkin (1966) and Vaks and Zinenko (1973) showed this formally by making a gradient expansion of the proton-proton interaction potential. Using the two-state symmetric/antisymmetric basis (ϕ_0, ϕ_1) for the protons, Vaks and Zinenko obtain

$$J(\underset{\sim}{r}_i - \underset{\sim}{r}_j) = V(\underset{\sim}{r}_i - \underset{\sim}{r}_j)\,\xi^i_{sa}\,\xi^j_{sa} \qquad (5.38)$$

where $\xi^{i}_{sa} = \langle 0|x|1\rangle_i$, $|0\rangle$ and $|1\rangle$ being the state vectors for the ground and first excited protonic states respectively and x the displacement from the centre of the respective bond. $V(\underset{\sim}{r}_i - \underset{\sim}{r}_j)$ is a structure factor depending on the positions $\underset{\sim}{r}_i$ and $\underset{\sim}{r}_j$ of the ith and jth proton respectively. Thus if the structure of the lattice does not change substantially on deuteration and if J is sufficiently short-range for the gradient expansion of V to be adequate, the above discussion implies that

$$\frac{J_H}{J_D} \approx \frac{\xi^{(H)2}_{sa}}{\xi^{(D)2}_{sa}} \approx \frac{\delta^2_H}{\delta^2_D} \qquad (5.39)$$

since

$$\langle 0|x|1\rangle \approx 2\int_0^\infty x|\phi_0|^2 dx = \delta,$$

provided that the ground state splitting is small.* Also $J \propto w$ as J is a linear combination of the Slater-Takagi parameters ε and w and $w >> \varepsilon$.

This type of relationship was first put forward tentatively by Silsbee, Uehling and Schmidt when they assumed that

$$\frac{\varepsilon_H}{\varepsilon_D} = \frac{\delta^2_H}{\delta^2_D} \qquad (5.40)$$

in order to explain the observed transition entropy changes of KDP and DKDP. However, Blinc and Žekš (1968), Blinc and Žekš (1974), Torstveit (1979) and Mackowiak, Stankowski, Žekš

---

* The assumption that $\xi^{(H)2}_{sa}/\xi^{(D)2}_{sa} \approx \delta^2_H/\delta^2_D$ can be tested in terms of the double Morse potential model as follows. The left hand side, evaluated directly from the double Morse potential wavefunctions is found to be equal to 0.654 at room temperature and atmospheric pressure. The right hand side, estimated from table 5.2 is equal to 0.665 at room temperature and atmospheric pressure. Thus $\xi^{(H)2}_{sa}/\xi^{(D)2}_{sa} \approx \delta^2_H/\delta^2_D$.

and Blinc (1979) have assumed that $J \propto \delta^2$ is valid on hydrostatic compression of the lattice. However this cannot be directly inferred from equation (5.40) as these authors suppose unless the classical dipolar interaction interpretation of J is correct. The quantum-mechanical treatment only leads to $J \propto \delta^2$ if the structure factors $V(\underset{\sim}{r}_i - \underset{\sim}{r}_j)$ in equation (5.38) do not change on compression.

To see this more clearly it is instructive to compare the effect of deuteration with the effect of compression on the lattice parameters. The changes in lattice parameters are summarized in table 5.9. As can be seen from the table, the most noticeable effect on deuteration is the change in δ, the lattice constant a and the tetrahedral angle θ are little changed. The effect of isotopic substitution is mainly to reduce the zero-point amplitude of the proton and since the potential is skew this results in the maxima of the deuterium probability density function being appreciably further from the centre of the O...O bond than those of the proton probability density function. However, on compression the change in a and θ are much more pronounced. Thus $J \propto \delta^2$ on compression cannot be directly implied from assumption (5.39) without further justification.

An attempt will now be made to calculate J(T,P) directly from the Raman response. The relationship $J \propto \delta^2$ will then be tested to see whether J can in any sense be treated as a dipolar interaction.

The protonic collective mode frequency has been seen to be best described by equation (5.35). From this equation

Table 5.9

Change in KDP lattice parameters on compression, deuteration and cooling. (Estimated from Table 5.2)

	$\Delta\delta$ (Å)	$\Delta\theta$ °	Δa (Å)	Δ(O...O) (Å)
14kbar compression (T = 295K)	0.03	0.80	0.11	0.021
Deuteration (T = 295K, P = 1 bar)	0.083	0.57	0.008	0.031
Cooling 295K → 128K (P = 1 bar)	0.026	0.10	0.026	0.011

$$J(T,P) = \left[\tilde{\Omega}(T,P) - \frac{\omega_a^2(T,P)}{\tilde{\Omega}(T,P)}\right] \frac{1}{\langle S^x \rangle} \qquad (5.41)$$

where

$$\tilde{\Omega}(T,P) = A\Omega_0(T,P)\exp(cT) + B\langle S^x \rangle .$$

The best estimate of $\Omega_0(295K, 1bar)$ was seen to be 320 cm^{-1} and this estimate can be used to determine $\Omega_0(T,P)$. $\omega_a(T,P)$ has been determined by Peercy

i) along the isobar P = 6.54 kbar (figure 5.6) and

ii) along the isotherm T = 295K (figure 5.7).

Equation (5.41) can therefore be used to determine J(T,P) along these same curves. These calculations were performed and the results, displayed in figures 5.11 and 5.12, will now be discussed.

i) J(T, 6.54 kbar) (figure 5.11). J increases approximately linearly with temperature at a rate of about 0.7% per 100K. Its value is typically about 425 cm^{-1}, which is a reasonable result. This seems to be the first time that the temperature dependence of J has been estimated in the literature. $\Omega_0(T, 6.54\ kbar)$ and $\tilde{\Omega}(T, 6.54\ kbar)$ have also been plotted for comparison purposes.

ii) J(295K, P) (figure 5.12). J shows a substantial increase with pressure. The rate of increase is highest at low pressures: $(1/J)\partial J/\partial P]_{P=0\ kbar}$ = 12% per kbar and $(1/J)\partial J/\partial P]_{P=10\ kbar}$ = 4% per kbar. $\Omega_0(295K, P)$ and $\tilde{\Omega}(295K, P)$ are also plotted for comparison purposes. This high rate of increase of J with pressure seems unrealistic. The most likely error is probably Peercy's low pressure values of ω_a: it is difficult

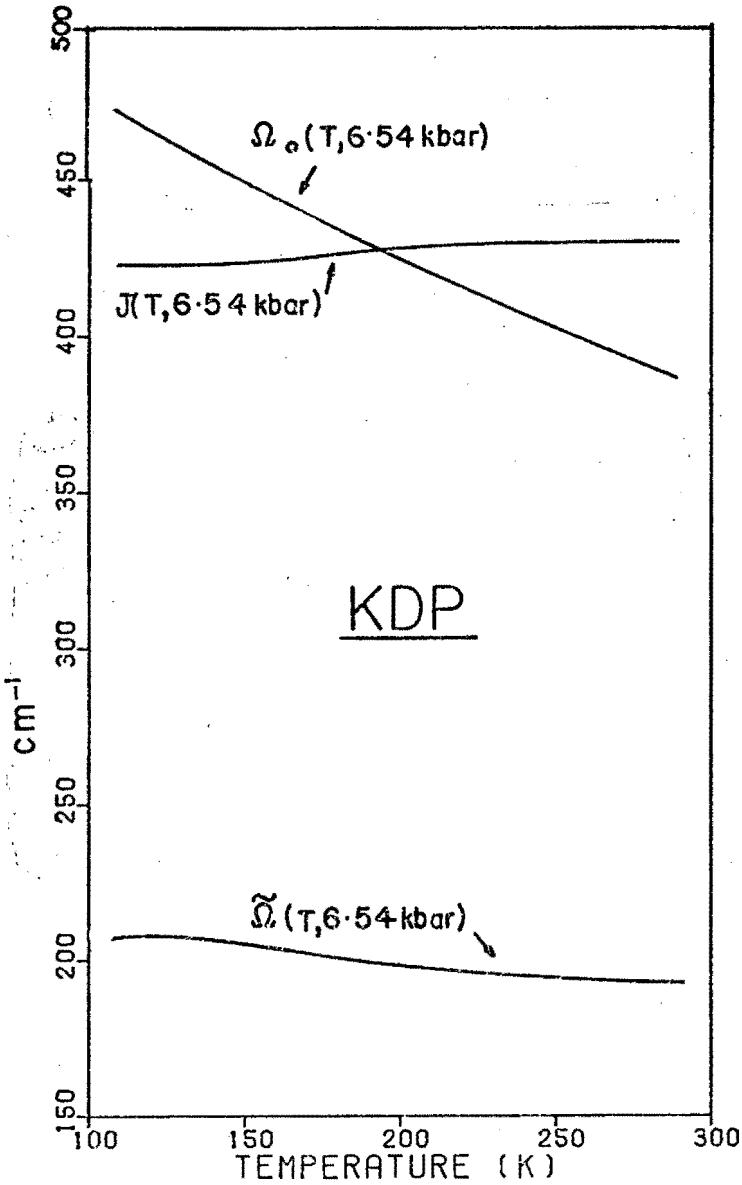

Figure 5.11. Predicted temperature dependence of J, $\tilde{\Omega}$ and Ω_0 at P = 6.54 kbar.

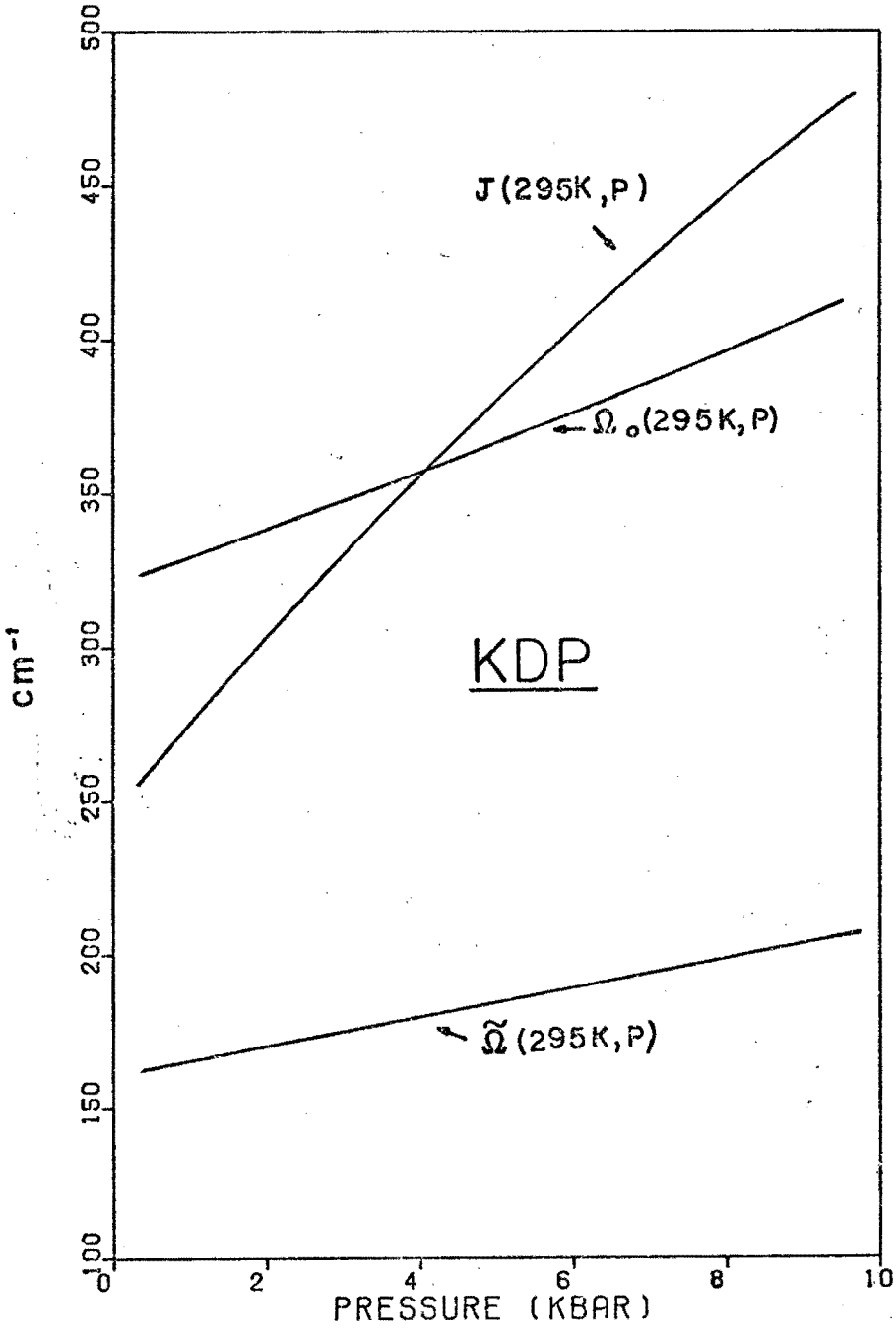

Figure 5.12. Predicted pressure dependence of J, $\tilde{\Omega}$ and Ω_0 at room temperature.

to determine ω_- and ω_+ accurately at low pressures as the soft mode is highly damped. The functional form of equation (5.41) makes the calculated J(T,P) very sensitive to errors in $\omega_a(T,P)$ and again the high pressure results are likely to be more accurate. The results do however indicate that J(295K, P) is an increasing function of pressure.

The dependence of J(T,P) on δ can now be determined. $\delta(T,P)$ was calculated along the same T,P-paths from the double Morse potential model and figure 5.13 then plots J(T,P) as a function of δ^2. If one attempts to describe J(T,6.54 kbar) by the functional form $J = a_o + a_1\delta^2$ one obtains $a_o = (400 \pm 18)$ cm^{-1} from which $J(T,6.54\text{ kbar}) \propto \delta^2$ may be safely rejected with a very high degree of confidence. J(295K,P) is clearly not proportional to δ^2 as is obvious from the result that J(295K,P) is an increasing function of pressure. This suggests that J may well be affected more by changes in the lattice parameter a and the angle θ between neighbouring tetrahedra (as defined by Nelmes (1980)) than by changes in the parameter δ. This supports the conclusion of Nelmes (1980) that the orientation of the tetrahedra may be more important in characterising the pressure response of KDP than is the parameter δ. Furthermore the substantial increase of J with pressure suggests that J cannot simply be treated as dipolar and that both long and short range effects must be included. The theory of the pressure dependence of T_c proposed by Blinc and Žekš (1974, chapter 6), which equates $d\ell nJ/dP$ to $2d\ell n\delta/dP$, cannot therefore be correct, and its application by Mackowiak, Stankowski, Žekš and Blinc (1979) to the pressure dependence of T_c in potassium dihydrogen

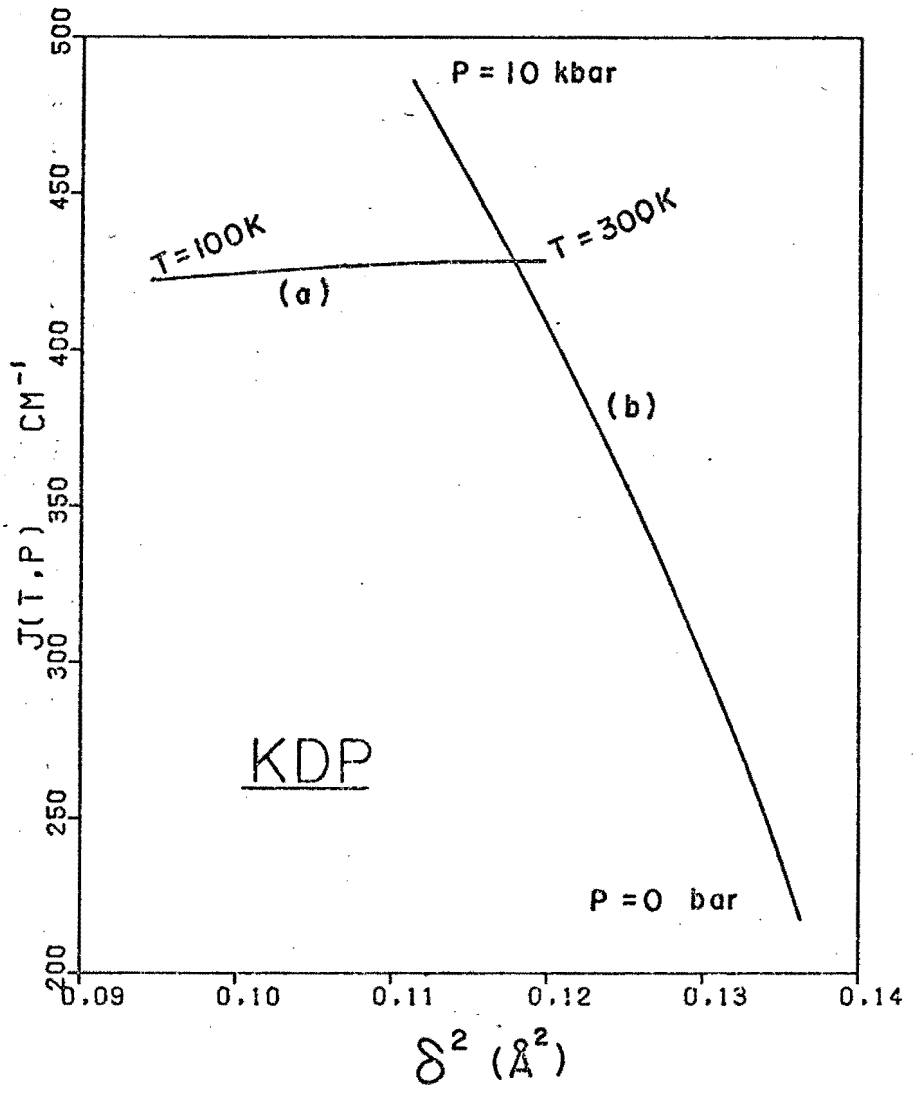

Figure 5.13. Predicted dependence of J(T,P) on the protonic inter-site distance δ, computed along
a) the isobar P = 6.54 kbar, and
b) the isotherm T = 295K.
The assumption that $J \propto \delta^2$ on the application of hydrostatic pressure or on cooling is strongly refuted.

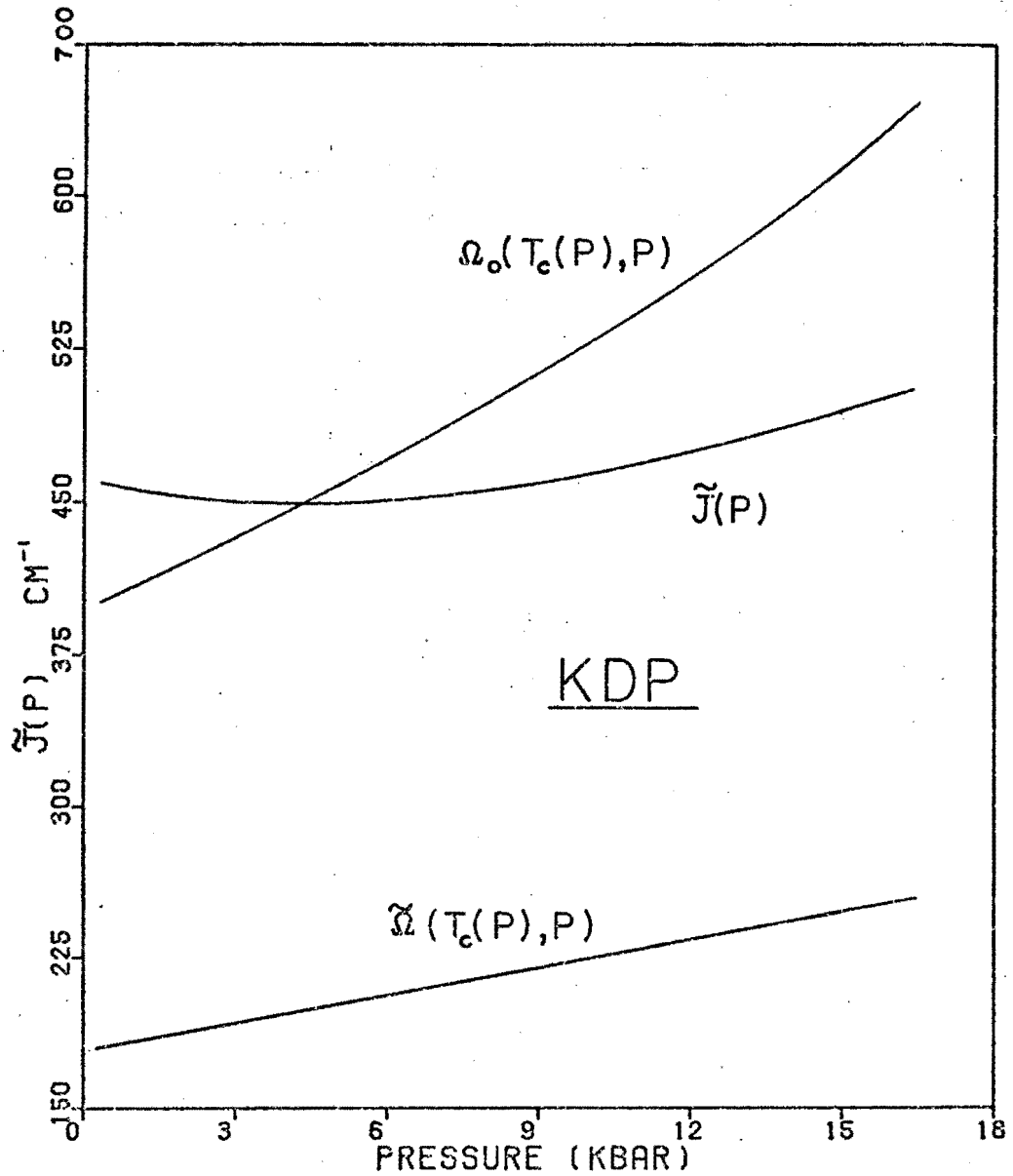

Figure 5.14. Predicted pressure dependence of $\tilde{J}$, $\tilde{\Omega}$ and Ω_0 at $T = T_c(P)$.

arsenate (KDA) is questionable.

Finally, the model can be used to estimate the pressure dependence of $\tilde{J}(T_-(P)P) \equiv \tilde{J}(P)$. Note that $\tilde{J}$ is defined only at the "clamped" Curie temperature. Equation (5.11) becomes, after including the renormalizations of the previous section,

$$\tilde{J}(T_-(P),P) = \tilde{\Omega}/\langle S^x \rangle_- \qquad (5.42)$$

where $\langle S^x \rangle_-$ is given by equation (5.36) with $T = T_-(P)$. $T_-(P)$ can be obtained from figure 5.5 (as $T_-(P) \approx T_c(P)$ and thus equation (5.42) can be used to determine $\tilde{J}(P)$. The results of this calculation are displayed in figure 5.14. $\tilde{J}(P)$ decreases slightly at first as P increases but thereafter increases rapidly with increasing P. This behaviour seems unrealistic particularly at the lower pressure and might again be caused by failure to take properly into account the large damping of the soft mode at low pressures. The high pressure results imply that $J \approx 2\tilde{\Omega}$ with $(1/J)\partial\tilde{J}/\partial P = 1\%$ kbar.

5.8 A Note on Soft Mode Damping

The soft mode in KDP is overdamped at room temperature and atmospheric pressure. However, Peercy (1973) showed that the soft mode became underdamped at pressure greater than 6 kbar and proposed that this resulted from an increase in the correlation length of the collective protonic excitation. Peercy's coupled mode analysis (1975) showed that the magnitude of the collective mode damping is also reduced with decreasing temperature.

Tuval and Nettleton (1976) formally examined the effect of introducing a strain-dependent proton-proton interaction

in the Kobayashi model, supposing that the proton-proton interaction is modulated by the acoustic lattice vibrations. This was able to explain effectively the observed damping of ultrasound in KDP crystals, but was less successful in explaining the damping of the soft-mode Raman response.

The discussion of the preceding section support the idea that the proton-proton interaction J is dependent on the distance between neighbouring protons in the lattice. However, the dependence of the tunnelling frequency Ω on the O...O distance is much greater than any corresponding effect on J, which suggests that a theory which includes the strain-dependence of J but neglects that of Ω is at best incomplete.

The simplest way of characterizing the distribution of Ω is to estimate its variance. This may be done as follows, (ignoring for simplicity the direct $B_{ij}S_i^xS_j^x$ coupling and the Blinc-Ribaric polarization factor A):

$$\begin{aligned}
\langle(\Omega - \langle\Omega\rangle)^2\rangle &= \langle\Omega^2\rangle - \langle\Omega\rangle^2 \\
&= \Omega_0^2\langle\exp(-2bQ)\rangle - \Omega_0^2\langle\exp(-bQ)\rangle^2 \\
&= \Omega_0^2[\exp(-2b\langle Q\rangle_c + \tfrac{1}{2}(2b)^2\langle Q^2\rangle_c) \\
&\quad - (\exp(-b\langle Q\rangle_c + \tfrac{1}{2}b^2\langle Q^2\rangle_c))^2] \\
&= \Omega_0^2[\exp(2b^2\langle Q^2\rangle) - \exp(b^2\langle Q^2\rangle)] \\
&= \Omega_0^2\exp(b^2\langle Q^2\rangle)[\exp(b^2\langle Q^2\rangle) - 1] \\
&= \langle\Omega\rangle^2[\exp(b^2\langle Q^2\rangle) - 1] \qquad (5.43)
\end{aligned}$$

where, once again, the subscript c represents a cumulant average (Kubo (1962a)). Q has again been assumed to obey a gaussian distribution law with zero mean so that all cumulants of third and higher orders vanish identically.

For KDP at room temperature and atmospheric pressure, $\exp(\frac{1}{2}b^2\langle Q^2\rangle)$ has been estimated as 1.42 (section 5.6.2). It

follows that the variance of Ω is about $[(1.42)^2 - 1]\langle\Omega\rangle^2 \approx \langle\Omega\rangle^2$. Despite the skewness of the distribution, this indicates a very broad distribution of Ω about its expected value.

Although nothing seems to be known about the proper mathematical description of a collective tunnelling mode where the individual tunnelling frequencies are randomly distributed with a large variance (comparable to the square of the mean value), one may surmise that the collective mode would be subject to frequent interruption due to the fluctuations in the tunnelling frequencies of the individual protons. This could be interpreted as a damping of the soft mode.

The pressure and temperature dependence of $\mathrm{var}(\Omega) \equiv \langle(\Omega - \langle\Omega\rangle)^2\rangle$ should then give some idea of the temperature and pressure dependence of the damping. Equation (5.43) is written as

$$\mathrm{var}(\Omega) \approx \langle\Omega\rangle^2 b^2 \langle Q^2\rangle. \qquad (5.44)$$

If the predominant temperature dependence of the right hand side of this equation comes from that of $\langle Q^2\rangle$ (which is proportional to T in the classical limit, cf. equation (5.30)), then a decrease in temperature implies a decrease in the variance of Ω and hence in the damping.

The reduction in the damping of the soft mode with increasing pressure may arise if b did not remain constant with change in pressure. Figure 5.9 suggests that if Ω is described by $\Omega(Q) = \Omega(0)\exp(-bQ)$, then b is smaller in value at higher pressures. (The graph of $\ln(\Omega)$ vs. 2R is not quite linear but flattens as R decreases.) This reduces the variance of Ω and thus reduces the damping.

This mechanism is put forward simply as a plausible suggestion but it does merit further theoretical investigation.

5.9 Conclusion

5.9.1 Summary of Results

We have shown in this chapter that the double Morse potential can be used as an accurate model for the protonic potentials in KDP. This potential has the important feature of being able to give details of how the proton tunnelling frequency and site-site separation vary with temperature and pressure.

The $\nu_s(OH)/\nu_s(OD)$ vibrational bands in the infrared spectra of KDP and DKDP have also been interpreted. For KDP, the band at 4600 cm^{-1}, observed by Viswanath and Miller, is assigned as a $|0\rangle \rightarrow |3\rangle$ transition and the band centred at about 2600 cm^{-1} as a $|1\rangle \rightarrow |2\rangle$ transition. For DKDP, the band centred at about 2600 cm^{-1} is assigned as a $|0\rangle \rightarrow |3\rangle$ transition and the band at about 1750 cm^{-1} as a $|1\rangle \rightarrow |2\rangle$ transition. The potential wells which give rise to these transitions are entirely consistent with the available crystallographic data. The single particle protonic tunnelling frequency is determined to be about 320 ± 10 cm^{-1} at room temperature and atmospheric pressure. This estimate neglects any static polarization effects which are responsible for "self-trapping" of the proton.

The soft-mode Raman analysis of Peercy (1975) has been extensively re-examined. The re-analysis showed that the temperature and pressure dependence of the single-particle tunnelling

frequency play an important role in determining the temperature and pressure dependence of the collective protonic mode frequency and can be calculated directly from the double Morse potential. The effect of the thermal variations in the hydrogen bond lengths is incorporated in the expression for the collective mode frequency, taking into account the exponential dependence of Ω on the hydrogen bond length. The effect on Ω of the decrease in the average O...O distance $\langle 2R \rangle$ with decreasing temperature has been shown to be similar in magnitude and opposite in sign to the effect on Ω of the decrease in the mean square displacement $\langle Q^2 \rangle$ with decreasing temperature. This resolves the difficulty raised by Nelmes regarding the effect of thermal contraction on the single particle tunnelling frequency. The Blinc-Ribarič polarization factor A is determined to be about 0.31 and there is no evidence to suggest that it is strongly pressure dependent. The magnitude B of the direct $S_i^x S_j^x$ coupling between the protons is determined to be about 90 cm^{-1}. The last three effects all combine to produce a renormalized single particle tunnelling frequency that is considerably lower than the "bare" single particle tunnelling frequency.

An attempt was made to calculate the temperature and pressure dependence of the direct $S_i^z S_j^z$ proton-proton interaction J, while allowing explicitly for the temperature and pressure dependence of the single-particle tunnelling frequency Ω. Although a realistic estimate of $(1/J)\partial J/\partial T]_{P=6.54\ \text{kbar}}$ was obtained ($\sim$0.7% per 100K), $(1/J)\partial J/\partial P$ could not be accurately evaluated, primarily due to the large damping at low pressures.

The assumption that the interaction between protons on neighbouring H-bonds can be regarded simply as proportional

to the square of the off-centre distance of the hydrogen-bonded particle has been criticised. It appears that the parameter J must include short-range interactions as well, whose strain dependence is very different from that of classically interacting dipoles.

$\tilde{J}(P)$ was also evaluated and was shown to increase with pressure at a rate of 1% per kbar for $P > 6$ kbar. Low pressure estimates again proved to be inaccurate.

Finally, the soft mode damping can be very simply understood in terms of a reduction in magnitude of the tunnelling frequency fluctuations with increased pressure or decreased temperature. This is a new idea and it complements the damping mechanism arising from a strain-dependent proton-proton interaction proposed by Tuval and Nettleton (1976).

5.9.2 Possible Further Developments

The above analysis leaves a number of possibilities for further development.

i) The assignment of the infrared bands for KDP and DKDP should be tested further by obtaining the IR spectrum for DKDP in the range 4000-8000 cm^{-1}. The 4600 cm^{-1} band observed for KDP should be absent from the DKDP spectrum.

ii) An attempt should be made to estimate the bandshapes for the infrared transitions. This could be done directly from the double Morse potential, using the methods employed in the preceding two chapters.

iii) The effect on the microscopic parameters of the change in the tetrahedral orientation θ with pressure should be further investigated. This concept has only recently been

introduced into the understanding of KDP and the above analysis suggests that it is important.

iv) Raman data should be collected at temperatures above room temperature so that the theoretical expressions for the single-particle tunnelling frequency can be further verified.

v) The proposed soft-mode damping mechanism should be further investigated.

vi) The difficulty raised by Peercy (1975) regarding the temperature dependence of $|G_i|^2$ is not resolved, as Δ is still predicted to increase with decreasing temperature, even after allowing for the renormalization and temperature dependence of Ω. This seems to point again to underlying difficulties in the coupled mode analysis. This is likely to be connected with the neglect of damping in Kobayashi's and the consequent phase ambiguities when phenomenological damping terms are introduced in the analysis of the Raman data.

CHAPTER SIX

CONCLUSION

The double Morse potential has proved useful in the analysis of three hydrogen-bonded systems, viz.

a) Chromous and Cobaltic acids

b) Carboxylic and Dicarboxylic acids

c) Potassium dihydrogen phosphate (KDP)

a) Chromous and Cobaltic acids

The controversy regarding the interpretation of the mid-infrared and neutron inelastic scattering spectra of chromous acid is resolved. The doublet peaks at 1923 cm^{-1} and 1613 cm^{-1} in the mid-infrared spectrum of deuterated chromous acid CrOOD are assigned to $|0\rangle \rightarrow |3\rangle$ and $|1\rangle \rightarrow |2\rangle$ transitions respectively. These transitions were described in terms of a double Morse potential characterized by parameters D, α, r_o and R (the first three parameters corresponding to those of a single Morse function and 2R corresponding to the O...O distance). On the assumption that the change in the protonic potential on deuteration can be accounted for by changing the parameter R (D, α and r_o remaining constant), infrared transition frequencies were predicted for CrOOH. The 226 cm^{-1} band is assigned to a tunnelling ($|0\rangle \rightarrow |1\rangle$) transition, the 1650 cm^{-1} band to a $|1\rangle \rightarrow |2\rangle$ transition and the 3400 cm^{-1} band to a $|0\rangle \rightarrow |3\rangle$ transition. Similar results were obtained for cobaltic acid.

This description in terms of the double Morse potential is entirely consistent with existing infrared and neutron

scattering spectra as well as with the existing crystallographic data. The assumption that the change in the protonic potential on deuteration can be described in terms of a change in R alone appears to be a good one. This is a stringent test as the change in O...O distance on deuteration is large, viz. 0.06Å. This suggests that a similar assumption may be used to describe the change in potential that accompanies thermal expansion or hydrostatic compression of hydrogen-bonded crystals.

b) Carboxylic and Dicarboxylic acids

The mid-infrared spectra of dimeric and deuterated dimeric formic acid have been examined. The 140 cm^{-1} upper state splitting proposed by Excoffon and Marechal is confirmed. The shape of the mid-infrared ν_s(OH) and ν_s(OD) spectral bands can be qualitatively reproduced by assuming that ν_s(OH) and ν_s(OD) frequencies are modulated by the O...O vibrations. (The details of the ν_s(OH) - ν_σ(O...O) coupling are neglected in the analysis.)

The $(COOH)_2$ cycles in crystalline adipic acid have also been examined. As an approximation the same double Morse potential parameters are used as for dimeric formic acid (except of course for R). The analysis shows that the anomalous intensity ratio observed for adipic acid cannot be explained in terms of the well shape alone and that electrical anharmonicity is probably therefore important. Proton tunnelling is also shown to be important in interpreting the polarization of the ν_s(OH) bands.

An estimate of 23 cm^{-1} is obtained for the protonic tunnelling frequency in crystalline formic acid. This is

consistent with an order-disorder interpretation of the phase transition.

c) Potassium dihydrogen phosphate (KDP)

A double Morse potential for the protonic motions in KDP was estimated from the infrared overtone and neutron crystallographic data for KDP. The resultant potential is able to give a reasonable interpretation of the mid-infrared bands for both KDP and DKDP. The change in the tunnelling frequency Ω for KDP with both temperature and pressure was calculated using the double Morse potential and the existing crystallographic data. The double Morse potential also gives accurate predictions of the change in the "site-site" separation δ on deuteration, cooling and hydrostatic compression. The temperature dependence of the soft-mode Raman data for KDP was re-analysed allowing for the temperature dependence of the tunnelling frequency. The apparent lack of temperature dependence of Ω that appeared in an earlier analysis (Peercy (1975)) is shown to be the result of two compensating effects:

i) A decrease in Ω with temperature due to the increase in O...O distance; and

ii) An increase in $\langle\Omega\rangle$ with temperature due to the increase in the thermal amplitude of the O...O thermal vibrations and the non-linear dependence of Ω on the O...O distance.

This explains why even though there is a considerable change in δ on cooling, Ω remains effectively temperature-independent. The analysis of the soft-mode Raman data also showed that the proton-proton interaction J is non-dipolar in character. The

relationship $J \propto \delta^2$ proves to be inappropriate for describing the change in J on compression.

The mean square dispersion of Ω was also estimated and is about equal to $\langle\Omega\rangle^2$, indicating a very skew distribution of Ω. This suggests that the damping of the soft-mode Raman response may well arise from the propagation of the collective mode being interrupted by fluctuations in the individual single-particle tunnelling frequencies.

The double Morse potential is thus seen to be an important tool in the analysis of hydrogen bond dynamics and should be of considerable use in understanding other hydrogen-bonded systems.

APPENDIX A

The Airy and Parabolic Cylinder functions

This appendix contains the definitions of the Airy and parabolic cylinder functions as required for the computation of the wavefunctions $\Phi(x)$. The definitions given are based on those in the mathematical handbook of Abramowitz and Stegun (1964).

A.1 The Airy functions

The Airy equation

$$y'' - xy = 0 \tag{A1}$$

has a pair of independent solutions the Airy functions $y = Ai(x)$ and $y = Bi(x)$ where

$$Ai(x) = d_1 f(x) - d_2 g(x) \tag{A2}$$

$$Bi(x) = 3^{\frac{1}{2}}[d_1 f(x) + d_2 g(x)] \tag{A3}$$

with $$f(x) = 1 + \frac{1}{3!}x^3 + \frac{1.4}{6!}x^6 + \frac{1.4.7}{9!}x^9 + \ldots\ldots \tag{A4}$$

$$g(x) = x + \frac{2}{4!}x^4 + \frac{2.5}{7!}x^7 + \frac{2.5.8}{10!}x^{10} + \ldots\ldots \tag{A5}$$

and $$d_1 = 3^{-2/3}/\Gamma(2/3)$$

$$d_2 = 3^{-1/3}/\Gamma(1/3)$$

where $\Gamma(x)$ is the gamma function.

Ai(x) and Bi(x) have the following asymptotic behaviour:

$$Ai(x) \sim \tfrac{1}{2}\pi^{-\frac{1}{2}}x^{-\frac{1}{4}}\exp(-t)\left[c_0 - \frac{c_1}{t} + \frac{c_2}{t^2} - \frac{c_3}{t^3} + \ldots\right],\ x > 0 \tag{A6}$$

$$Bi(x) \sim \pi^{-\frac{1}{2}}x^{-\frac{1}{4}}\exp(t)\left[c_0 + \frac{c_1}{t} + \frac{c_2}{t^2} + \frac{c_3}{t^3} + \ldots\right],\ x > 0 \tag{A7}$$

$$Ai(x) \sim \pi^{-\frac{1}{2}}x^{-\frac{1}{4}}\left[\sin\left(t + \frac{\pi}{4}\right)\left(1 - \frac{c_2}{t^2} + \frac{c_4}{t^4} - \frac{c_6}{t^6} + \ldots\right) - \cos\left(t + \frac{\pi}{4}\right)\left(\frac{c_1}{t} - \frac{c_3}{t^3} + \frac{c_5}{t^5} - \ldots\right)\right],\ x < 0 \tag{A8}$$

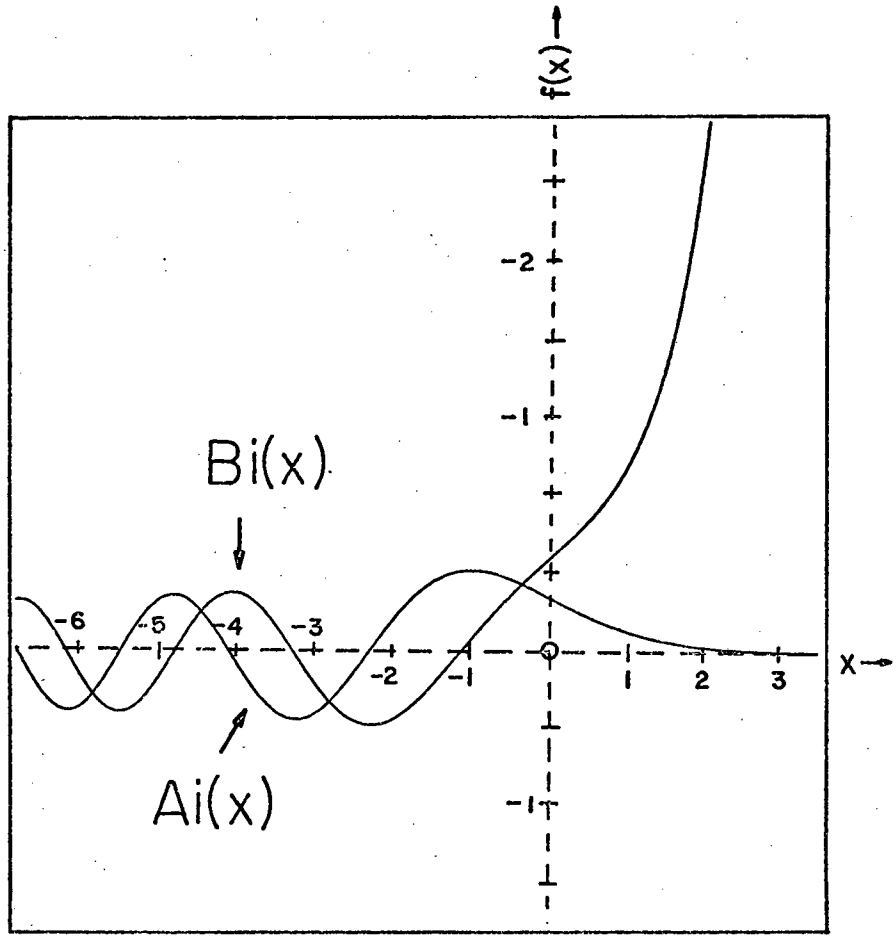

Figure A1. The Airy functions Ai(x) and Bi(x).

$$\mathrm{Bi}(x) \sim \pi^{-\frac{1}{2}}x^{-\frac{1}{4}}\left[\cos\left(t + \frac{\pi}{4}\right)\left(1 - \frac{c_2}{t^2} + \frac{c_4}{t^4} - \frac{c_6}{t^6} + \ldots\right)\right.$$

$$\left. + \sin\left(t + \frac{\pi}{4}\right)\left(\frac{c_1}{t} - \frac{c_3}{t^3} + \frac{c_5}{t^5} - \ldots\right)\right], \quad x < 0 \qquad (A9)$$

with $t = 2/3\ x^{3/2}$ and

$$c_k = \frac{(2k + 1)(2k + 3)\ldots(6k - 1)}{216^k\ k!} \qquad (A10)$$

Ai(x) and Bi(x) are plotted in Figure A1.

From equation (A7) it follows that $\mathrm{Bi}(x) \to \infty$ as $x \to \infty$. Thus when transforming the Schrödinger equation to the Airy equation in equations (2.4) - (2.13), the solutions $\mathrm{Bi}(\tau)/|\phi'|^{-\frac{1}{2}}$ are inappropriate as approximation for Φ, as $\Phi(x) \to 0$ when $x \to 0$. However, from (A6), $\mathrm{Ai}(x) \to 0$ as $x \to \infty$ and thus $\mathrm{Ai}(\tau)/|\phi'|^{-\frac{1}{2}}$ becomes the correct approximation to use for Φ in regions of the form (b,∞). This point was mentioned without qualification in Section 2.2.

The power series expansions (A2) and (A3) are absolutely convergent and thus may be differentiated termwise to yield Ai'(x) and Bi'(x). It is necessary to have expressions for these derivatives when solving the matching equation(2.44). So

$$\mathrm{Ai}'(x) = d_1 f'(x) - d_2 g'(x), \qquad (A11)$$

$$\mathrm{Bi}'(x) = 3^{\frac{1}{2}}[d_1 f'(x) + d_2 g'(x)] \qquad (A12)$$

$$f'(x) = \frac{1}{2!}\ x^2 + \frac{1.4}{5!}\ x^5 + \frac{1.4.7}{8!}\ x^8 + \ldots \qquad (A13)$$

$$g'(x) = 1 + \frac{2}{3!}\ x^3 + \frac{2.5}{6!}\ x^6 + \frac{2.5.8}{9!}\ x^9 + \ldots \qquad (A14)$$

For computational purposes, the power series expansions (A4), (A5), (A13) and (A14) proved to be rapidly convergent and yielded Ai(x) and Ai'(x) to the desired accuracy without

difficulty.

A.2 The Parabolic Cylinder functions

One form of the parabolic cylinder equation is

$$y'' - (\tfrac{1}{4}x^2 + a)y = 0. \qquad \text{(A15)}$$

Two independent solutions are

$$y_1(x;a) = 1 + a\frac{x^2}{2!} + a_4\frac{x^4}{4!} + a_6\frac{x^6}{6!} + \ldots \qquad \text{(A16)}$$

$$y_2(x;a) = x + a\frac{x^3}{3!} + a_5\frac{x^5}{5!} + a_7\frac{x^7}{7!} + \ldots \qquad \text{(A17)}$$

with $a_0 = a_1 = 1$

$a_2 = a_3 = a$

$a_{n+2} = a.a_n + \tfrac{1}{4}n(n-1)a_{n-2}$.

Clearly, y_1 is even in x and y_2 odd in x. (A16) and (A17) are absolutely convergent for all a and may be differentiated termwise to give

$$y_1'(x;a) = a_2x + a_4\frac{x^3}{3!} + a_6\frac{x^5}{5!} + \ldots \qquad \text{(A18)}$$

$$y_2'(x;a) = 1 + a_3\frac{x^2}{2!} + a_5\frac{x^4}{4!} + \ldots \qquad \text{(A19)}$$

The power series expansions (A16)-(A19) all proved to be rapidly convergent when computing $y_1(x;a)$, $y_2(x;a)$, $y_2'(x;a)$ and $y_2'(x;a)$.

APPENDIX B

Reduction and Computation of Phase Integrals

When calculating asymptotic approximations to the wave-functions $\Phi(x)$, integrals of the form

$$\int_{z_1}^{z_2} |E - V(z)|^{\frac{1}{2}} \, dz \qquad \text{(B1)}$$

have to be repeatedly evaluated.

B.1 Reduction of the integral

In this section it will be shown that if $V(x)$ is defined by (1.7), then the different forms of the integral (B1) that arise in the computing of the asymptotic approximations can all be reduced to combinations of elliptic integrals.

The various forms of the integral (B1) that arise in section (2.2) are as follows:

i) $\int_{-a}^{a}(V(u) - E)^{\frac{1}{2}}du$, a real [cf (2.27)]

ii) $\int_{x}^{b}(E - V(u))^{\frac{1}{2}}du$, $a<x<b$ [cf (2.31)]

iii) $\int_{x}^{b}(E - V(u))^{\frac{1}{2}}du$, $0<x<b$, a pure imaginary [cf Case II, region 2]

iv) $\int_{b}^{x}(V(u) - E)^{\frac{1}{2}}du$, $x>b$, a real [cf (2.32)]

v) $\int_{b}^{x}(V(u) - E)^{\frac{1}{2}}du$, $x>b$, a pure imaginary [cf Case II, region 2]

vi) $\int_{a}^{x}(E - V(u))^{\frac{1}{2}}du$, $a<x<b$ [cf (2.26)]

vii) $\int_{o}^{x}(E - V(u))^{\frac{1}{2}}du$, $0<x<b$, a pure imaginary [cf (2.35)]

viii) $\int_{x}^{a}(V(u) - E)^{\frac{1}{2}}du$, $0<x<a$ [cf (2.25)]

ix) $\int_{-Im(a)}^{Im(a)}(E - V(iv))dv$, a pure imaginary [cf (2.37)]

Consider first the integrals (i) - (viii).

From (1.7)

$$E-V(u) = E - D\{2\exp[-2\alpha(R-r_o)]\cosh 2\alpha u - 4\exp[-\alpha(R-r_o)]\cosh\alpha u\}.$$

Let $t = \cosh\alpha u$ and $t' = \cosh\alpha x$. Then

$$|E - V(u)|^{\frac{1}{2}}du = (D^{\frac{1}{2}}/\alpha)\,|E/D + 2\exp[-2\alpha(R-r_o)] + 4\exp[-\alpha(R-r_o)]t - 4\exp[-2\alpha(R-r_o)]t^2|^{\frac{1}{2}}\,\frac{dt}{|t^2-1|^{\frac{1}{2}}}. \qquad (B2)$$

Consider the quadratic in t in the numerator. According to (2.1) and (2.2) it will have two real roots* $t_+ \equiv \cosh\alpha b$ and $t_- \equiv \cosh\alpha a$, given by

$$t_{\pm} = \gamma \pm (\gamma^2 + \gamma^2 E/D + \tfrac{1}{2})^{\frac{1}{2}} \qquad (B3)$$

where $\gamma = \exp[\alpha(R - r_o)]/2$. For the double minimum potential $\gamma > 1$ and so the two cases that arise are

Case I Below the barrier : $t_+ > t_- > 1 > -1$

Case II Above the barrier : $t_+ > 1 > t_- > -1$

(or $t_+ > 1 > -1 > t_-$)

It has already been pointed out in Section 2.2 that when $t_- < -1$, a is complex (not pure imaginary) and the Liouville transformations then become far more difficult to perform. Hence in Case II only the first set of inequalities will be considered. (B2) may then be written as

$$|E - V(u)|^{\frac{1}{2}}du = (D^{\frac{1}{2}}/\alpha)\left|\frac{(t - t_-)(t - t_+)}{(t - 1)(t + 1)}\right|^{\frac{1}{2}} dt \qquad (B3)$$

In general integrals of this form can be evaluated only in terms of elliptic integrals. This is done as follows.

---

* The case where either t_+ or t_- is complex can only occur if $E < V(u)$ for all u, a situation which does not arise physically.

Let the roots of the numerator and denominator of the right hand side of (B3) be represented by α_i; i = 1,2,3,4 with $\alpha_1 \geq \alpha_2 \geq \alpha_3 \geq \alpha_4$. The integrals (i) - (viii) above then become (remembering that V is even in u):

i') $2C \int_{\alpha_3}^{\alpha_2} \left[\frac{(\alpha_1-t)(\alpha_2-t)}{(t-\alpha_3)(t-\alpha_4)}\right]^{\frac{1}{2}} dt, \quad \alpha_1=t_+, \ \alpha_2=t_-, \ \alpha_3=1, \ \alpha_4=-1$

ii') $C \int_{t'}^{\alpha_1} \left[\frac{(\alpha_1-t)(t-\alpha_2)}{(t-\alpha_3)(t-\alpha_4)}\right]^{\frac{1}{2}} dt, \quad \alpha_1=t_+, \ \alpha_2=t_-, \ \alpha_3=1, \ \alpha_4=-1$

iii') $C \int_{t'}^{\alpha_1} \left[\frac{(\alpha_1-t)(t-\alpha_3)}{(t-\alpha_2)(t-\alpha_4)}\right]^{\frac{1}{2}} dt, \quad \alpha_1=t_+, \ \alpha_2=1, \ \alpha_3=t_-, \ \alpha_4=-1$

iv') $C \int_{\alpha_1}^{t'} \left[\frac{(t-\alpha_1)(t-\alpha_2)}{(t-\alpha_3)(t-\alpha_4)}\right]^{\frac{1}{2}} dt, \quad \alpha_1=t_+, \ \alpha_2=t_-, \ \alpha_3=1, \ \alpha_4=-1$

v') $C \int_{\alpha_1}^{t'} \left[\frac{(t-\alpha_1)(t-\alpha_3)}{(t-\alpha_2)(t-\alpha_4)}\right]^{\frac{1}{2}} dt, \quad \alpha_1=t_+, \ \alpha_2=1, \ \alpha_3=t_-, \ \alpha_4=-1$

vi') $C \int_{\alpha_2}^{t'} \left[\frac{(\alpha_1-t)(t-\alpha_2)}{(t-\alpha_3)(t-\alpha_4)}\right]^{\frac{1}{2}} dt, \quad \alpha_1=t_+, \ \alpha_2=t_-, \ \alpha_3=1, \ \alpha_4=-1$

vii') $C \int_{\alpha_2}^{t'} \left[\frac{(\alpha_1-t)(t-\alpha_3)}{(t-\alpha_2)(t-\alpha_4)}\right]^{\frac{1}{2}} dt, \quad \alpha_1=t_+, \ \alpha_2=1, \ \alpha_3=t_-, \ \alpha_4=-1$

viii') $C \int_{t'}^{\alpha_2} \left[\frac{(\alpha_1-t)(\alpha_2-t)}{(t-\alpha_3)(t-\alpha_4)}\right]^{\frac{1}{2}} dt, \quad \alpha_1=t_+, \ \alpha_2=t_-, \ \alpha_3=1, \ \alpha_4=-1$

where $C = 2(D^{\frac{1}{2}}/\alpha)\ \exp\ [-\alpha(R-r_o)]$.

Following Byrd and Friedman (1971), the integrals (i')-(viii') are all sums of elliptic integrals:

i") $$2C\int = 2C\frac{(\alpha_1-\alpha_3)(\alpha_2-\alpha_3)g}{2\beta^4} \times [-\beta^2 E(k)+(\beta^2+k^2)F(k)+ (\beta^4-k^2)\Pi(\beta^2;k)] \qquad (254.18,362.20)$$

ii") $$C\int = C\frac{(\alpha_1-\alpha_2)(\alpha_2-\alpha_3)\beta^2 g}{2\beta^4(k^2-\beta^2)} \times \left\{\beta^2[E(k)-E(\theta,k)]+(\beta^2-k^2)[F(k)-F(\theta,k)]+(\beta^4-2\beta^2+k^2)[\Pi(\beta^2;k)-\Pi(\beta^2;\theta,k)]+ \frac{\beta^4\sin\theta\cos\theta(1-k^2\sin^2\theta)^{\frac{1}{2}}}{1-\beta^2\sin^2\theta}\right\} \qquad (256.19,362.18)$$

iii") $$C\int = C\frac{(\alpha_1-\alpha_2)(\alpha_2-\alpha_3)g}{2\beta^2(k^2-\beta^2)} \times \left\{\beta^2[E(k)-E(\theta,k)]+(k^2-\beta^2)[F(k)-F(\theta,k)]+(2k^2\beta^2-\beta^4-k^2)[\Pi(\beta^2;k)-\Pi(\beta^2;\theta,k)]+ \frac{\beta^4\sin\theta\cos\theta(1-k^2\sin^2\theta)^{\frac{1}{2}}}{1-\beta^2\sin^2\theta}\right\} \qquad (256.17,362.16)$$

iv") $$C\int = \frac{C(\alpha_1-\alpha_2)^2\beta^2 g}{2\beta^2(\beta^2-1)(k^2-\beta^2)} \times \left\{\beta^2 E(\theta,k)+(k^2-\beta^2)F(\theta,k)+ (\beta^4-k^2)\Pi(\beta^2;\theta,k) - \frac{\beta^4\sin\theta\cos\theta(1-k^2\sin^2\theta)^{\frac{1}{2}}}{1-\beta^2\sin^2\theta}\right\} \qquad (258.19,362.15)$$

v") $$C\int = C\frac{(\alpha_1-\alpha_3)(\alpha_1-\alpha_2)\beta^2 g}{2\beta^4(\beta^2-1)} \times \left\{-\beta^2 E(\theta,k)+(\beta^2+k^2-2\beta^2k^2)F(\theta,k)+ (2\beta^2k^2-\beta^4-k^2)\Pi(\beta^2;\theta,k)+ \frac{\beta^4\sin\theta\cos\theta(1-k^2\sin^2\theta)^{\frac{1}{2}}}{1-\beta^2\sin^2\theta}\right\} \qquad (258.17,362.19)$$

vi") $$C\int = \frac{C(\alpha_1-\alpha_2)(\alpha_2-\alpha_3)\beta^2 g}{2\beta^4(k^2-\beta^2)} \times \left\{\beta^2 E(\theta,k)+(\beta^2-k^2)F(\theta,k)+ (\beta^4-2\beta^2+k^2)\Pi(\beta^2;\theta,k) - \frac{\beta^4\sin\theta\cos\theta(1-k^2\sin^2\theta)^{\frac{1}{2}}}{1-\beta^2\sin^2\theta}\right\}$$

(256.19,362.18)

vii") $$C\int = \frac{C(\alpha_1-\alpha_2)(\alpha_2-\alpha_3)g}{2\beta^2(k^2-\beta^2)} \left\{\beta^2 E(\theta,k)+(k^2-\beta^2)F(\theta,k)+ (\beta^4-2\beta^2+k^2)\Pi(\beta^2;\theta,k) - \frac{\beta^4\sin\theta\cos\theta(1-k^2\sin^2\theta)^{\frac{1}{2}}}{1-\beta^2\sin^2\theta}\right\}$$

(256.17,362.16)

viii") $$C\int = \frac{C(\alpha_1-\alpha_3)(\alpha_2-\alpha_3)g}{2\beta^4} \times \left\{-\beta^2[E(k)-E(\theta,k)]+(\beta^2+k^2)[F(k)-F(\theta,k)]+(\beta^4-k^2)[\Pi(\beta^2;k)-\Pi(\beta^2;\theta,k)] \frac{-\beta^2\sin\theta\cos\theta(1-k^2\sin^2\theta)^{\frac{1}{2}}}{1-\beta^2\sin^2\theta}\right\}$$

(254.18,362.20)

where $g = 2[(\alpha_1-\alpha_3)(\alpha_2-\alpha_4)]^{-\frac{1}{2}}$,

β^2, k^2 and θ are defined for each integral in Table B1 and F,E and Π are the standard elliptic integrals (e.i.'s) defined by

$F(\theta,k) = \int_0^{\theta}(1-k^2\sin^2\phi)^{-\frac{1}{2}}d\phi$ (Incomplete e.i. of the 1st kind)

$F(k) \equiv F(\pi/2,k) = \int_0^{\pi/2}(1-k^2\sin^2\theta)^{-\frac{1}{2}}d\phi$ (Complete e.i. of the 1st kind)

$E(\theta,k) = \int_0^{\theta}(1-k^2\sin^2\phi)^{\frac{1}{2}}d\phi$ (Incomplete e.i. of the 2nd kind)

$E(k) \equiv E(\pi/2,k) = \int_0^{\pi/2}(1-k^2\sin^2\phi)^{\frac{1}{2}}d\phi$ (Complete e.i. of the 2nd kind)

$\Pi(\beta^2;\theta,k) = \int_0^{\theta}(1-\beta^2\sin^2\theta)^{-1}(1-k^2\sin^2\phi)^{-\frac{1}{2}}d\phi$ (Incomplete e.i. of the 3rd kind)

$$\Pi(\beta^2;k) \equiv \Pi(\beta^2;\ \pi/2,k) = \int_0^{\pi/2}(1-\beta^2\sin^2\phi)(1-k^2\sin^2\phi)^{-\frac{1}{2}}d\phi$$

(Complete e.i. of the 3rd kind)

The numbers in brackets in (i")-(viii") refer to the formulae used in Byrd and Friedman to perform the reduction.

Integral (ix) is still outstanding. From the analysis of Case II in Section 2.2,

$$E\text{-}V(iv) = E-D\{2\ \exp[-2\alpha(R-r_o)]\cos 2\alpha v-4\ \exp[-\alpha(R-r_o)]\cos\alpha v\}.$$

Let $t = \cos\alpha v$. Then

$$(E-V(iv))^{\frac{1}{2}}dv = (D^{\frac{1}{2}}/\alpha)\{E/D+2\ \exp[-2\alpha(R-r_o)]+4\ \exp[-\alpha(R-r_o)]t - 4\ \exp[-2\alpha(R-r_o)]t^2\}^{\frac{1}{2}}\ \frac{dt}{(1-t^2)^{\frac{1}{2}}} \qquad (B4)$$

The numerator is quadratic in t and has roots given by

$$t_{\pm} = \gamma \pm (\gamma^2+\gamma^2E/D+\tfrac{1}{2})^{\frac{1}{2}}$$

As $\gamma>1$ for the double minimum potential $V(x)$, $t_+ > 1$ and so only t_- can possibly give a real value for v from $t = \cos\alpha v$. Hence put

$$t_- \equiv \cos\,[\alpha\,\mathrm{Im}(a)].$$

Note that $|t_-|\leq 1$ is assumed. For if $t_- > 1$ then the level E would lie below the barrier, and the integral (ix) would not arise. If $t < -1$, then a is complex, a case that cannot be dealt with by the method developed in Section 2.2.

(B4) becomes

$$(E-V(iv))^{\frac{1}{2}}dv = (D^{\frac{1}{2}}/\alpha)\left[\frac{(t_+-t)(t-t_-)}{(1-t)(1+t)}\right]^{\frac{1}{2}}dt.$$

Integral (ix) then becomes, as V is even in v,

ix') $$2C\int_{\alpha_3}^{1}\left[\frac{(\alpha_1-t)(t-\alpha_3)}{(\alpha_2-t)(t-\alpha_4)}\right]^{\frac{1}{2}}dt, \quad \alpha_1=t_+,\alpha_2=1,\alpha_3=1,\alpha_4=-1$$

where $C = 2(D^{\frac{1}{2}}/\alpha)\ \exp\,[-\alpha(R-r_o)]$.

Following Byrd and Friedman, (ix') may be written as

$$\text{ix"}) \quad 2C\int = \frac{2C(\alpha_1-\alpha_3)(\alpha_3-\alpha_4)\beta^2 g}{2\beta^4(\beta^2-1)} \times \left\{-\beta^2 E(k)+(\beta^2+k^2-2\beta^2k^2)F(k) + (2\beta^2k^2-\beta^4-k^2)\Pi(\beta^2;k)\right\} \qquad (254.17,362.19)$$

where g,E,F and Π are defined as above and β^2 and k^2 are given in Table B1.

Equations (i") - (ix") are now the desired computational forms required for the phase integrals.

B.2 Computation of the elliptic integrals F,E and Π

In the program developed for determining asymptotic approximations to Φ, the Harwell Subroutine Library* subroutines FBØ1A, FBØ2A and FBØ3A were used for computing the elliptic integrals F,E and Π. FBØ1A evaluates complete elliptic integrals of the first and second kind, FBØ2A evaluates incomplete elliptic integrals of the first and second kind and FBØ3A evaluate complete elliptic integrals of the third kind.

As the version of the Harwell library used had no subroutine available for computing incomplete elliptic integrals of the third kind, a subroutine was developed for this purpose using the algorithm given in Section 17.7 of Abramowitz and Stegun (1964).

All these subroutines proved to be very successful for computing the various elliptic integrals.

---

* See Appendix D

Table B1

Elliptic integral arguments used when reducing $\int_{z_1}^{z_2} |E-V(z)|^{\frac{1}{2}} dz$. ($\alpha_{ij}=\alpha_i-\alpha_j$)

Integral form	k^2	$\sin^2\theta$	β^2
(i), (viii), (ix)	$\alpha_{23}\alpha_{14}\alpha_{13}^{-1}\alpha_{24}^{-1}$	$\alpha_{24}\alpha_{23}^{-1}(t'-\alpha_3)(t'-\alpha_4)^{-1}$	$\alpha_{23}\alpha_{24}^{-1}$
(ii), (iii), (vi), (vii)	$\alpha_{12}\alpha_{34}\alpha_{13}^{-1}\alpha_{24}^{-1}$	$\alpha_{13}\alpha_{12}^{-1}(t'-\alpha_2)(t'-\alpha_3)^{-1}$	$\alpha_{12}\alpha_{23}^{-1}$
(iv), (v)	$\alpha_{14}\alpha_{23}\alpha_{13}^{-1}\alpha_{24}^{-1}$	$\alpha_{24}\alpha_{14}^{-1}(t'-\alpha_1)(t'-\alpha_2)^{-1}$	$\alpha_{14}\alpha_{24}^{-1}$

APPENDIX C

Accuracy of Energy Eigenvalue Estimates

As mentioned in section 2.3, it is very difficult to give a good estimate of the accuracy of the method developed in chapter 2 for determining the energy eigenvalues and energy wavefunctions in the double Morse potential. However, an attempt will now be made to obtain some estimate of the errors involved and to give a qualitative discussion of their most likely sources.

The method involved matching in both value and derivative two asymptotic approximations $\Phi_n^{(1)}$ and $\Phi_n^{(2)}$ at a common boundary point $x = c$. $\Phi_n^{(1)}$ is an approximation to the true wavefunction in the region $|x| < c$ and $\Phi_n^{(2)}$ is an approximation to the true wavefunction in the region $|x| > c$. Equation (2.44) must be satisfied at the point $x = c$ in order for Φ_n to be an approximate eigenfunction of the Hamiltonian. For convenience, c was chosen in that chapter to be equal to x_m, the displacement of the potential minima from the centre of the bond. The method is clearly dependent on the position of the point c at which the matching is performed.

As is shown in figure 2.3, the point c must lie either between the turning points a and b (if the energy level is below the barrier) or between the point $x = 0$ and the turning point b (if the energy level lies above the barrier). Consider now the case of an energy level lying below the barrier. If the point c is chosen too close to the point $x = b$, then the asymptotic approximation $\Phi_n^{(1)}$ in the region $a < x < c$ may cease to be a good approximation to the true wavefunction near to the point $x = c$ due to the proximity of the turning

point b. Similarly, inaccuracies might be expected if the point c were chosen to lie too close to the point x = a. The point c must therefore be chosen so that both $\Phi_n^{(1)}$ and $\Phi_n^{(2)}$ are sufficiently close in value to the true wavefunction at x = c. As the point $x = x_m$ lies approximately halfway between the turning points a and b, this is probably a good choice for c. The effect on the energy eigenvalues of varying the position of c should be most pronounced for the lowest lying levels i.e. those levels for which the turning points a and b lie closest together. Furthermore, the effect should also be more pronounced for deuterated species that it is for protonated species as the energy levels are situated lower down in the well in the deuterated case. For energy levels lying above the barrier, the choice of x_m for c is expected to be reasonable as above the barrier the points b, x_m and a are much further apart than they are for a level lying below the barrier. (Recall that in this case a is pure imaginary and the three points mentioned should be considered as lying in the complex plane.)

Whereas the choice of c mentioned above appeared to yield no abnormal behaviour or instabilities in all the calculations of chapters 3, 4 and 5, it is interesting to test just what effect varying the position of the point c has on the energy eigenvalues.

The double Morse potentials that will be used are those given in chapter 3 for CrOOH and CrOOD (see table 3.). c is varied in the range $0 < |x_m - c| < 0.02\text{Å}$ and the resultant variations in the energy level positions found. These are plotted for CrOOH and CrOOD in figures C1 and C2 respectively. As can be seen, the most marked effect is that upon

the positions of the lowest lying levels: the total variation of 0.04Å in c results in the position of the E_o level changing by 47 cm^{-1} relative to the bottom of the well for CrOOH and by 43 cm^{-1} relative to the bottom of the well for CrOOD. The corresponding change in the E_3 level position is 15 cm^{-1} for CrOOH and 11 cm^{-1} for CrOOD.

The changes in the transition frequencies are less pronounced in magnitude as they depend only upon the relative displacement of the respective levels. Table C1 shows the percentage variation of the ν_s(OH) and ν_s(OD) infrared transition frequencies for CrOOH and CrOOD respectively as c is varied by 0.02Å on either side of x_m. The greatest variation is in the $|0\rangle \rightarrow |1\rangle$ transition frequency for CrOOD ($\sim$9%), as might be expected from the above remarks. However, as the magnitude of the ground state splitting is only 8 cm^{-1} for CrOOD, this is not at all serious.

The turning points a and b for the ground state wavefunctions are calculated to be separated by about 0.14Å for CrOOD and by about 0.22Å for CrOOH. The variation in c by 0.02Å on either side of the point $x = x_m$ is hence substantial and should place a severe test on the accuracy of the asymptotic approximations in the vicinity of a neighbouring turning point. Thus the above error estimates are probably generous upper bounds for the true error and the above analysis suggests that the method developed is numerically stable as regards determining the transition frequencies. It should be capable of giving accurate estimates (to within $\sim$2%) of the $|0\rangle \rightarrow |1\rangle$, $|1\rangle \rightarrow |2\rangle$ and $|0\rangle \rightarrow |3\rangle$ infrared transition frequencies of a given double Morse potential.

Table C1. Percentage variation in predicted CrOOH and CrOOD infrared transition frequencies due to a change of 0.04Å in the position of wavefunction "matching point" c.

Transition	CrOOH Frequency	CrOOH Variation	CrOOD Frequency	CrOOD Variation
$\|0\rangle \rightarrow \|1\rangle$	226 cm^{-1}	6%	8 cm^{-1}	9%
$\|1\rangle \rightarrow \|2\rangle$	1650 cm^{-1}	2%	1613 cm^{-1}	2%
$\|0\rangle \rightarrow \|3\rangle$	3400 cm^{-1}	1%	1923 cm^{-1}	2%

APPENDIX D

Computer Program Libraries Used

All the computer programs needed for the computations contained in this thesis were written by the author, with the exception of:

a) The subroutines FBØ1A, FBØ2A, FBØ3A, NBØ1A, NSØ1A and VBØ1A, which were obtained from the Harwell Subroutine Library (AERE, Harwell, England, 1974); and

b) The non-linear regression routine NREG, which was obtained from the Madison Academic Computer Centre (University of Wisconsin, U.S.A., 1972).

Both of these program libraries are available at the University of Cape Town Computer Centre where the computing was performed.

REFERENCES

Abramowitz, M. and I.A. Stegun, 1965, *Handbook of Mathematical Functions with Formulas, Graphs and Mathematical Tables*, (Government Printing Office, Washington, D.C.).

Almenningen, A., O. Bastiansen and T. Motzfeldt, 1970, *Acta Chem. Scand. 24*, 747.

Auvert, G. and Y. Marechal, 1979a, *Chem. Phys. 40*, 51.

Auvert, G. and Y. Marechal, 1979b, *Chem. Phys. 40*, 61.

Auvert, G. and Y. Marechal, 1979c, *J. Physique, 40*, 735.

Bacon, G.E. and R.S. Pease, 1953, *Proc. Roy. Soc. A220*, 397.

Bacon, G.E. and R.S. Pease, 1955, *Proc. Roy. Soc. A230*, 359.

Baker, A.N., 1954, *J. Chem. Phys. 22*, 1625.

Blinc, R. and D. Hadži, 1958, *Molec. Phys. 1*, 391.

Blinc, R., 1960, *J. Phys. Chem. Solids 13*, 204.

Blinc, R. and M. Ribarič, 1963, *Phys. Rev. 130*, 1816.

Blinc, R. and S. Svetina, 1966a, *Phys. Rev. 147*, 423.

Blinc, R. and S. Svetina, 1966b, *Phys. Rev. 147*, 430.

Blinc, R. and B. Žekš, 1968, *Helv. Phys. Acta 41*, 700.

Blinc, R. and B. Žekš, 1972, *Adv. Phys. 21*, 693.

Blinc, R. and B. Žekš, 1974, *Soft Modes in Ferroelectrics and Antiferroelectrics*, ed. E.P. Wohlfarth, (North Holland, Amsterdam).

Blinc, R., B. Žekš, J.F. Sampaio, A.S.T. Pires and F.C. Sa Barreto, 1979, *Phys. Rev. B20*, 1991.

Bournay, J. and Y. Marechal, 1974, *Chem. Phys. Lett. 27*, 180.

Bournay, J. and Y. Marechal, 1975, *Spectrochimica Acta, 31A*, 1351.

Byrd, P.F. and M.D. Friedman, 1971, *Handbook of Elliptic Integrals for Engineers and Scientists*, (Springer-Verlag, Berlin).

Claydon, M.F., N. Sheppard, B.C. Stace and J.A. Upfield, 1975, *Chem. Comm.*, 31.

Cochran, W., 1960, *Adv. Phys. 9*, 387.

Cochran, W., 1961, *Adv. Phys. 10*, 401.

Cochran, W., 1969, *Adv. Phys. 18*, 157.

Davis, T.D. and R.E. Christoffersen, 1973, *Chem. Phys. Lett. 20*, 317.

De Gennes, P.G., 1963, *Solid State Comm., 1*, 132.

Delaplane, R.G., J.A. Ibers, J.R. Ferraro and J.J. Rush, 1969, *J. Chem. Phys. 50*, 1920.

Douglass, R.M., 1957, *Acta Cryst. 10*, 423.

Erdélyi, A., 1956, *Asymptotic Expansions*, (Dover, New York).

Excoffon, P. and Y. Marechal, 1972, *Spectr. Acta 28A*, 269.

Ford, K.W., D.L. Hill, M. Walkano and J.A. Wheeler, 1959, *Ann. Phys. 7*, 239.

Frazer, B.C. and R. Pepinsky, 1953, *Acta Cryst. 6*, 273.

Godzik, K.D. and A. Blumen, 1974, *Phys. Stat. Sol (b) 66*, 569.

Hamilton, W.C. and J.A. Ibers, 1963, *Acta Cryst. 16*, 1209.

Haurie, M. and A. Novak, 1966, *J. Chim. Phys. 63*, 1584.

Havlin, S. and H. Sompolinsky, 1979, *J. Phys. C12*, 3135.

Heading, J., 1962, *Introduction to Phase-Integral Methods*, (Methuen, London).

Hill, R.M. and S.K. Ichiki, 1968, *J. Chem. Phys. 48*, 838.

Holtzberg, F., B. Post and I. Fankuchen, 1953, *Acta Cryst. 6*, 127.

Housty, J. and M. Hospital, 1965, *Acta Cryst. 18*, 693.

Ibers, J.A., C.H. Holm and C.R. Adams, 1961, *Phys. Rev. 121*, 1620.

Imry, Y., I. Pelah and E. Wiener, 1965, *J. Chem. Phys. 43,* 2332.

Janoschek, R.E., G. Weidemann, H. Pfeiffer and G. Zundel, 1972, *J. Am Chem. Soc. 92,* 2387.

Jeffreys, H. and B.S. Jeffreys, 1956, *Methods of Mathematical Physics,* (University Press, Cambridge).

Jeffreys, H., 1962, *Asymptotic Approximations,* (Oxford University Press, London).

Kaminow, I.P. and T.C. Damen, 1968, *Phys. Rev. Lett, 20,* 1968.

Karle, I.L. and J. Karle, 1954, *J. Chem. Phys. 22,* 43.

Kobayashi, K.K., 1968, *J. Phys. Soc. Japan 24,* 497.

Kubo, R., 1962a, *J. Phys. Soc. Japan 17,* 1100.

Kubo, R., 1962b, *Fluctuation, Relaxation and Resonance in Magnetic Systems,* Ed. D. ter Haar (Oliver and Boyd, Edinburgh).

Kwei, G.H. and R.F. Curl, 1960, *J. Chem. Phys. 32,* 1592.

Lagakos, N. and H.Z. Cummins, 1974, *Phys. Rev. B10,* 1063.

Lawrence, M.C. and Robertson, G.N., 1979, *Chem. Phys. Lett. 63,* 447.

Lawrence, M.C. and Robertson, G.N., 1980, *Ferroelectrics 25,* 363.

Lerner, R.G., B.P. Dailey and J.P. Friend, 1957, *J. Chem. Phys. 26,* 680.

Lines, M.E. and A.M. Glass, 1977, *Principles and Applications of Ferroelectrics and Related Materials,* (Oxford University Press, London).

Mačkowiak, M., J. Stankowski, B. Žekš and R. Blinc, 1979, *Phys. Rev. B19,* 1651.

Maradudin, A.A., I.P. Ipatova, E.W. Montroll and G.H. Weiss, 1971, *Theory of Lattice Dynamics in the Harmonic Approximation, (Solid State Physics Suppl. 3)*, 2nd ed. (Academic Press, New York).

Meyer, G.H., R.J. Nelmes and C. Vettier, 1980, in press.

Miller, W.H., 1968, *J. Chem. Phys. 48*, 1651.

Nagle, J.F. and H.J. Morowitz, 1978, *Proc. Natl. Acad. Sci. U.S.A. 75*, 298.

Nelmes, R.J., 1980, *Ferroelectrics 24*, 237.

Nørlund Christensen, A., P. Hansen and M.S. Lehmann, 1976, *J. Sol. Stat. Chem. 19*, 299.

Nørlund Christensen, A., P. Hansen and M.S. Lehmann, 1977, *J. Sol. Stat. Chem. 21*, 325.

Novak, A., 1974, *Structure and Bonding, 18*, 177.

Olver, F.W.J., 1975, *Phil. Trans. Roy. Soc. 278A*, 137.

Peercy, P.S., 1973, *Phys. Rev. Lett. 31*, 6.

Peercy, P.S., 1975, *Phys. Rev. B12*, 2725.

Peterson, S.W. and H.A. Levy, 1957, *Acta Cryst. 10*, 70.

Pshenichnov, E.A. and N.D. Sokolov, 1961, *Optika I Spektroskopiya 11*, 16.

Reid, C., 1959, *J. Chem. Phys. 30*, 182.

Rush, J.J. and J.R. Ferraro, 1966, *J. Chem. Phys. 44*, 2496.

Samara, G.A., 1967, *Phys. Lett. 25A*, 664.

Samara, G.A., 1971, *Phys. Rev. Lett. 27*, 103.

Samara, G.A., 1973, *Ferroelectrics 5*, 25.

Savel'ev, V.A. and N.D. Sokolov, 1975, *Chem. Phys. Lett. 34*, 281.

Schomaker, V. and J.M. O'Gorman, 1947, *J. Am. Chem. Soc. 69*, 2638.

Schuster, P., G. Zundel, and C. Sandorfy, 1975, *The Hydrogen Bond* (3 vols.) (editors), (North Holland, Amsterdam).

Senko, M.E., 1961, *Phys. Rev. 121*, 1599.

She, C., T.W. Broberg, L.S. Wall and D.F. Edwards, 1972, *Phys. Rev. B6*, 1847.

Sheppard, N., 1979, private communication.

Silsbee, H.B., W.A. Uehling and V.H. Schmidt, 1964, *Phys. Rev. 133*, A165.

Slater, J.C., 1941, *J. Chem. Phys. 9*, 16.

Snyder, R.G. and J.A. Ibers, 1962, *J. Chem. Phys. 36, 1356*.

Somorjai, R.L. and D.F. Hornig, 1962, *J. Chem. Phys. 36*, 1980.

Takagi, Y., 1948, *J. Phys. Soc. Japan 3*, 271.

Temme, F.P. and T.C. Waddington, 1973, *J. Chem. Phys. 59*, 817.

Ter Haar, D., 1964, *Selected Problems in Quantum Mechanics*, (Infosearch, London).

Tokunaga, M. and T. Matsubara, 1966, *Progr. Theor. Phys. 35*, 581.

Tokunaga, M., 1966, *Progr. Theor. Phys. 36*, 857.

Torstveit, S., 1979, *Phys. Rev. B20*, 4431.

Tuval, Y. and R.E. Nettleton, 1976, *J. Phys. C9*, 1159.

Umebayashi, H., B.C. Frazer, G. Shirane and W.B. Daniels, 1967, *Solid St. Comm. 5*, 591.

Vaks, V.G. and A.I. Larkin, 1965, *Zh. Eksp. Teor. Fiz. 49*, 975. (*Sov. Phys. - JETP. 22*, 678 (1966)).

Vaks, V.G. and V.I. Zinenko, 1973, *Zh. Eksp. Teor. Fiz. 64*, 650. (*Sov. Phys. - JETP. 37*, 330 (1973)).

Viswanath, R.S. and P.J. Miller, 1979, *Solid State Comm. 29*, 163.

Zelsmann, H.R., F. Bellon, Y. Marechal and B. Bullemer, 1970, *Chem. Phys. Lett. 6*, 513.

Zelsmann, H.R. and Y. Marechal, 1974, *Chem. Phys. 5*, 367.

Zelsmann, H.R. and Y. Marechal, 1977a, *Chem. Phys. 20*, 445.

Zelsmann, H.R. and Y. Marechal, 1977b, *Chem. Phys. 20*, 459.